FLEXURAL AND LONG-TERM BEHAVIOR OF CFRP-STRENGTHENED REINFORCED CONCRETE BEAMS

Von der Fakultät für Bauingenieurwesen und Geodäsie

der Gottfried Wilhelm Leibniz Universität Hannover

zur Erlangung des Grades eines

DOKTOR DER INGENIEURWISSENSCHAFTEN

Dr.-Ing.

genehmigte Dissertation

von

M.Sc. Mohamed Morsy Abd El-Ghaffar Salem

geboren am 01.06.1972, in El-Fayoum/Ägypten

2012

Die vorliegende Arbeit wurde als Dissertation im Rahmen des Promotionsverfahrens an der Fakultät für Bauingenieurwesen und Geodäsie der Leibniz Universität Hannover eingereicht und angenommen.

Referent: Univ.-Prof. Dr.-Ing. Nabil A. Fouad

Korreferenten: Univ.-Prof. Dr.-Ing. Ludger Lohaus

Kommissionsmitglieder: Univ.-Prof. Dr.-Ing. Steffen Marx

Vorsitz: Univ.-Prof. Dr.-Ing. Martin Achmus

Tag der Promotion: 12.12.2012

Dedicated to my Mother, Soul of my Father, and my family
With great gratitude for their encouragement, support, help and everything they done for me.

Acknowledgements

Mohamed Morsy Abd El-Ghaffar Salem

Hannover, December 2012

FLEXURAL AND LONG-TERM BEHAVIOR OF CFRP-STRENGTHENED REINFORCED CONCRETE BEAMS

Mohamed Salem

Abstract

The repair and strengthening or retrofitting of existing concrete structures to resist higher design loads (wind loads, earthquake loads, and bridges loads), has traditionally been accomplished using conventional materials and construction techniques. Externally bonded steel plates, steel or concrete jackets and external post tensioning are just some of the many traditional techniques available. In the context of the strengthening of the reinforced concrete structures, advanced composite materials have the potential for leading to innovative solutions.

The main objective of this study is to evaluate the flexural and creep behavior of the CFRP-strengthened reinforced concrete beams under normal conditions. To achieve this objective; an experimental and numerical investigation were conducted. The experimental specimens were tested in the laboratory of the Institute for Building Physics in the Leibniz of Hannover, Faculty of Civil Engineering and Geodesy. The tested specimens were twelve simply supported reinforced concrete beams; six of the RC beams were strengthened with external bonded CFRP to the tension side of the reinforced concrete beams.

The tested specimens were divided into two parts; the first part consists of six beams; three un-strengthened reinforced concrete beams (control beams); and three FRP-strengthened reinforced concrete beams. The flexural behavior of the CFRP-strengthened reinforced concrete beams was investigated experimentally and numerically using Abaqus finite element program. Furthermore, a parametric study using the calibrated finite element model was also evaluated. The experimental and FE model showed that using CFRP for strengthened reinforced concrete beams improve the stiffness of the reinforced concrete beam, increase the ultimate capacity, and also decreased the cracks in the tension side of the reinforced concrete beam. Also the properties of epoxy adhesive had no significant effect in the ultimate capacity of the strengthened system.

The second part were three un-strengthened reinforced concrete beams (control beams); and three CFRP-strengthened reinforced concrete beams. The creep behavior of the CFRP-strengthened reinforced concrete beams under constant applied load and normal

weathering condition was investigated experimentally and numerically. In addition parametric study using the calibrated finite element model was also evaluated. The parameter used in the parametric study was the effect of different material properties of epoxy adhesive. The experimental and FE investigation showed that using CFRP for strengthened reinforced concrete beams decreases the creep deflection of the CFRP-strengthened reinforced concrete beam with value depends on the ratio of the CFRP plate length/breadth to beam span/breadth. Furthermore, using CFRP decreased the initial deflection and decreased the cracks in the tension side of the strengthened beam. Also it can be observed from the parametric study that; the length of CFRP plate should be extended to the supports and the CFRP plate breadth should be not less than the half of the beam breadth to get the full effect of the CFRP plate on the ultimate capacity and also to decrease the creep deflection of the CFRP-strengthened RC beams. It is also suggested to use epoxy adhesive with combined high modulus of elasticity and high glass transition temperature to resist the change in the interface behavior due to the creep of the strengthened system. Furthermore, it has been proven that the creep coefficient of concrete which estimated using code equation can be used to evaluate the creep deflection of CFRP-strengthened reinforced concrete beams.

DAS BIEGE- UND LANGZEITVERHALTEN VON CFK-VERSTÄRKTEN STAHLBETONBALKEN

Mohamed Salem

Kurzzusammenfassung

Die Instandsetzung und Verstärkung oder die Ertüchtigung bestehender Betonbauten zur Kompensierung höheren Lastannahmen (Windlasten, Erdbebenlasten und Brückenlasten) wurden in der Vergangenheit durch die traditionelle Verwendung von herkömmlichen Materialien und Bautechniken ausgeführt. Extern geklebte Stahlplatten, Stahl- oder Betonumantelung und extern vorgespannter Beton sind einige der vielen verfügbaren, traditionellen Techniken. Im Zusammenhang mit der Verstärkung der Stahlbetonkonstruktionen, haben fortschrittliche Verbundmaterialien das Potenzial für innovativen Lösungen.

Das Hauptziel dieser Abreit ist die Bewertung des Biege- und Kriechverhaltens von CFK-verstärkten Stahlbetonbalken unter normalen Bedingungen. Um dieses Ziel zu erreichen, wurden eine experimentelle und numerische Untersuchung durchgeführt. Die experimentellen Stahlbetonbalken wurden im Labor des Instituts für Bauphysik getestet. Die getesteten Proben waren zwölf einfach gelagerte Stahlbetonbalken; sechs von ihnen wurden mit externen CFK-gebundenen auf der Zugseite der Stahlbetonbalken verstärkt.

Die geprüften Balken wurden in zwei Gruppen geteilt. Der erste Teil besteht aus sechs Balken; drei Stahlbetonbalken (als Kontrollbalken) und drei CFK- verstärkte Stahlbetonbalken. Das Biegeverhalten der CFK-verstärkten Stahlbetonbalken wurde experimentell und numerisch mittels des Finite-Elemente-Programms "Abaqus" untersucht. Dazu wurde eine Parameterstudie unter Verwendung der Finite-Elemente-Modell durchgeführt.

Das experimentelle Programm und das FE-Modell zeigen, dass die Verwendung von CFK-verstärkten Stahlbetonbalken eine Verbesserung der Steifigkeit der Stahlbeton-Balken bewirkt, die Tragfähigkeit erhöht und die Rissbreite auf der Zugseite des Stahlbetonbalkens verkleinert wird. Es wird auch festgestellt, dass die Klebereigenschaften (Epoxy-Kleber) kaum Einfluss auf die Tragfähigkeit des verstärkten Systems hat.

Der zweite Teil besteht aus sechs Balken; drei Stahlbetonbalken (als Kontroll-Balken) und drei CFK-verstärkten Stahlbetonbalken. Das Kriechverhalten der CFK- verstärkten Stahlbetonbalken unter konstanten angelegten Lasten und normalen Witterungsbedingungen wurde experimentell und numerisch untersucht. Eine Parameterstudie unter Verwendung der Finite-Elemente-Modell wurde ebenfalls durchgeführt und ausgewertet.

Die experimentellen Untersuchungen und das FE-Modell zeigen, dass bei der Verwendung von CFK zur verstärktung von Stahlbetonbalken das Kriechen des CFK-verstärkten Stahlbetons, in Abhängigkeit von dem Verhältnis der CFK-Platte Länge / Breite zu Stahlbetonbalken Länge / Breite, abnimmt. Die Verwendung von CFK reduziert die anfängliche Verformung und minimiert die Rissbreite in der Zugseite der verstärkten Stahlbetonbalken. Auch kann mit der parametrischen Studie beobachtet werden, dass die Länge der CFK-Platte an der Auflager angeschlossen werden sollte (d.h. CFK mit einer Länge gleich der Stahlbetonspannweite) um die Tragfähigkeit der verstärkten Systeme zu verbessern. Auch die Breite des CFK sollte nicht weniger als die Hälfte der Stahlbalkenbreite betragen. Es wird auch empfohlen, Epoxy-Klebstoff mit einem hohem Elastizitätsmodul und hoher Glasübergangstemperatur zu verwenden, um der Veränderung des Verhaltens durch das Kriechen des gestärkten Systems zu widerstehen. Weiterhin kann die Kriechzahl aus Beton, die mit Code Gleichung abgeschätzt werden, verwendet werd, um das Kriechen der CFK-verstärkten Stahlbetonbalken auszuwerten.

Schlüsselwörter:

Stahlbetonbalken, CFK, Biegesteifigkeit verstärkt, Durchbiegung, langfristige Ablenkung, Auflast

Table of Contents

List of Figures

List of Tables

List of Symbols

Greek symbols

φ	:	strength reduction factor
β	:	factor depend on the strength of the concrete
σ	:	stress
ε	:	total elastic plus time-dependent strain
ν	:	Poisson's ratio
ψ	:	The angle of dilatancy
η	:	Benzeggagh and Kenane (BK) material parameter
ε'_s	:	compression steel reinforcement strain
$\varepsilon(t)$	:	Strain at time t.
$\beta(t_o)$	:	Factor for the effect of concrete age at loading, t_0.
ε'_o	:	stress-dependent and time-independent elastic strain
ε'_t	:	stress-dependent and time-dependent coefficient
α_1	:	Factor depends on the plastic strain, stress and temperature
η_1, η_2	:	Viscosity
ε_c	:	concrete strain
σ_c	:	applied stress
ε_{cr}	:	Creep strain
$\varepsilon_{cr}(t,t_0)$	:	the creep strain at time t
ε_{cu}	:	Ultimate compressive strain for concrete
ε_{fe}	:	FRP Effective strain
ψ_{frp}	:	reduction factor for FRP
ε_{frp}	:	FRP strain
ε_{fu}	:	FRP ultimate strain
β_H	:	coefficient depending on the relative humidity and the notional size of the
σ_n, τ_s, τ_t	:	the cohesive tensile and shear stresses of the interface
ε_o	:	Initial strain
ε_s	:	tension steel reinforcement strain

δ_u	:	Deflection at ultimate load
$\dot{\bar{\varepsilon}}_{cr}$	:	the uniaxial equivalent creep strain rate
$\tilde{\varepsilon}_t^{pl}, \tilde{\varepsilon}_C^{pl}$	:	Tension, and compression equivalent plastic strains
$\beta_c(t, t_o)$	:	Coefficient describes the progress of creep with time after loading.
$\varphi_{frp}(t)$	:	creep coefficient for FRP composite laminate

Latin symbols

A, n, m	:	Material parameters
A_1	:	Factor $= 0.85 f_c' \beta\, b$
A_2	:	factor $= \dfrac{s_0 - s_e}{s_o}$
a_a	:	air content
A_c	:	Cross-sectional area
ACI	:	American Concrete Institute
$A_{f,max}$	:	maximum cross-sectional area of FRP
$A_{f,min}$	:	minimum cross-sectional area of FRP
AFRP	:	Aramid Fiber Reinforced Polymer
A_{frp}	:	Area of FRP
a_i, b_i, a_d, b_d	:	constants depends on temperature which are fitted with the variations of the rheological model parameters
A_s	:	Area of tension steel reinforcement
A'_s	:	Area of compression steel reinforcement
ASTM	:	American Society for Testing and Materials
B	:	Factor depend on elastic and initial slip $= \dfrac{s_e}{2(s_0 - s_{e)}}$
B_1	:	constant $= (A'_s E_s + A_{frp} E_{frp}) \varepsilon_{cu} - A_s f_y$
b_c	:	Reinforced concrete beam width
b_f	:	width of the FRP plate
c_1	:	constant $= -(A'_s E_s d' + A_{frp} E_{frp} d_{frp}) \varepsilon_{cu}$
C3D8R	:	Eight-node brick element
C3D8R	:	Eight-node brick element
C_c	:	internal force in compression concrete $= \beta x b\, f'_c$

C_E	:	the environment-reduction factor for various FRP materials
CEB-FIP	:	Comité Euro-International du Béton - fédération internationale du béton
CFRP	:	Carbon Fiber Reinforced Polymer
COH3D8	:	Eight-node cohesive element
C'_s	:	internal force in compression steel reinforcement = $A'_s f'_s$
$D(t)$	:	rheological function
d_{frp}	:	depth of fiber reinforced polymer
d_s	:	depth of tension steel reinforcement
d'_s	:	depth of compression steel reinforcement
$E(T)$	:	the modulus of Elasticity at temperature T
E_c	:	concrete modulus of elasticity at 28 days
E_{frp}	:	FRP modulus of elasticity
E_s	:	modulus of elasticity of steel reinforcement
$f(K_a)$	:	function of the stiffness of the adhesive layer = 1
$f_1(\sigma)$	:	Function of stress
$f_2(t)$	:	Function of time
$f_3(T)$	:	Function of temperature
f'_c	:	Concrete compressive strength.
f_{cm}	:	the mean compressive strength of concrete
f_{co}	:	the critical strength of concrete
FE	:	Finite Element
f_{frp}	:	FRP stress
FRP	:	Fiber Reinforced Polymer
f_s	:	tension steel reinforcement stress
f'_s	:	compression steel reinforcement stress
f_t	:	Concrete tensile strength
G_a	:	interface shear modulus
G_c	:	concrete shear modulus
G_F	:	total interfacial fracture energy

G_F^a	:	fracture energy of the ascending branch
GFRP	:	Glass Fiber Reinforced Polymer
G_o, G_∞	:	the shear modulus parameters
$G_{Tc}, G_{Ic}, G_{IIc},$	:	Fracture energy
h	:	the notional size of the concrete member in mm
h_a	:	Average thickness of a member in mm
k_m	:	limit values factor for the ultimate strain
K_o	:	The initial stiffness of the bond-slip model; $K_o = \frac{1}{\frac{t_a}{G_a} + \frac{t_c}{G_c}}$
LVDT	:	linear variable differential transformer
M_n	:	nominal bending moment at failure
M_u	:	The ultimate bending moment
n	:	dimensionless material constant
N.A.	:	Neutral axis
n_{frp}	:	number of layers of FRP
P_{cr}	:	Load at first crack
P_u	:	ultimate load
$R, R_E, R_\sigma,$	:	Parameters depend on concrete properties
RC	:	Reinforced Concrete
RH	:	the relative humidity for the surrounding
s	:	slip
S_0	:	corresponding slip to local bond strength τ_{max}
S_1	:	the slump in mm
S_e	:	the elastic component of initial slip s_o; $s_e = \frac{\tau_{max}}{K_o}$
S_f	:	Slip at interface failure
t	:	thickness of reinforced concrete beam
t	:	Time
T	:	Temperature
t_o	:	Age of concrete at loading,
T3D2	:	Two-node truss element

t_a	:	the interface thickness in mm
t_c	:	the effective thickness of concrete = 5 mm
t_{frp}	:	thickness of fiber reinforced polymer (FRP)
T_{frp}	:	internal force in tension FRP = $A_{frp} f_{frp}$
T_g	:	Glass transition temperature
T_s	:	internal force in tension steel reinforcement = $A_s f_s$
u	:	Perimeter of the member in contact with the atmosphere
V/S	:	Volume to surface ratio in mm
x	:	depth of neutral axis
α	:	parameter controls the shape of the descending branch of the bond-slip curve (τ~s)
β_w	:	FRP-to-concrete width ratio
γ	:	shear strain
γ_a	:	Correction factor for air content
γ_{at}	:	Correction factor for thickness of member
γ_c	:	correction factors
γ_{la}	:	Correction factor for loading age
γ_{RH}	:	Correction factor ambient relative humidity
γ_s	:	Correction factor for slump of fresh concrete
γ_ρ	:	Correction factor for fine to total aggregate ratio
ρ_a	:	fine to total aggregate ratio
σ_{ult}	:	Ultimate stress
τ	:	Shear stress
τ_{max}	:	local bond (Shear) strength
φ_∞	:	constant = 2.35
$\varphi_\infty(t_o)$	:	Ultimate creep coefficient
$\varphi(t,t_0)$	:	the creep coefficient
φ_o	:	notional creep coefficient
φ_{RH}	:	factor of relative humidity
$\beta(f_{cm})$:	:	factor for the effect of concrete strength

Chapter 1   Introduction

1.1 General

The repair and strengthening or retrofitting of existing concrete structures to resist higher design loads (increasing in the affecting loads such as wind loads, earthquake loads, and bridges loads as a result of the continued updates of the Egyptian and international loading codes), correct deterioration-related damage, or increased ductility has traditionally been accomplished using conventional materials and construction techniques. Externally bonded steel plates, steel or concrete jackets and external post tensioning are just some of the many traditional techniques available. In the context of the strengthening of the reinforced concrete structures, advanced composite materials have the potential for leading to innovative solutions.

These advanced composites used in structures rehabilitation are being developed from fibers, polymers, metals and composites of these materials. While the concept of composites have been used in building, bridges, and several structures, the application of fiber reinforced polymer (FRP) for rehabilitation and strengthening of reinforced concrete structures is widely used. The FRP composites combine the strength of the fibers with the stability of the polymer resins. They are defined as polymer matrix, that are reinforced with fibers or other reinforcing material with a sufficient aspect ratio (length to thickness) to provide a desirable reinforcing function in one or more directions. The fiber reinforced polymer composite materials are different from traditional construction materials such as steel, aluminum and concrete because their properties depending on the direction of the fibers.

Fiber reinforced polymer systems with their high versatility (excellent strength-to-weight and stiffness-to weight ratios, high durability, corrosion resistance) can be used to rehabilitate a deteriorated structural member, strengthen a functionally obsolete structural member to resist increased loads due to changes in use of the structure, or address design or construction errors. To assess suitability of a fiber reinforced polymer system for a particular application, the condition assessment of the existing structure should be performed and the best treatment option should be then determined based on the assessment (ACI Committee 440, 2002).

Several researches had been carried out to investigate the flexural behavior of the strengthened reinforced concrete structures externally bonded with FRP. Failure capacity, deflection, durability, and creep are some of the important criteria in the design of CFRP strengthened reinforced concrete structures and must be kept within allowable limits, several control measures, such as appropriate design and construction procedures and the use of appropriate materials to provide higher beam stiffness, have been recommended by the American Concrete Institute (ACI Committee 435R , 1995). Fibre-reinforced polymer

systems that have a high resistance to creep deformation should also offer improved deflection characteristics of beams under service load, (Phillips L.N. , 1989).

Long-term performance is a much-recognized but less-addressed issue in the field of reinforced concrete (RC) structures strengthened with externally bonded carbon fibre reinforced polymer (CFRP) system. This type of structure may show increased deflections and crack widths over time and may also fall short of the safety margin against the ultimate collapse state when subjected to weathering effects in addition to sustained loading. Although concrete is proven to be well-resistant against both of them, concerns prevail as regards to the degradation in performance of externally bonded CFRP laminates over long period of exposure to weathering. The creep effect on CFRP laminates due to sustained loading would be another concern as this may accelerate the degradation due to weathering effects, (Saha & Tan, 2005).

Also the possibility to determine the creep deflection of the strengthening system using the international code equations for the concrete needs more studies.

1.2 Objective and Scope

Evaluation of flexural short- and long-term behavior of the CFRP-strengthened RC beams, especially the effect of the creep phenomenon on the behavior of the strengthened beams during the life time of the structure was set as the aim of this thesis, the following will be studied:

- The creep coefficient which can be used to estimate the deflection due to creep of the strengthening system.

- Effect of CFRP, epoxy and different load level on the creep deflection.

- Effect of temperature on the creep behavior of epoxy interface.

- Ability of using the code equation for estimating the creep coefficient of the concrete to estimate the creep deflection of CFRP-strengthened RC beams.

To achieve this objective the following can be summarized:

- Review for previous research about studying the flexural and long-term behavior of CFRP strengthened reinforced concrete structures.

- Estimating the possible influence of CFRP- strengthened material on flexural and creep response of the strengthened concrete structures.

- Conducting short-term experiments on the CFRP-strengthened RC beams under different loading conditions to attain some mechanical properties of the tested specimens that could help understand and justify their long-term performance.

- Developing finite element models simulating the performance of the studied CFRP-strengthened RC beams using some different material properties of the concrete, epoxy and CFRP attained through short-term experiments.

- Validating the finite element models by comparing its results with the experimental ones.

- Using the calibrated finite element model for parametric study to estimate the effect of applied load level, CFRP plate length and breadth ratio and epoxy interface type on the creep deflection of the CFRP-strengthened RC beams

- Using the calibrated finite element model for parametric study to evaluate the effect of temperature level on the creep strain of the epoxy interface.

- Evaluating the applicability of the FEM model and traditional equations available in international codes for calculating the creep response of CFRP- strengthened RC beams.

- Addresses recommendation and conclusions that must be taken into account when using the CFRP for strengthening RC beams for the designers.

1.3 Limitation

This study was conducted under laboratory weather condition; and the age of concrete at loading was about 9 months. It should be taken into consideration the glass transition temperature for the epoxy adhesive (it must be not less than 50 ^{o}C), also the effect of the fire not included in this study, but it must be using fire protection method if using FRP-strengthened RC beams inside buildings may be exposed to fire.

1.4 Outline of Thesis

The thesis contains six chapters covering the listed objective.

Chapter One: includes an introduction and plan of the research work, the objectives and the scope, and the content of the present study are also included.

Chapter Two: deals with the literature review of durability behavior of reinforced concrete beam strengthened by FRP composite.

Chapter Three: introduces the experimental work of this study; including the details and fabrication of the tested specimens, test setup and instrumentations, and materials used in the specimens.

Chapter Four: describes the experimental test results, exploiting the experimental results, and discussion of the results.

Chapter Five: discusses the finite element model used to simulate the experimental specimens, exploiting and validate the FE model results compared with experimental results

 Chapter Six discus the numerical results and using the FE model to study some parametric study by using different material properties.

Chapter Seven: summarizes conclusions and recommendations for the future studies.

Chapter 2   Literature Review

2.1 General

The strengthening of reinforced concrete structures using concrete/steel jackets, and/or external bonded steel plates techniques were widely in some countries. These techniques are very easy to carry out, but the most difficult with these techniques is the increase of section dimensions and the heavy weight of the materials used in strengthening. In the recent years, externally bonded fibre reinforced polymers (FRP) has becomes a popular technique for repairing, retrofitting and strengthening of existing concrete structures all over the world because of the special mechanical and physical properties of these composites (excellent strength-to-weight and stiffness-to weight ratios, high durability, and corrosion resistance). In fact, there may be several reasons for the need of strengthening and upgrading concrete structures, such as expired design life, changes in functionality; damage caused by mechanical actions and environmental effects, more stringent design requirements, original design and construction errors. However, the long-term performance of FRP-bonded beams under service loads is still a concern.

In many fibre-reinforced polymer (FRP) composite structures, both the short-term and long-term durability of the material is of importance. While the structure may not fail when subjected to stresses over a short period of time, it may be prone to failure or increased strain when subjected to stresses over an extended period of time. Even if failure does not occur, the slow deformation of the composite material may cause the structure to become less and less effective. The characterization of the long-term performance of FRP composites is especially important because of the viscoelastic behavior of the polymer matrix. FRP matrices exhibit a glass transition, T_g, a temperature above which the properties of the composite degrade significantly. Typically, it is necessary that the application temperature for the composite structure is below the glass transition in order to assure that the mechanical stiffness and creep resistance of the material is satisfactory. However, the glass transition relaxation occurs over a range of temperatures, so creep testing and predictions of long-term creep behavior at particular application temperatures are important so that the material's long-term mechanical performance can be evaluated.

2.2 Flexural strengthening reinforced concrete structures with FRP

Since 1982, externally bonded FRP sheets/strips have been successfully applied to reinforced concrete beams. Meier, et al., (1995) suggested that CFRP laminates could replace steel plates with overall cost savings emanating from the simplicity of the strengthening method because:

- FRPs do not corrode;
- FRPs are easy to handle in the construction site and can be bonded to structure without expensive scaffolding; and

- FRPs are available in long lengths, therefore no joints are necessary.

These FRP materials can be externally bonded to the tension face of concrete structures with any desirable shape via a thin layer of epoxy adhesive and thus enhance stiffness and strength of the structures to be strengthened.

Advanced composite materials offer advantages such as low weight, excellent, a range of elastic moduli, high resistance to corrosion, high strength, availability in long lengths thus avoiding the need for lapping, and good fatigue and creep characteristics. Recent studies have shown that advanced composite materials can strengthen structural elements such as columns and beams, leading to great economic benefit in repairing damaged structures (An W., et al., 1991), and (Meier & Kaiser, 1991). However, the choice of the composite and the manufacturing and application procedures must be well defined to assure that the retrofitted structural elements will consistently have the required performance.

There are a number of applications of FRP composites as the strengthening material of reinforced concrete elements. FRP composite strips can be bonded to the external tension zones of beams and slabs thus increasing the flexural strength of the element (Figure 2-1).

Figure 2-1: Reinforced concrete beams and slabs strengthened with FRPs ((Amélie Grésille, 2009)

Dat Duthinh & Monica Starnes, (2001) studied the Strengthening of Reinforced Concrete Beams with Carbon FRP experimentally; seven concrete beams reinforced internally

with steel and externally with CFRP laminate applied after the concrete had cracked were tested under four-point bending. Results show that FRP is very effective for flexural strengthening. As the amount of steel increased, the additional strength provided by the carbon decreases. Compared to a beam reinforced heavily with steel only, the beams reinforced with both steel and carbon have adequate deformation capacity, in spite of their brittle mode of failure. Clamping or wrapping of the ends of the FRP laminate combined with adhesive bonding is effective in anchoring the laminate.

Philip A. Ritchie, et al., (1991) studied the effectiveness of external strengthening using fiber reinforced plastic (FRP) plates. A series of 16 under-reinforced beams was tested. Plates of glass, carbon, and aramid fibers were bonded to the tension side of the beams using a two-part epoxy. FRP is attractive for this application due to its good tensile strength, low weight, and resistance to corrosion. An iterative analytical method was developed to predict the stiffness and maximum strength in bending of the plated beam. Increases in stiffness (over the working load range) from 17 to 99 percent and increases in strength (ultimate) from 40 to 97 percent were achieved for the beams with FRP plates. Predicted and actual load-deflection curves showed fairly good agreement, although generally the theoretical curves were stiffer. Experimental failure did not occur in the maximum moment region on many of the beams, despite attempts at end anchorage to postpone the local shear failure. The ultimate loads of the beams that did fail in the maximum region were within about 5 percent of predicted values.

M.R. Esfahani, et al., (2006) investigated the flexural behaviour of reinforced concrete beams strengthened using Carbon Fibre Reinforced Polymers (CFRP) sheets. The effect of reinforcing bar ratio ρ on the flexural strength of the strengthened beams is examined. Twelve concrete beam specimens with dimensions of 150 mm width, 200 mm height, and 2000 mm length were manufactured and tested. Beam sections with three different reinforcing ratios, ρ, were used as longitudinal tensile reinforcement in specimens. Nine specimens were strengthened in flexure by CFRP sheets. The other three specimens were considered as control specimens. The width, length and number of layers of CFRP sheets varied in different specimens. The flexural strength and stiffness of the strengthened beams increased compared to the control specimens. From the results of this study, it is concluded that the design guidelines of ACI Committee 440, (2002) and ISIS Canada, (2001) overestimate the effect of CFRP sheets in increasing the flexural strength of beams with small ρ values compared to the maximum value, ρ_{max}, specified in these two guidelines. With the increase in the ρ value in beams, the ratios of test load to the load calculated using ACI 440 and ISIS Canada increased. Therefore, the equations proposed by the two design guidelines are more appropriate for beams with large ρ values. In the strengthened specimens with the large reinforcing bar ratio, close to the maximum code value of ρ_{max}, failure occurred with adequate ductility.

Several studies have been conducted on the use of Glass or Carbon FRP as flexural strengthening reinforcement of concrete beams ((Toutanji, et al., 2006), and (Kachlakev D & McCurry DD., 2000)). The researchers showed the behavior in terms of load-deflection, load-

strain, failure patterns and structural ductility. All beams showed a considerable increase in ultimate load capacity by (40% to 200%) compared to control beams.

2.2.1   FRP types used for structures strengthening

FRP composites are formed by embedding continuous fibres in a resin matrix which binds the fibres together. Common fibres include carbon, glass, and aramid fibres while common resins are epoxy, polyester, and vinyl ester resins. The most widely used FRP composites are glass-fibre-reinforced polymer (GFRP) composites, carbon-fibre-reinforced polymer (CFRP) composites, and aramid-fibre-reinforced polymer (AFRP) composites. The mechanical properties for GFRP, CFRP, and AFRP were summarized in Table 2-1.

Table 2-1: Typical mechanical properties for GFRP, CFRP and AFRP composites
(J. G. Teng, et al., 2003)

Unidirectional advanced composite materials	Fibre content % by weight	Density kg/m^3	Longitudinal tensile modulus GPa	Tensile strength MPa
Glass fibre/polyester GFRP laminate	50-80	1600-2000	20-55	400-1800
Carbon/epoxy CFRP laminate	65-75	1600-1900	120-250	1200-2250
Aramid/epoxy AFRP laminate	60-70	1050-1250	40-125	1000-1800

In terms of structural use of FRP composites, one very important property common to all three types of FRPs is that their stress–strain behavior is linearly elastic until rupture (Figure 2-2). This has two major structural consequences. First, these materials do not possess the ductility that steels have, and their brittleness may limit the ductile behavior of RC members strengthened with FRP composites. For example, an RC beam bonded with an FRP soffit plate may fail by either FRP rupture or crushing of concrete, both of which are brittle failure modes. In such beams, failure by concrete crushing is permissible, as the FRP rupture mode is also brittle. This contrasts with normal RC beam design where steel yielding should be ensured to precede concrete crushing. Nevertheless when used to provide confinement for concrete, these materials can greatly enhance the strength and ductility of columns. The second implication of the brittle behavior of FRPs is that stress redistribution is limited. Consequently, the design of FRP strengthening measures for RC structures should not be based on existing methods for RC structures without due justification, (J. G. Teng, et al., 2003).
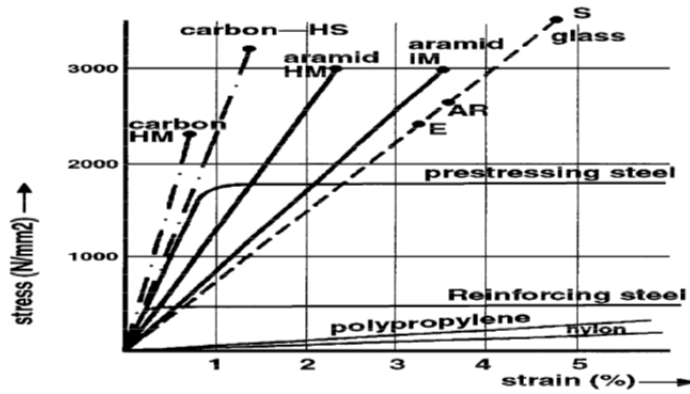
Figure 2-2: Comparison of stress-strain behavior of steel and FRPs (ACI Committee 440, 2002)

2.2.2   Failure mode of FRP strengthened RC beams

Most of the failure modes observed in the beam tests carried out by Meier, et al., (1995), Ritchie PA, et al., (1991), and Smith ST & Teng JG., (2002) are illustrated in Figure 2-3.

a) FRP rapture

e) Concrete cover separation

b) Crushing of compressive concrete

d) Interfacial debonding at plate end

c) Shear failure

f) Intermediate flexural/shear cracks induced interfacial debonding
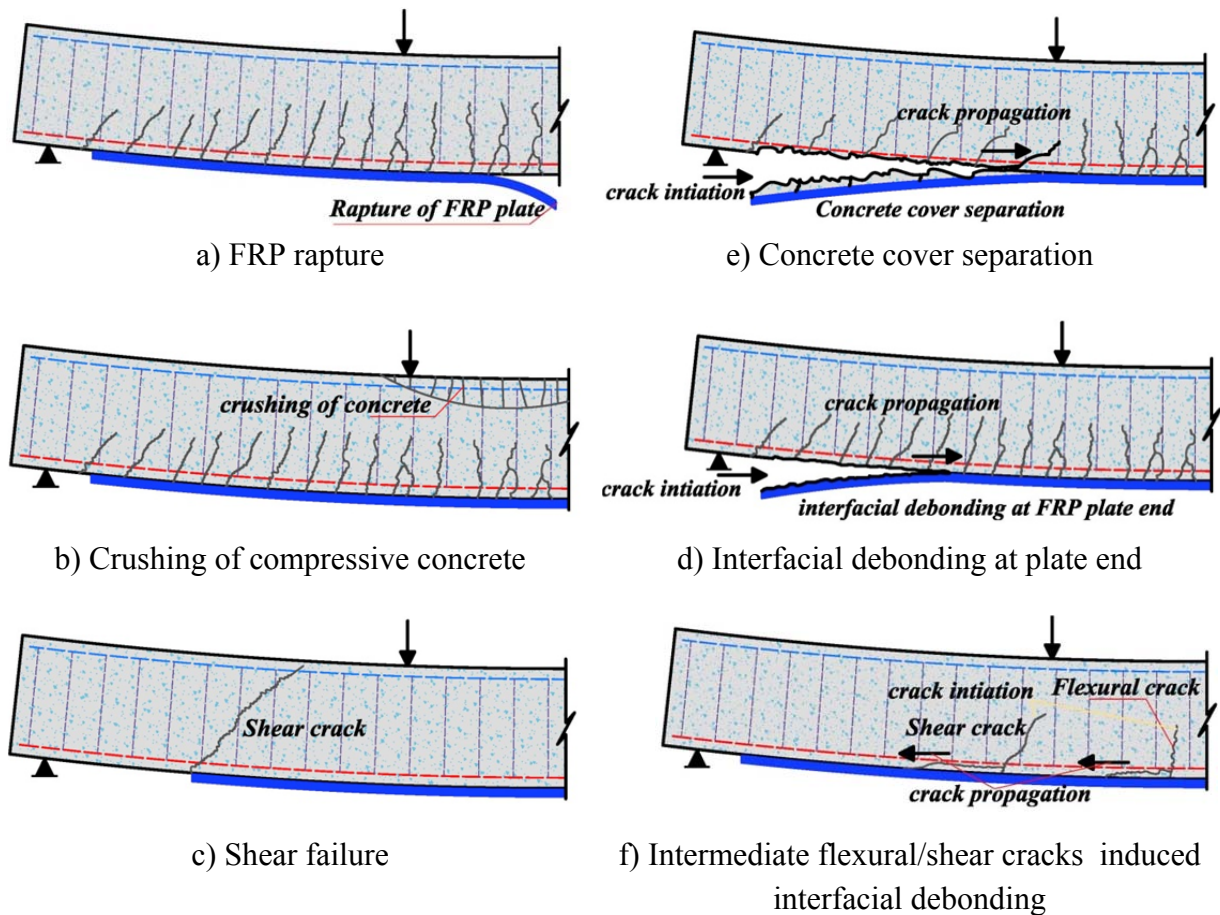
Figure 2-3: Failure modes in reinforced concrete beams strengthened with FRPs

8

Possible failure modes of FRP strengthened beams are classified into two types. The first type of failure includes the common failure modes such as concrete crushing and FRP rupture based on complete composite action.

The second type of failure is a premature failure without reaching full composite action at failure. This type of failure includes: end cover separation, end interfacial delamination, flexural crack induced debonding and shear crack induced debonding. Different failure mechanisms in experimental tests were reported by (Aram MR, et al., 2008), (Pham H & Al-Mahaidi R , 2004) and (Teng GJ, et al., 2003). Premature failures can significantly limit the enhancement property and the ultimate flexural capacity of the retrofitted beams. Several studies were conducted to identify methods of preventing premature failure with the aim of improving the load capacity and ductility of RC beams. Researchers studied the use of end anchorage techniques, such as U-straps, L-shape jackets, and steel clamps for preventing premature failure of RC beams strengthened with CFRP ((Ceroni F , 2010); and (Jumaat MZ & Alam MA , 2010)). In particular, their practical implementations for flexural strengthening are numerous ((Costa IG & Barros JAO, 2010); (Tan KH, et al., 2009); and (Wang YC & Hsu K , n.d.)). It is seen that most of the conducted experiments to validate the design methodology for FRP flexural strengthening, consisted of rectangular or T-beams on which the strengthening was applied to the positive moment region of the member.

2.2.3   Ultimate flexural capacity

The American Concrete Institute, (ACI Committee 440, 2002), proclaims that flexural behavior of strengthened systems can be analysed using the following assumptions:

- FRPs have a linear elastic stress-strain relationship up to failure;
- Strain compatibility and equilibrium;
- Maximum concrete strain of 0.003; and
- Tensile strength of concrete could be ignored.

The stress in each material is calculated based on strain compatibility, force equilibrium, and the governing failure mode. The strain in the FRP has been shown to exhibit three distinct stages of beam behavior corresponding to: uncracked section of the beam, cracked section with elastic steel, and finally the section with plastic steel ending with rupture of the FRP (Meier & Kaiser, 1991). Consequently, flexural failures are highly governed by the amount of FRP relative to the amount of the existing steel and beam dimensions

ACI Committee 440F (ACI Committee 440, 2002); used a rectangular stress block similar to that used in normal reinforced concrete beams as shown in Figure 2-4. In order to prevent debonding of the FRP laminate, a limitation should be placed on the strain level developed in the laminate.
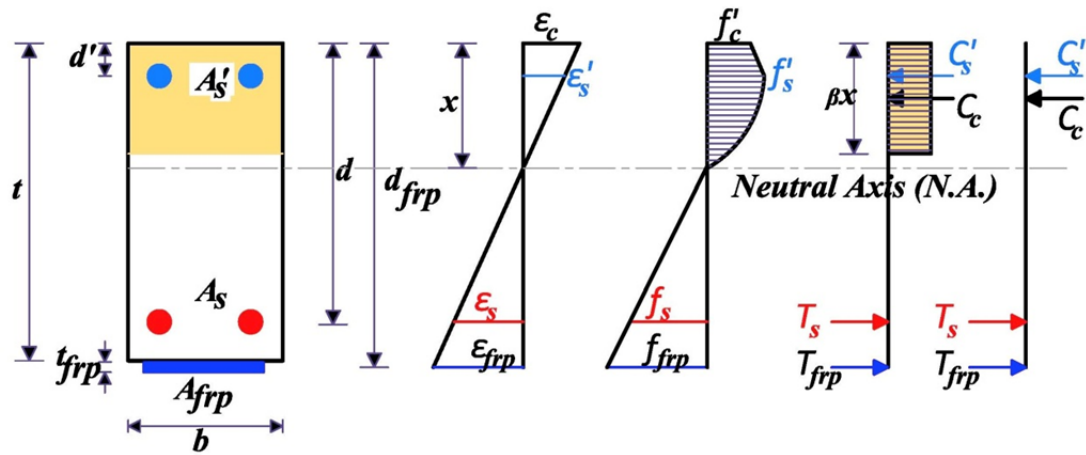
Figure 2-4: Internal strain and stress distribution for a rectangular section under flexure at ultimate stage.

ACI Committee 440F applies limit values for the ultimate strain of FRP given by the following equations:

$$\varepsilon_{fu} = C_E \cdot \varepsilon_{frp} \tag{2-1}$$

$$\varepsilon_{fe} \leq k_m \cdot \varepsilon_{fu} \tag{2-2}$$

$$k_m = \begin{cases} \dfrac{1}{60\varepsilon_{fu}}\left(1 - \dfrac{n_{frp}E_{frp}t_{frp}}{360000}\right) \leq 0.90, & n_{frp}E_{frp}t_{frp} \leq 180000 \\[4mm] \dfrac{1}{60\varepsilon_{fu}}\left(\dfrac{90000}{n_{frp}E_{frp}t_{frp}}\right) \leq 0.90, & n_{frp}E_{frp}t_{frp} > 180000 \end{cases} \tag{2-3}$$

Wher;

C_E : the environment-reduction factor for various FRP materials (C_E = 0.5-0.95)

ε_{fu} : FRP ultimate strain

E_{frp}: FRP modulus of elasticity

t_{frp}: FRP thickness

ε_{fe} : FRP Effective strain

n_{frp}: number of layers of FRP

The nominal bending moment at failure is given by:

$$M_n = f_s A_s \left(d - \frac{\beta x}{2} \right) + \psi_{frp} A_{frp} E_{frp} \varepsilon_{fe} \left(d_{frp} - \frac{\beta x}{2} \right)$$
$$+ A'_s f'_s \left(\frac{\beta x}{2} - d' \right)$$

(2-4)

Where; ψ_{frp} is a reduction factor for FRP (the recommended value of the factor $\psi_{frp} = 0.85$), and β factor depend on the strength of the concrete (β $= 0.65 - 0.85$ the most used value β$= 0.8$) . The ultimate bending moment is calculated by the following equation:

$$M_u = \varphi M_n$$

(2-5)

Based on ACI440, to provide appropriate ductility, the design bending moment is calculated provided that the tension steel strain be greater than 0.005. Therefore, a strength reduction factor given by Equation (2-6) should be used, where ε_s is the strain in the steel at the ultimate limit state.

$$\varphi = \begin{cases} 0.9, & \varepsilon_s \geq 0.005 \\ 0.7 + \frac{0.2(\varepsilon_s - \varepsilon_y)}{0.005 - \varepsilon_y}, & \varepsilon_y < \varepsilon_s < 0.005 \\ 0.7, & \varepsilon_s \leq \varepsilon_y \end{cases}$$

(2-6)

This equation sets the reduction factor at 0.90 for ductile sections and 0.70 for brittle sections where the steel does not yield, and provides a linear transition for the reduction factor between these two extremes.

In general for the RC beam, the ultimate moment of resistance of doubly reinforced concrete beam is calculated by the following equation:

$$M_n = f_y (A_s - A'_s) \left[d_s - \frac{f_y (A_s - A'_s)}{2(0.85 f'_c b)} \right] + f_y A'_s (d_s - d')$$

(2-7)

For FRP strengthened reinforced concrete beam; the minimum cross-sectional area of FRP to avoid FRP rupture failure is

$$x = d_f \frac{\varepsilon_{cu}}{\varepsilon_{cu} + \varepsilon_{fu}}$$

(2-8)

11

$$A_{f,min} = \frac{0.75(0.85\, f_c'\, b\, \beta\, x) + f_s' A_s' - f_y A_s}{f_{fu}}$$ (2-9)

The maximum cross-sectional area of FRP to preclude concrete crushing failure is

$$x = d_s \frac{\varepsilon_{cu}}{\varepsilon_{cu} + \varepsilon_y}$$ (2-10)

$$A_{f,max} = \frac{0.75(0.85\, f_c'\, b\, \beta\, x) + f_s' A_s' - f_y A_s}{f_{fu}}$$ (2-11)

At ultimate state, the tension failure will be the yielding of the steel in tension followed by concrete crushing (Figure 2-4). The ultimate moment of resistance after strengthening is

$$M_n = 0.85 f_c' \beta x\, b \left(d_f - \frac{\beta x}{2} \right) + E_s \varepsilon_s'\, A_s'\, (d_f - d') + f_y A_s (d_f - d_s)$$ (2-12)

x can solved by the following equation

$$x = \frac{-B_1 + \sqrt{B_1{}^2 - 4A_1 c_1}}{2A_1}$$ (2-13)

Where $A_1 = 0.85 f_c' \beta\, b$,

$B_1 = \left(A_s' E_s + A_{frp} E_{frp} \right) \varepsilon_{cu} - A_s f_y$

$c_1 = -(A_s' E_s d' + A_{frp} E_{frp} d_{frp}) \varepsilon_{cu}$

2.2.4 Bond between FRP and concrete

The bonding of fiber reinforced plastics (FRP) plates/sheets to the tension side of a concrete beam was found to be an effective technique for flexural FRP-strengthening structures. This bond property can be represented by the bond stress-slip relationship, the experimental and theoretical studies investigated interfacial shear bond behaviors commonly based on direct shear tests (single and double fig), various bond stress-slip relationships have been proposed (Dai el al. 2005, Nakaba et al. 2001).

The evaluated interface characteristic parameters include average shear bond strength, effective bond length, maximum shear bond stress, interfacial fracture energy, as well as the local bond stress-slip relationship

a)   double shear test   b)   single shear test
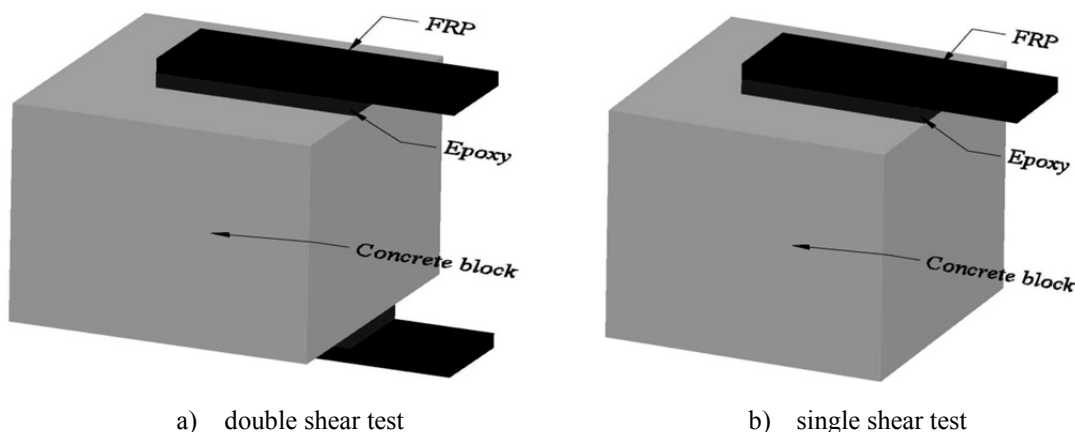
Figure 2-5: interface shear test

Debonding is often observed at discontinuities such as laminate ends and existing crack mouths within the retrofit span (Meier U, 1992) where high concentration of shear and peel stresses can be found.

For the strengthened member, failure often occurs by debonding of FRP from the concrete substrate, which can initiate from the end of the FRP plate or the mouth of a flexural or flexural/shear crack (Figure 2-3; (d), (e), and (f)). Failure initiated from the plate end is often attributed to the presence of high shear and normal stress concentrations.

The elastic stress distributions around the plate end have been derived in various studies (El-Mihilmy MT & Tedesco JW, 2001). Knowing the elastic stresses, the applied load at the occurrence of plate end debonding can be obtained with the use of concrete failure criterion under multi-axial stress (El-Mihilmy MT & Tedesco JW, 2001) and (Saadatmanesh H, & Malek AM., 1998).

Another possible location for interfacial crack to occur is the mouth of a major flexural/shear crack in the beam. Loading of a FRP strengthened RC beam will lead to the formation of flexural/shear cracks along the span. When loading is increased, the crack will tend to propagate upwards but crack opening at the bottom is resisted by the FRP plate. Elastic analysis performed by Leung (Leung C. K. Y, 2001) shows that very high interfacial shear stresses are induced at the vicinity of the crack, leading to debonding of the FRP plate (Figure 2-3(f)). From experimental observations, the debonded plate always carries with it a thin layer (a few mm; about 5 mm) of concrete, implying that the debonding is occurring at a distance from the concrete/adhesive interface. This observation can be explained as follow. Firstly, penetration of adhesive into the concrete may increase the strength of a thin layer of material right next to the interface. Secondly, high shear stresses acting along the

concrete/adhesive interface will produce micro-cracks that tend to propagate away from the interface at a certain angle (along the principal compression direction). The interaction and coalescence of these inclined cracks will produce the final debonding surface inside the concrete, (Jinlong Pan & Christopher K.Y. Leung, 2007).

Debonding can also initiate at the bottom of cracks in the concrete member, and propagate towards the end of the FRP plate. This mode of failure has been experimentally observed by Wu Z., et al., (1997), and Teng J. G., et al., (2000). Crack-induced debonding at the FRP/concrete interface is not a linear process. In tests on pre-cracked beams conducted by Hearing B. & Buyukozturk O., (2000), strain gages were put along the FRP plate right below the crack and also at its vicinity. Initially, the gage right under the crack showed a much higher strain value than the neighboring gages. As loading was increased, the strain difference between the gages became smaller and smaller. This can be explained in terms of damage along the interface, which reduces the shear transfer capability between the concrete and the FRP. With a lower shear stress along the interface, there is a smaller change in FRP strain from one point to another. This experimental observation indicates that interfacial debonding is a progressive process involving material softening along the interface, which should be taken into account in the modeling of crack-induced debonding.

Cover delamination or FRP debonding can occur if the force in the FRP cannot be sustained by the substrate. In order to prevent debonding of the FRP laminate, a limitation should be placed on the strain level developed in the laminate. Equation (2-3) gives an expression for a bond-dependent coefficient k_m (ACI Committee 440, 2002).

2.2.4.1   *Bond-slip model*

Modeling of debonding in structural members strengthened with externally bonded reinforcements with finite element model was studied due to its critical importance of debonding failures in bonded joints. The bond stress versus slip (τ~s) relationship is the very important law to describe the interface performance of FRP-strengthened RC structures.

Based on such finite element bond-slip curves and some calibration with a large test database, three bond-slip models were developed (Lu, et al., 2005)

➢ **Precise model:**

The first of the three bond-slip models is referred to as the precise model as it takes explicit account of the effect of the adhesive layer, which is important when the adhesive is much softer than those currently in common use. It has been reported that very soft adhesive layers can increase the interfacial fracture energy (Dai J G & Ueda T, 2003). The bond stress versus slip (τ~s) for precise model developed by Lu, et al.,(2005) shown in Figure 2-6
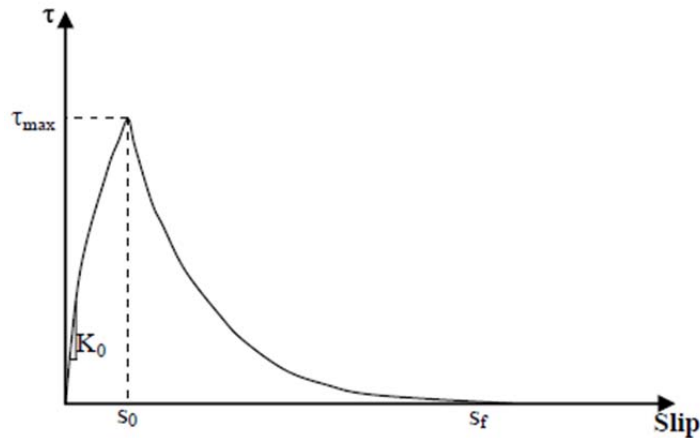
Figure 2-6: Bond-slip curve, precise model by (Lu, et al., 2005)

The precise model describes the ascending and descending branches separately using the following equations:

$$\tau = \tau_{max}\left(\sqrt{\frac{s}{s_o A_2} + B^2} - B\right) \quad \text{for } s \le s_o \tag{2-14}$$

$$\tau = \tau_{max} e^{-\propto(\frac{s}{s_o}-1)} \quad \text{for } s > s_o \tag{2-15}$$

Where

$A_2 = \frac{s_0 - s_e}{s_o}$

$B = \frac{s_e}{2(s_0 - s_e)}$

$s_e = \frac{\tau_{max}}{K_o}$, the elastic component of s_o

$K_o = \frac{1}{\frac{t_a}{G_a} + \frac{t_c}{G_c}}$; The initial stiffness of the bond-slip model Figure 2-6

t_a is the interface thickness in mm

t_c : is the effective thickness of concrete whose deformation forms part of the interfacial slip and may be taken as 5mm unless this thickness is specifically measured during the test.

G_a, G_c : are the shear modulus for interface and concrete respectively in GPa.

The local bond strength τ_{max} and the corresponding slip s_o are given by:

$$\tau_{max} = 1.5\,\beta_w f_t \tag{2-16}$$

$$s_o = 0.0195\,\beta_w f_t + s_e \tag{2-17}$$

FRP-to-concrete width ratio β_w can be expressed as

$$\beta_w = \sqrt{\frac{2.25 - \dfrac{b_f}{b_c}}{1.25 + \dfrac{b_f}{b_c}}} \tag{2-18}$$

b_c and b_f are the widths of the concrete and the FRP plate respectively.

The parameter α controls the shape of the descending branch and is given by:

$$\propto = \tau_{max}\frac{s_o}{G_F - G_F^a} \tag{2-19}$$

Where the total interfacial fracture energy can be expressed as:

$$G_F = 0.308\beta_w^2\sqrt{f_t}\,f(K_a) \tag{2-20}$$

The fracture energy of the ascending branch G_F^a can be calculated as:

$$G_F^a = \tau_{max}s_o\left(\frac{2A}{3}\left(\frac{1 + A \cdot B^2}{A}\right)^{3/2} - B - \frac{2}{3}A \cdot B^3\right) \tag{2-21}$$

Where $f(K_a)$ is a function of the stiffness of the adhesive layer. Based on finite element results, for normal adhesives with $K_a \geq 2.5$GPa/mm, the effect of adhesive layer stiffness on G_F is very small, so it is proposed that $f(K_a)=1$ for normal adhesives.

➢ **Simplified model:**

The precise model is accurate but complicated. For normal adhesives, a simplified model (Figure 2-7) without a significant loss of accuracy can be easily obtained. This is because the initial stiffness of the bond-slip curve is much larger than the secant stiffness at the peak point when a normal adhesive of a reasonable thickness is used. Therefore, the initial

stiffness can be approximated as infinity. Furthermore, the interfacial fracture energy G_F has little relationship with the stiffness of the adhesive layer. Based on these two simplifications, the following simplified bond-slip model can be obtained:
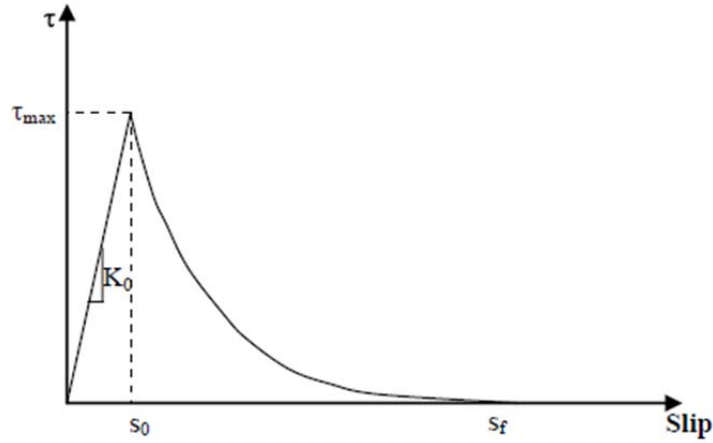
Figure 2-7: Bond-slip curve, simplified model by (Lu, et al., 2005)

$$\tau = \begin{cases} \tau_{max}\sqrt{\dfrac{s}{s_o}}, & s \leq s_o \\[3mm] \tau_{max}e^{-\alpha(\frac{s}{s_o}-1)}, & s > s_o \end{cases} \qquad (2\text{-}22)$$

Where:

$$s_o = 0.0195\,\beta_w f_t \qquad (2\text{-}23)$$

$$G_F = 0.308\beta_w^2\sqrt{f_t} \qquad (2\text{-}24)$$

$$\alpha = \dfrac{1}{\dfrac{G_F}{\tau_{max}s_o} - \dfrac{2}{3}} \qquad (2\text{-}25)$$

Where τ_{max} and β_w can be evaluated using Equation (2-16)and Equation (2-18) respectively.

> ➢ **Bilinear model:**

Further simplification was made to the simplified model, leading to a simple bilinear model (Figure 2-8) which can be used to derive an explicit design equation for the ultimate load. This bilinear model has the same local bond strength and total fracture energy, so the ultimate load remains unchanged if the bond length is longer than the effective bond length. This bilinear model is described by the following equations:
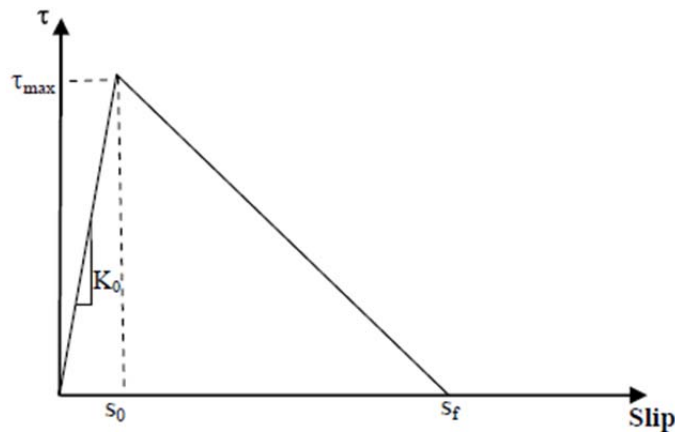
Figure 2-8: Bond-slip curve, bilinear model by (Lu, et al., 2005)

$$\tau = \begin{cases} \tau_{max} \dfrac{s}{s_o}, & s \le s_o \\ \tau_{max} \dfrac{s_f - s}{s_f - s_o}, & s_o < s \le s_f \end{cases} \qquad (2\text{-}26)$$

Where

$$s_f = \frac{2G_F}{\tau_{max}} \qquad (2\text{-}27)$$

τ_{max} , s_o, and β_w can be evaluated using Equation (2-16), Equation (2-17), and Equation (2-18) respectively.

2.2.4.2   *Anchorage effect on FRP end*

The effects of various anchor systems were investigated by Hollaway L. C. & Mays G. C., (1999) as shown in Figure 2-9. According to their research, the beams with end anchors showed greater moment capacity and deformability than un-anchored beams by delaying premature debonding failure.

a)   Bolt anchor

b)   Mechanical clamping system

c)   U-wrap anchor with GFRP
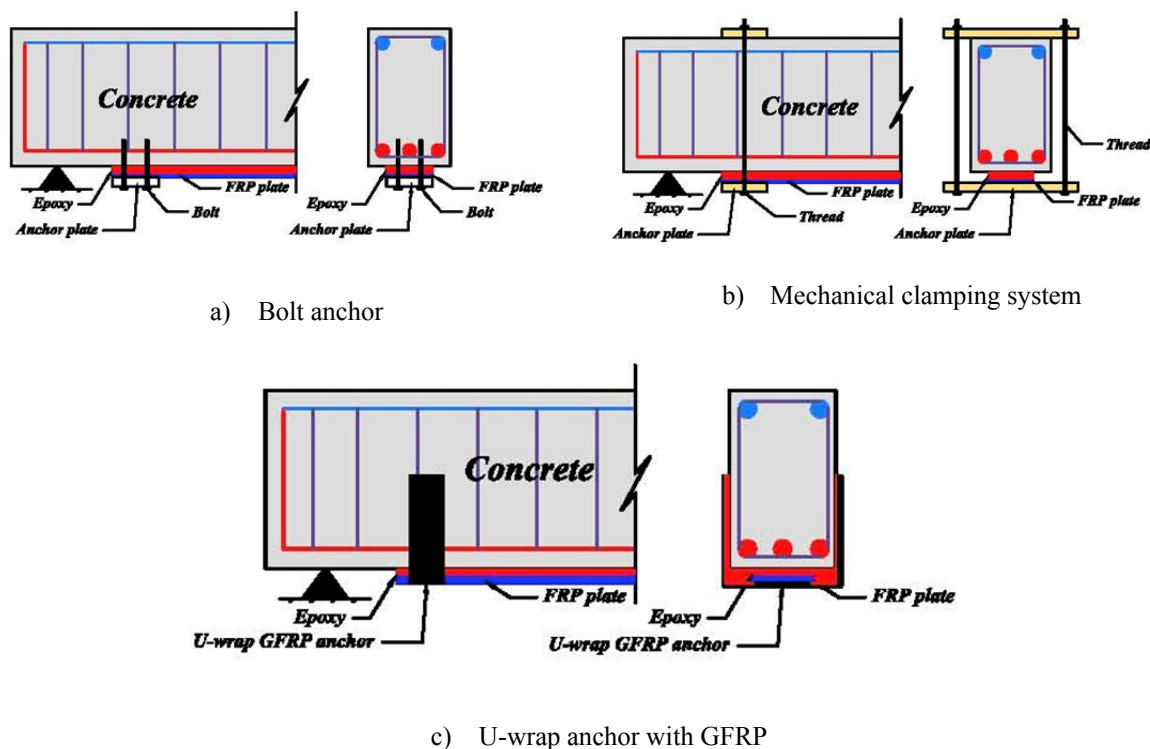
Figure 2-9: Plate end anchorage systems, (Hollaway L. C. & Mays G. C., 1999)

2.3 Durability

Durability of FRP systems is the subject of considerable ongoing research (Steckel, et al., 1999a). The engineer should select an FRP system that has undergone durability testing consistent with the application environment. Durability testing may include hot-wet cycling, alkaline immersion, freeze-thaw cycling, and ultraviolet exposure. Any FRP system that completely encases or covers a concrete section should be investigated for the effects of a variety of environmental conditions including those of freeze/thaw, steel corrosion, alkali and silica aggregate reactions, water entrapment, vapor pressures, and moisture vapor transmission ((Soudki & Green, 1997); (Christensen, et al., 1996); and (Toutanji, 1999))

Studies in the early 1990's revealed serious durability problems for glass FRP bars in alkaline environments such as in concrete. Sen, et al., (1993) placed 8 pre-tensioned beams with steel and glass FRP strands in saltwater with 15% concentration, and subjected them to wet/dry cycles simulating tidal effects in coastal areas. Half of the beams were pre-cracked at

mid-span. The beams were tested to capacity at periodic intervals and compared against unexposed control specimens.

A complete loss in the effectiveness of glass FRP strands was noticed after only 6 months in the pre-cracked beams and after 15 months in the un-cracked beams. There was no comparable loss of capacity in the specimens with steel strands. Saadatmanesh & Tannous , (1998) evaluated durability of eight types of glass FRP bars, and two types of carbon and one type of aramid FRP tendons by simulating accelerated exposure to seven different field conditions. Test results indicated long-term durability problems for glass bars, whereas carbon and aramid tendons performed well in harsh environments. Tannous & Saadatmanesh, (1999) also carried out a durability study on FRP bars made from alkali resistant glass. Test variables included temperature, matrix material (polyester and vinylester), chemical solution, and ultraviolet radiation. They also tested FRP-RC beams in flexure to examine the effect of exposure to deicing salts. Test results showed that alkali resistant glass did not improve the behavior of bars in the aggressive field conditions. While most research on strength and stiffness of FRP-RC beams has focused on their short-term behavior, there are few and limited studies on their long-term response. Hundley & Dolan, (1996) tested glass, aramid and carbon FRP tendons for their short-term characteristic creep-rupture times, i.e., the time a material will sustain the load before ultimate fracture. Tests were conducted at stress levels of 90% and 100% of the respective static strength of the tendons. Wang, et al., (1999) carried out tests on the bond creep of eight types of FRP bars. The average creep slip of FRP bars was only slightly larger than that of steel bars. Pullout tests, however, showed that bond strength of aramid bars decreased by about 15% as a result of sustained loads. Fuhr, et al., (1993) and Huston, et al., (1992) have successfully measured strains in concrete structures using fiber optic sensors. Initially, there were concerns regarding the alkali reaction with silicon in the glass fibers. However, jacketing the fibers with plastic buffers made of Kevlar has resolved the problem. Avoiding deterioration pinching and micro bending of sensors during concrete placement and compaction is still a difficult task. Maaskant, et al., (1997) installed fiber optic instrumentation in a prestressed concrete bridge in Canada.Amore promising approach is to embed the sensors in FRP bars and tendons during pultrusion. Kalamkarov, et al., (2000) subjected such tendons to sinusoidal and trapezoidal loads of 11 kN (2.5 kip) magnitude inside a temperature chamber. They showed that performance of the sensors was not affected by either the load or the ambient temperatures within the range of $-40°$ and $+60°C$.

Amir, (2002) studied the Creep and Durability of Environmentally Conditioned FRP-RC Beams Using Fiber Optic Sensors, and he found that the accelerated environmental conditioning increases creep rate of FRP bars and results in 2%–3% moisture absorption. Presence of salt in the solution does not affect creep rate of FRP-RC beams or moisture absorption of FRP bars. Effect on strength and stiffness of FRP is about3%for saline solutions and none for moisture. Environmental conditioning lowers post-cracking stiffness of the beams due to stiffness degradation of FRP and loss of bond between FRP and concrete. Fiber

optic sensors are less sensitive than foil gages to temperature effects, but must be handled properly during construction and secured carefully against harsh environments.

Chajes M. J., et al., (1994) and Ross C. A., et al., (1999) found an increase in the flexural strength and stiffness of the beams with FRP composite laminates. However, no studies have been reported on the long-term deflections of FRP-bonded RC beams.

Tan T.H. & Saha M.K., (2006) studied the long-term deflection characteristics of externally FRP-bonded beams under sustained loads. Nine reinforced concrete beams 9 (100x125 mm in cross section and 2000 mm in total length), six of which were externally bonded with glass FRP composite laminates, were subjected to sustained loads for 2 years. The test parameters were the FRP ratio and sustained load level. The long-term deflections of the beams were reduced 23 and 33% with a FRP ratio of 0.64 and 1.92%, respectively. The total beam deflections were accurately predicted by the adjusted effective modulus method, and overestimated by about 20% by the effective modulus method.

Michael J. Chajes, et al., (1995) studied the Durability of concrete beams externally reinforced with composite fabrics. The study represented the second half of a research project at the University of Delaware concerning the flexural strengthening of concrete beams using externally applied composite fabrics. Initial results showed that significant increases in flexural capacity can be achieved by epoxy-bonding composite fabrics to the tension face of reinforced concrete beams. The study deals with the environmental durability of the concrete-epoxy fabric system. The three types of fabric studied are made of aramid, E-glass and graphite fibres. To determine the durability of this type of strengthening procedure under aggressive environments, 48 small-scale reinforced-concrete beams were exposed to freeze/thaw or wet/dry cycling in a calcium chloride solution, and an additional 12 beams were left in a control environment. Of the 60 beams, 45 were reinforced with aramid, E-glass, and graphite composite fabrics (15 with each type), and 15 had no external reinforcement (unwrapped). By varying the time of exposure to the different conditions and loading the beams to failure following the environmental testing, the durability of the externally reinforced beams was assessed. The tests indicated that chloride exposure in both wet/dry and freeze/thaw environments causes degradation to the beams' strength, with the wet/dry condition being slightly more severe. Both conditions led to some deterioration of the bond between the composite fabric and the concrete. Of the three types investigated, the graphite-reinforced beams proved to be the most durable, losing less than 15% of their 140% strength increase over the unwrapped beams after 100 cycles of exposure.

Separate studies have been reported on FRP-bonded RC beams subjected to weathering ((Almusallam T. H., et al., 2001); (Leung H. Y. , et al., 2001); (Liew Y. S. & and Tan K. H. , 2003)) or sustained loading (Saha M. K. & Tan K. H., 2004). A study by (Almusallam T. H., et al., 2001) revealed that under an exposure period of twelve months, neither did the solar radiation nor the wet-dry condition cause any significant influence on the flexural strength or rigidity of the beams (150 mm x 150 mm x 1200 mm) bonded with glass FRP laminates. A

study by Leung, Balendran, and Lim (2001) on carbon FRP-bonded concrete beams (of dimensions 75 mm x 75 mm x 300 mm, without any internal reinforcement) showed improvement in the loading response when the beams were exposed to elevated temperature (during heating/cooling cycles) while water immersion for a long time (tested up to six months) gave rise to reduction in flexural capacity.

Liew Y. S. & and Tan K. H. , (2003) studied the accelerated weathering effects of tropical climate on RC beams (100 mm x 100 mm x 700 mm) bonded with glass FRP laminates. They concluded that the glass FRP-strengthened beams showed the same failure mode when protected from weathering effects while short-term (less than one month) outdoor weathering enhances the flexural behavior. They also concluded that periods of six to nine months exposure resulted in the change in failure mode with a marginal drop of 2% in flexural capacity whereas weathering for more than six years reduced the flexural strength by 15% due to deterioration of bond between FRP and concrete.

Saha & Tan, (2005) carried out a study on glass FRP-bonded RC beams subjected to sustained loading under tropical weathering is reported. Beams were observed for long-term deflections and cracking due to sustained loading over different periods of time, after which they were unloaded and subsequently tested to failure. Beams subjected to outdoor tropical weathering for six months showed 8% larger deflections and 15% larger crack widths compared to those kept under ambient laboratory condition. Under accelerated weathering in a chamber, similar increase in deflections and crack widths were observed. Also, after six months of accelerated weathering, the ultimate flexural strength was about 17% and 12% less for beams bonded with uni- and bi-directional glass FRP laminates, respectively, compared to the un-weathered reference beams. The failure mode changed from concrete crushing to FRP rupture with weathering period, indicating the deterioration of FRP laminates. The effect of weathering was more detrimental in the presence of sustained loads.

Based on experimental evaluations of externally strengthened RC beams, David E. & Neuner J. D, (2001) and Karbhari V. M. & Engineer M., (1996) concluded that long-term exposure to humidity may cause a significant decrease in their load-carrying capacity. The study of Karbhari V. M. & Engineer M., (1996) also revealed that, depending on the compatibility of the fibers and the resin, even short-term exposure of CFRP to humidity may significantly degrade the beam strengthening system. Similarly, Juska T., et al., (2000) analyzed data related to thermal exposure and freezing and thawing and concluded that elevated temperature and freezing-and-thawing cycles have significant detrimental effects on FRP composite systems. Benmokrane B., et al., (2000) studied the effects of an alkaline solution on FRP composites and confirmed that an alkaline environment may cause degradation of both the stiffness and strength of various FRP composites.

Nabil F. Grace, (2004) concluded that The load-carrying capacity of beams strengthened with CFRP plates or fabrics is reduced after long-term exposure to 100% humidity, dry heat, freezing and thawing, and thermal expansion environmental conditions.

The most significant reduction (33%) in the ultimate load of strengthened beams is due to long-term exposure to 100% humidity. The onset of delamination was the primary mode of failure of strengthened beams with and without exposure to environmental conditions and repeated loads. (Evaluating the durability of externally bonded carbon fiber-reinforced polymer plates and fabric exposed to the environment)

The decision maker requires information on lifecycle performance of the structure and durability as well as underpinning social and economic factors to make an informed decision.

Liew, (2003) studied the accelerated weathering effect of tropical climate on RC beams strengthened with GFRP laminates, and concluded that a weathering period of 6–9 months resulted in the change in failure mode with a marginal drop of 2% in flexural capacity whereas weathering for more than 6 years reduced the flexural strength by 15% due to deterioration of bond between FRP laminate and concrete.

2.4 Creep

Creep may be defined as an increase of the strain with time (time-dependent deformation), when constant stress is applied to this material. It occurs as a result of long term exposure to high levels of stress that are below the yield strength of the material. Creep is more severe in materials that are subjected to heat for long periods, and near melting point. Creep always increases with temperature. The rate of this deformation is a function of the material properties, exposure time, exposure temperature and the applied structural load.

Relaxation is the time-dependent decrease of stress under the condition of constant deformation and temperature. For many structural materials, both the creep and the relaxation can be observed above a certain critical temperature.

In general when a specimen form plastic material is subjected to constant load and temperature, it deforms continuously (as shown in Figure 2-11). The initial strain is roughly predicted by its stress-strain modulus. Three stages can be considered in a typical creep curve: the first stage (primary or reduced creep), the second stage (secondary or stationary creep) and the third stage (tertiary or accelerated creep). During the primary creep stage the creep rate decreases to a certain value (minimum creep rate). The secondary stage is characterized by the approximately constant creep rate. During the tertiary stage the strain rate increases. At the end of the tertiary stage creep rupture of the specimen occurs, (Naumenko & Altenbach, 2007).
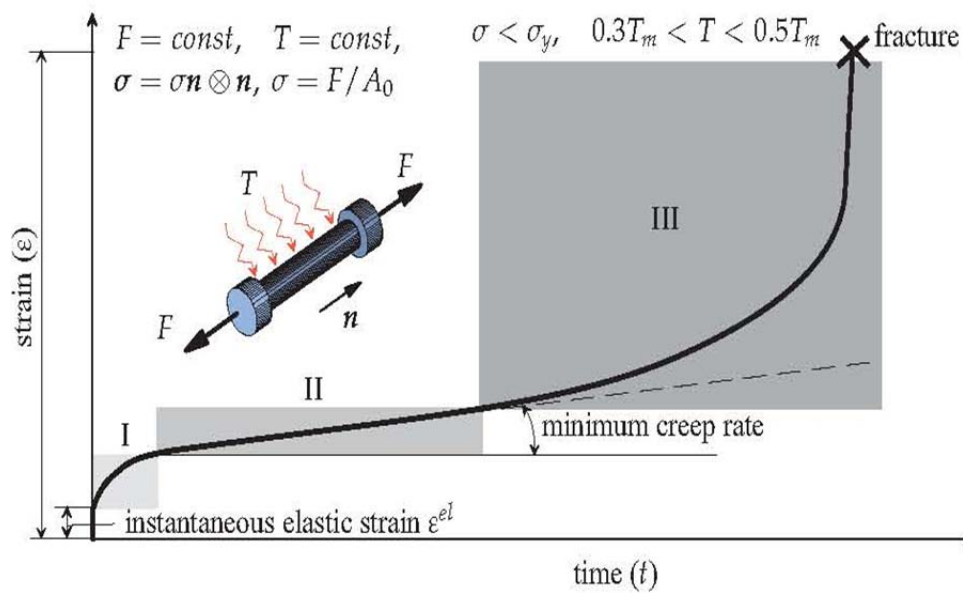
Figure 2-10: Strain vs. time curve under constant load F and temperature T. I - primary creep, II - secondary creep, III - tertiary creep (Naumenko and Altenbach 2007).

The shape of the creep curve and the duration of the creep stages depend strongly on the stress and temperature values, Figure 2-11. The dependencies on stress and temperature are of primary interest to an engineer designing some structure or machine.
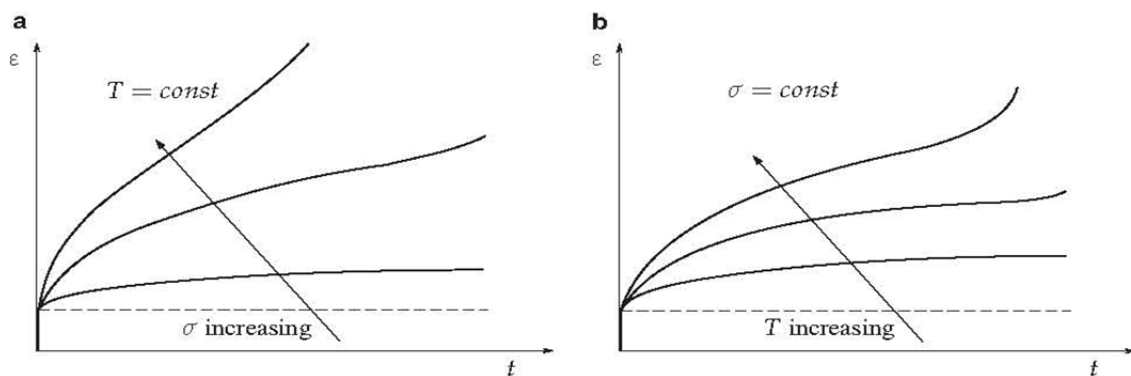
Figure 2-11: Influence of stress and temperature on the creep behavior. a. Stress dependence,

b. temperature dependence (Naumenko and Altenbach 2007)

2.4.1   Creep Model Equations

The creep deformation under constant load depends on three parameters: stress σ, time t, and temperature T, therefore the most general creep equation is

$$\varepsilon_{cr} = f(\sigma, t, T) \tag{2-28}$$

This equation can be written as follow:

$$\varepsilon_{cr} = f_1(\sigma)f_2(t)f_3(T) \tag{2-29}$$

The response of the specimen loaded by σ_0 at time t = 0 can be divided into an elastic and a plastic part as

$$\varepsilon_0 = \frac{\sigma_0}{E(T)} + \varepsilon_p(\sigma_0, T) \tag{2-30}$$

Where E(T) is the modulus of Elasticity at temperature T. The creep strain in Figure 2-10 can then be expressed according to

$$\varepsilon_{cr} = \varepsilon(t) - \varepsilon_0 \alpha_1 t^k \tag{2-31}$$

Where:

α_1 depends on the plastic strain, stress and temperature.

$\kappa < 1$ in the primary, $\kappa = 1$ in the secondary, and $\kappa > 1$ in the tertiary creep stage. These terms correspond to a decreasing, constant, and increasing strain rate, respectively, and were introduced by Andrade, (1910). These three creep stages are often called transient creep, steady creep, and accelerating creep; respectively.

A wide range of creep model equations are in use today to represent the time-dependent deformation behavior of engineering materials. Many of these comprise components originating from a small number of classical representations of primary, secondary, and/or tertiary creep deformation. The multi-cast creep data assessment inter-comparisons involved the application of 10 models by 10 different analysts.

The creep strain (2-31) can be described by the simple formula

$$\varepsilon_{cr} = A\sigma^n t^m \tag{2-32}$$

Where the parameters *A, n, and m* depend on the temperature. They can be determined in a uniaxial creep test.

If the stress σ in (4.3) is assumed to be constant the creep rate $d \approx \dot{\varepsilon}_{cr}$ is given by

$$\varepsilon_{cr} = Am\sigma^n t^{m-1} \tag{2-33}$$

The strain rate equation (2-33) contains stress and time as variables and is therefore called the time-hardening-law.

2.4.2 Creep of concrete

Creep may be defined as an increase in strain with time due to sustained loading. Shrinkage, on the other hand, is load-independent and occurs as the concrete reduces in volume with time. In plain concrete, there would be a uniform reduction in concrete volume. But in the case of reinforced concrete, the reinforcement bars will inhibit the shrinkage in concrete volume and therefore cause curvature to occur (Fling 1974; Salmon et al. 1974). Major factors affecting the rate and ultimate values of creep and shrinkage of concrete include compressive strength, stress level at which the concrete is subjected to, environmental conditions during curing and during the life of the structure, age at loading, and mix proportions (Paulson et al. 1989).

Many theoretical models which aim to predict the time-dependent behaviour of concrete are available ((Bazant Z.P., 1988); (Gilbert R.I., 1988); and (Kak Tien Chong, et al., 2008)). The creep strain in the normal direction (tension or compression) can be calculated based on the recommendations of ((CEB-FIP Model Code, 1990), (ACI Committee-209R-92, 1997), and (ACI Committee 318, 1999)) which have been widely investigated

2.4.2.1 CEB-FIP Model Code, 1990

The creep strain can be predicted by the following equation:

$$\varepsilon_{cr}(t, t_o) = \frac{\sigma_c}{E_c} \cdot \varphi(t, t_o) \tag{2-34}$$

Where;

$\varepsilon_{cr}(t, t_o)$: is the creep strain at time t

σ_c : is the applied stress

$\varphi(t, t_0)$: is the creep coefficient

E_c : is the concrete modulus of elasticity at 28 days.

The creep coefficient, $\varphi(t, t_0)$, is usually used to describe the magnitude of the creep deformations. It is defined as the total deformation (including creep) divided by the instantaneous deformation

The creep coefficient $\varphi(t, t_0)$ can be calculated from the following expression:

$$\varphi(t, t_o) = \varphi_o \beta_c(t, t_o) \tag{2-35}$$

Where

φ_o : is the notional creep coefficient

$\beta_c(t, t_o)$: is a coefficient that describes the progress of creep with time after loading.

The notational creep coefficient can be estimated as follows:

$$\varphi_o = \varphi_{RH} \cdot \beta(f_{cm}) \cdot \beta(t_o) \qquad (2\text{-}36)$$

Where

φ_{RH} : is a factor that takes the relative humidity into account,

$\beta(f_{cm})$: is a factor for the effect of concrete strength, and

$\beta(t_o)$: is a factor for the effect of concrete age at loading, t_o.

The factor φ_{RH} is calculated with the following equation:

$$\varphi_{RH} = 1 + \frac{1 - RH/100}{0.46(\frac{h}{100})^{1/3}} \qquad (2\text{-}37)$$

where

RH : is the relative humidity for the surrounding, expressed in percentage and

h : is the notional size of the concrete member in mm, calculated as:

$$h = \frac{2A_c}{u} \qquad (2\text{-}38)$$

Where

A_c: Cross-sectional area (in mm^2)

u : Perimeter of the member in contact with the atmosphere (in mm)

The factor $\beta(f_{cm})$ is calculated with the following expression:

$$\beta(f_{cm}) = \frac{5.3}{\sqrt{f_{cm}/10}} \qquad (2\text{-}39)$$

Where

f_{cm} : is the mean compressive strength of concrete, in MPa at the age of 28 days

The factor $\beta(t_o)$ is calculated from the following equation:

$$\beta(t_o) = \frac{1}{0.1 + t_o^{0.2}} \qquad (2\text{-}40)$$

The coefficient $\beta_c(t, t_o)$ can be calculated using the following expression:

$$\beta_c(t, t_o) = \left[\frac{(t - t_o)/t_1}{\beta_H + (t - t_o)/t_1} \right]^{0.3} \qquad (2\text{-}41)$$

$$\beta_H = 150\left[1 + \left(1.2\frac{RH}{100}\right)^{18}\right] \cdot \frac{h}{100} + 250 \leq 1500 \tag{2-42}$$

Where

t: is the age of concrete in days at the moment considered,

t_0 : is the age of concrete in days when loaded

t_1 = 1 day

β_H: is a coefficient depending on the relative humidity and the notional size of the concrete member

2.4.2.2   *ACI 209R-92*

The creep coefficient is estimated as follows:

$$\varphi(t,t_o) = \varphi_\infty(t_o) \cdot \frac{(t - t_o)^{0.6}}{10 + (t - t_o)^{0.6}} \tag{2-43}$$

Where

$\varphi(t,t_o)$: Creep coefficient at time t

$\varphi_\infty(t_o)$: Ultimate creep coefficient

t_o : Time of loading

The ultimate creep coefficient can be expressed as:

$$\varphi_\infty(t_o) = \gamma_c \cdot \varphi_\infty \tag{2-44}$$

The constant φ_∞ = 2.35 is recommended. The correction factors γ_c consist of the following terms:

$$\gamma_c = \gamma_{la} \cdot \gamma_{RH} \cdot \gamma_{at} \cdot \gamma_s \cdot \gamma_\rho \cdot \gamma_a \tag{2-45}$$

Where

γ_{la} : Correction factor for loading age. For loading ages later than 7 days and moist cured concrete, γ_{la} = 1.25 x to-0.118, for loading ages later than 1-3 days and γ_{la} = 1.13 x to-0.094

γ_{RH} : Correction factor ambient relative humidity. For ambient relative humidity greater than 40%, γ_{RH} = 1.27 − 0.0067 RH; (RH is the ambient relative humidity in %)

γ_{at} : Correction factor for thickness of member. When the average thickness or volume to surface ratio of a structural member differs from 150 mm or 38 mm, respectively, two methods are offered for estimating the factor of member size γ_{at}:

➢ **average-thickness method**

For an average thickness of a member smaller than 150 mm, the factors are given by ACI-209 Report. For an average thickness of a member larger than 150 mm and up to about 300 to 380 mm, the correction factor for thickness is given as:

$\gamma_{at} = 1.14 - 0.00092\, h_a$ during the first year after loading

$\gamma_{at} = 1.10 - 0.00067\, h_a$ for ultimate values

Where

h_a = Average thickness of a member in mm.

➢ **volume-surface ratio method**

$$\gamma_{at} = \frac{2}{3} \cdot \left[1 + 1.13 e^{-0.0213\left(\frac{v}{s}\right)}\right]$$

Where

$\frac{v}{s}$: Volume to surface ratio in mm

γ_s : Correction factor for slump of fresh concrete;

$\gamma_s = 0.82 + 0.00264\, S_1$

S_1 : is the slump in mm.

γ_ρ : Correction factor for fine to total aggregate ratio.

$\gamma_\rho = 0.88 + 0.0024\, \rho_a$

ρ_a : is fine to total aggregate ratio

γ_a : Correction factor for air content. $\gamma_a = 0.46 + 0.09 a_a$

a_a is air content.

2.4.3 Creep of epoxy

Epoxy-based structural adhesives have emerged as a critical component for assembling structural parts due to their high strength-to-weight ratio, excellent adhesion properties, and superior thermal stability (Kinloch , 1987). A structural adhesive can be defined as a load-bearing material with high modulus and strength that can transmit stress without loss of

structural integrity. Compared with other joining methods, such as welding or bolting, epoxy-based structural adhesives provide exceptional advantages, including distributing stresses equally over a large area while minimizing stress concentrations, joining dissimilar materials, and reducing the overall weight and manufacturing costs. However, epoxy resins, being viscoelastic in nature, exhibit unique time-dependent behavior. This leads to a great concern in assessing their long-term load-bearing performance, mainly because of a lack in fundamental knowledge of the viscoelastic behavior of epoxy-based structural adhesives. There is also a general concern regarding the lack of a long-term performance database for epoxy structural adhesives and the lack of a theory/ model that can reliably predict the creep behavior of epoxy adhesives. Significant work is still required to develop accurate models for the prediction of the long-term behavior of epoxy adhesives, especially under different testing conditions.

Maksimov R.D. & Plume R., (2001) investigated the long-term creep of EDT-10 epoxy resin specimens under tension for 5.7 years. The experimental results showed that the EDT-10 epoxy resin exhibits considerable creep—the total strains, after the action of constant stresses over 5.7 years, exceed the instantaneous ones by 4.3 to 4.7 times (fig). In this case, in the stress and time intervals examined, the creep of resin is of a damping character, i.e., the deformation rate decreases in time.
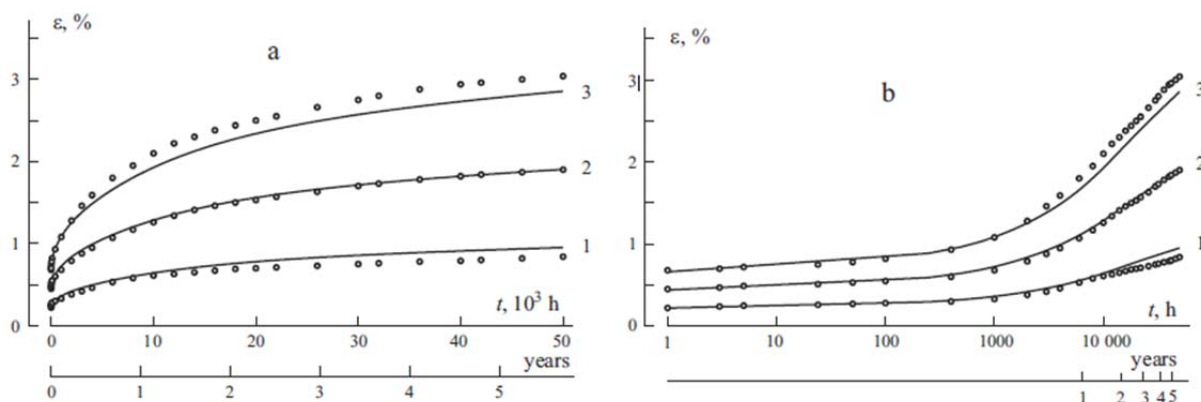
Figure 2-12: Creep curves ε(t) (a) and ε(log t) (b) for an EDT-10 epoxy resin at different stress levels: 6.8 (1), 13.6 (2), and 20.4 MPa (3). Dots are experimental data and lines are approximations; used by (Maksimov R.D. & Plume R., 2001)

Miguel Miravalles & IIP Dharmawan, (2007) studied the experimental and numerical creep behavior of adhesive for epoxy specimens (dogbone shape, they were 225 mm long and had a thickness of 2 mm; Figure 2-13) under tension. The results showed that at high stress values (approx 80% of σ_{ult}) under constant loads, the behaviour of structural adhesives changes significantly and failure is reached very quickly; and the FE model with abaqus presented good agreement with the experimental test, as shown in Figure 2-14.

30

a)   specimens   b)   test setup

Figure 2-13: adhesive creep test used by (Miguel Miravalles & IIP Dharmawan, 2007)
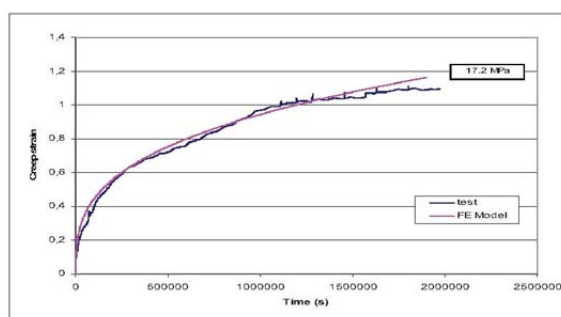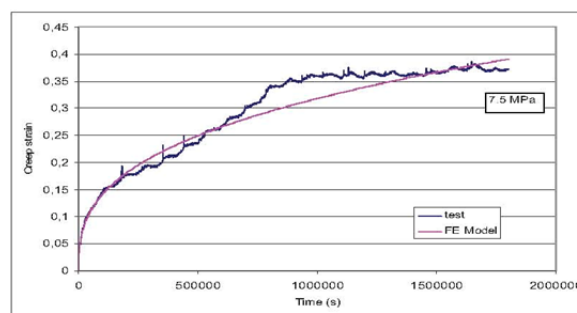
a)   Epoxy A   b)   Epoxy B

Figure 2-14: Comparison of the experimental results and the FE Model by (Miguel Miravalles & IIP Dharmawan, 2007)

C. Mazzotti & M. Savoia, (2005) investigated the long-term behavior of bond between concrete and FRP plates. Three different bonded lengths (from 100 mm to 400 mm) have been adopted. Seven to eleven strain gauges (depending on bonded lengths) along FRP plates have been used to measure longitudinal strains. A mechanical system able to apply a traction force constant in time to the extremity of plates has been designed. In order to eliminate strain thermal drift, long-term tests have been carried out in climatic room with standard ambient conditions; fig . Strains have been measured during time by using an automatic control system. Strain profile evolutions with time along the bonded length have been recorded. At the moment, time duration of tests is about 6 months.

It is shown that a significant redistribution of shear stresses along the anchorage occurs due to creep deformations at the interface level. A set of short-term delamination tests on identical specimens has also been performed and considered as reference tests. At the end of tests (loading time about 1 year), specimens subject to long – term loading will be loaded up to failure in identical conditions as reference specimens, in order to estimate if a long – term loading reduces bond strength of FRP anchorage.
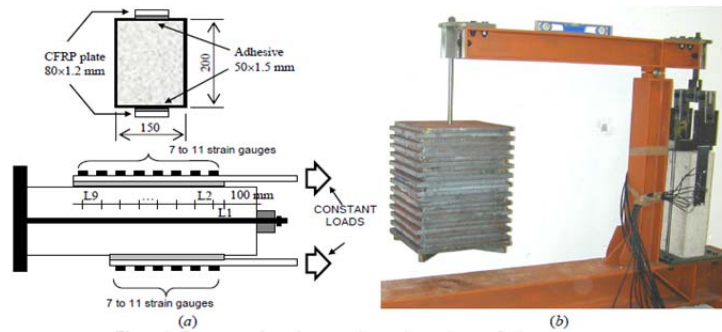
Figure 2-15: Geometry of specimens and experimental setup for long – term tests used by (C. Mazzotti & M. Savoia, 2005)

Pania Meshgin, et al., (2009) investigated the experimental and analytical long-term behavior of epoxy at the interface between the concrete and the fiber-reinforced-polymer (FRP). Double shear experiments under sustained service load were performed on nine specimens composed of two concrete blocks connected by FRP sheets bonded to concrete using epoxy. The primary investigation parameters included the ratio of shear stress to ultimate shear strength, the epoxy thickness and the epoxy time-before-loading. Loading was sustained for periods up to nine months.

It showed that the magnitude of shear stress to ultimate shear strength and the epoxy time before loading could be the most critical parameters affecting creep of epoxy at the concrete–FRP interfaces. It was also found that the creep of epoxy can result in failure at the interfaces due to the combined effect of relatively high shear stress to ultimate shear strength and thick epoxy adhesive. This can have an adverse effect on the designed performance of reinforced concrete (RC) structures strengthened with FRP. Based on the experimental observations, rheological models were developed to simulate the long-term behavior of epoxy at the concrete–FRP interfaces. It is shown that the long-term behavior of epoxy at the interfaces can be properly modelled by analytically for both loading and unloading stages

E. Ferrier , et al., (2011) studied the creep behavior of the concrete-composite interface using the double-lap shear test (Figure 2-16). Four types of epoxy (Table 2-2) with glass transition temperatures ranging from 45 to 80 ^{o}C were used for the FRP/concrete interface; the bonded joints were subjected to thermo-stimulated experiments to assess their creep behavior as a function of time and temperature under shear loading 40% of the ultimate bond strength.
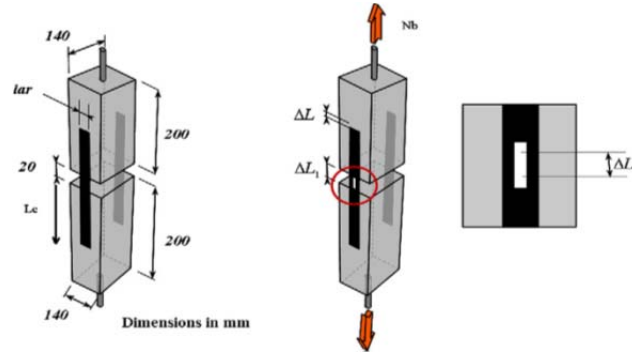
Figure 2-16: Double-lap shear test principle used by (E. Ferrier , et al., 2011)

Table 2-2: material characteristics for epoxy interface used by (E. Ferrier , et al., 2011)

Material	Epoxy A	Epoxy B	Epoxy C	Epoxy D
Young modulus (GPa)	3200	3200	3200	12000
Glass transition temperature T (^{o}C)	46	55	80	55

The results showed that the shear modulus decreased with 20% for high modulus epoxy and 70% for low modulus epoxy due to creep dependence; and the creep strain increased due to temperature for the epoxy with low glass transition temperature less than 50 ^{o}C ; this increase was three times the epoxy with glass transition temperature more than 50 ^{o}C .

A rheological model based on Kelvin–Voight elements connected in series for simulated the creep epoxy polymer used by E. Ferrier , et al., (2011); as shown in Figure 2-17, the adhesive shear strain (γ) could be determined as a function of time (t) temperature T, average shear stress (τ_0) and rheological function D(t) from equation (2-46) :

$$
\begin{aligned}
\gamma(t) = \ & \tau_o \cdot D(t) \\
= \ & \tau_o \\
& \cdot \left[\frac{2}{G_o} + \frac{G_o - G_\infty}{G_o \cdot G_\infty} \cdot e^{\frac{-t(G_o \cdot (G_\infty - G_o))}{\eta_1 \cdot G_\infty}} + \frac{G_o - G_\infty}{G_o \cdot G_\infty} \right. \\
& \left. \cdot e^{\frac{-t(G_o \cdot (G_\infty - G_o))}{\eta_2 \cdot G_\infty}} \right]
\end{aligned}
\tag{2-46}
$$

Where; η_1, η_2 were considered equal for each temperature, based on the fitting of experimental results.

G_o, and G_∞, are the shear modulus parameters can be calculated from the curve fitting shown in Figure 2-18.

$G_o = a_i + b_i \, T$, $G_\infty = a_d + b_d \, T$, Parameters a_i, b_i, a_d, b_d are constants which are fitted with the variations of the rheological model parameters.
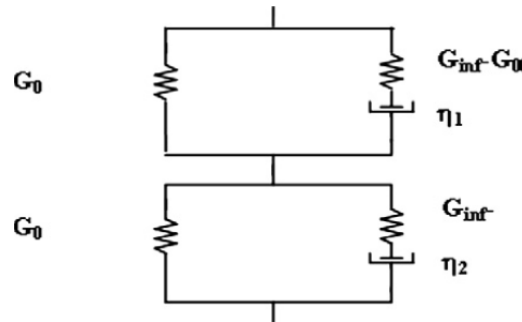
Figure 2-17: Rheological model by (E. Ferrier , et al., 2011)
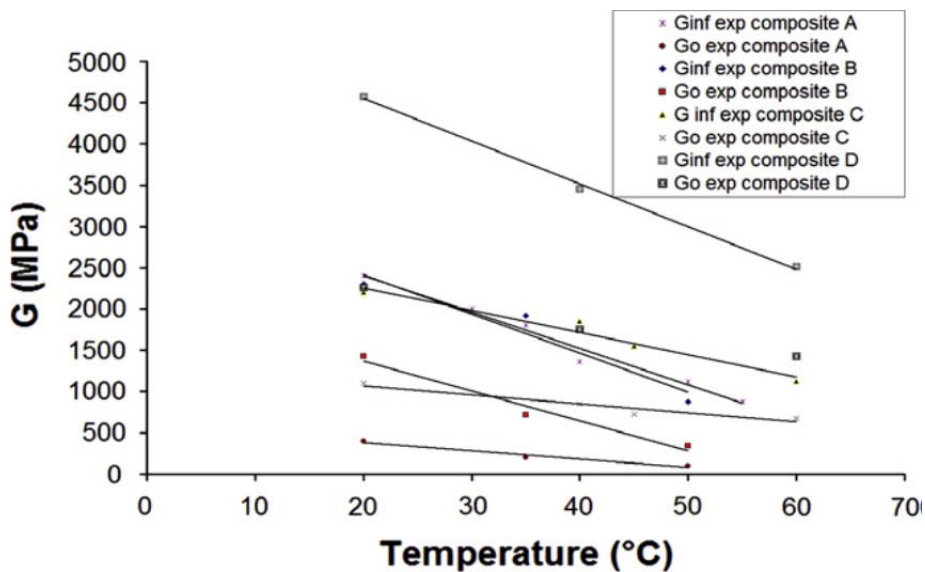
Figure 2-18: Evolution of the rheological parameters with the test temperature by (E. Ferrier , et al., 2011)

2.4.4   Creep of FRP

Many of the fibres (Glass, and Carbon) used for civil engineering applications are linear elastic, but the overall behavior of the laminate may exhibit some level of viscoelasticity due to the matrix. While, Aramid fibres exhibit significant creep which together with the creep of the matrix and the adhesive, may radically affect the efficiency of the strengthening system over time. Fibres are also characterized by a phenomenon called creep or stress rupture, for

which the strength of the material significantly decreases over time, especially for Glass and Aramid fibres. For this, the existing codes and design guidelines for structural strengthening introduce limits on the stress and strain of the FRP in the serviceability limit state (ACI Committee 440, 2002). In this study the creep rupture effects are out of the scope, and the behavior of the FRP is assumed linear viscoelastic, a perfect bonding is assumed between the fibres and the matrix, and the stresses arising from the differences in Poisson's ratios are assumed to be negligible (Maksimov R.D. & Plume R., 2001). For simplicity it is assumed that the mechanical properties of each constituent do not change, (Lee S.M, 1989)

Findley W. N. , (1960) suggested a simple power law relationship based on a linear viscoelastic approach that simulates creep of FRP laminates under sustained loads as

$$\varepsilon = \varepsilon'_o + \varepsilon'_t t^n \tag{2-47}$$

Where;

ε : total elastic plus time-dependent strain;

ε'_o : stress-dependent and time-independent elastic strain;

ε'_t : stress-dependent and time-dependent coefficient

n: dimensionless material constant, which is independent of stress magnitude

t : time after loading in hours.

In the other hand, the creep effects of FRP composite laminates can be considered using an effective modulus of elasticity for FRP similar to that of concrete using ACI approach (ACI Committee-209R-92, 1997); as follow:

$$E_{frp}(t) = \frac{E_{frp}}{1 + \varphi_{frp}(t)} \tag{2-48}$$

The creep coefficient for FRP composite laminate, $\varphi_{frp}(t)$, is defined as the increment in FRP strain with time divided by the instantaneous strain, that is

$$\varphi_{frp}(t) = \frac{\varepsilon_{frp}(t) - \varepsilon_{frp}(t_o)}{\varepsilon_{frp}(t_o)} \tag{2-49}$$

The increment in FRP strain is most obvious in the bidirectional form of reinforcement, whereas it is the least in case of unidirectional FRP. However, the value of $\varphi_{frp}(t)$ can be derived from the following relationship for a given stress level (Holmes M. & Just D. J, 1983).

$$\varepsilon_{frp}(t) = \varepsilon_{frp}(t_o) \left(\frac{t}{t_0}\right)^m \tag{2-50}$$

Where

t:time in hours after application of loading;

t_0=1 hour;

m: slope of the best-fit line relating $log\ \varepsilon_{frp}(t)$ and $log(\frac{t}{t_0})$.

The value of $\varphi_{frp}(t)$ can be expressed as the following equation:

$$\varphi_{frp}(t) = \left(\frac{t}{t_0}\right)^{m} - 1 \tag{2-51}$$

In many fiber-reinforced polymer (FRP) composite structures, both the short-term and long-term durability of the material is of importance. While the structure may not fail when subjected to stresses over a short period of time, it may be prone to failure or increased strain when subjected to stresses over an extended period of time. Even if failure does not occur, the slow deformation of the composite material may cause the structure to become less and less effective. The characterization of the long-term performance of FRP composites is especially important because of the viscoelastic behavior of the polymer matrix. FRP matrices exhibit a glass transition, T_g, a temperature above which the properties of the composite degrade significantly. Typically, it is necessary that the application temperature for the composite structure is below the glass transition in order to assure that the mechanical stiffness and creep resistance of the material is satisfactory. However, the glass transition relaxation occurs over a range of temperatures, so creep testing and predictions of long-term creep behavior at particular application temperatures are important so that the material's long-term mechanical performance can be evaluated.

W.K. Goertzen & M.R. Kessler, (2006) investigated the creep behavior of a carbon fiber/epoxy matrix composite was studied through tensile and flexural creep testing. No creep rupture failures were observed in short-term (less than 1600 h) room temperature tensile creep tests at loads up to 77% ultimate tensile strength (UTS). For elevated temperature flexural creep compliance data taken at isotherms between 30 and 75 ∘C, the principle of time–temperature superposition held. Master curves were generated by shifting the data by hand and also using the constant activation energy of the glass transition relaxation to estimate the shift factors. It was shown that the constant activation energy assumption worked fairly well, but only for temperatures below the onset T_g of the material. Predictions were made concerning the creep levels at the end of a proposed 50-year design life.

2.5   Fire protection

In the last decade, a few fire tests have been conducted on FRP-strengthened RC beams to generate fire endurance ratings.

Most of these tests were under standard fire exposure aimed at obtaining fire resistance ratings, rather than studying the response of FRP-strengthened members under fire conditions. Thus, there is a lack of understanding of the response of FRP-strengthened RC beams under realistic fire, loading, and failure limit states. This lack of fire test data and fire design methods is posing a major obstacle for wider use of FRP in buildings and parking structures (ACI Committee 440, 2002).

In the event of fire, the properties of FRP deteriorate quickly, resulting in rapid loss of strength and stiffness above glass transition temperature (T_g), (H. Blontrock , et al., 1999) . Typically, the glass transition temperatures for commonly used polymers vary between 60 to 82°C (ACI Committee 440, 2002). Therefore, FRP sheets used without fire protection will lose their strength and stiffness at early stages of fire exposure (Brea Williams, et al., 2006).

When used in buildings, structural members are to satisfy fire resistance ratings prescribed in building codes. Fire resistance is the duration during which a structural member exhibits resistance with respect to strength, integrity and stability and depends on many factors including structural geometry, material used in construction and characteristics of fire. A fire resistance rating is the fire resistance of a member rounded off to nearest hour or half-hour. Concrete due to its low thermal conductivity, high thermal capacity and slower loss of strength and stiffness properties performs reasonably well under fire. Therefore, concrete structures are often used without any fire protection. However, when strengthened with external FRP system, concerns like loss of strength, stiffness and bond, flame spread, smoke generation and toxicity associated with fire are to be addressed (L.A. Bisby, 2003). Guidelines on design and application of FRP at ambient temperature are available in different codes of practice (ACI Committee 440, 2002). However, the codes do not specify any fire guidelines and assume that the FRP is lost in the event of fire. (ACI Committee 440, 2002) recommends that FRP-strengthened members must meet all building and fire code guidelines spelled out for RC structures. Further, it requires that the prestrengthened RC structure must be capable of withstanding the service loads (1.2 times the dead load and 0.85 times the live load) in order to prevent collapse that might arise from failure of FRP under fire exposure.

Brea Williams, et al., (2006) investigated experimentally and numerically the performance in fire of insulated FRP-strengthened concrete slabs. Four different supplemental fire insulation systems are examined (Figure 2-19) through standard fire tests, and a numerical model to predict member behavior in fire is presented. Model predictions are shown to satisfactorily agree with test data. The results of this study indicate that appropriately designed and insulated FRP-strengthened concrete slabs are capable of achieving satisfactory fire endurances.
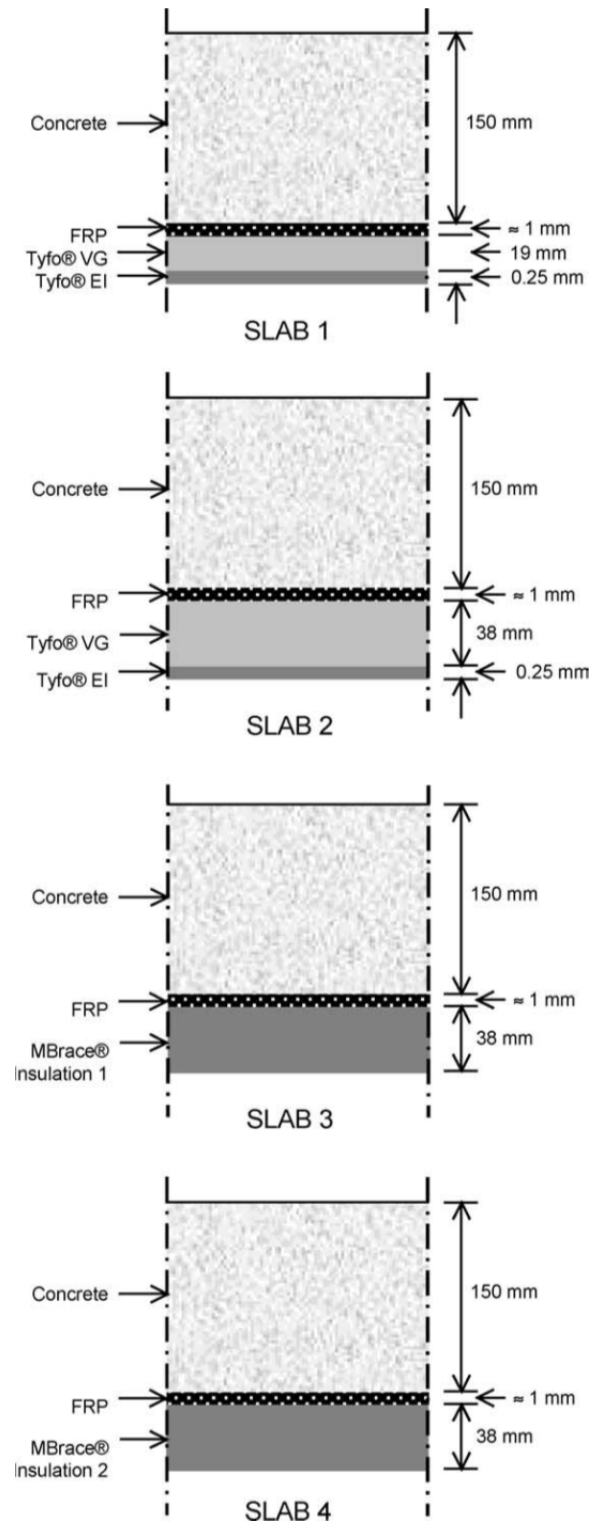
Figure 2-19: Through-thickness details of the four insulated FRP-strengthened reinforced concrete slab specimens tested, (Brea Williams, et al., 2006)

According to (ASTM. E119, 2002) fire endurance criteria, a 4-h fire endurance rating (based on thermal criteria only) can be achieved with 38 mm of any of the four insulation

schemes examined herein. A smaller thickness of Insulation System 1 (19 mm) provided approximately 2 h of fire protection for a 150 mm thick reinforced concrete slab, (Brea Williams, et al., 2006).

Aqeel Ahmed & Venkatesh Kodur, (2011) studied the experimental behavior of FRP-strengthened RC beams subjected to design fire exposure. The results from fire resistance experiments on five rectangular reinforced concrete (RC) beams are presented (Figure 2-20); four of these RC beams were tested after being strengthened with carbon fiber reinforced polymer (CFRP), while the remaining one was tested as a control RC beam specimen. The beams were tested by exposing them to fire and service load, computed based on the nominal capacity of an unstrengthened/strengthened beam in accordance with ((ACI Committee 318, 1999), and (ACI Committee 440, 2002)) provisions. The test variables included type of fire exposure, anchorage zone, insulation type, and restraint conditions. The data from the fire tests is used to evaluate the thermal and structural response, as well as failure patterns in FRP-strengthened RC beams. The test results indicate that the anchorage configuration plays a critical role in limiting the deflections of the strengthened beam after debonding of the FRP occurs at T_g ±10 °C, where T_g is the glass transition temperature. Also, FRP-strengthened RC beams supplemented with 25 mm thick spray-applied insulation can survive failure under (ASTM. E119, 2002)standard fire or a design fire. Further, the fire-induced axial restraint force significantly increases the fire resistance of FRP-strengthened/unstrengthened RC beams, provided that the location of restraining force is below the geometric centroid of the beam and that the beam's deflection is sufficiently small along the entire span.
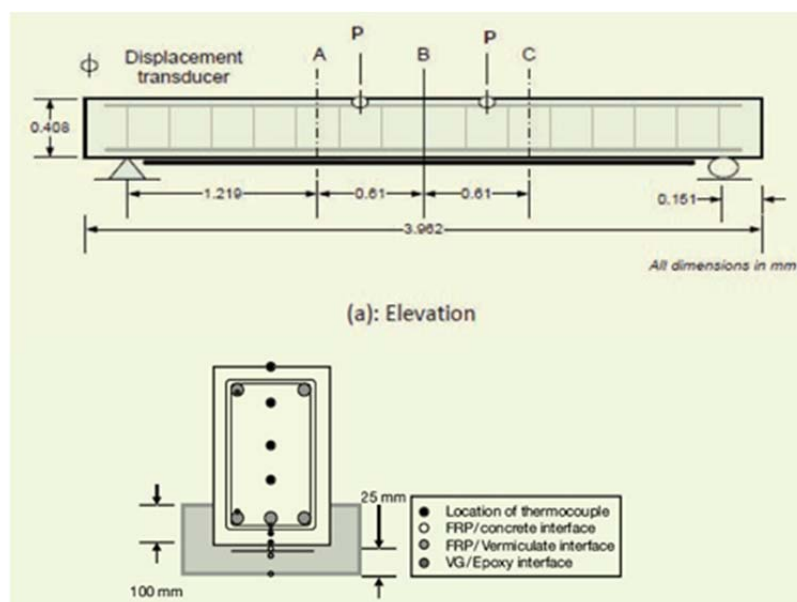
Figure 2-20: Elevation and cross-sectional details of tested FRP-strengthened RC beam, together with fire scenarios, (Aqeel Ahmed & Venkatesh Kodur, 2011)

39

2.6   Long-term behavior of FRP strengthened RC structures

The short-term response of concrete beams strengthened with FRP has been widely studied and reported. One of the main characteristics of strengthened beams is the debonding failure mechanism of the FRP at the edges and near cracks, which results from relatively high shear and vertical normal stress at the adhesive interfaces. Under sustained loads, these stresses become dependent upon the creep characteristics of the concrete, as well as those of the adhesive and the FRP. Since composite and polymer materials exhibit different creep characteristics to concrete, the creep behavior of the strengthened member may lead to stress redistributions. This may eventually lead to debonding failures over time, although the structure may be subjected to sustained loads that are less than its short-term failure loads. In order to shed light on this effect, as well as, on the stresses redistribution at cracked sections and on the creep behaviour of strengthened members in general, an understanding of the effect of creep on the deformations, internal forces and stresses is required, bearing in mind the dependence of the creep strains on the variable stress level and their interaction with environmental effects (temperature, humidity, etc.), which make predicting the behaviour of strengthened members a challenging and difficult task.

The numerous studies that have been carried out to date on FRP-strengthened concrete elements have mainly focussed on the static and short-term responses; very little work has been done regarding the long-term performance. Several researchers have investigated the long-term deflections for concrete beams. (Washa G.W. & Fluck P.G. , 1952) investigated the effect of the compression steel and found that the compression reinforcement in simply supported reinforced concrete beams is very effective in reducing the deflections. The results of Washa and Fluck were later confirmed by (Paulson K.A., et al., 1991), who noted that compression reinforcement has a significant effect in reducing the long-term deflections. The efficiency of this reinforcement is more pronounced in normal strength concrete beams than high strength concrete beams.

Analytical methods ((Ghali A. & Favre R., 1986); (Tan K. H., et al., 1994); and (Gilbert R. I., 1999), along with ACI approach (ACI Committee 318, 1999), are available for the determination of time-dependent deflections of RC beams. The time dependent deflections can be predicted by using either the effective modulus method (EMM) or the adjusted EMM (AEMM), by incorporating appropriate creep and shrinkage models, such as those recommended by ACI (ACI Committee-209R-92, 1997).

Nikolaos Plevris & Thanasis C. Triantafillou, (1994) investigated the time-dependent behavior of RC members strengthened with FRP laminates analytically; and concluded that CFRP, and GFRP appears to be the best composite materials for the external strengthened of concrete structures.

Al Chami, et al., (2009) investigated the creep behavior of experiments on the time-dependent behavior of carbon FRP-strengthened concrete beams. Twenty-six reinforced concrete beams with dimensions 100 x 150 x 1800 mm, with and without bonded CFRP laminates, Different reinforcement ratios were used to evaluate the contribution of the external reinforcement on the creep resistance of the beams. High levels of sustained load were used in order to determine the maximum sustained load that can be applied without any risk of creep failure. The applied sustained loads varied from 59% to 78% of the ultimate static capacities of the un-strengthened beams. For most of the long-term tests, the applied sustained loads were higher than the service loads. This was done to account for the fact that strengthening is typically required when a structure is expected to carry increased service loads. The results confirm that FRP strengthening is effective for increasing the ultimate capacities of the beams; however, there is virtually no improvement in performance with regard to the long-term deflections.

Tan T.H. & Saha M.K., (2006) studied the long-term deflection characteristics of externally FRP-bonded beams under sustained loads. Nine reinforced concrete beams 9 (100x125 mm in cross section and 2000 mm in total length), six of which were externally bonded with glass FRP composite laminates, were subjected to sustained loads for 2 years. The test parameters were the FRP ratio and sustained load level. The long-term deflections of the beams were reduced 23 and 33% with a FRP ratio of 0.64 and 1.92%, respectively. The total beam deflections were accurately predicted by the adjusted effective modulus method, and overestimated by about 20% by the effective modulus method.

Yousef A. Al-Salloum & Tarek H. Almusallam, (2007) studied the effect of different environmental conditions on the creep behavior of concrete beams reinforced with glass fiber reinforced polymer (GFRP) bars under sustained loads is investigated. This is achieved through testing concrete beams reinforced with GFRP bars and subjected to a stress level of about 20–25% of the ultimate stress of the GFRP bars. Reference beams were loaded in the temperature controlled laboratory (24 $\pm$ 3 ^{o}C). Other test beams were either completely or partially immersed in different environments (tap-water and sea-water) at elevated temperature (40 $\pm$ 2 ^{o}C) to accelerate the reaction. During the exposure period, which lasted for ten months, strains in concrete and GFRP bars as well as the mid-span deflections were recorded for all considered environmental conditions. The results show that the creep effect due to sustained loads was significant for all environments considered in the study and the highest effect was on beams subjected to wet/dry cycles of sea-water at 40 $\pm$ 2 ^{o}C.

Stierwalt D.D. & Hamilton III H.R. , (2005) examined the creep behavior of masonry walls strengthened with FRP composites compared to that of conventional reinforcement. Eight full-scale (40 in wide by 96 in tall [1.02 m x 2.44 m]) unreinforced concrete masonry walls were constructed for testing long-term deflections out-of-plane. The walls were strengthened with externally bonded CFRP or GFRP composites. Two additional walls were constructed with mild steel reinforcement grouted in the centre cell of the specimens. Long-

term deflections due to creep in FRP reinforced walls were shown to be about 22–56% higher than those of steel reinforced walls.

S. Benyoucef , et al., (2007) investigated the time-dependent behavior of RC beams bonded with thin composite plate theoretically by including the effect of the adherend shear deformations. The time effects considered here are those that arise from shrinkage and creep deformations of the concrete. The influence of creep and shrinkage effect relative to the time of the casting and the time of the loading of the beams is taken into account. Numerical results from the present analysis are presented to illustrate the significance of time-dependent of adhesive stresses. The study showed that the interfacial stresses take a peak value during the first months and begin to decrease until they become almost constant after a very long time. In addition, the interfacial shear stress is affected considerably by the relative humidity, contrary to the interfacial normal stress which is affected slightly.

Chapter 3   Experimental Program

3.1   General

This chapter presents the details of the experimental program undertaken in this study. The main goal of the experimental program is highlighted. The fabrication process, specimen configurations, test setup, instrumentation, and testing procedures for Phases I and II of the experimental program are provided. Finally, material characteristics are identified.

The main objective of the experimental program conducted within the scope of this thesis is to investigate the failure (ultimate) behavior and long-term and creep behavior of reinforced concrete beams strengthened with CFRP laminates in flexure and to use the experimental results for validating the finite element model which will be used on additional parametric study. To achieve this aim, an experimental program consisted of two parts is tested.

Part I consisted of two groups were tested up to failure to investigate the flexural behavior of reinforced concrete beam strengthened with CFRP laminates and comparing the results with the un-strengthened beams.

The Part II consisted of two groups and tested under constant load in the lab condition to investigate the time dependent behavior (creep) of reinforced concrete beams strengthened with externally bonded Carbon fiber reinforced polymer (CFRP) laminates and comparing results with un-strengthened beams. Detailed information about the experimental program and tested specimens is provided in Figure 3-1.
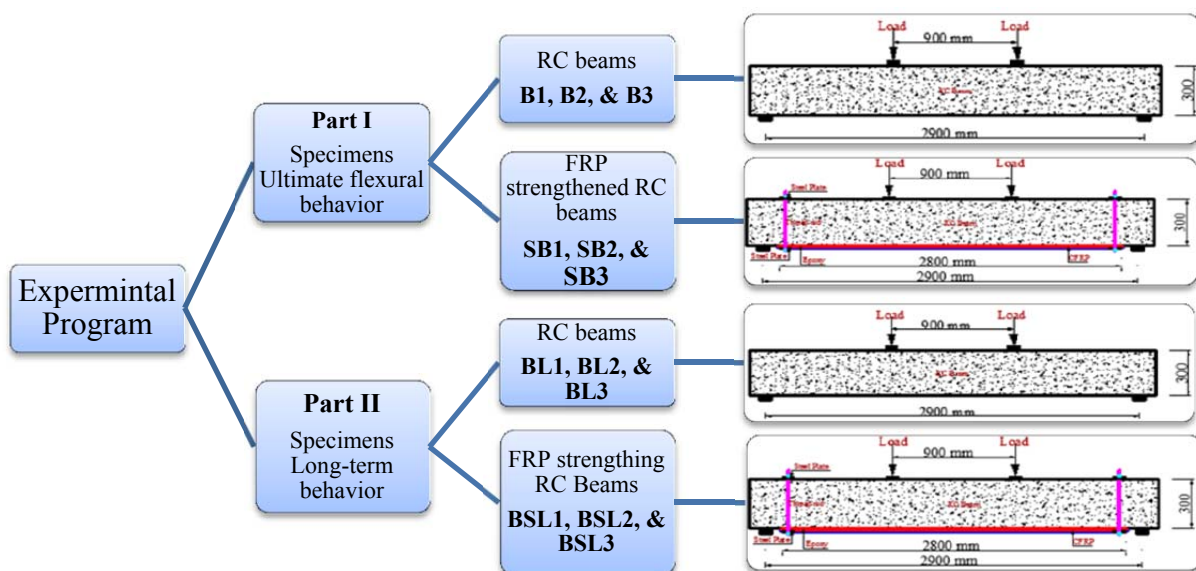
Figure 3-1: detailed of experimental program and tested specimens

3.2 Part I specimens (short-term specimens)

3.2.1 Details of Part I

This section describes the first Part of the experimental program undertaken to evaluate the flexural behavior of concrete members retrofitted with CFRP strengthening techniques. The fabrication process, instrumentation, and testing of the specimens are also discussed.

Six simply supported reinforced concrete beams with a span of 2900 mm and depth of 300 mm, while the breadth is 120 mm were prepared and constructed. Shear reinforcement consisted of ϕ8 mm steel stirrups, uniformly spaced at 100 mm. The top reinforcement consisted of two ϕ10 mm steel bars running along the full length of the beam. The bottom reinforcement consisted of two ϕ16 mm steel bars running along the full length of the beam, as shown in Figure 3-2. The longitudinal and transverse reinforcement for the tested beams were determined according to the Euro code and Egyptian Code of practice requirement for the maximum reinforcement in the section.
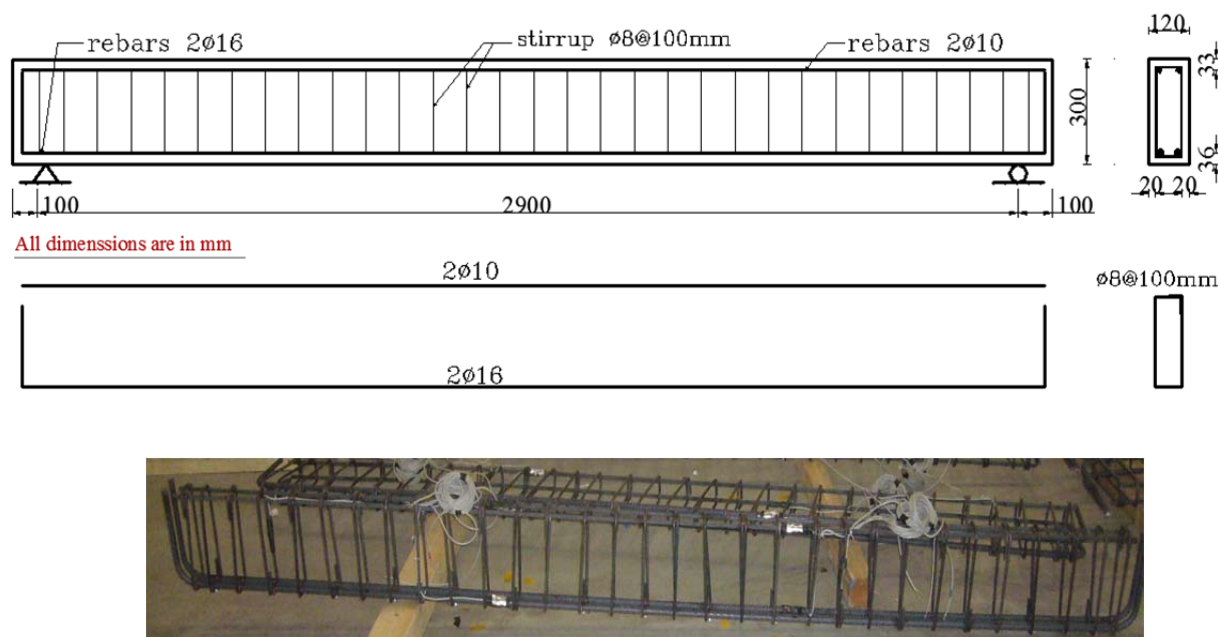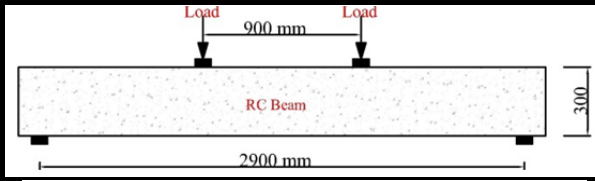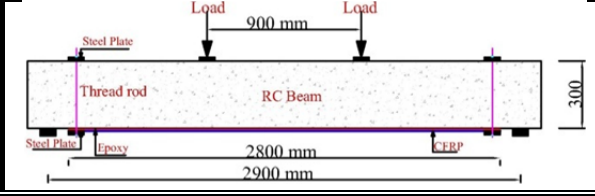
Figure 3-2: Reinforcement details of Part I specimens

This Part divided into two groups; the first group is the controlled reinforced concrete beams and consisted of three specimens B1, B2, and B3, while the other three specimens SB1, SB2, and SB3 were strengthened with externally bonded CFRP laminates used for the second group. With the maximum moment occurring at the mid-span section of the beam,

failure could be due to either debonding of the CFRP. The specimens were adequately designed to avoid concrete crushing and premature failure due to shear. Detailed information about the tested specimens is provided in Table 3-1.

Table 3-1: details of tested specimens Part I

Beam No.	Series	Description of specimen	Epoxy	CFRP layer
B1	Control beams 1st group		---	---
B2				
B3				
SB1	Strengthened beams 2nd group		Sikadur 30	1x1.2 mm-layer
SB2				
SB3				

3.2.2   Fabrication of the Part I Specimens

Six wood frameworks with the same shape and size of specimens were prepared and constructed in the Pferdestall laboratory of the Institute of building Physics, in Hannover, Germany. Casting of the Part I specimens is illustrated in Figure 3-3. After 24 hours from casting concrete the forms were removed and the specimens were cured with water for 28 days in the laboratory environment.

Figure 3-3: Casting of the Part I specimens

3.2.3   CFRP-Strengthening reinforced concrete beams procedure

The tension surface of three specimens was prepared by grinding and sand-blasting and the dust particles were removed by airbrush. Then an 80 mm wide, 2800 mm length, and 1.2 mm thick CFRP laminate was bonded with SikaDur 30 epoxy resin. At the cut-off points of the CFRP composite laminate near the end of the beam, steel plates attached transversely to prevent premature plate-end debonding of the CFRP composite laminate. The nominal thickness of CFRP system (epoxy and composite) for one layer was 2 mm. The details of strengthening concrete beams with CFRP are shown in Figure 3-4.

Figure 3-4: Strengthening concrete beams with CFRP

3.2.4   Instrumentation of Part I

Strains: The concrete strain in the compression and tension zone of the beam was measured using two demc points and LVDTs between the two points in the both sides. The strain in the CFRP was monitored using three electrical strain gauges. While the strain in the top and bottom steel reinforcement was measured using electrical strain gauges embedded in concrete.

Slip monitoring: The slip at the free ends of the CFRP reinforcement was measured using LVDTs.

Deflections: The deflection at mid-span and under the load was monitored on both sides of the beam using two LVDTs.

The instrumentation used to monitor the behavior of the bond specimens during testing is shown in Figure 3-5.
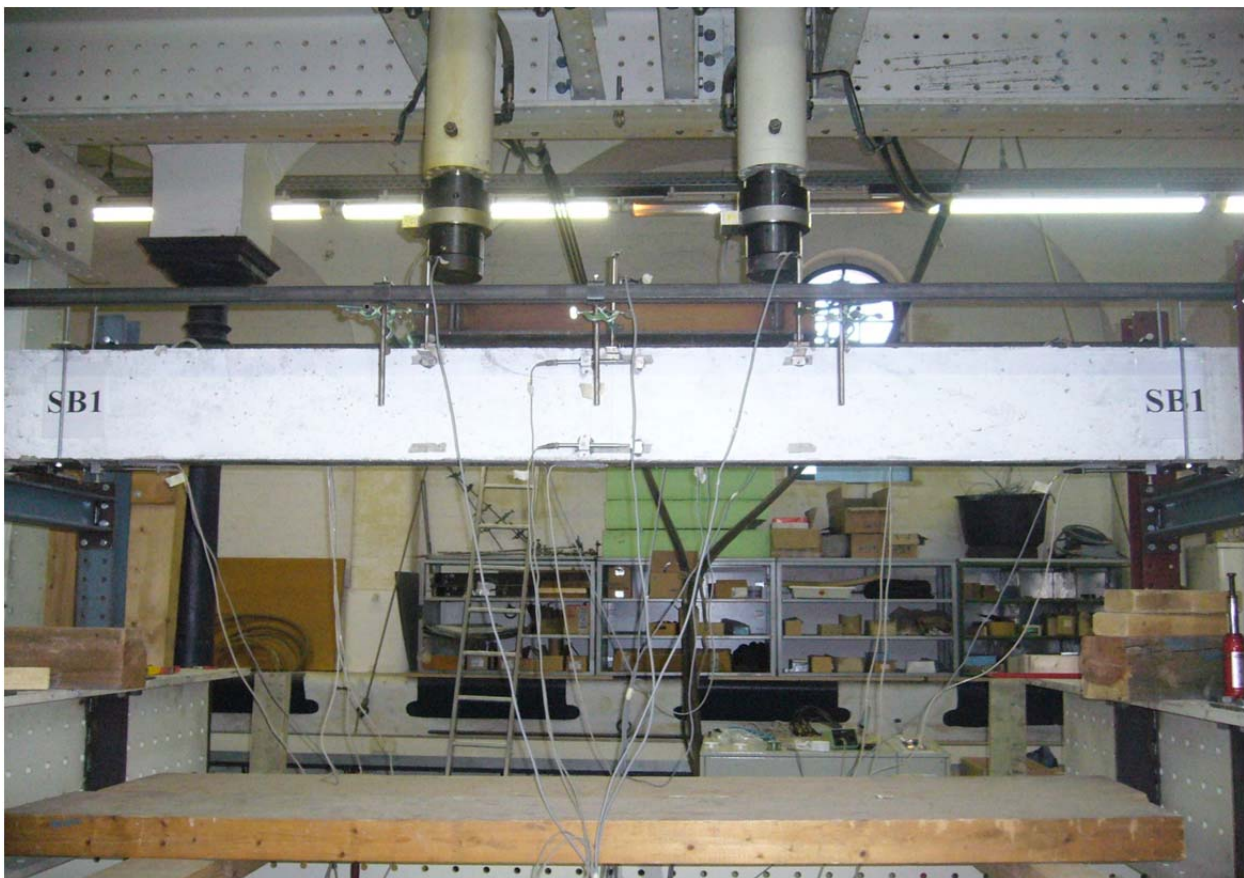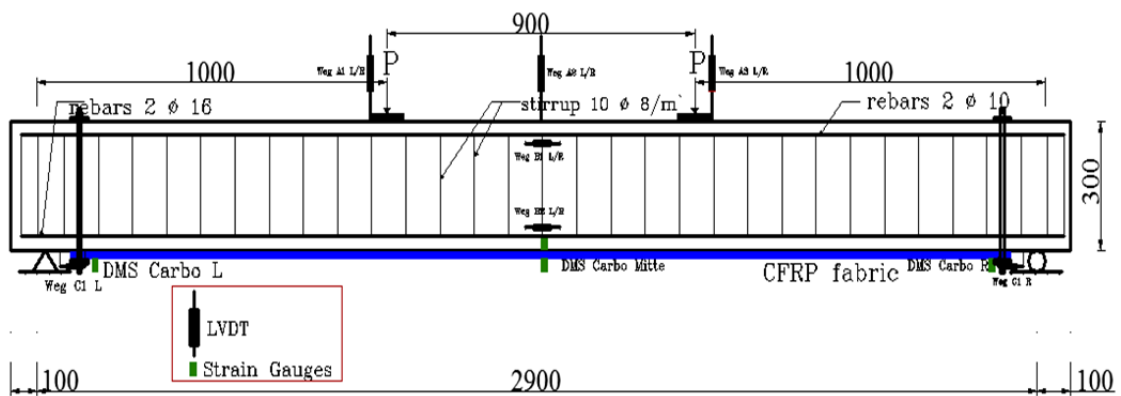
Figure 3-5: Instrumentation used for Part I specimens

3.2.5   **Testing Setup of Part I**

The beams were tested under a concentrated load applied at two points. 160KN testing machine was used to apply the load. The rate of loading was 3.0 mm/min up to failure. Figure 3-6 shows the test set-up in the lab.
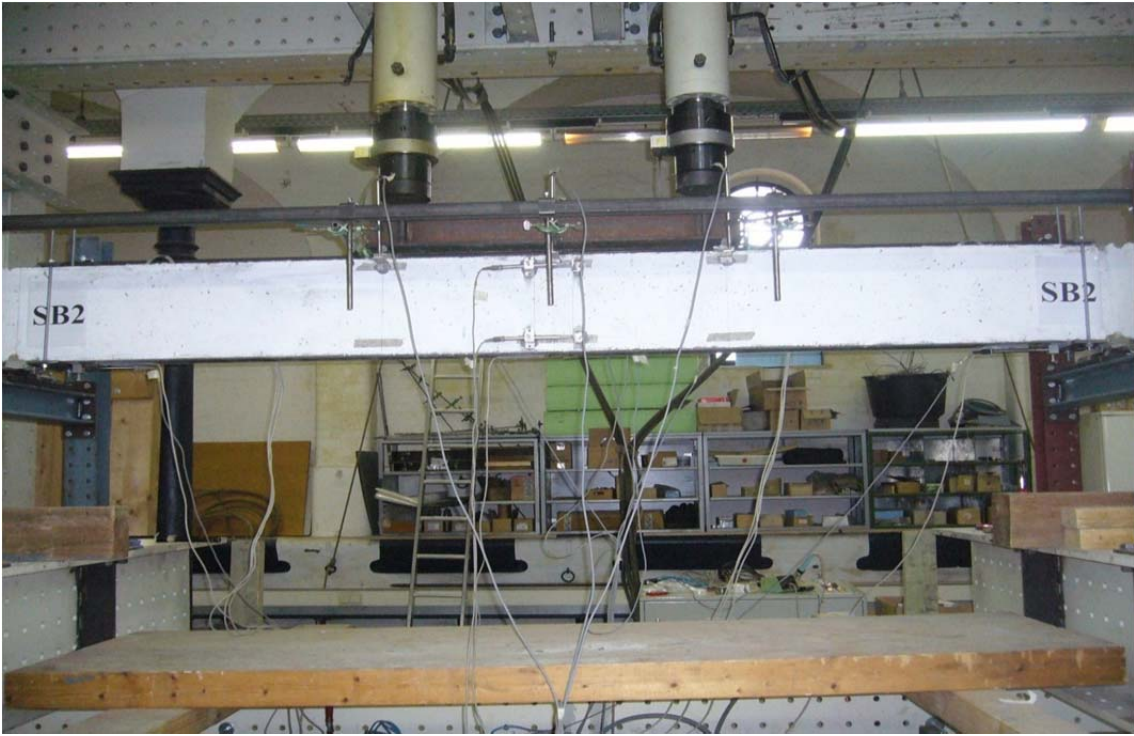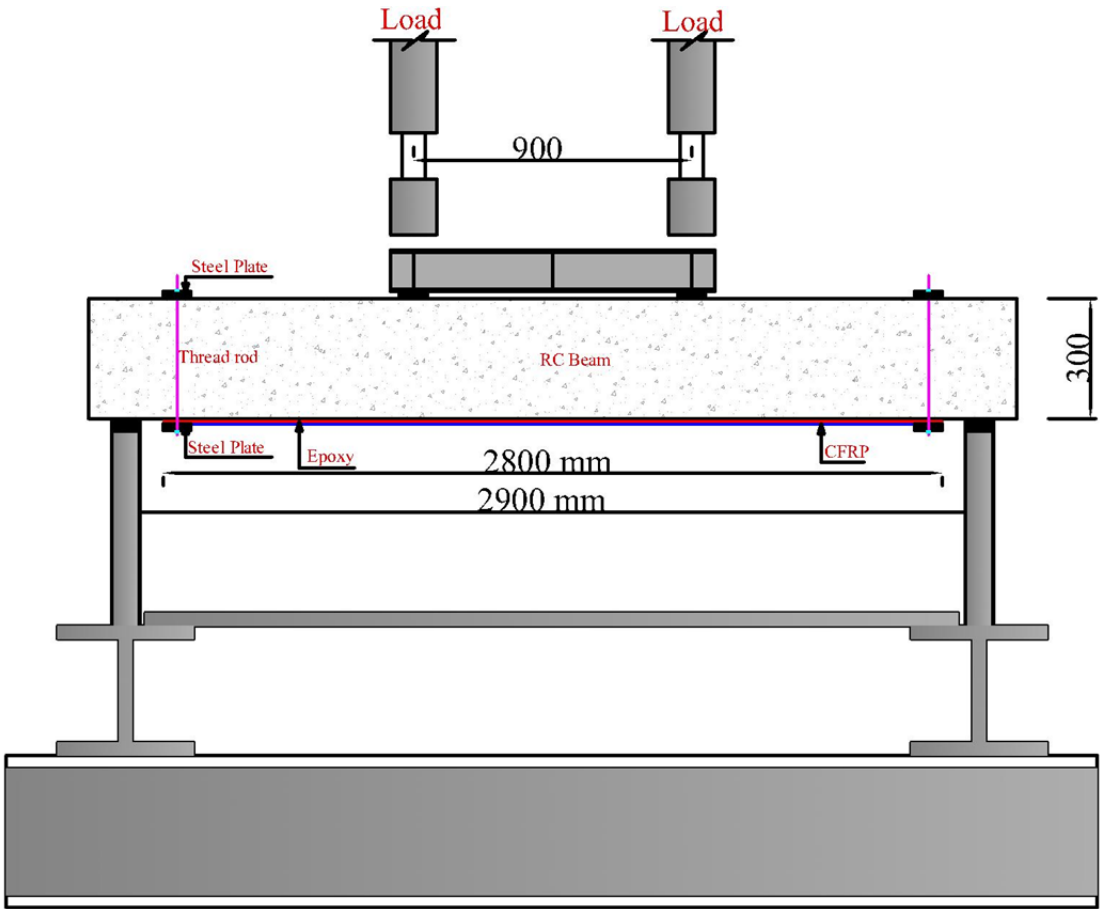
Figure 3-6: Test set-up for Part I specimens

3.3   Part II specimens (long-term specimens)

3.3.1   Details of Part II

This section describes the first Part of the experimental program undertaken to evaluate the long-term behavior of concrete members retrofitted with CFRP strengthening techniques. The fabrication process, instrumentation, and testing of the specimens are also discussed.

Six simply supported reinforced concrete beams with a span of 2900 mm and depth of 300 mm, while the breadth is 120 mm were prepared and constructed. Shear reinforcement consisted of ф8 mm steel stirrups, uniformly spaced at 100 mm. The top reinforcement consisted of two ф10 mm steel bars running along the full length of the beam. The bottom reinforcement consisted of two ф16 mm steel bars running along the full length of the beam, as shown in Figure 3-7. The longitudinal and transverse reinforcement for the tested beams were determined according to the Euro code and Egyptian Code of practice requirement for the maximum reinforcement in the section.
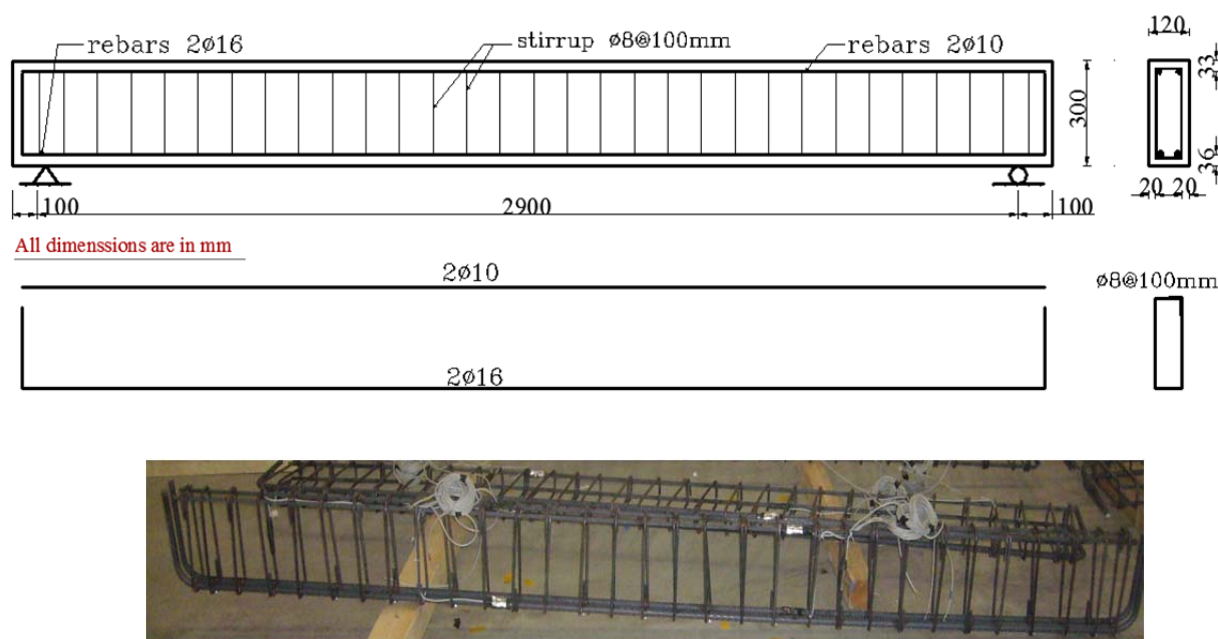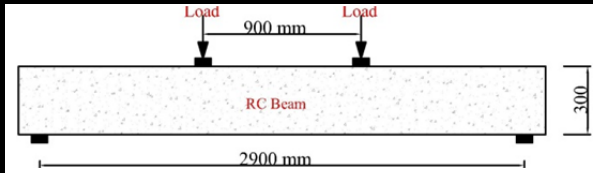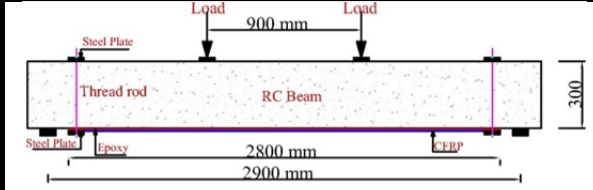
Figure 3-7: Reinforcement details of Part II specimens

This Part divided into two groups; the first group is the controlled reinforced concrete beams and consisted of three specimens B1, B2, and B3, while the other three specimens SB1, SB2, and SB3 were strengthened with externally bonded CFRP laminates used for the second group. With the maximum moment occurring at the mid-span section of the beam, failure could be due to either debonding of the CFRP. The specimens were adequately designed to avoid concrete crushing and premature failure due to shear. Detailed information about the tested specimens is provided in Table 3-2.

Table 3-2: details of tested specimens Part II

Beam No.	Series	Description of specimen	Epoxy	CFRP layer
BL1	Control beams 1st group		---	---
BL2				
BL3				
BSL1	Strengthened beams 2nd group		Sikadur 30	1x1.2 mm-layer
BSL2				
BSL3				

3.3.2 Fabrication of the Part II Specimens

Six wood frameworks with the same shape and size of specimens were prepared and constructed in the Marienwerder laboratory of the Institute of building Physics, in Hannover, Germany. Casting of the Part II specimens is illustrated in Figure 3-8. After 24 hours from casting concrete the forms were removed and the specimens were cured with water for 28 days in the laboratory environment.

Figure 3-8: Casting of the Part II specimens

50

3.3.3 CFRP- Strengthening reinforced concrete beams procedure

The tension surface of three specimens was prepared by grinding and sand-blasting and the dust particles were removed by airbrush. Then an 80 mm wide, 2800 mm length, and 1.2 mm thick CFRP laminate was bonded with SikaDur 30 epoxy resin (Sika Detuschland, n.d.). At the cut-off points of the FRP composite laminate near the end of the beam, steel plates attached transversely to prevent premature plate-end debonding of the CFRP composite laminate. The nominal thickness of CFRP system (epoxy and composite) for one layer was 2 mm. The details of strengthening concrete beams with CFRP are shown in Figure 3-9.

Figure 3-9: Strengthening concrete beams with CFRP

3.3.4 Instrumentation of Part II

Strains: The concrete strain in the compression and tension zone of the beam was measured using two demc points and Watches between the two points in the both sides. The strain in the CFRP was monitored using three electrical strain gauges. While the strain in the top and bottom steel reinforcement was measured using electrical strain gauges embedded in concrete.

Slip monitoring: The slip at the free ends of the CFRP reinforcement was measured using watches.

Deflections: The deflection at mid-span and under the load was monitored on both sides of the beam using two watches.

The instrumentation used to monitor the behavior of the bond specimens during testing is shown in Figure 3-10.
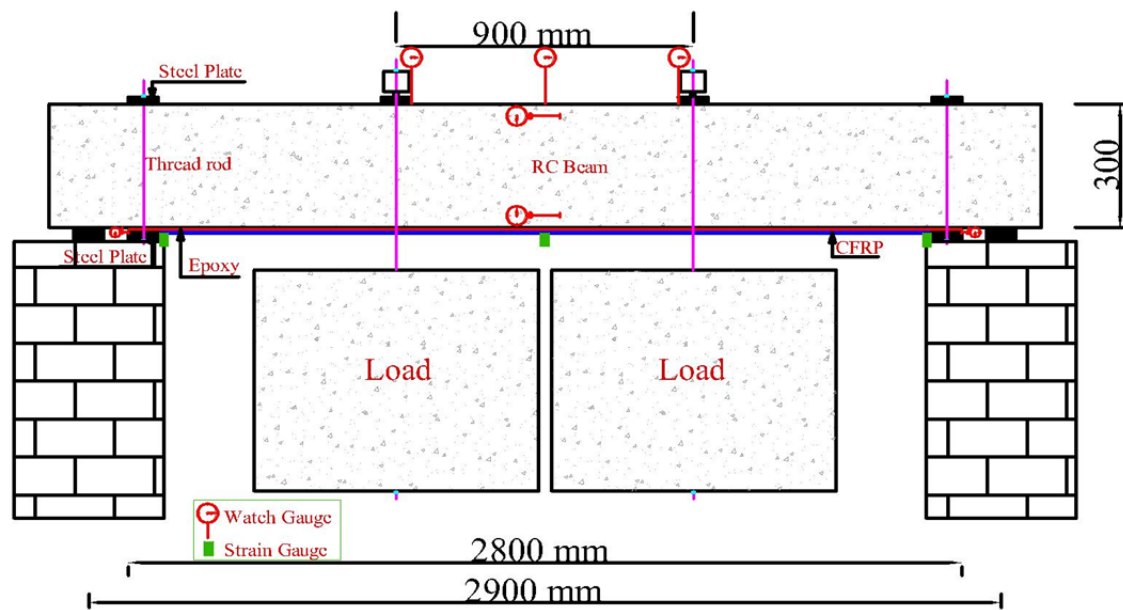
Figure 3-10: Instrumentation used for Part II specimens

3.3.5   Testing Setup of Part II

The beams were tested under a concentrated load applied at two points. Concrete blocks were casting in the lab and used for loading. the design service load used for creep test was 50% - 60% from the prediction of the ultimate load, but due to unexpected change in the compressive strength of the concrete from the concrete supplier, (compressive strength was increased from 25MPa to 44 MPa) , the ultimate load was higher than the calculated, and the service load used for creep test was changed to be 34% from the ultimate load. Figure 3-11 shows the test set-up in the lab.
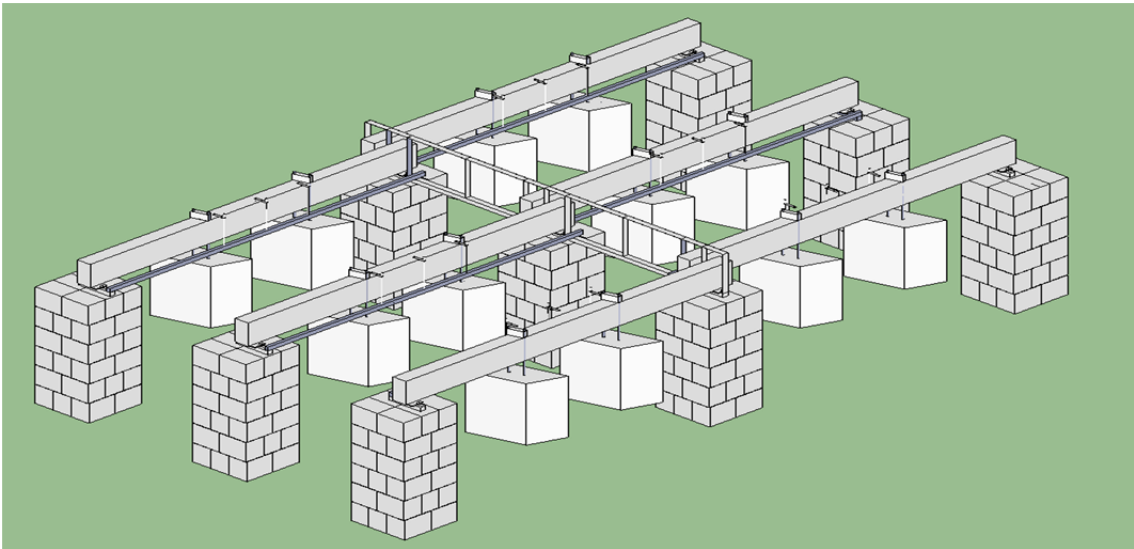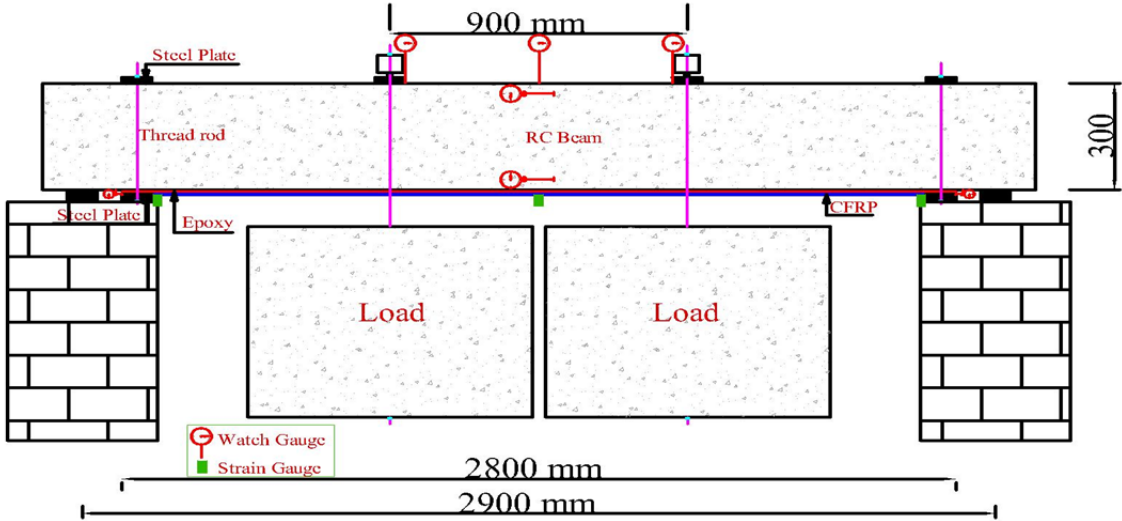
Figure 3-11: Test set-up for Part II specimens

3.4 Materials

3.4.1   Concrete

A precast concrete C20/25 X0 F3 0-16 with 16 mm maximum size of aggregate was used for constructing all specimens. Cubes with dimensions 150 x 150 x 150 mm and cylinders with 150 mm diameter and 300 mm length were (shown in Figure 3-12) casted and tested after 28 days, and during the test. The average compressive strength of the concrete was 44 MPa, while the average modulus of elasticity was 23941 MPa, and the tensile strength was 2.6 MPa. The properties of concrete summarized in Table 3-3.

Cubes and cylinders

Compressive strength test   Young's modulus test   Tensile strength test

Figure 3-12: Concrete cubes and cylinders tests

Table 3-3: mechanical properties of concrete

Compressive strength, f'_c (MPa)	44
Modulus of elasticity, E_c (MPa)	23941
Tensile strength, f_{ct} (MPa)	2.6
Poisson's ratio, ν	0.2
Angle of dilatancy	38
Ultimate strain (%)	0.0035
Fracture energy G_F (N/mm)	0.079

3.4.2   Reinforcement Steel bars

Deformed reinforcement bars (S500) of 8, 10, and 16 mm diameter have been used for stirrups, top and bottom reinforcement respectively. The yield stress of the steel was 490 MPa, and the modulus of elasticity was 200 GPa. The properties of the reinforcing steel were determined according to Euro code and Egyptian Standard Specifications, Ess. 262/1989. Table 3-4 shows the mechanical properties of reinforcement steel bars.

Table 3-4: mechanical properties of Steel

Yield stress, f_{sy} (MPa)	490
Modulus of elasticity, E_s (GPa)	200
Poisson's ratio, ν	0.30

3.4.3   FRP plate

The carbon fiber reinforced polymer (CFRP) composite employed in this study was manufactured by Sika Corporation (Sika Detuschland, n.d.) (Sika Carbodur S812/120). This fabric, with a width of 80 mm and a thickness of 1.2 mm, is a high strength, unidirectional carbon fiber. Typical Minimum Requirement Chart- Spec Writer to customize per product for Sika CarboDur Strip shown in Table 3-5.

Table 3-5: Typical Minimum Requirement Chart- Spec Writer to customize per product for Sika CarboDur Strip

Property	Requirement	ASTM Test Method
Laminate Tensile Strength, In primary fiber direction	2,800 MPa	D3039
Laminate Tensile Modulus, In primary fiber direction	165,000 MPa	D3039
Laminate Elongation at break	1.70 %	D3039
Laminate Thickness	1.2mm	
Fiber Volume, minimum	68%	D2563

3.4.4   Epoxy Resin

SikaDur 30 epoxy was used to bond the carbon fiber reinforced polymer (CFRP) system to concrete face.

Commercially available epoxy adhesive (Sikadur 30‑ Sika EU Inc.) was used for bonding the CFRP plates and bars to the concrete. The maximum tensile strength of the Sikadur 30 adhesive is 25MPa, Modulus of elasticity is 4.5GPa, and compressive strength

59.3MPa at 7days at 23°C based on the data provided by manufacturer. The mechanical properties of the epoxy interface shown in Table 3-3-6

Table 3-3-6: mechanical properties of Epoxy

Modulus of elasticity, E_c (GPa)	12
Shear Modulus, G_a (GPa)	4.5
Tensile strength, f_{ct} (MPa)	25
Poisson's ratio, ν *(assumed)*	0.38
Ultimate strain (%)	1
Fracture energy (N/m)	0.41

Chapter 4   Analysis and discussion of experimental results

4.1 Introduction

This chapter presents the analysis and discussion of the data produced by testing. In each test measurements are taken for, applied loads, deflection of mid-span, deflection under applied load, concrete strain, strains of steel, and strains of CFRP. The discussion of test results will be in view of mode of failure, the load – deflection behavior, and the load – flexural strains of these beams.

4.2 Experimental Results of Part I

This part consisted of two groups were tested up to failure to investigate the flexural behavior of reinforced concrete beam strengthened with CFRP laminates and comparing the results with the unstrengthened beams.

The first group (control beams; B1, B2, and B3) consisted of three simply supported reinforced concrete beams with dimensions 2900x120x300 mm. The beams were tested in lab conditions up to failure

The second group (FRP-strengthened reinforced concrete beams; SB1, SB2, and SB3) consisted of three simply supported reinforced concrete beams with dimensions 2900x120x300 mm strengthened with CFRP laminates bonded to the tension face of these beams. The beams were tested in lab conditions up to failure.

The beams were tested in four point bending. This load case was chosen because it gives constant maximum moment and zero shear in the section between the loads, and constant maximum shear force between support and load. The moment was linearly varying between supports and load.

4.2.1   Mode of failure and crack patterns

From the test results of the first group beams (control beams) B1, B2, and B3, it can be noticed that:

The first crack for B1, B2, and B3 beams was observed at the under-load in the tension side and later at mid-span at average load P = 8.83 KN. As the load increased, flexural cracks propagated approximately vertical upgrade until yielding of steel bars at P = 45 KN with widening of cracks. The average ultimate load recorded was P ≈ 49.75 kN with flexure mode of failure at mid span due to the yielding of reinforcement in the tension zone. It was observed that the reinforced concrete beams (control beams) were failed in a ductile manner and gives large deflection before the final failure as expected. The results of load and deflection shown in Table 4-1, while the cracks pattern was shown in Figure 4-1.

Table 4-1: Cracking, Loads, mode of failure and deflection of the tested control beams

Specimen	First Crack load P_{cr} (kN)	Ultimate load P_u (kN)	Deflection δ_u (mm)	**Mode of failure**
B1	8.5	49.72	18.94	flexural, mid-span
B2	9.0	49.37	18.72	flexural, mid-span
B3	9.0	50.17	19.04	flexural, mid-span
Average	**8.83**	**49.75**	**18.9**	flexural, mid-span

a) Beam B1
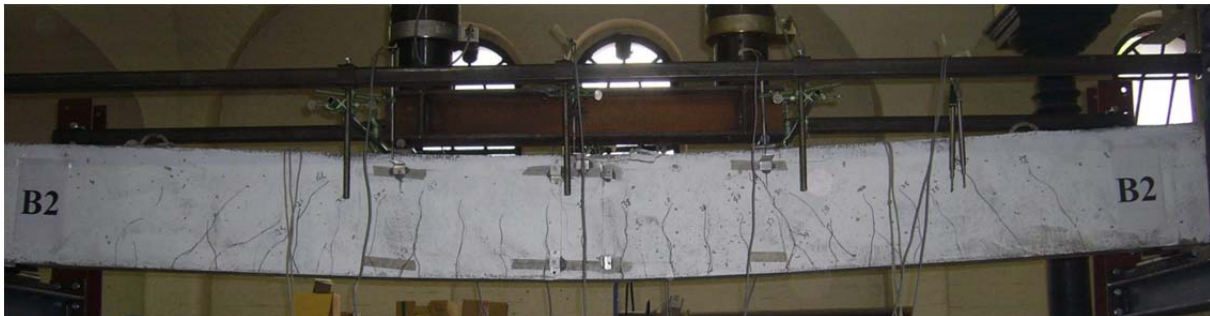
b) Beam B2

c) Beam B3

Figure 4-1: cracks pattern of RC control beams.

In the other hand; from the test results of the first group beams SB1, SB2, and SB3, (FRP-strengthened RC beams) it can be noticed that:

The first crack for SB1, SB2, and SB3 beams was observed at the under-load in the tension side and later at mid-span at load P = 10 KN. As the load increased, flexural cracks propagated approximately vertical upgrade until yielding of steel bars at P = 64 kN with widening of cracks. The ultimate load recorded was P = 78.347 KN with failure along the epoxy interface layer which is the weak part between CFRP and concrete; the summary of the test results shown in Table 4-2, while the cracks pattern was shown in Figure 4-2.

Table 4-2: Cracking, Loads, mode of failure and deflection of the tested FRP-strengthened RC beams

Specimen	First Crack load P_{cr} (kN)	Ultimate load P_u (kN)	Deflection δ_u (mm)	Mode of failure
SB1	10	78.61	30.91	CFRP-debonding
SB2	10	76.84	29.66	CFRP-debonding
SB3	10	79.59	32.42	CFRP-debonding
Average	**10**	**78.347**	**30.997**	CFRP-debonding
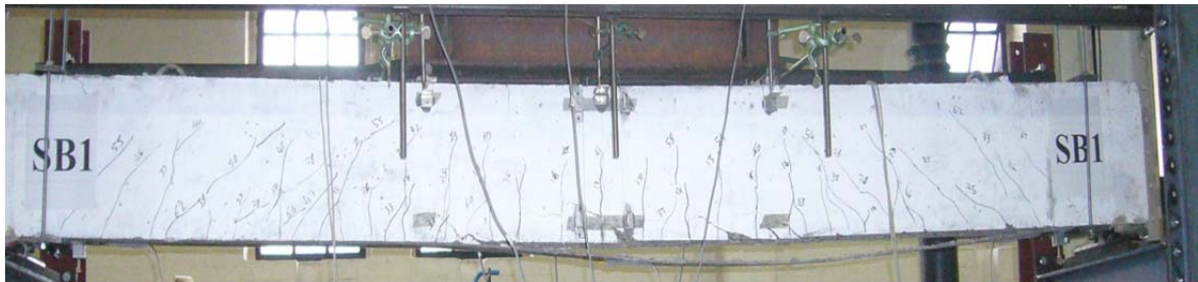
a) Beam SB1

b) Beam SB2

c) Beam SB3

Figure 4-2: cracks pattern of FRP-strengthened RC beams.

4.2.2   Load versus deflection relationship

The load versus mid-span deflection curves for the control beams are shown in Figure 4-3. It is clear that the beam failed in a ductile manner and gives large deflection before the final failure as expected. The effect of the own weight of the tested beams was not included in the calculation of the test loads as it was neglected. The difference between the three specimens is small, and the average value of the load-deflection relationship which plotted in the figure will be used as a reference for reinforced concrete controls beams in this study.
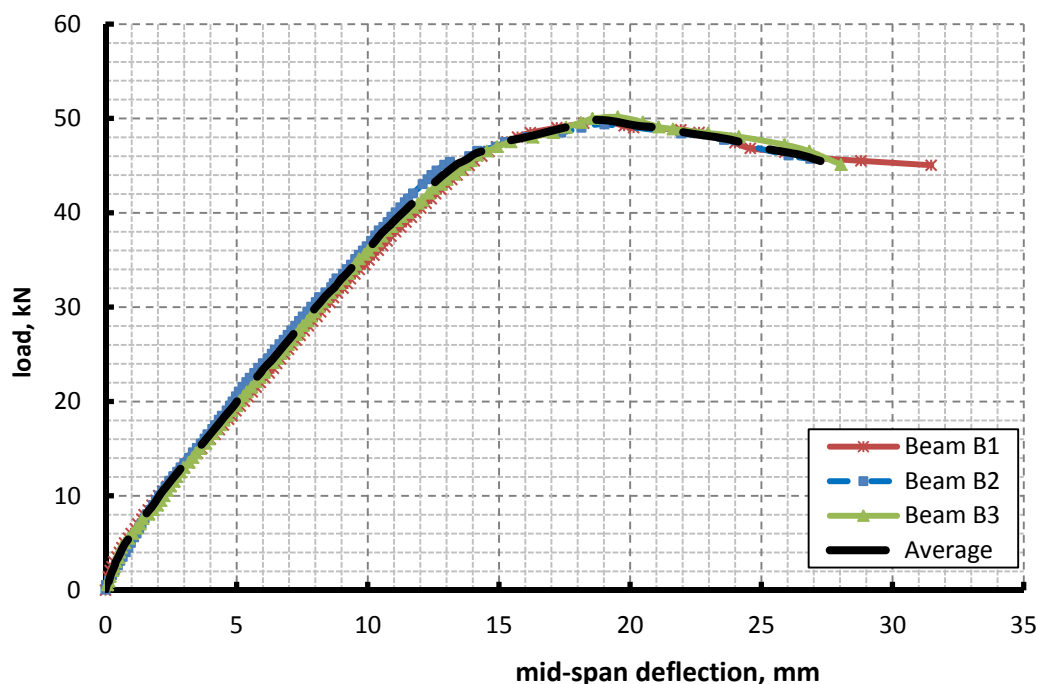
Figure 4-3: Load Mid-span Deflection of Part I controls beam.

The curve includes a linear response up to the load 8.5 kN. The appearance of a crack was first noted at load 8.5 kN. The mid-span deflection curve illustrates the nonlinearities at cracking of the concrete. After 45 kN load flexural cracks formed and widened as loading increased. The maximum load was 49.75 kN as shown in the figure. After maximum load, the cracks did not grow in length but the flexural cracks width increased in the constant moment region.

For the FRP-strengthened reinforced concrete beams; the load-deflection diagram shown in Figure 4-4 indicate that the behavior of the strengthened beams is nearly the same to RC beams up to cracking and at small load, while the using of CFRP increasing the stiffness of the strengthened beams As the load increased, flexural cracks propagated approximately vertical upgrade until yielding of steel bars at P = 64 kN with widening of

cracks. The debonding initiates at a region near to under load and propagate at the end of the CFRP plate because the shear stress was concentrated at this region. The failure load of the FRP-strengthened RC beams was 78.347 kN and after this load the load suddenly dropped down due to the deponding of the CFRP plate and interface failure.
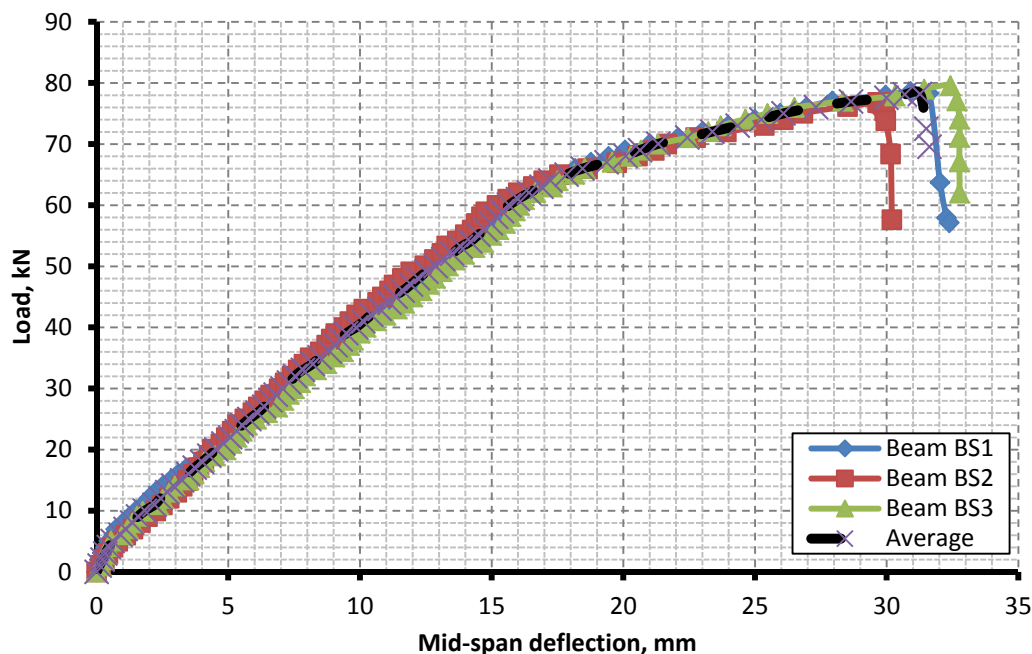
Figure 4-4: Load-Mid-span Deflection of FRP-strengthened RC beams.

4.2.1　Ultimate load and deflection at ultimate load comparison

The increasing in ultimate load of strengthened beams ΔP was compared to the controlled beam ultimate load $P_{u,rc}$ to evaluate the percentage of ultimate load increasing ($\Delta P_u /P_{uo}$) due to using CFRP in strengthened reinforced concrete beam, the data was shown in Table 4-3; it can be observed that the CFRP increased the ultimate load by about 57.48 % comparing to the control beams. While the increasing percentage in deflection $\Delta\delta_u$ was 64%, the main load versus deflection for control beams and FRP-strengthened RC beams shown in Figure 4-5.

Table 4-3: ultimate load and deflection comparison.

Specimen	P_u (kN)	δ_u (mm)	$\Delta P_u = (P_{u,frp} - P_{u,rc})/P_{u,rc}$ %	$\Delta\delta_u=(\delta_{u,frp}-\delta_{u,rc})/\delta_{u,rc}$ %
Control beam	49.75	18.9		
CFRP-strengthened RC beam	78.347	30.997	57.48	64
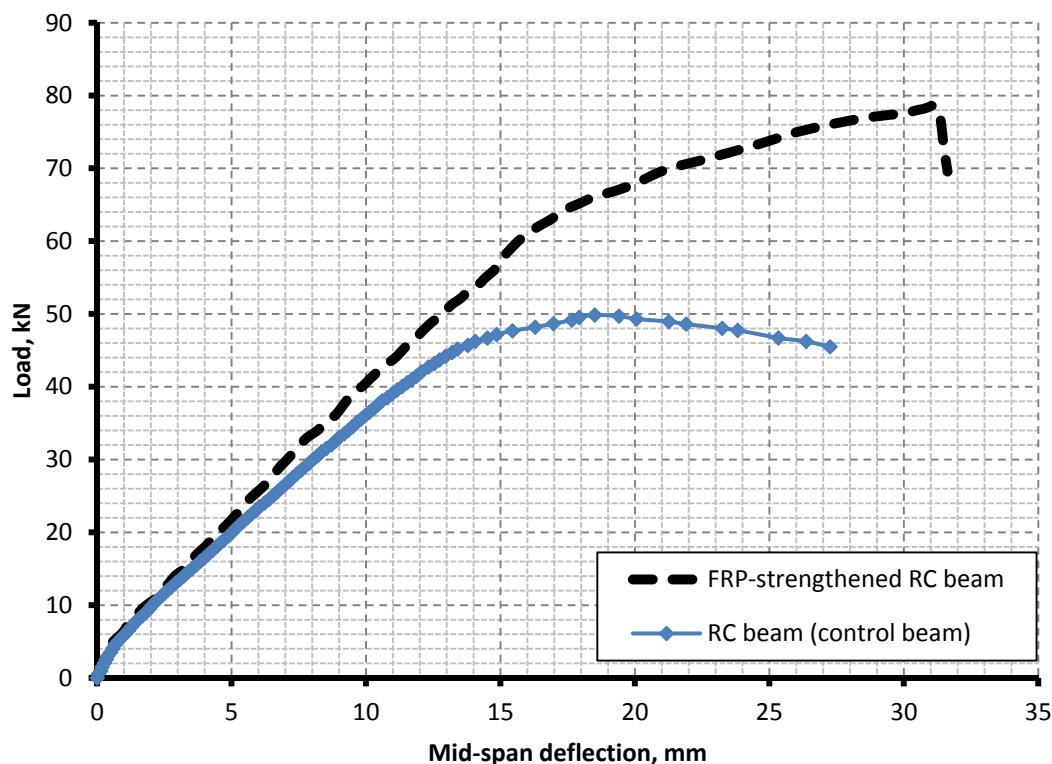
Figure 4-5: average Load-Mid-span Deflection of FRP-strengthened RC beams and control beams.

The load-deflection diagram shown in Figure 4-5 indicate that the behavior of the strengthened beams is nearly the same to RC beams up to cracking and at small load; while the using of CFRP increasing the stiffness of the strengthened beams (expressed by the slope of the load-deflection curves), also increased the yielding load of reinforcement bar, and the ultimate load compared to control beam.

4.2.2   Strain in reinforcement bars

The load-strain in steel reinforcement relationship shown in Figure 4-6; from the figure it can be observed that due to the strengthened with CFRP the yield load for the reinforcement steel bar in tension side is higher than in control beam by 37 %; and the strain at yield load was 2800×10^{-6} and 3200×10^{-6} for control beam and FRP-strengthened RC beam respectively.

While in compression reinforcement the slope of the covers was typically up to beam failed in each specimen. The experimental results for tested specimens were summarized in Table 4-4.
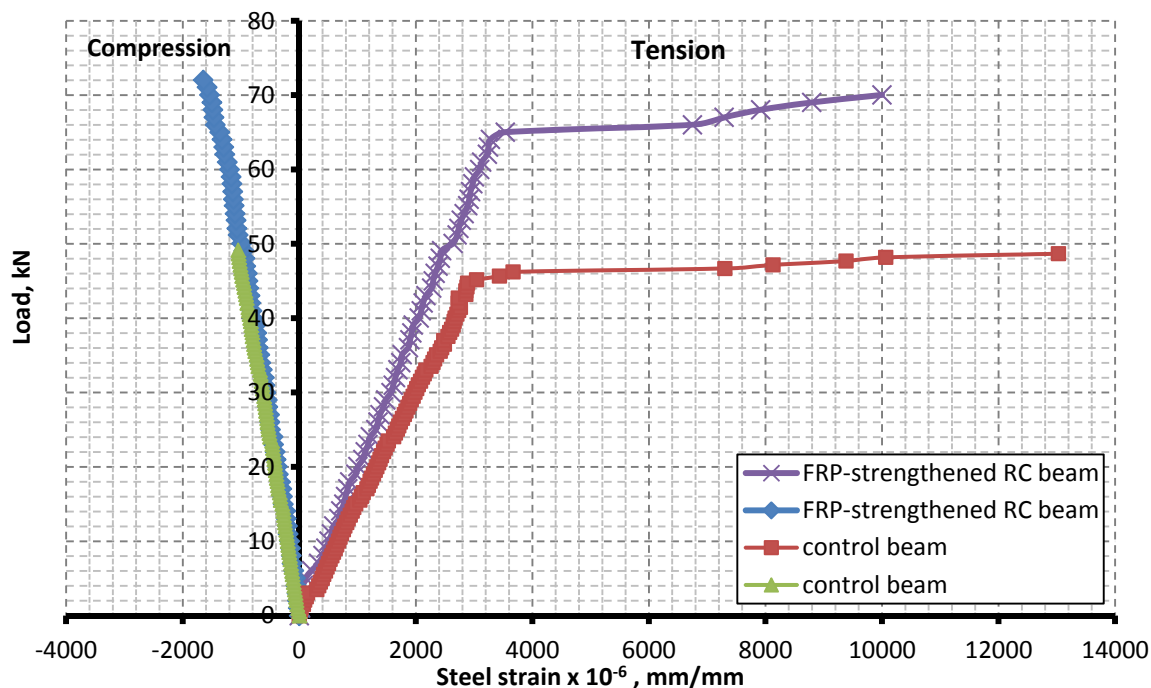
Figure 4-6: Load-steel reinforcement strain of FRP-strengthened RC beams and control beams.

Table 4-4: average strian in reinforcement steel bars at differnet applied load.

Specimen	Applied load P (kN)	Tension reinforcement strain ε_{st} x 10^{-6}	Compression reinforcement strain ε_{sc} x 10^{-6}
Control beam	10	675.29	-201.82
	45	3044.84	-965.847
	49.75	20305.96	-1059.07
FRP-strengthened RC beam	10	511.7128	-169.02
	45	2298.374	-881.265
	50	2638.586	-988.18
	65	3534.705	-1366.08
	78.347	Strain gage defect	-1740.27

4.2.3   Strain variation along CFRP

The strain variation of CFRP with the applied load shown in Figure 4-7; the strain was increased on the CFRP plate for the strain gage at the mid-span and decreased at CFRP plate

end strain gage. This is due to the full bond between CFRP and concrete and the proportion between CFRP-strain and the moment along the beam span. The rate of increasing in CFRP strain was high after the yield of steel reinforcement, and the slope of the curve changed as shown in Figure 4-7. The experimental CFRP-strain results for tested specimens were summarized in Table 4-5.
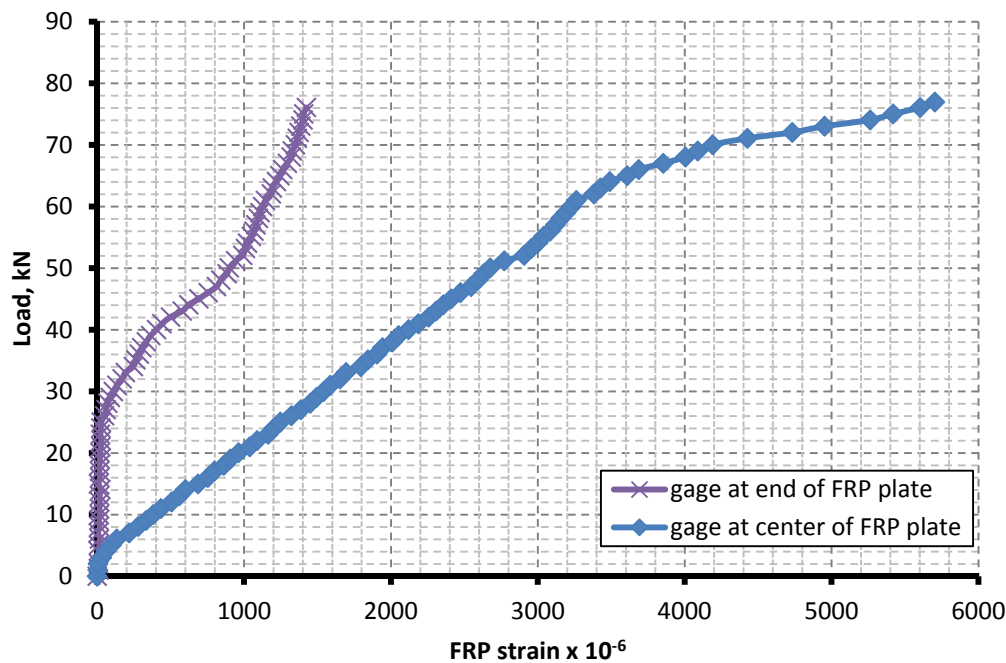
Figure 4-7: Load-CFRP strain for FRP-strengthened RC beam.

Table 4-5: average strian in CFRP plate at differnet applied load.

Specimen	Applied load P (kN)	CFRP-strain at center of CFRP plate ε_{FRP} x 10^{-6}	CFRP-strain at CFRP plate end ε_{FRP} x 10^{-6}
FRP-strengthened RC beam	10	380.80	14.21
	65	3608.64	1243.74
	78.347	6375.38	1539.53

4.2.4   Slip of CFRP plate

To evaluate the slip of CFRP plate; two LVDT's were used one at each side at the end of CFRP plate to measure the slip between CFRP and concrete at the CFRP plate end.

It was observed that the debonding of CFRP plate occurred suddenly at the failure load and the LVDT record only the slip at failure load and failed with debonding of CFRP plate.

4.2.5   Strain variation over the beam depth

In the control specimens, the variation of strain over the beam depth was linear, as shown in Figure 4-8. In the FRP-strengthened RC beam, the measured strain was linear only for small loads. As the load increased up to the beam ultimate capacity, the measured strain variation over the beam depth became nonlinear as shown in Figure 4-8(b). This can be due to the fact that the sliding of the CFRP plate reduced its measured strain. For the ultimate load of FRP-strengthened RC beam the reinforcement strain gage was broken; the diagram did not include the variation of strain along the depth of FRP-strengthened RC beams at ultimate load. The experimental results of strain at mid-span for tested specimens were summarized in Table 4-6.
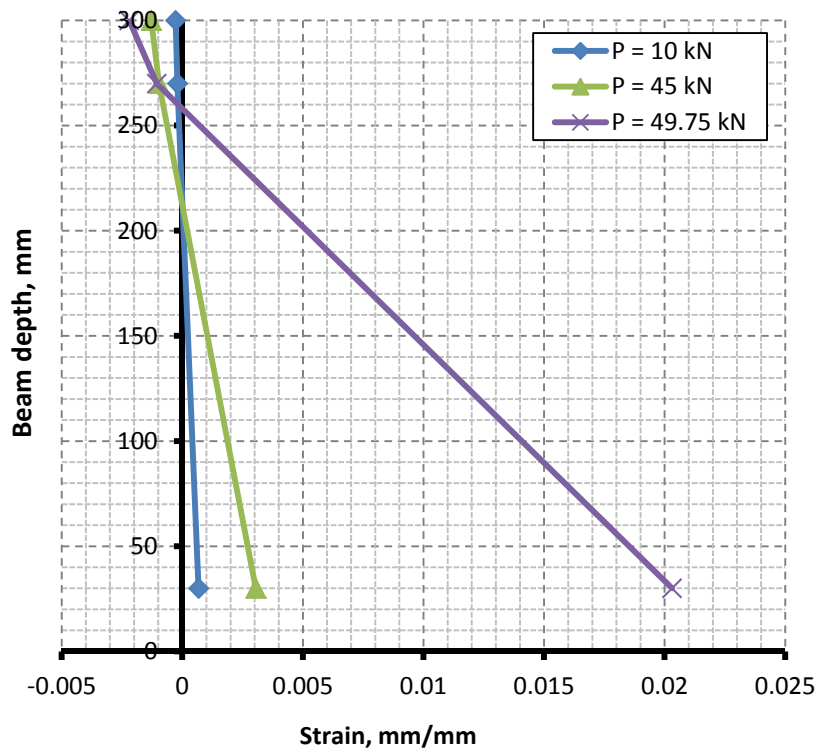
a)   Control beam
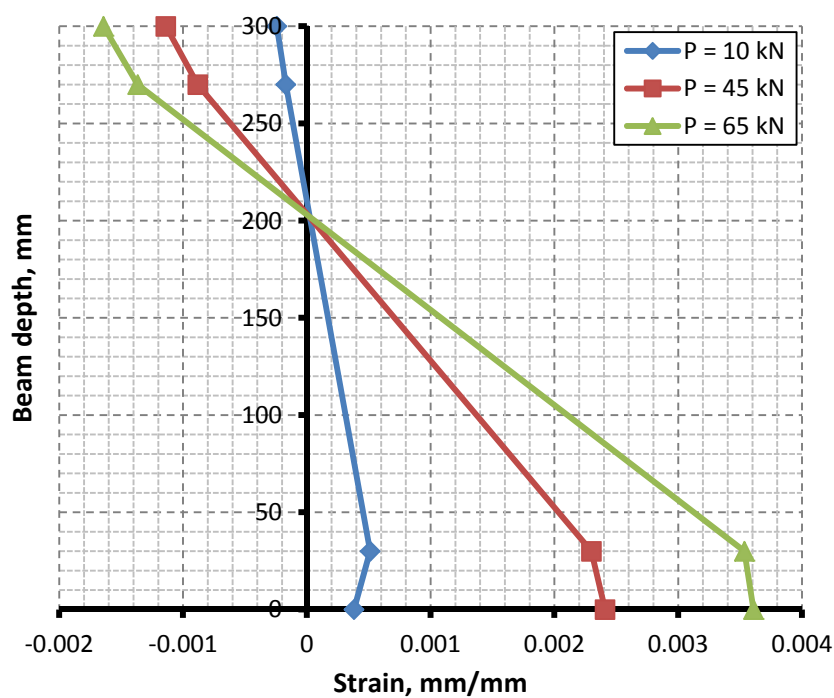
b) FRP-strengthened RC beam

Figure 4-8: strain variation along beam depth at mid-span.

Table 4-6: average strian along beam depth at differnet applied load.

| Specimen | Applied load | Concrete strain | reinforcement strain | | CFRP strain |
	P (kN)	ε_{cc}	Compression ε_{sc} x 10^{-6}	Tension ε_{st} x 10^{-6}	ε_{FRP} x 10^{-6}
Control beam	10	-0.000275	-201.82	675.29	----
	45	-0.00129	-965.85	3044.84	
	49.75	-0.0022	-1059.07	20305.96	
FRP-strengthened RC beam	10	-0.00024	-169.02	511.71	380.80
	45	-0.00114	-881.27	2298.37	2409.31
	65	-0.00164	-1366.08	3534.71	3608.64
	78.347	-0.0024	-1740.27	Strain gage defect	6375.38

4.3   Experimental Results of Part II (Creep test results)

The Part II consisted of two groups were tested under constant load (34% of the ultimate load) in the lab condition to investigate the time dependent behavior (creep) of reinforced concrete beams strengthened with externally bonded carbon fiber reinforced polymer (CFRP) laminates and comparing results with unstrengthened beams.

The first group (control beams; BL1, BL2, and BL3) consisted of three simply supported reinforced concrete beams with dimensions 2900x120x300 mm. The beams were tested in lab conditions under constant load to predict creep behavior of RC beam.

The second group (FRP-strengthened reinforced concrete beams; SBL1, SBL2, and SBL3) consisted of three simply supported reinforced concrete beams with dimensions 2900x120x300 mm strengthened with CFRP laminates bonded to the tension face of these beams. The beams were tested in lab conditions under constant load to investigate the CFRP effect in the creep behavior of strengthened RC beams.

The beams were tested on four point bending. This load case was chosen because it gives constant maximum moment and zero shear in the section between the loads, and constant maximum shear force between support and load. The moment was linearly varying between supports and load.

4.3.1   Long-term deflection

4.3.1.1   Long-term deflection for control beams

The total deflection and creep deflection at mid-span of the control beams under constant load (34% of ultimate load) in the room condition shown in Figure 4-9 and Figure 4-10, respectively. It can be observed that the three specimens nearly had the same long-term deflection. The average value of them for the creep strain was considered in this study. It can be observed that the increase rate of mid-span deflection in the first 90 days was high, and the rate was decreased with the time. The instantaneous deflection δ_o was 5.23 mm and after 90 days the total deflection was, 6.88 mm while after 515 days was 7.80 mm; this means about 64% δ_{cr}, from the 515 days creep strain occurred in the first 3 months. Where $\delta_{total,t} = \delta_o + \delta_{cr,t}$. The experimental result of long-term deflection and creep deflection for control beams during the test was summarized in Table 4-7 and Table 4-8.
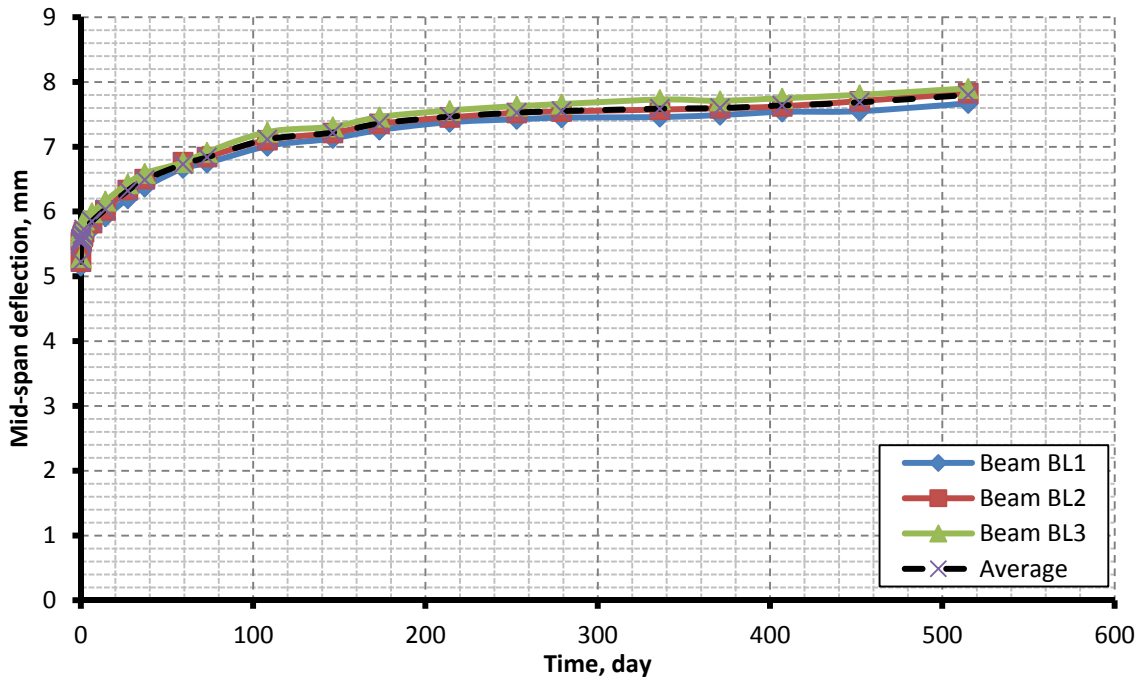
Figure 4-9: long-term total mid-span deflection.
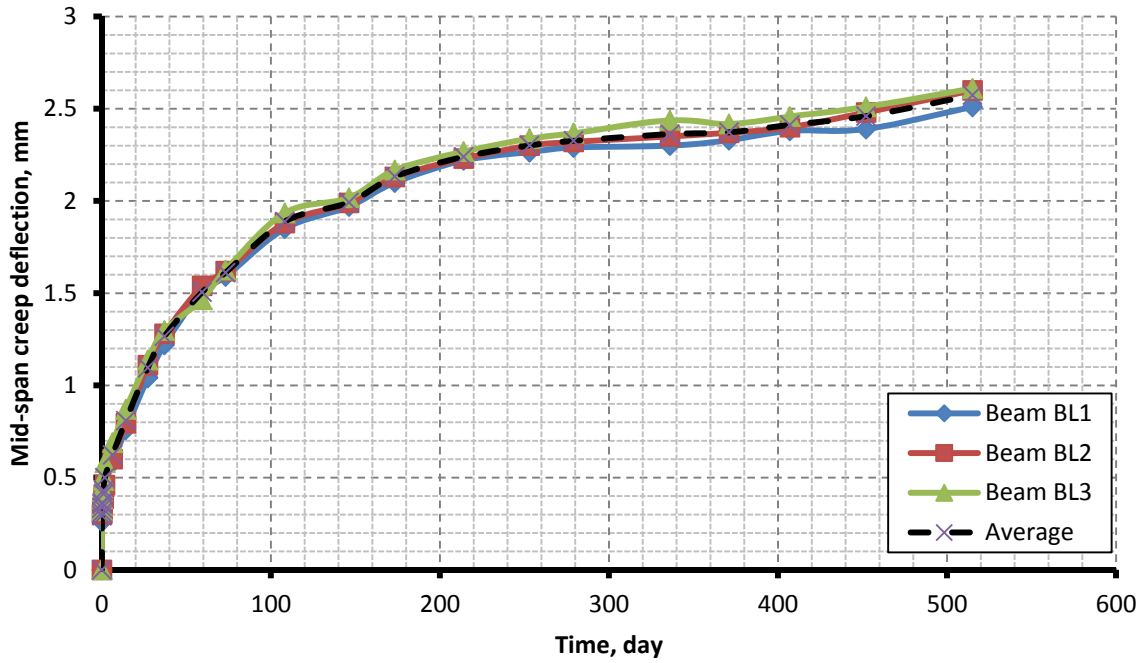
Figure 4-10: long-term creep deflection at mid-span.

68

Table 4-7: long-term total deflection of RC control beams.

Time, day / Specimen	0	30	60	90	180	365	515
BL1	5.16	6.26	6.67	6.88	7.29	7.46	7.67
BL2	5.23	6.4	6.77	6.85	7.38	7.58	7.83
BL3	5.29	6.49	6.76	6.92	7.48	7.63	7.9
Average	**5.23**	**6.38**	**6.73**	**6.88**	**7.38**	**7.58**	**7.80**

Table 4-8: long-term creep deflection of RC control beams.

Time, day / Specimen	0	30	60	90	180	365	515
BL1	0	1.1	1.51	1.72	2.13	2.3	2.51
BL2	0	1.17	1.54	1.62	2.15	2.35	2.6
BL3	0	1.2	1.47	1.63	2.19	2.34	2.61
Average	**0**	**1.15**	**1.5**	**1.65**	**2.15**	**2.35**	**2.57**

4.3.1.2   Long-term deflection for CFRP-strengthened RC beams

The total deflection and creep deflection at mid-span of the FRP-strengthened RC beams under constant load (34% of ultimate load, 53% of control beam ultimate load) in the room condition shown in Figure 4-11 and Figure 4-12, respectively. It can be observed that the three specimens nearly had the same long-term deflection. The average value of them for the creep strain was considered in this study. It can be observed that the increase rate of mid-span deflection in the first 90 days was high, and the rate was decreased with the time. The instantaneous deflection δ_o was 6.38 mm and after 90 days the total deflection was, 8.52 mm while after 515 days was 9.635 mm; this means about 66% δ_{cr}, from the 515 days creep strain occurred in the first 3 months. Where $\delta_{total,t} = \delta_o + \delta_{cr,t}$. The experimental result of long-term deflection and creep deflection for control beams during the test was summarized in Table 4-9 and Table 4-10.
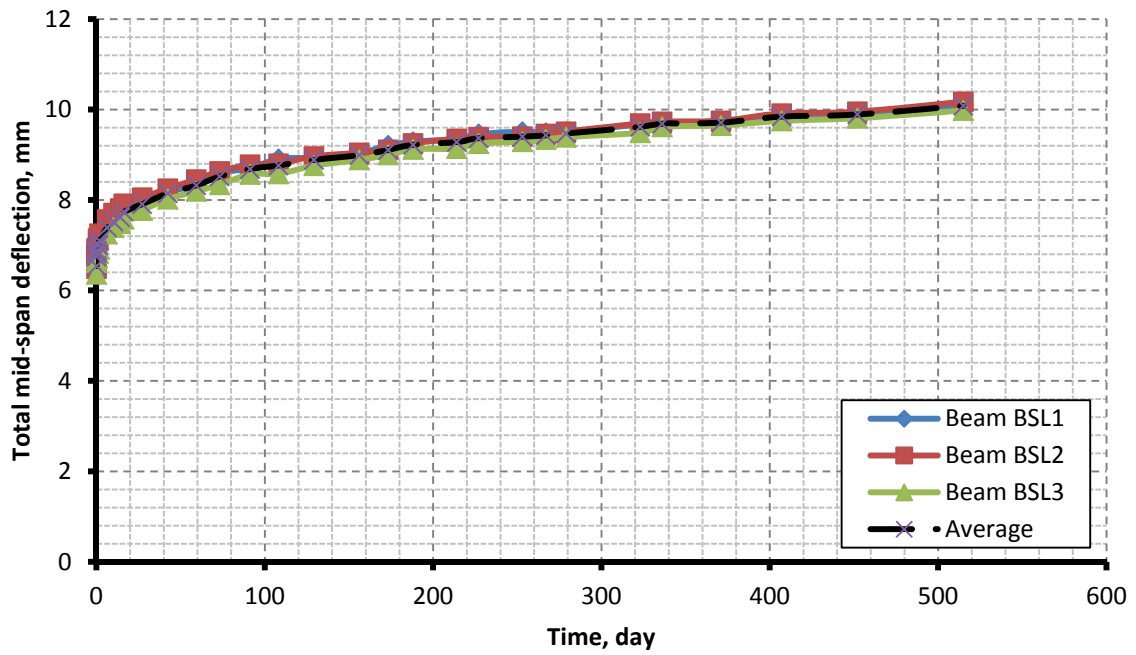
Figure 4-11: long-term total mid-span deflection.
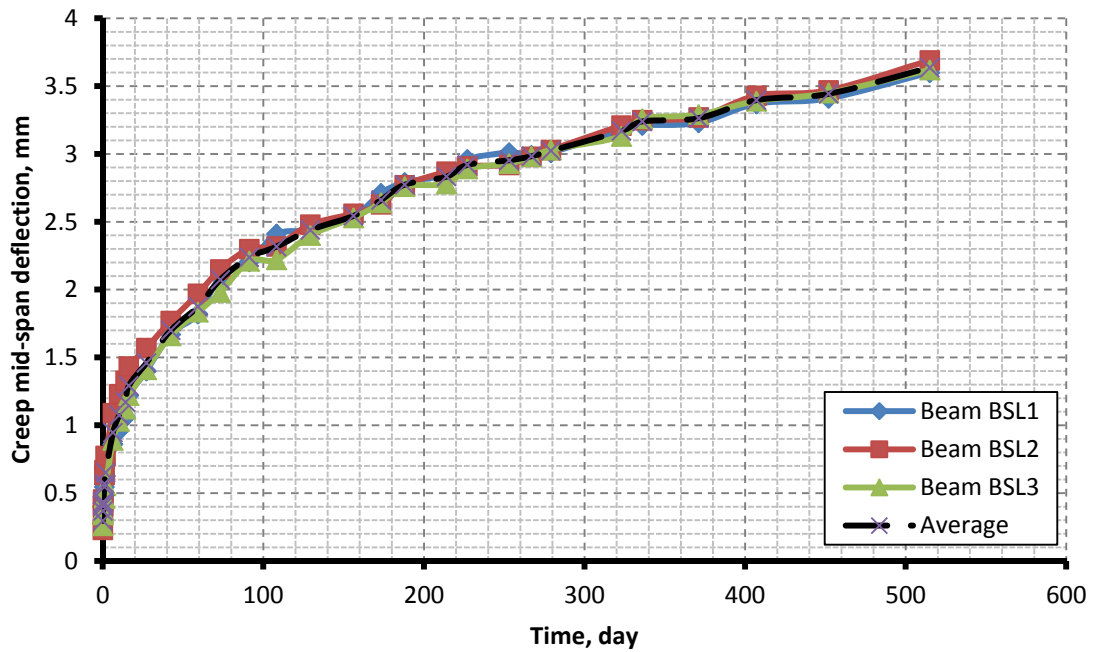
Figure 4-12: long-term creep deflection at mid-span.

Table 4-9: long-term total deflection of FRP-strengthened RC beams.

Time, day / Specimen	0	30	60	90	180	365	515
BSL1	6.5	7.94	8.32	9.25	9.21	9.73	10.1
BSL2	6.485	8.06	8.46	9.19	9.07	9.75	10.175
BSL3	6.36	7.77	8.2	9.05	9.12	9.65	9.98
Average	**6.45**	**7.92**	**8.33**	**9.16**	**9.13**	**9.71**	**10.09**

Table 4-10: long-term creep deflection of CFRP-strengthened RC beams.

Time, day / Specimen	0	30	60	90	180	365	515
BSL1	0	1.44	1.82	2.75	2.71	3.23	3.6
BSL2	0	1.575	1.975	2.705	2.585	3.265	3.69
BSL3	0	1.41	1.84	2.69	2.76	3.29	3.62
Average	**0**	**1.48**	**1.88**	**2.72**	**2.69**	**3.26**	**3.64**

4.3.1.3   *Creep deflection comparison*

The Figure 4-13 and Figure 4-14 shows the creep deflection at mid-span for average control and CFRP-strengthened RC beams; it can observed that the applied load for FRP-strengthened RC beam was more than that for control beam with 53% while the increase in creep deflection was 23%; and the increase in total deflection with the same value 23% while the increase in initial deflection 22%; this mean that the rate of creep deflection proportional to the initial deflection and increase with the same rate. In the other hand for the same applied load to control beam or CFRP-strengthened RC beams; from the experimental test result for Part I the initial deflection for the CFRP-strengthened RC beams was smaller than that for control beam this will decrease the creep deflection of the CFRP-strengthened RC beams due to the effect of using CFRP plate for strengthening the RC beam.

And for increasing the control beam applied load up to 53% from ultimate load the initial deflection will increase and the creep deflection will increase to be more than that for CFRP-strengthened RC beam.
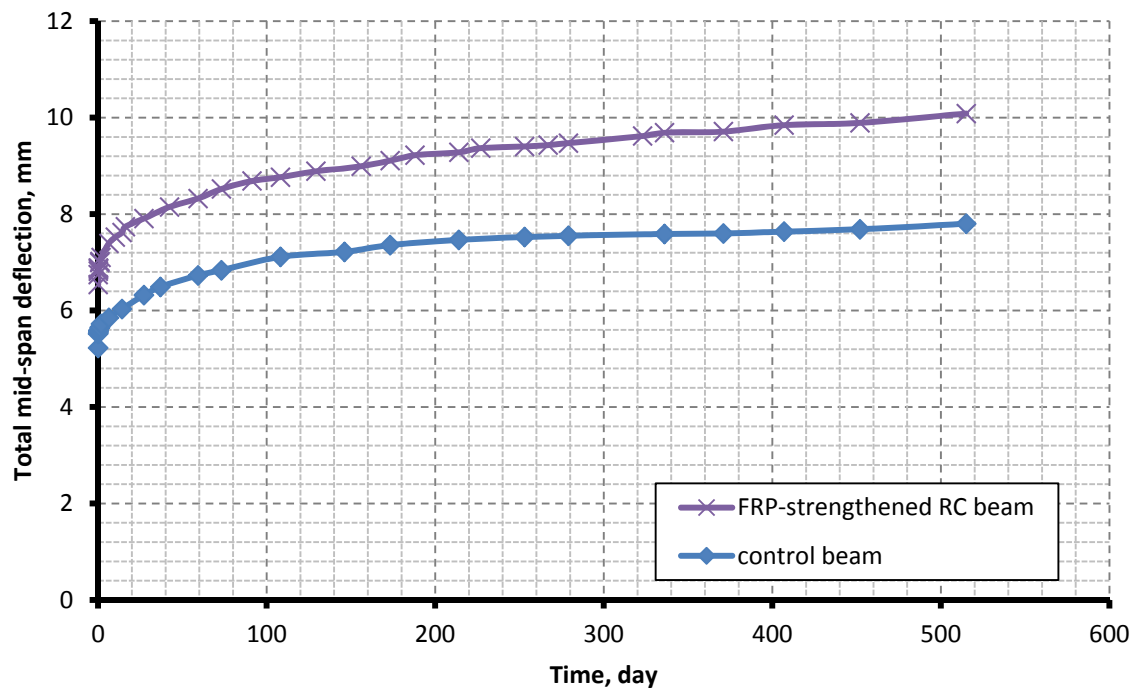
Figure 4-13: long-term total mid-span deflection.
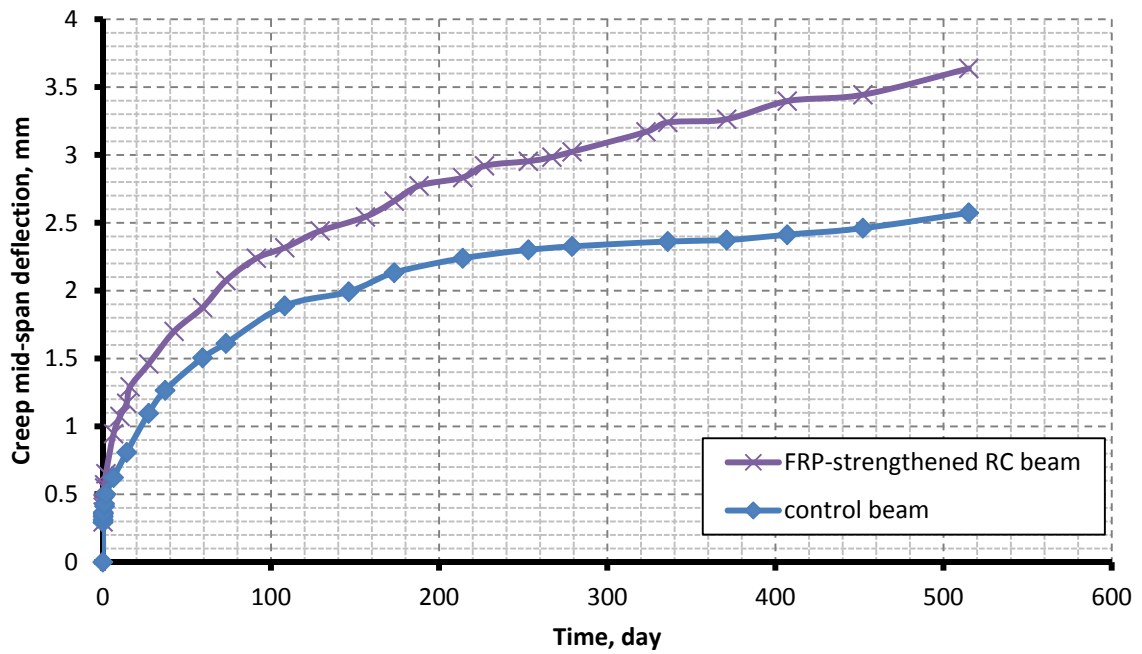
Figure 4-14: long-term creep deflection at mid-span.

4.3.2   Long-term CFRP-strain at mid-span

The initial strain at the mid-span of the CFRP plate for the average of the three tested specimen was 1449.49×10^{-6} mm/mm after applying the load; while after 90 days it was 1621×10^{-6} mm/mm, and after 515 days from loading it was 1717.43×10^{-6} mm/mm. The total long-term CFRP-strain at the mid-span of the CFRP plate increased due to creep by about 18.5% in 515 days. It can be observed that 65 % from the creep strain at 515 days occurred in the first 90 days. The CFRP creep strain versus time relationship shown in Figure 4-15 and the experimental test results for the average of the three specimens were summarized in Table 4-11.
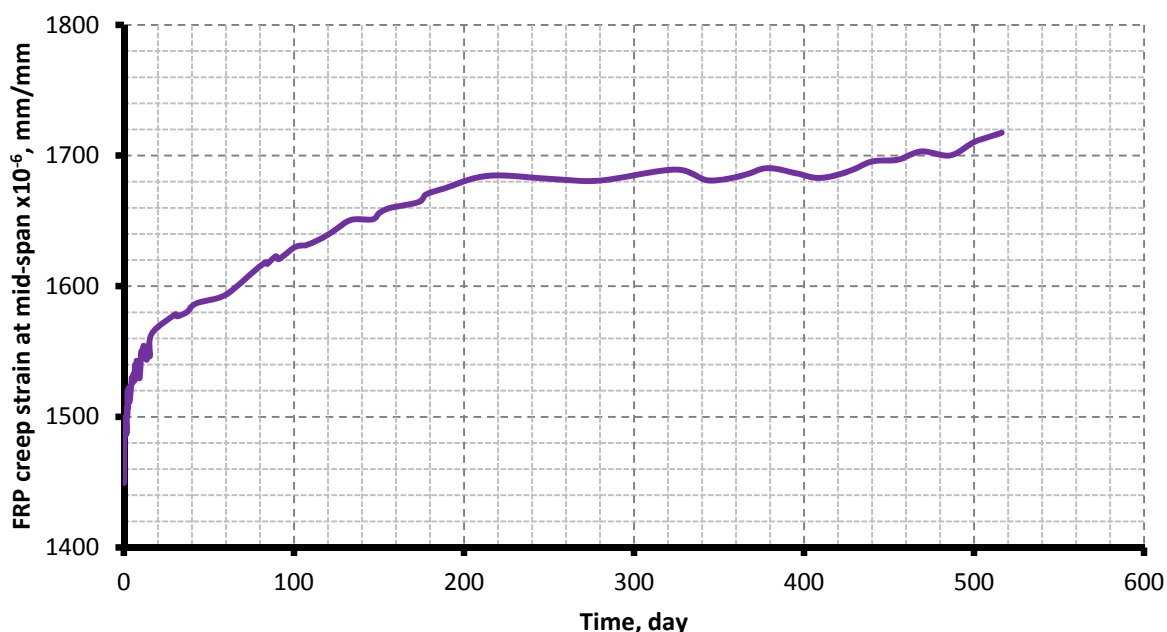
Figure 4-15: long-term CFRP creep strain at mid-span.

Table 4-11: long-term total CFRP-strain at mid-span of FRP-strengthened RC beams $(\varepsilon_{frp} \times 10^{-6})$.

Time, day Specimen	0	30	60	90	180	365	515
Average CFRP-strengthened RC beam	1449.49	1578.53	1593.06	8.52	1621	1684.88	1717.43

73

4.3.3   Long-term reinforcement steel bars strain at mid-span

The long-term strain at mid-span of the reinforcement steel bars in tension and compression of the test specimens shown in Figure 4-16; it can be observed that the difference in the creep strain of the reinforcement in the tension side is very small while the applied load of the FRP-strengthened RC beams is higher that of the control beams with 53% because of the CFRP plate in the tension increase the stiffness of the beams and the CFRP carried the additional tension stress. While in the compression side the creep strain in the FRP-strengthened RC beams was higher than that of the control beams as expected.
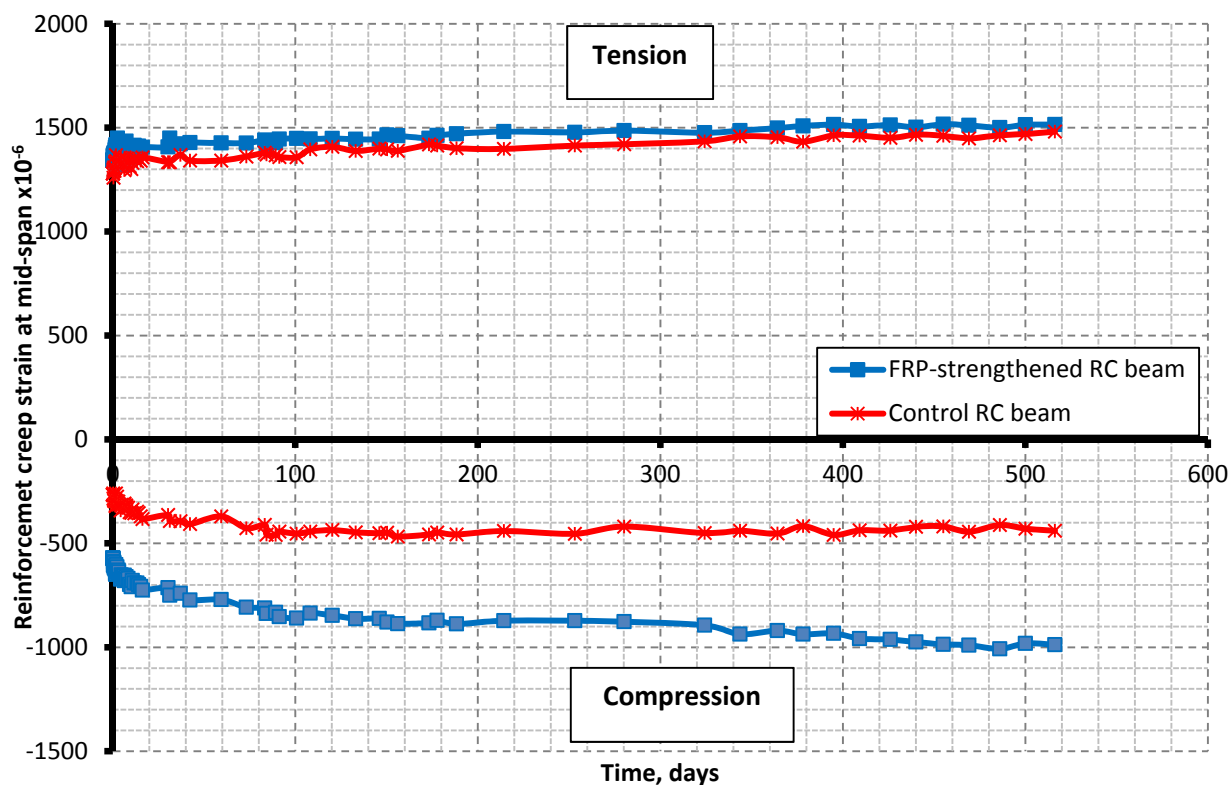
Figure 4-16: long-term reinforcement steel bars strain at mid-span in tension and compression.

The experimental test results for the average of the three controls and FRP-strengthened RC beams specimens summarized in Table 4-12 and Table 4-13.

Table 4-12: long-term tension reinforcement steel bars-strain at mid-span of tested beams (ε_s x10^{-6}).

Time, day Specimen	0	30	60	90	180	365	515
Control RC beam	1280.57	1333.87	1343.23	1359.15	1401.43	1432.73	1475.40
Average CFRP-strengthened RC beam	1343.29	1407.56	1425.59	1444.79	1470.39	1508.30	1503.87

Table 4-13: long-term compression reinforcement steel bars-strain at mid-span of tested beams (ε_s x10^{-6}).

Time, day Specimen	0	30	60	90	180	365	515
Control RC beam	265.95	392.59	426.72	443.34	457.01	458.90	469.71
Average CFRP-strengthened RC beam	570.80	749.75	807.19	852.83	887.36	937.02	973.42

4.3.4   Long-term CFRP slip

To evaluate the slip of CFRP plate; two watch-gages were used one at each side at the end of CFRP plate to measure the slip between CFRP and concrete at the CFRP plate end.

During the test duration there is no change was observed.

4.3.5   Long-term concrete strain

The creep strain in concrete in compression and tension were evaluated using two watch-gages; one in tension and one in compression side, it was observed a thin cracks in the tension side of every specimen. The crack width in the tension side can be evaluated using the watch-gage and the number of cracks between the distance of the two points of the gage. It was observed that one thin crack was produced between the measuring two points and the initial crack width was about 0.185 mm for control beams and 0.165 mm for FRP-strengthened RC beams.

The creep concrete strain for control beams is little higher than that of CFRP-strengthened RC beam as shown in Figure 4-17.
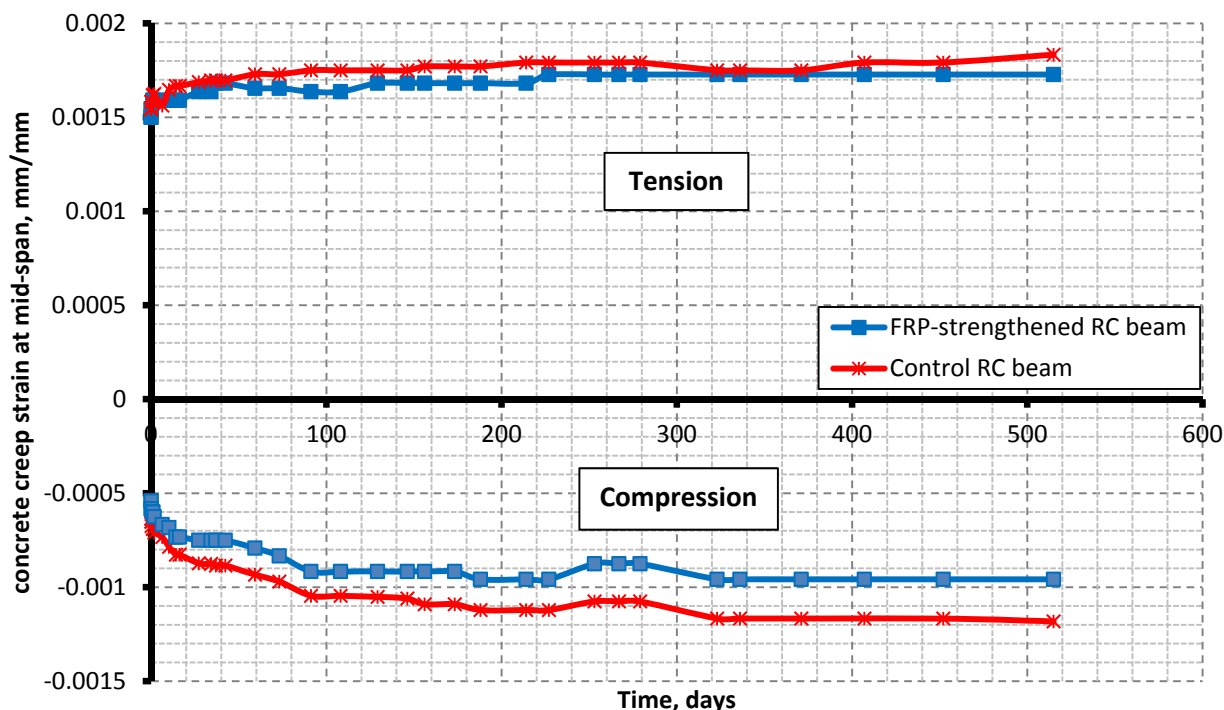
Figure 4-17: long-term concrete strain at mid-span in tension and compression.

4.4 Summary of experimental analysis

In this chapter, an experimental program consists of twelve full dimensioned specimens (six reinforced concrete beams, and six CFRP-strengthened reinforced concrete beams) was constructed and tested to investigate the flexural and long-term behavior of CFRP-strengthened RC beams . These specimens were divided into two parts; Part I was tested to investigate the flexural behavior of the CFRP-strengthened RC beams, while Part II was tested to investigate the long-term behavior of CFRP-strengthened RC beams. The results obtained from the tested specimens were plotted and analyzed and the following can be drawn:

➢ The ultimate flexural capacity and the total ultimate deflection of the CFRP-strengthened RC beams were increased by about 50% and 64% respectively compared to unstrengthening beams due to increasing in the stiffness of the strengthening system, while the cracks width in the tension face of the RC beam was limited due to strengthening with externally bonded CFRP plate. The increasing in ultimate capacity depends on the CFRP length and breadth.

➢ Most of the creep occurs in the first 90 days from applying load. The total deflection after one year was increased by about 55 % from the immediately deflection due to the effect of the creep of the system.

➢ The increasing in creep deflection was proportional to the load level and with nearly the same increasing value of the applied load level which means there was no significant effect of the Strengthened RC beams externally by CFRP on the creep deflection because the creep of CFRP and epoxy was very small and can be neglected compared to the creep of the concrete.

➢ There is no slip observed between CFRP and concrete, and the cracks width is limited in the tension side of the strengthened RC beam due to the effect of externally bonded CFRP in increasing the stiffness of the beams.

The effect of CFRP length/breadth, the epoxy type, compressive strength, reinforcement ratio, and CFRP ratio on the behavior of the strengthening system is some of the parameters used to investigate the flexural behavior of the strengthening beams in the next chapter using the Abaqus finite element modeling program. While the effect of CFRP, epoxy type, and temperature of different types of epoxy interface are used to investigate the long-term behavior of the strengthening system using the calibrated model.

Chapter 5   Finite Element Modeling of long-term behavior

5.1 Introduction

This chapter presents the finite element model built to simulate flexural and creep behavior of CFRP-strengthened reinforced concrete beams tested experimentally in chapter 3, the detail of the CFRP-strengthened RC beam and the controlled RC beam are shown in Figure 5-1. The FE model is used to perform the parametric study to predict the flexural and creep of the CFRP-strengthened reinforced concrete beams.

In this approach, the finite element (FE) computer program (Abaqus , 2010), was used to perform a failure analysis and suppositions of the power law creep model of rectangular reinforced concrete beams strengthened by externally bonded CFRP plate under flexural; and to verify the integrity of the numerical results by comparing them with those obtained experimentally. According to the symmetry of the beam; a quarter of three-dimensional finite element model was developed to reduce the computational time required for the analysis of the long-term behavior of the CFRP-strengthened RC beams under flexural load.
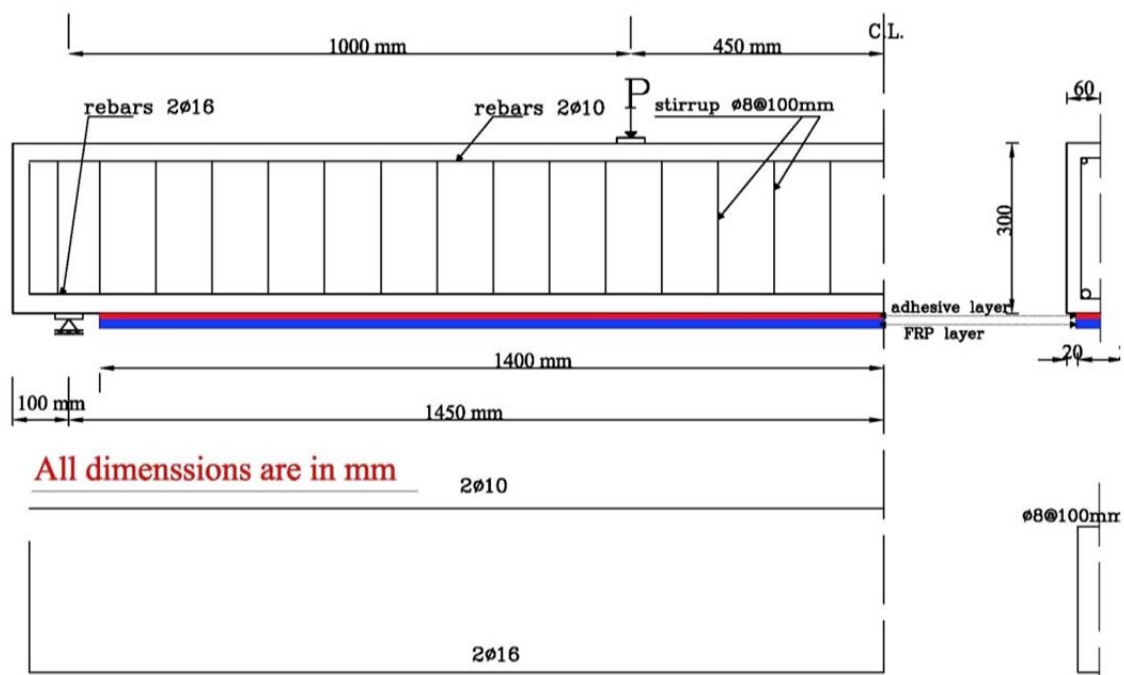
(a) FRP strengthened RC beam used for FEM

(b)   control RC beam used for FEM
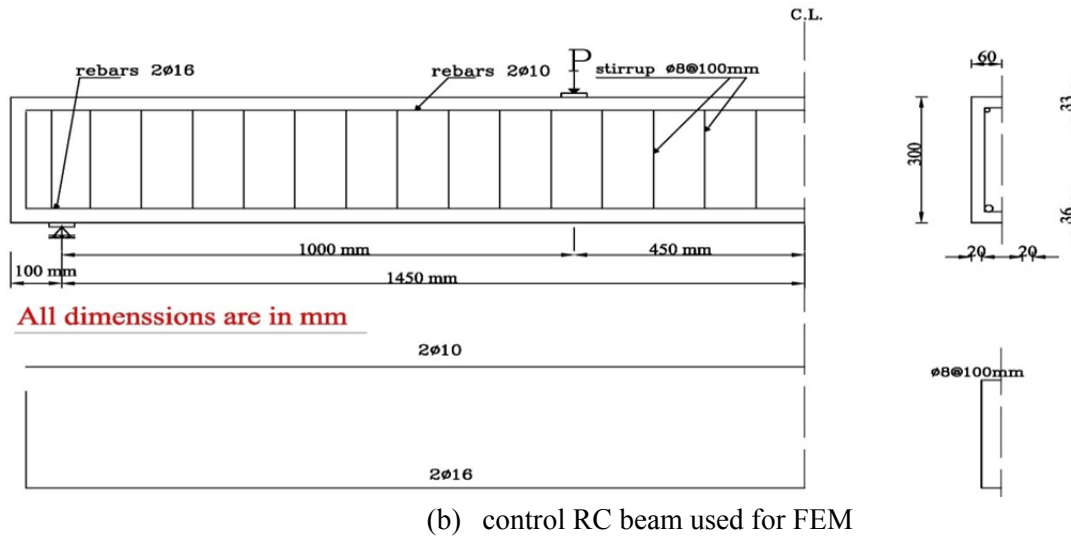
Figure 5-1: details of specimens used in FE model.

To study the long-term behavior of CFRP-strengthened reinforced concrete beams, numerical model includes the nonlinear behavior of the constitutive materials; reinforcement bars, concrete, epoxy adhesive and CFRP, separately was developed to investigate the ultimate capacity of the CFRP-strengthened RC beams and validate the model by comparing the results obtained from the finite element model with the results obtained from the experimental program. The calibrated model will be used to predict the long-term behavior of the CFRP-strengthened RC beams under service load.

Numerical analysis of reinforced concrete structures is customarily performed by static implicit FE solvers where the integration scheme is for example full Newton–Raphson. The solution is obtained from equilibrium iterations minimizing the error of the solution. The outcome is a reliable and stable solution.

5.2   Creep Modeling by Abaqus

(Abaqus , 2010) FE program was used to model the creep behavior of CFRP strengthened reinforced concrete beam using the power law. There were two types of creep model with power low; first one is the time hardening form of power law creep model (Equation (5-1)) which is used when the stress state remains essentially constant during analysis; and the second type is strain hardening equation of power law creep model (Equation (5-2)) which is used when the stress state varies during analysis, (Abaqus online documentation v 6.10.1).

$$\dot{\bar{\varepsilon}}_{cr} = A\tilde{\sigma}^n t^m \tag{5-1}$$

$$\dot{\bar{\varepsilon}}_{cr} = (A\tilde{\sigma}^n[(m+1)\bar{\varepsilon}_{cr}]^m)^{\frac{1}{m+1}} \tag{5-2}$$

79

Where, $\dot{\bar{\varepsilon}}_{cr}$ is the uniaxial equivalent creep strain rate; σ is the uniaxial equivalent deviatoric stress, $\bar{\varepsilon}_{cr}$ is the equivalent creep strain, and A, n, m are user defined parameters; these constants are defined according to experimental data.

The time hardening form was used in this study, it is available in Abaqus FE program. To model the creep behavior of CFRP-strengthened reinforced concrete beams the parameters A, n, and m are required for every materials used in finite element model.

In order to obtain the values of A, n, and m; the equation (5-1) was integrated with respect to time and the creep strain can be expressed as the following equation:

$$\varepsilon_{cr} = A\sigma^n \frac{t^{m+1}}{m+1} \tag{5-3}$$

In a simplified way the equation (5-3) can be written as following:

$$\varepsilon_{cr} = M_o t^{m1} \tag{5-4}$$

Where $M_o = \frac{A\sigma^n}{m+1}$, and $m_1 = m+1$

Therefore the M_o parameter can be written as:

$$M_o = M_1 \sigma^n \tag{5-5}$$

And $M_1 = \frac{A}{m+1}$

To obtain the parameters in equation (5-5) M_1 and n, the Logarithmic function (LN-function) is used and the equation (5-6) can be written as follow:

$$\ln(M_o) = \ln(M_1) + n \ln(\sigma) \tag{5-6}$$

By using the curve fitting option in excel; the relationship between LN(M_o) and LN(σ) was drawn and the equation of the fitting curve was used to get A and n.

This expression was used to obtain the constants for reinforced concrete, epoxy, and CFRP using results from creep test and using the curve fit tool to obtain these parameters.

5.3 Material properties and constitutive models

The materials used in the analysis are the concrete, steel reinforcing bars, epoxy adhesive, and CFRP. Abaqus material library included most of reliable constitutive models applicable for these materials. Therefore, the input material properties and associated constitutive models are only discussed.

The material properties was divided into two parts; first part was used for estimate the flexural behavior of the CFRP-strengthened RC beams up to failure to insure that the model will match the experimental results for the ultimate capacity and can be used for predicting the long-term behavior of the CFRP-strengthened RC beams. Furthermore, the second part was used to estimate the creep parameters for those materials to use these parameters in the input file of the calibrated model to predict the long-term behavior of the CFRP-strengthened RC beams under service flexural load.

5.3.1   Reinforced Concrete Model

To model the creep of the reinforced concrete material; first it should be understood the behavior of concrete and reinforced steel bars until failure and after that the creep parameters of the reinforced concrete material will be estimated using the Abaqus creep modeling approach.

5.3.1.1   Concrete Model

A concrete damage plasticity model is used in this study to present the inelastic behavior of concrete. The model is based on the scalar plastic damage models proposed by Lubliner J, et al., (1989) and by Lee J & Fenves LG., (1998). It assumes that the two main failure mechanisms of the concrete are tensile cracking and compressive crushing of the concrete material. Both of these phenomena are the result of micro-cracking. The evolution of the yield (or failure) surface is determined by two hardening variables, $\tilde{\varepsilon}_t^{pl}$ and $\tilde{\varepsilon}_C^{pl}$, each of them linked to degradation mechanisms under tensile or compressive stress conditions, as shown in Figure 5-2. If E_o is the initial elastic stiffness of the material, the stress-strain relations under uniaxial tension and compression loading are as follow, respectively:

$$f_t = (1 - d_t)E_0\big(\varepsilon_t - \tilde{\varepsilon}_t^{pl}\big) \tag{5-7}$$

$$f_c = (1 - d_c)E_0\big(\varepsilon_c - \tilde{\varepsilon}_c^{pl}\big) \tag{5-8}$$

Where the subscripts t and c refer to tension and compression, respectively; $\tilde{\varepsilon}_t^{pl}$ and $\tilde{\varepsilon}_C^{pl}$, are the equivalent plastic strains. The degradation of the elastic stiffness is characterized by two damage variables, d_t and d_c, which are assumed to be functions of the plastic strains, temperature, and field variables.

Particular details of the mathematical implementation of these ideas are given by Lubliner J, et al., (1989), and modified by Lee J & Fenves LG., (1998). The basic parameters required by this formulation are as follows:

$$f_t = f_t(\tilde{\varepsilon}_t^{pl}, \dot{\tilde{\varepsilon}}_t^{pl}, \theta, f^\alpha)$$
$$d_t = d_t(\tilde{\varepsilon}_t^{pl}, \theta, f^\alpha); \qquad 0 \le d_t \le 1$$
$$\bar{f}_t = f_t/(1 - d_t)$$

a) tension

$$f_c = f_c(\tilde{\varepsilon}_c^{pl}, \dot{\tilde{\varepsilon}}_c^{pl}, \theta, f^\alpha)$$
$$d_c = d_c(\tilde{\varepsilon}_c^{pl}, \theta, f^\alpha); \qquad 0 \le d_c \le 1$$
$$\bar{f}_c = f_c/(1 - d_c)$$
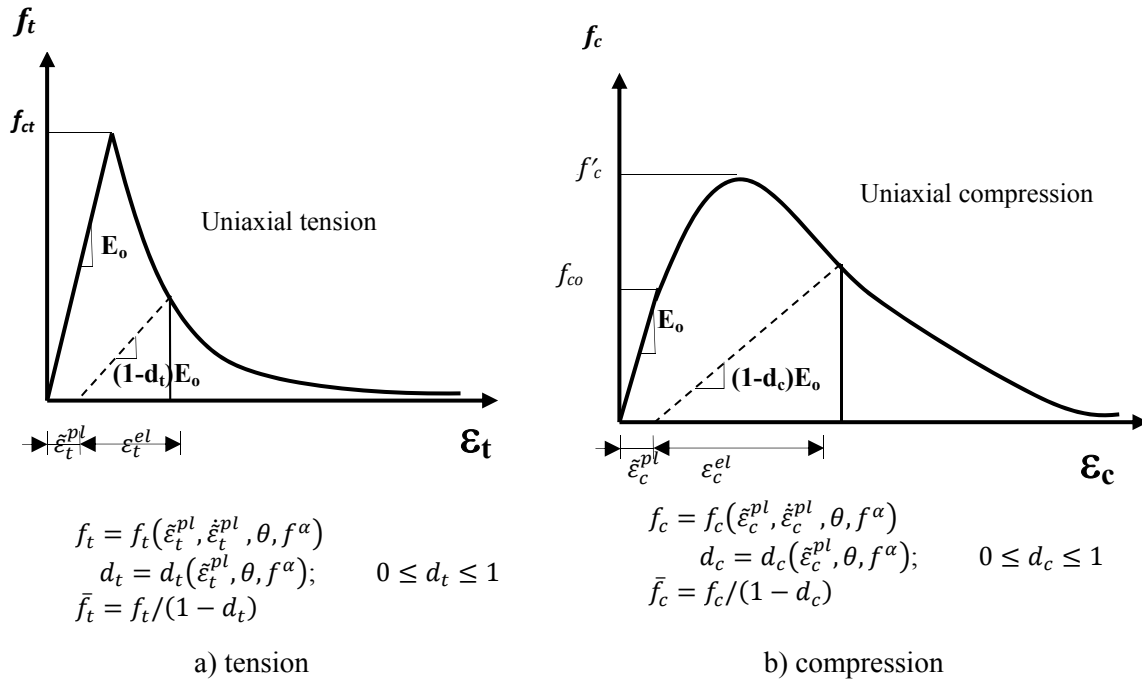
b) compression

Figure 5-2**:** Concrete behavior under uniaxial loading in a) tension b) compression, (ABAQUS 6.10-1, 2010)

5.3.1.1.1 The stress–strain curve of concrete under uniaxial compression

The stress-strain relationship for the concrete under uniaxial compression, (Eurocode 2, 1992), (CEB-FIP Model Code, 1990) recommendations, and (Saenz, 1964) shown in Figure 5-3. For this model, a uniaxial nonlinear stress-strain relationship proposed by (Saenz, 1964) was used as a basic stress-strain curve, and linear behavior was assumed up to $f_{co} = 0.4$ f'_c (f_{co} is the critical stress; $f_{co} = 0.4 f'_c$; (Eurocode 2, 1992)); which may be associated with the stress at which the volumetric strain reaches its maximum (Lubliner J, et al., 1989); f'_c is the compressive strength , and E_c is the modulus of elasticity.

(a) Eurocode 2, 1992/CEB-FIP Model Code, 1990

$$\sigma_C = f_c' \left[\frac{k\eta_c - \eta_c^2}{1+(k-2)\eta_c} \right]$$

$E_c = 9500(f_c')^{1/3}$

$\varepsilon_o = 0.0022$ $\varepsilon_{cu} = 0.0035$

(b) Saenz, 1964

$$\sigma_C = \frac{E_c\varepsilon_c}{1+(R+R_E-2)\left(\frac{\varepsilon_c}{\varepsilon_o}\right)-(2R-1)\left(\frac{\varepsilon_c}{\varepsilon_o}\right)^2+R\left(\frac{\varepsilon_c}{\varepsilon_o}\right)^3}$$

$E_c = 4700\sqrt{f_c'}$

$\varepsilon_o = 1.71\frac{E_c}{f_c'}$ $\varepsilon_{cu} = 0.0035$
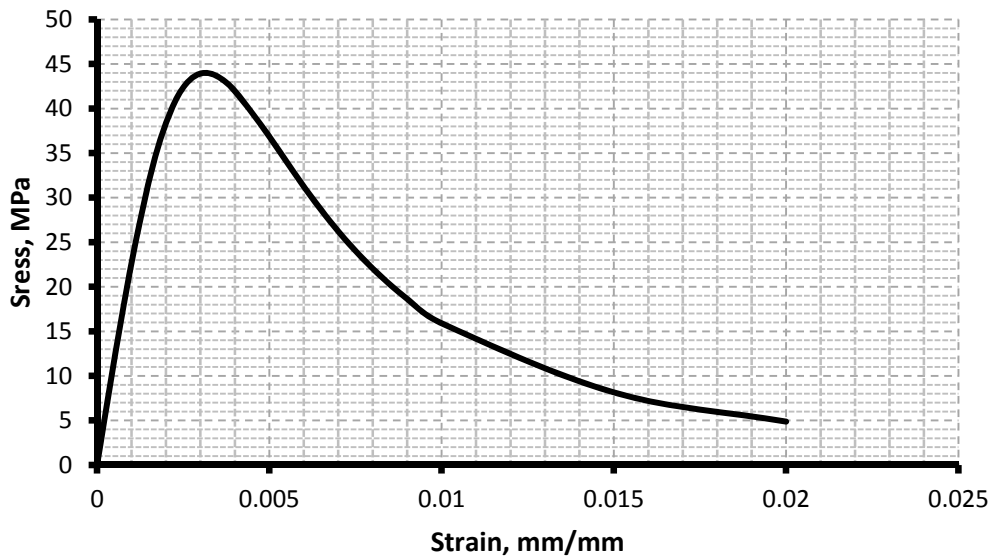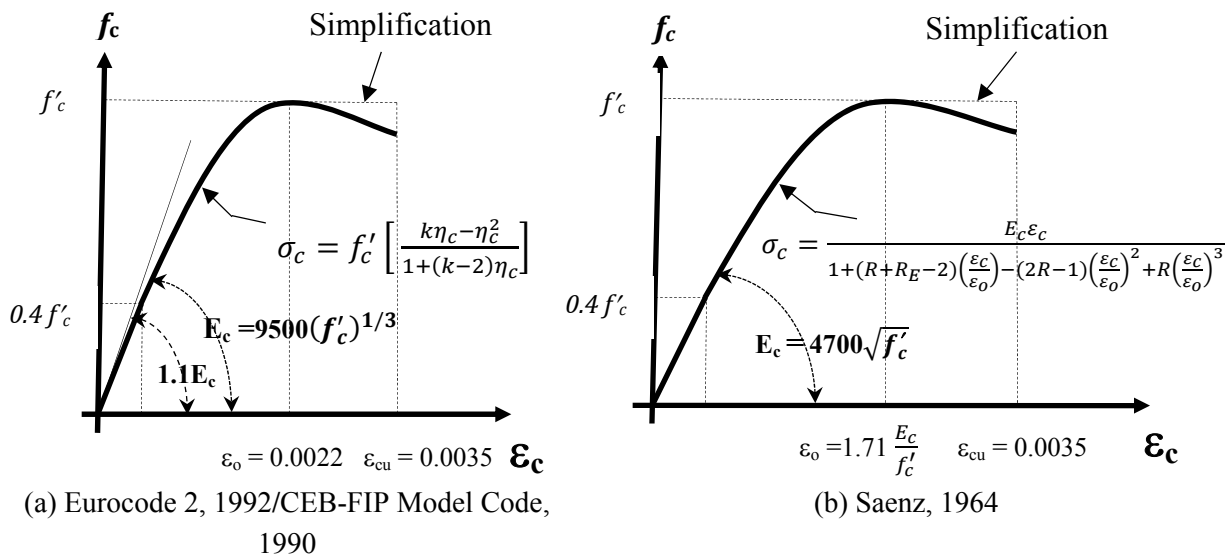
(c) concrete stress-strain curve used in this study

Figure 5-3**:** Stress-strain behavior of concrete under uniaxial compression

The Poisson's ratio ($\nu_c = 0.20$ is recommended in this study) controls the volume changes of concrete for stresses below the critical stress level, f_{co} (in the elastic region). The value of this parameter assumed to be 0.2 in this study. After the critical stress level is reached, the concrete exhibits an increase in plastic volume under pressure (Chen W-F., 1982). The angle of dilatancy ($\psi = 38°$ is recommended in this study) is the parameter used to model this behavior (in the inelastic region).

For non-linear analysis, the stress-strain (f_c-ε_c) relation for concrete in compression from Figure 5-3(b) is recommended by (Saenz, 1964). The model is defined by the following form:

$$f_c = \frac{E_c \varepsilon_c}{1 + (R + R_E - 2)\left(\frac{\varepsilon_c}{\varepsilon_o}\right) - (2R - 1)\left(\frac{\varepsilon_c}{\varepsilon_o}\right)^2 + R\left(\frac{\varepsilon_c}{\varepsilon_o}\right)^3} \qquad (5\text{-}9)$$

Where, f_c' is the compressive strength, and E_c is the elastic modulus of concrete which is calculated according to (ACI Committee 318, 1999) Equation *(5-10)* :

$$E_c = 4700\sqrt{f_c'} \qquad (5\text{-}10)$$

And ε_o was calculated according to Equation (5-11) by (MacGregor, 1997)

$$\varepsilon_o = 1.71\frac{E_c}{f_c'} \qquad (5\text{-}11)$$

Where,

$$E_o = \frac{f_c'}{\varepsilon_o} \qquad (5\text{-}12)$$

and

$$R_E = \frac{E_c}{E_o} \qquad (5\text{-}13)$$

And R was calculated according to Equation *(5-14)*:

$$R = \frac{R_E(R_\sigma - 1)}{(R_E - 1)^2} - \frac{1}{R_E} \qquad (5\text{-}14)$$

Where $R_E = R_\sigma = 4$ were used as reported by (Hu & Schnobrich, 1989)

5.3.1.1.2 The softening curve of concrete under uniaxial tension

For the concrete in tension, tensile strength, f_{ct}, can be obtained from the splitting test results [12], and the fracture energy, G_F, can be calculated from the load deflection behavior of notched concrete beams; once the parameters (f_{ct}, G_F) is available, then the softening curve for concrete can be determined. Otherwise, it is important to estimate these parameters.

Hillerborg, et al., (1976) suggested a linear softening curve for concrete tension behavior, as shown in Figure 5-4(a), and proposed a crack opening width, w_c, of 0.01~0.02 mm based on experiments. The (CEB-FIP Model Code, 1990) and (Hillerborg, 1985) proposed a bilinear curve, as shown in Figure 5-4(b) & (c). FE analyses were performed in the current study using these three types of tension stiffening model, but there was almost no difference in term of overall load-deflection behavior between different tension stiffening

models. Therefore, the bi-linear tension stiffening model proposed by Hillerborg, (1985) was adopted in the further simulation.

(a) Hilleborg model (1976)

(b) CEB-FIP model (1990)

(c) Hilleborg model (1985)
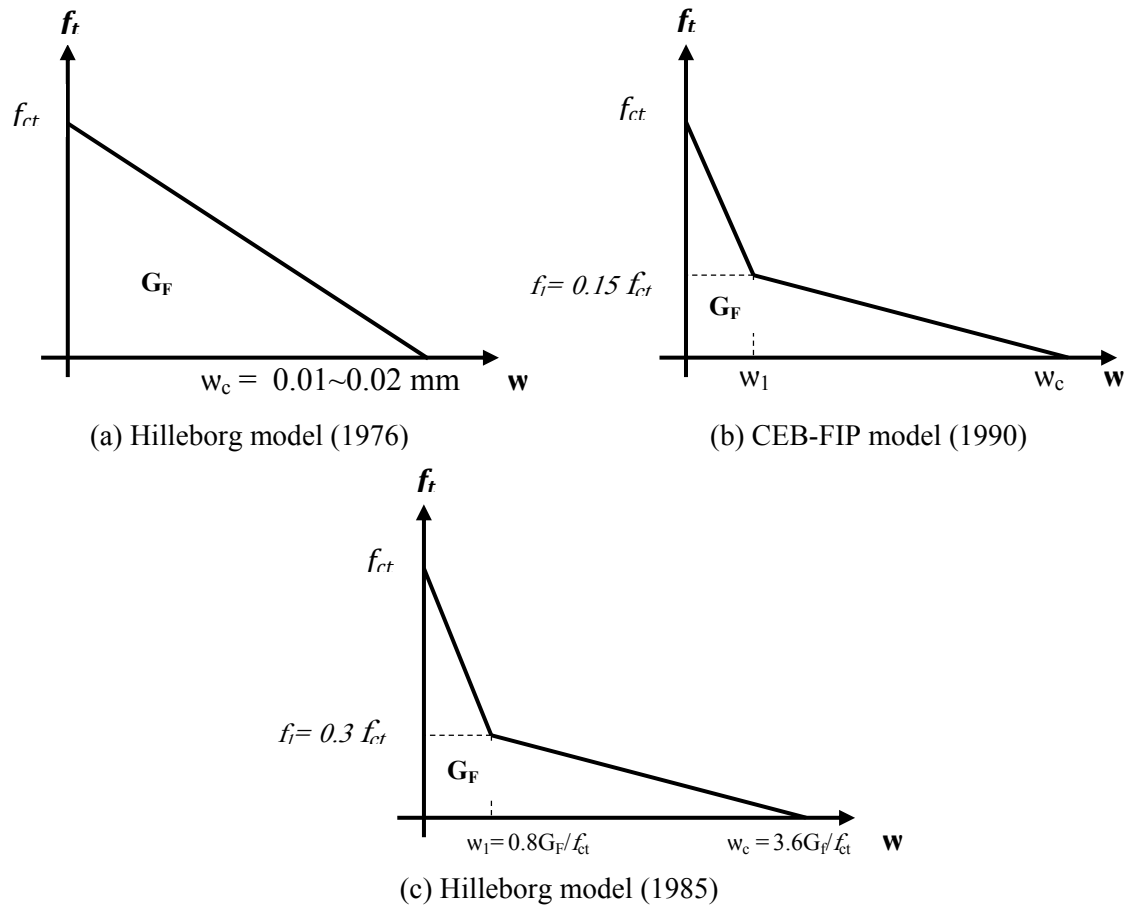
Figure 5-4: Concrete tension stiffening models

f_{ct} (MPa) is the tensile strength of the concrete which can be estimated from equation (5-15), (ACI Committee 318, 1999)

$$f_{ct} = 0.35\sqrt{f_c'} \qquad (5\text{-}15)$$

And the parameter associated with the softening part of the curve is fracture energy, G_F (N/m). The fracture energy for mode I, G_F (N/m), is the area under the softening curve and is according to (CEB-FIP Model Code, 1990), (Bazant ZP & Becq-Giraudon E, 2002) estimated as equation (5-16)

$$G_F = G_{F0}\left(\frac{f_c'}{f_{co}}\right)^{0.7} \qquad (5\text{-}16)$$

Where, f_c' (MPa) is the concrete compressive strength, f_{co} =10 MPa, and G_{F0} (N/mm) is base value of fracture energy which depends on maximum aggregate size d_{max}(mm), G_{F0} = 0.025, 0.030, 0.038 for d_{max}(mm) = 8, 16, and 32 respectively.

Once these parameters (f_{ct},G_F) have been determined, different analytical expressions can be used to approximate the softening curve.

The mechanical properties of concrete used in this study shown in Table 5-1.

Table 5-1: mechanical properties of concrete

Compressive strength, f'_c (MPa)	44
Modulus of elasticity, E_c (MPa)	23941
Tensile strength, f_{ct} (MPa)	2.6
Poisson's ratio, v	0.2
Angle of dilatancy	38
Ultimate strain (%)	0.0035
Fracture energy G_F (N/mm)	0.079

5.3.1.2   Steel reinforcing bar Model

The constitutive behavior of steel is predicted using an elastic perfectly plastic model, as described in (Abaqus , 2010). In this approach, the steel behavior is elastic up to when the yield stress is reached. At this point, the material yields under constant load (Figure 5-5). The parameters required by this formulation are the modulus of elasticity (E_s = 200 GPa), Poisson's ratio (v=0.3) and yield stress (f_{sy} = 490 MPa).

A two-node truss element was used for modeling the steel reinforcement (main reinforcement, compressive reinforcement, and stirrups) as shown in Figure 5-6. This element was embedded to the concrete assuming that there is a perfect bond between the concrete and steel reinforcement.
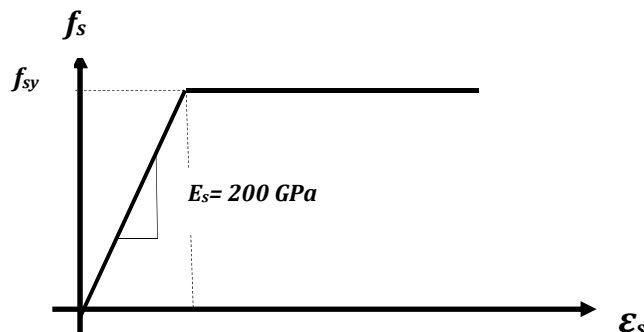
Figure 5-5: Stress-strain relationship for steel
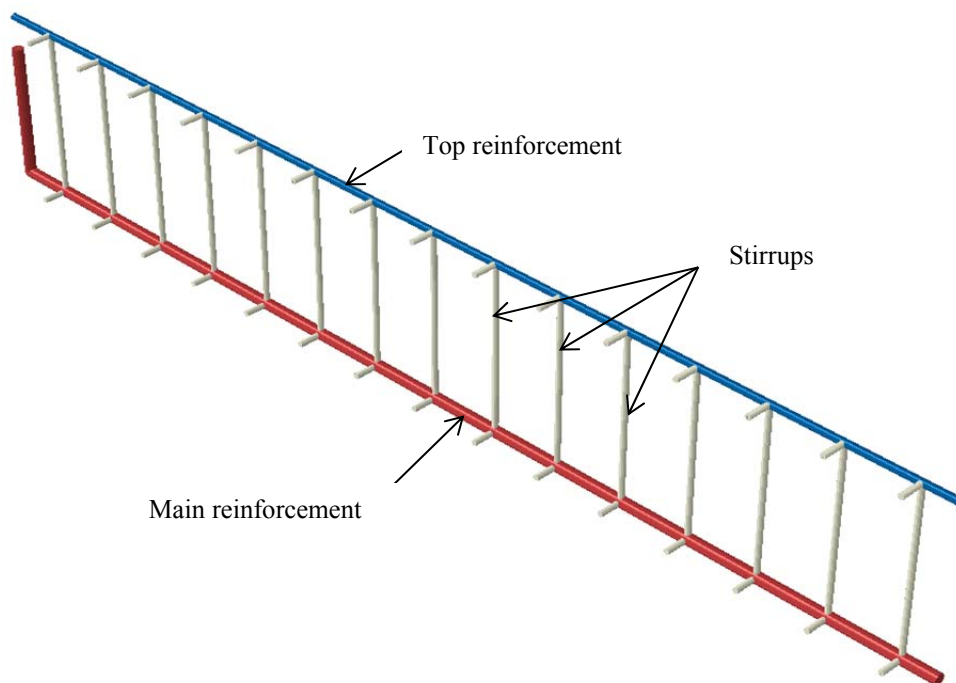
Figure 5-6: Modeling the steel reinforcement embedded in the concrete beam

The embedded element technique is used to specify that an element or group of elements is embedded in "host" elements. The embedded element technique can be used to model rebar reinforcement. Abaqus searches for the geometric relationships between nodes of the embedded elements and the host elements. If a node of an embedded element lies within a host element, the translational degrees of freedom at the node are eliminated and the node becomes an "embedded node." The translational degrees of freedom of the embedded node are constrained to the interpolated values of the corresponding degrees of freedom of the host element. Embedded elements are allowed to have rotational degrees of freedom, but these rotations are not constrained by the embedding. Multiple embedded element definitions are allowed.

The mechanical properties of the reinforced steel bars used in this study shown in Table 5-2

Table 5-2: mechanical properties of Steel

Yield stress, f_{sy} (MPa)	490
Modulus of elasticity, E_s (GPa)	200
Poisson's ratio, ν	0.30

5.3.1.3   **Creep Parameters of reinforced Concrete**

The creep response of the reinforced concrete beam under flexural loading based on experimental results is presented in Figure 5-7. Based on equation (5-4), the creep parameters for concrete can be determined by fitting the experimental creep deflection (Δ_{cr}) at the mid-span of the reinforced concrete beam under constant flexural load with time.
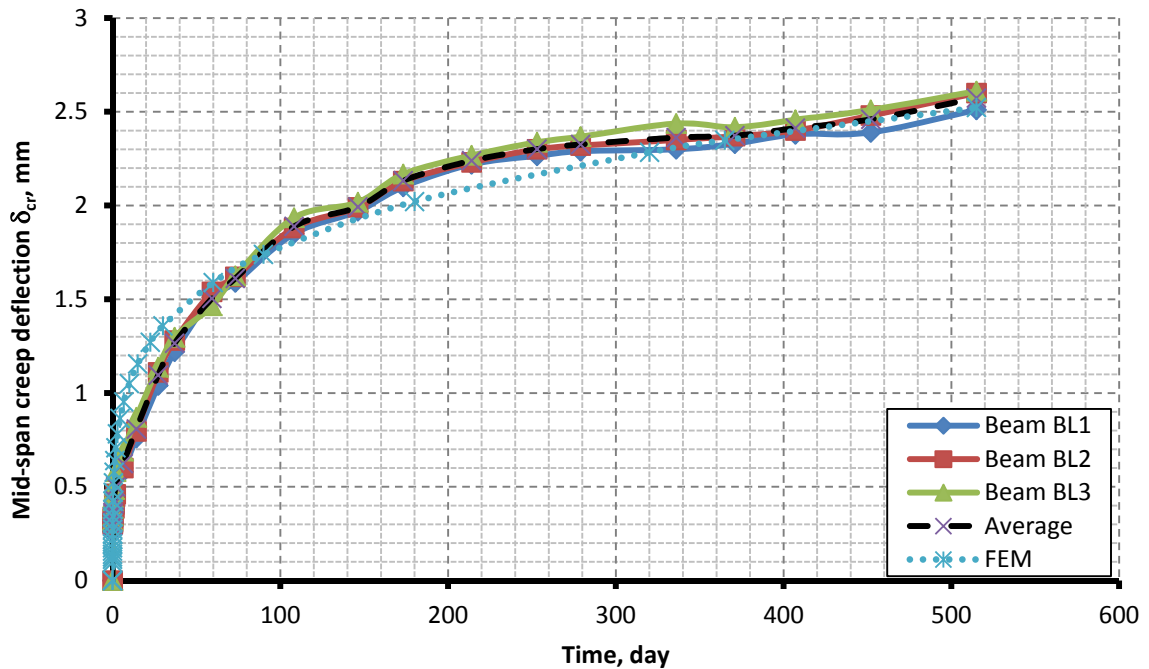
Figure 5-7: FE creep of RC beam.

Using the trendline equation in excel, the parameter m_1 was obtained ($m_1 = m+1 = 0.25$). In Abaqus power law form the parameter (m) is needed which can be determined from the previous calculated parameter m_1 ($m = 1-m_1 = -0.75$).

To evaluate the parameters A, and n; the relationship between the creep response and applied stress was assumed to be linear; therefore, the stress-dependent parameter n in Equation (5-5) was considered to be 1.0. Using an average value of n and σ, the power law model equation is used to predict creep response of the concrete beam under constant bending stress can be written as:

$$\varepsilon_{cr} = A\sigma^n \frac{t^{m+1}}{m+1} = 5.3x10^{-6} \, \sigma \, \frac{t^{0.285}}{0.285} = 1.86x10^{-5}\sigma \, t^{0.25} \qquad (5\text{-}17)$$

The resulting values for creep parameters determined based on Equation (5-4) and curve fitting tool was given in Table 5-3.

Table 5-3: creep parameters for reinforced concrete beam used in FE analysis

Material	A	n	m
Concrete	5.3E-6	1	-0.75

These values of A, n, and m give well result for the creep behavior of reinforced concrete beam and were used for studying the creep behavior of CFRP-strengthened reinforced concrete beam.

5.3.2   Cohesive zone (epoxy) modeling

5.3.2.1   Short-*term epoxy material modeling*

Cohesive elements implemented in the commercial finite element package ABAQUS can be represented as two cohesive surfaces separating from each other under shear or/and normal stresses. In this study, the bilinear traction separation law is defined by a linear elastic response, a strength criteria and a damage evolution law based on energies. The use of cohesive elements together with a traction separation law (Figure 5-8) is briefly described in the following part. Detailed descriptions of cohesive elements in (Abaqus , 2010) are available for the reader in Abaqus user manual (2010).
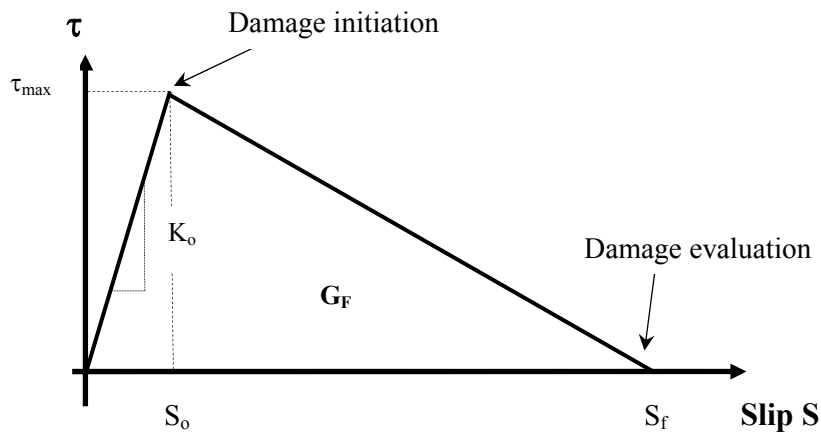
Figure 5-8: Bilinear traction-separation law.

The behavior of the interface prior to initiation of damage is described as linear-elastic.

The nominal traction vector consists of three components in three-dimensional problems: σ_n, τ_s and τ_t which represent the normal and shear tractions, respectively.

The stiffness is determined according to Equation (5-18) (Guo ZG, et al., 2005).

$$K_o = \frac{1}{\frac{t_a}{G_a} + \frac{t_c}{G_c}}$$

(5-18)

Where t_a is the adhesive thickness, t_c is the effective thickness of concrete whose deformation forms part of the interfacial slip and was taken as 5 mm, and G_a= 4.5 GPa and G_c=9.975 GPa are the shear modulus of adhesive and concrete respectively.

The damage initiation starts when a quadratic stress criterion is fulfilled. The strength of the adhesive in the normal and shear directions are used as input data.

$$\left(\frac{\sigma_n}{\sigma_n^o}\right)^2 + \left(\frac{\tau_s}{\tau_s^o}\right)^2 + \left(\frac{\tau_t}{\tau_t^o}\right)^2 = 1 \tag{5-19}$$

Where σ_n, τ_s and τ_t are the cohesive tensile and shear stresses of the interface, and the subscript refers to the direction of the stress component. The values used for this study were:

$\sigma_n^o = f_{ct}$ = 2.6 MPa and $\tau_s^o = \tau_t^o = \tau_{max}$. An upper limit for the maximum shear stress, τ_{max}, is provided by the expression, (Lu, et al., 2005):

$$\tau_{max} = 1.5\ \beta_w\ f_{ct} \tag{5-20}$$

Where

$$\beta_w = \sqrt{\frac{\left(2.25 - \frac{b_{FRP}}{b_{beam}}\right)}{\left(1.25 + \frac{b_{FRP}}{b_{beam}}\right)}} \tag{5-21}$$

Where b_{FRP}, b_{beam}, and f_{ct}, are CFRP width, beam width and concrete tensile strength respectively.

In this study, the energy-based Benzeggagh and Kenane (BK) damage evolution criterion shown in Equation 5-15 was used (Benzeggagh M. L. & Kenane M. , 1996)

$$G_{Tc} = G_{Ic} + (G_{IIc} - G_{Ic})\left[\frac{G_{shear}}{G_T}\right]^{\eta} \tag{5-22}$$

Where $G_{shear} = G_{II} + G_{III}$ and $G_T = G_I + G_{shear}$, η is the BK material parameter, G_{Ic} and G_{IIc} are the fracture toughness in mode I and II respectively, and G_{II}=G_{III}.

The fracture energy, G_F, can be estimated from Equation 5-16

$$G_F = 0.308\ {\beta_w}^2\ \sqrt{f_{ct}} \tag{5-23}$$

The values of fracture energy used for this study were G_I= 0.08 N/mm, G_{II}=G_{III}= 0.41 N/mm, and η=1.48

The mechanical properties of Epoxy used in this study obtained from Sika manufactory (Sikadur 30) and estimated using traction separation law shown in Table 5-4

Table 5-4: mechanical properties of Epoxy

Modulus of elasticity, E_c (GPa)	12
Shear Modulus, G_a (GPa)	4.5
Tensile strength, f_{at} (MPa)	25
Poisson's ratio, v *(assumed)*	0.38
Ultimate strain (%)	1
Fracture energy (N/m)	0.41

5.3.2.2   *Creep Parameters of Epoxy*

The creep parameter for adhesive was estimated based on the shear creep test data reported by (E. Ferrier , et al., 2011) for different 4 types of epoxy adhesive at the interface between concrete and CFRP.

The results of the creep shear strain versus time curves of the epoxy adhesive at every applied shear stress level are shown in Figure 5-9.
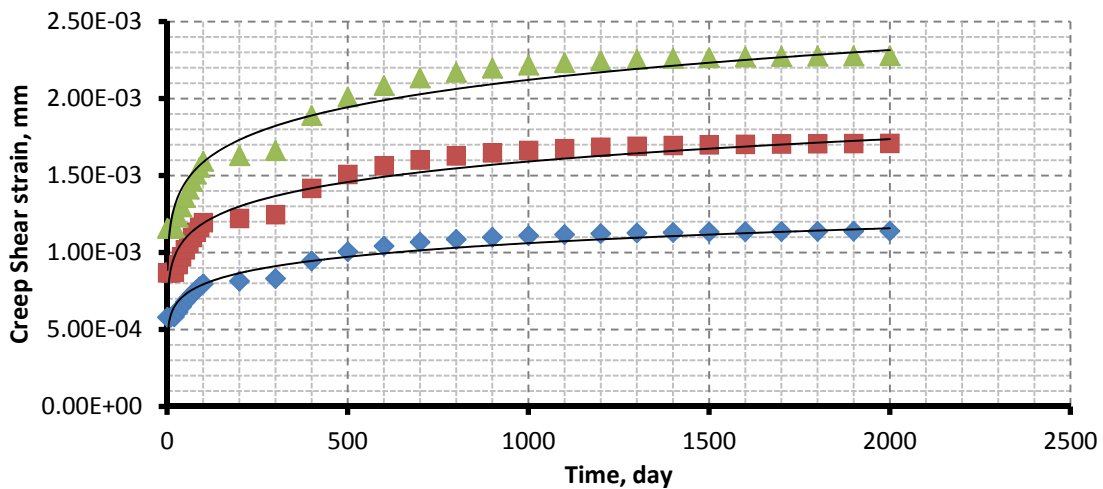
Figure 5-9: creep shear strain versus time result for the epoxy interface (E. Ferrier , et al., 2011) .

In order to estimate the parameters M_o, and m_1; the trendline function in excel was used to get the creep shear stain as a function of time at different applied stress level and comparing the fitting function with the equation (5-25). In this case the parameter m, (m= -0.8241) is obtained and is used in the finite element input for creep parameters of the epoxy interface. On the other hand, to estimate the parameters A, and n; the relationship between the creep response and applied stress was assumed to be linear; therefore, the stress-dependent parameter n in the Equation (5-26) was considered to be 1.0.

From the LN (M_o)-LN (σ) relationship as shown in Figure 5-10 the parameters n, M_1 can be evaluated and the creep parameters for the epoxy adhesive is estimated.

(a) Constant M_o , M_1, and n   (b) Constant (m_1= m+1)
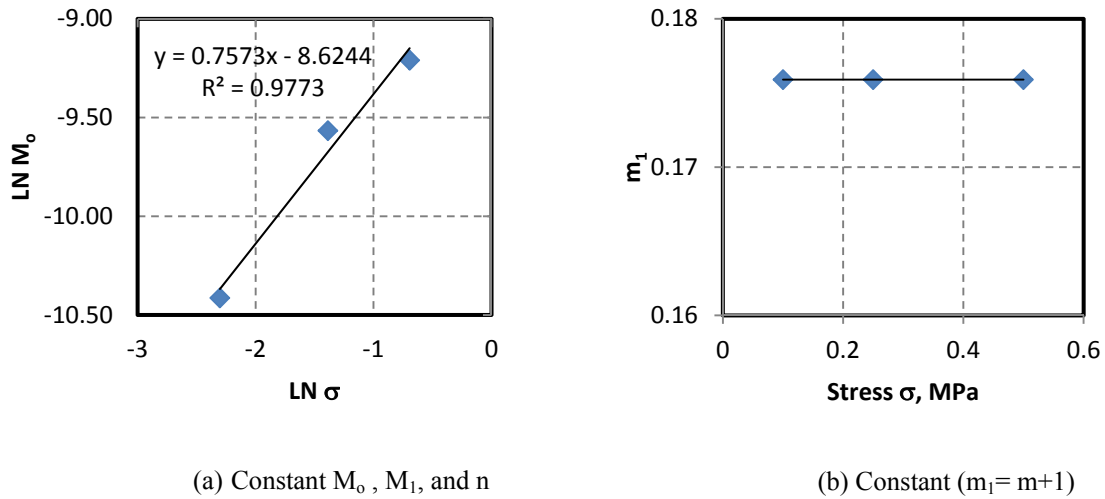
Figure 5-10: Constants M0 and M1, n, and m for the epoxy interface tested by (E. Ferrier , et al., 2011).

The parameters A, n, and m used in this study are shown in Table 5-5.

Table 5-5: creep parameters for epoxy interface used in FE analysis

Material	A	n	m
Epoxy	3.16036E-05	0.7573	-0.8241

5.3.3   CFRP modeling

5.3.3.1   Short-*term CFRP material modeling*

The CFRP material was considered as linear elastic isotropic until failure as shown in Figure 5-11 The material properties were obtained from Sika manufacture (S812) as in

Table 5-6.
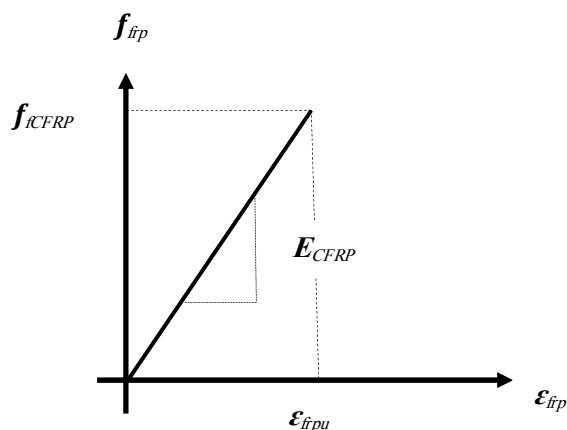
Figure 5-11: Stress-strain relationship for CFRP plate

Table 5-6: mechanical properties of CFRP

Modulus of elasticity, E_c (GPa)	165
Tensile strength, f_{CFRP} (MPa)	3400
Poisson's ratio, ν	0.3
Ultimate strain (%)	1.7

5.3.3.2   *Creep Parameters of CFRP*

In order to evaluate the time-dependent response of CFRP composites based on the test data, also the same procedure was used to evaluate the creep parameters based on the test data for CFRP creep test by (Fukuta Y., et al., 2008); and based on the previous studies; the change in creep strain of CFRP was about 2% to 8%, the curve data fitting tools was used and the evaluated creep parameter for CFRP shown in Table 5-7.
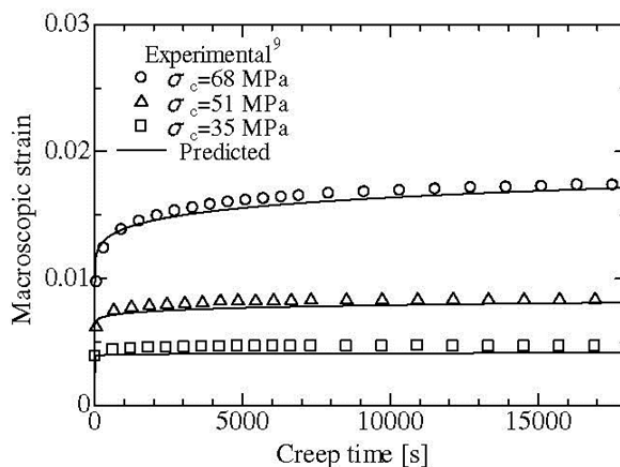
Figure 5-12: CFRP creep-strain relationship (Fukuta Y., et al., 2008)

Table 5-7: creep parameters for CFRP used in FE analysis

Material	A	n	m
CFRP	4E-008	1	-0.9

5.4 Geometric model

5.4.1 Short-term Model

One-quarter of the rectangular reinforced concrete beam was modeled due to two plans of symmetry as shown in Figure 5-13. An eight-node brick element was used to model the concrete and the CFRP plate. A two-node truss element was used for modeling the steel reinforcement, which was embedded in the concrete beam, assuming that there is a perfect bond between the concrete and steel reinforcement. (8-Node 3-D cohesive elements were used to model the interface layer. The cohesive interface elements are composed of two surfaces separated by a thickness. The relative motion of the bottom and top parts of the cohesive element measured along the thickness direction represents opening or closing of the interface. The relative motion of these parts represents the transverse shear behavior of the cohesive element. The element types used in the modeling are summarized in Table 5-8.

Abaqus/standard (Abaqus , 2010) was used for these simulations. The total deflection applied was divided into a series of deflection increments. Newton method iterations provide convergence, within tolerance limits, at the end of each deflection increment. In addition automatic stabilization and small time increments were used to avoid a diverged solution. Since the geometry of the beams, loading and boundary conditions were symmetrical, only one quarter of a beam was modeled with boundary conditions shown in Figure 5-14 and typical finite element mesh as shown in Figure 5-15.

Table 5-8: Element types used in FE analysis

Material	Description	Code	Additional information
Concrete	Eight-node brick	C3D8R	Reduced integration
Steel	Two-node truss	T3D2	Embedded element
Epoxy	Eight-node cohesive	COH3D8	Cohesive element
CFRP	Eight-node brick	C3D8R	Reduced integration

To verify the FE analysis and mesh sensitivity, three different mesh sizes were selected for the simulation of the strengthened and un-strengthened beam as shown in Figure 5-15 (a), (b), and (c). The load-deflection curves obtained from FE model at different mesh size were compared. The FE models with the different mesh sizes were found to represent the behavior of CFRP-strengthened reinforced concrete beams well as shown in Figure 5-16. Although the beam stiffness was slightly stiffer and the ultimate load was slightly higher as the mesh size

was finer, the difference was negligible. Therefore, the fine mesh in Figure 5-15 (b) was selected for the rest of the simulations.
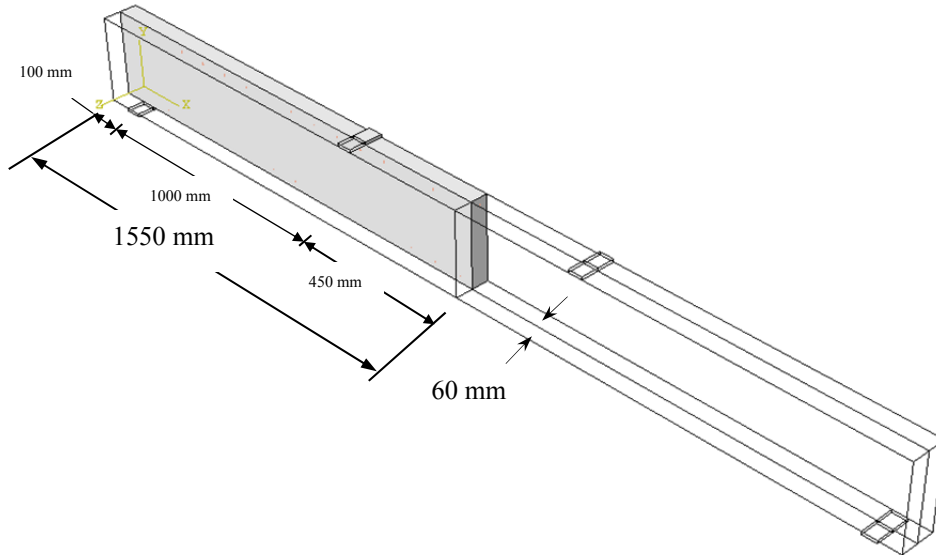
Figure 5-13: One-quarter of the beam was modeled due to two plans of symmetry

a)   Boundary condition for FE model

b) RC beam (control beam)   c) CFRP-strengthened Rc beam
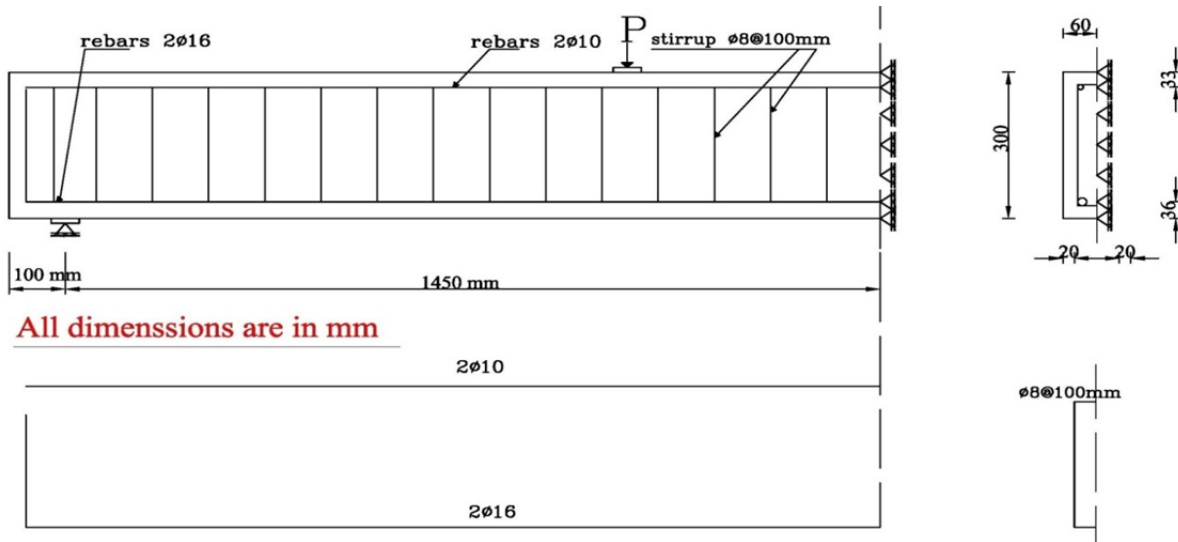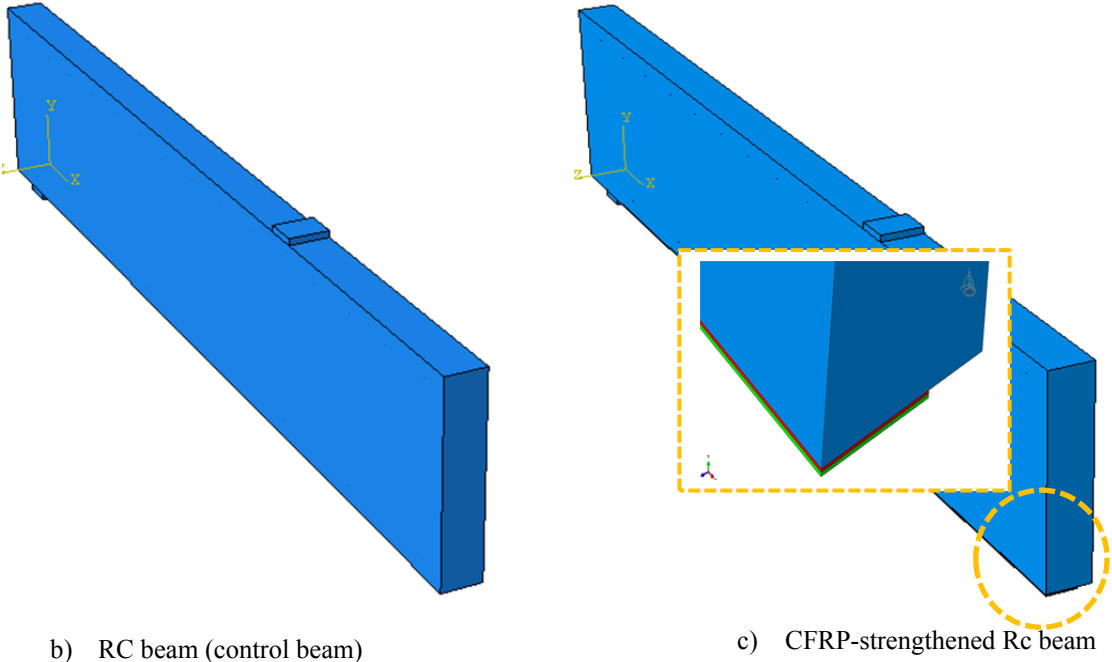
Figure 5-14: details and boundary condition for FE model

(c) Finer mesh   (d) Fine mesh   (e) Coarse mesh
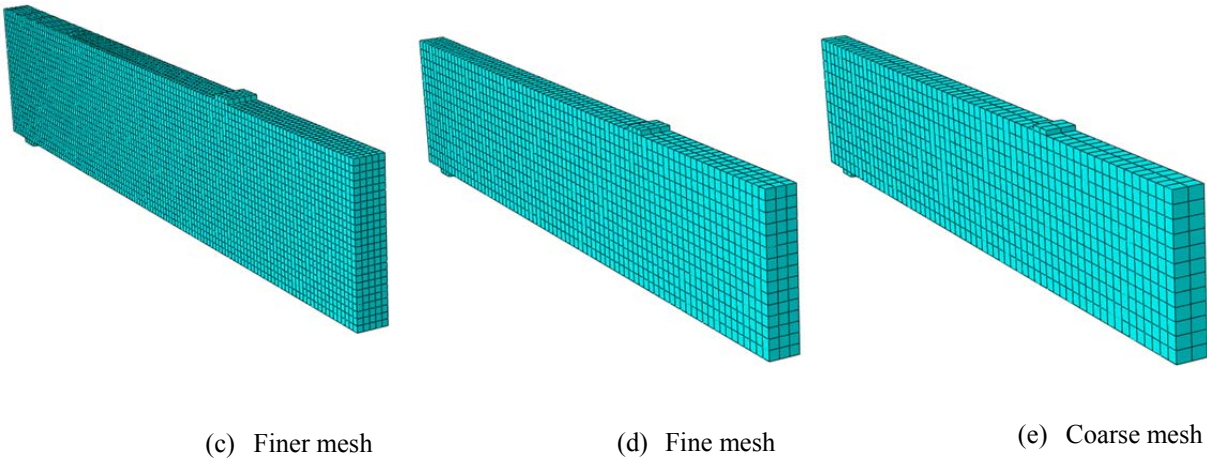
Figure 5-15: Mesh size used for FE model

96
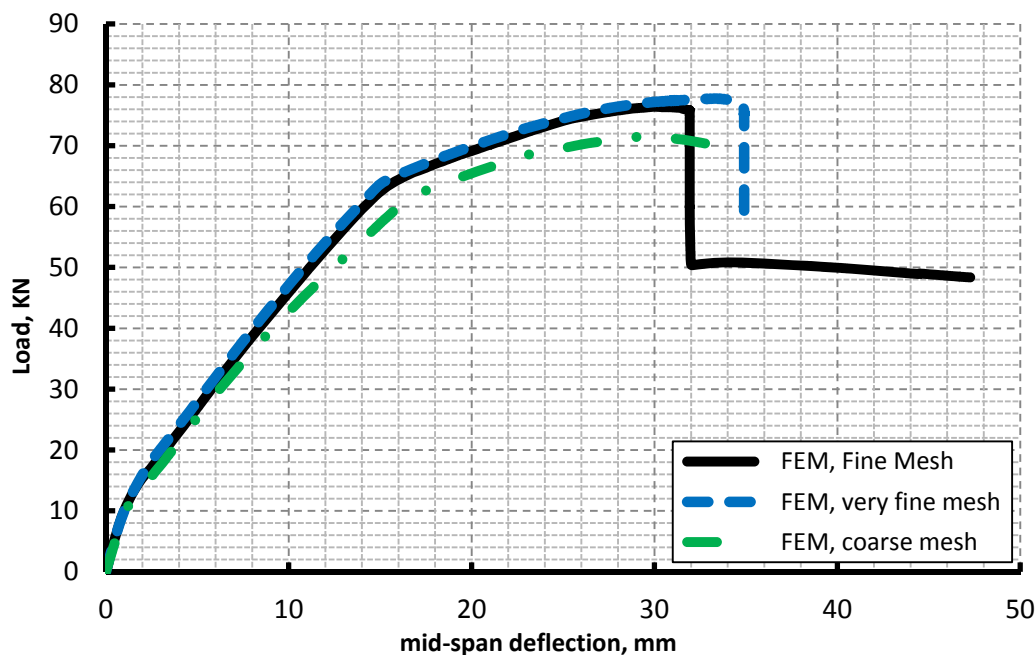
Figure 5-16: load-deflection curve of FRP-strengthened RC-beams for different mesh size.

5.4.2   FEM Creep Deformation of CFRP strengthened RC Beam

A 3D-finite element model, developed in the Abaqus finite element program (Abaqus 2010), was used to validate the power law creep model of the Reinforced concrete, Epoxy, and CFRP composites. The numerical results are compared with those obtained experimentally. The finite element (FE) creep analysis was performed by using the material properties and creep parameters obtained from fitting curves with the Equation (5-4) as discussed in this chapter. The same 3D-model used for simulating the flexural behavior of CFRP-strengthened RC beams (as shown in Figure 5-17) was used for studying the creep deformation of the strengthened beams.

The eight-node brick element (C3D8R) was used for modeling the concrete, steel paltes, and CFRP laminates. The reinforcement steel bars were modeled using two-node truss element (T3D2). The interface between the concrete and CFRP layers were modeled by cohesive element (COH3D8) using the Abaqus fully bonded Tie multi-constraint option (Abaqus , 2010). The final CFRP-strengthened RC beam was simulated by using eight sequential steps, and the results of each step were recorded.
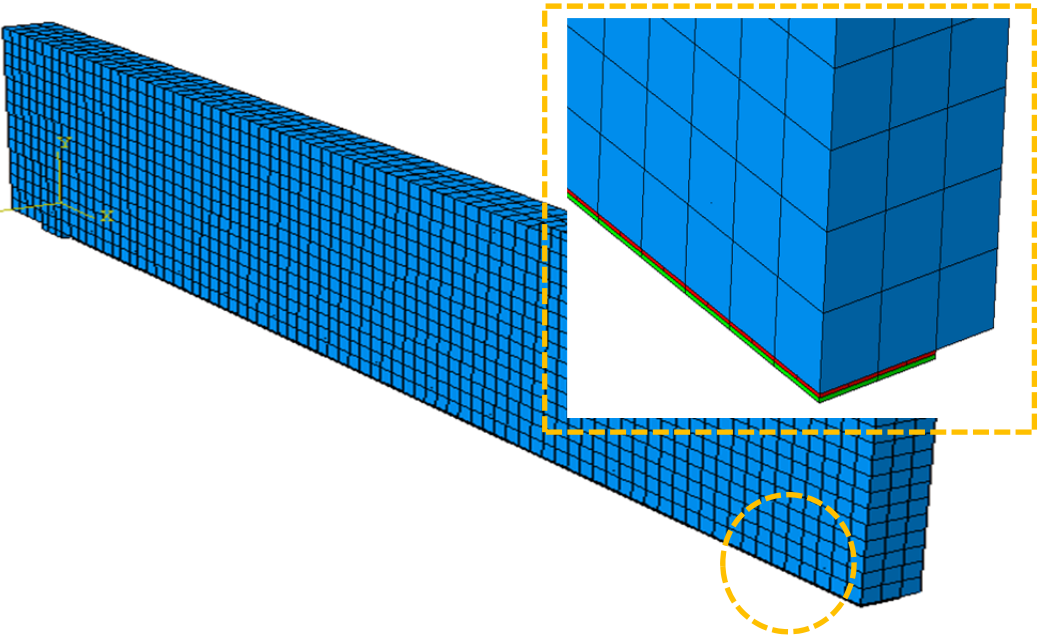
Figure 5-17: FE model used in this study

Chapter 6   Analysis and discussion of numerical results

6.1 Numerical Model verification

3D finite element model developed in chapter 5 was validated with the results obtained from the experimental test to estimate the failure load for the CFRP-strengthened RC beams at different CFRP plate length/breadth, and epoxy type. Also the calibrated model will be used to predict the long-term behavior of the CFRP-strengthened RC beams for different parametric study.

6.1.1   Load deflection comparison

The load-deflection relationship for both of reinforced concrete beam (controlled beams) and CFRP-strengthened reinforced concrete beams were shown in Figure 6-1. It can be seen that the CFRP increase the ultimate load and the bending resistance of the reinforced concrete beams by about 47% more than the un-strengthened beams. The increasing in ultimate capacity is due to the effect of composite action between external bonded CFRP and reinforced concrete beam on increasing the stiffness of the CFRP-strengthened RC beams.

The ultimate load and corresponding deflection comparison between FEM and experimental test were shown in Table 6-1.

Table 6-1: load-deflection results comparison between FEM and experimental test

Specimen		P_u (kN)	δ_u (mm)
Control RC- beam	Experimental	49.75	18.9
Control RC- beam	**FEM**	**51.56**	**15.57**
CFRP strengthened RC- beam	Experimental	78.347	30.997
CFRP strengthened RC- beam	**FEM**	**76.4212**	**30.0682**
CFRP strengthened RC- beam with plate at end of CFRP plate	FEM	77.006	31.2627

The load-deflection at mid-span obtained from FE model and that obtained from experimental test were shown in Figure 6-2; it can be observed that the stiffness of the FE model is higher than the stiffness of the experimental specimen and this occurred till the yield of reinforcement steel bars, but at the failure load the difference in ultimate capacity and corresponding deflection between both of the FEM and experimental test was accepted and the model gives good result for the failure behavior of control beams and CFRP-strengthened RC beams. Also the transverse steel plates at the CFRP plate end has insignificant effect on the ultimate capacity. In this study the developed 3D FE model without plate at the end of

CFRP plate was used to study the short- and long-term behavior of CFRP-strengthened RC beams.
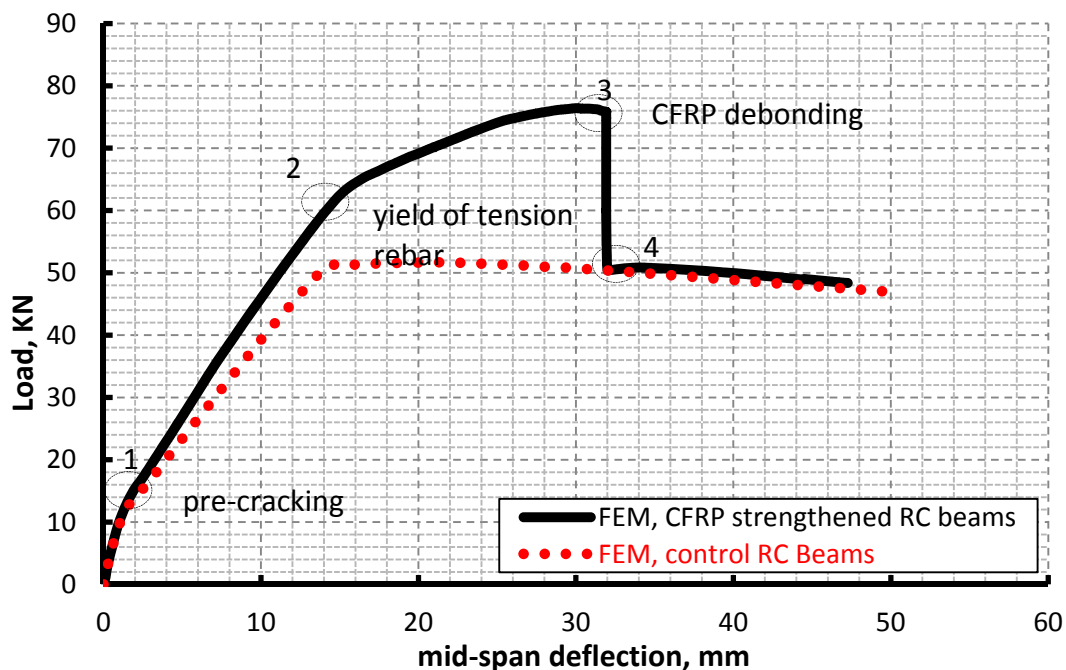
Figure 6-1: load-deflection curve comparison between control beams and CFRP-strengthened RC-beams.
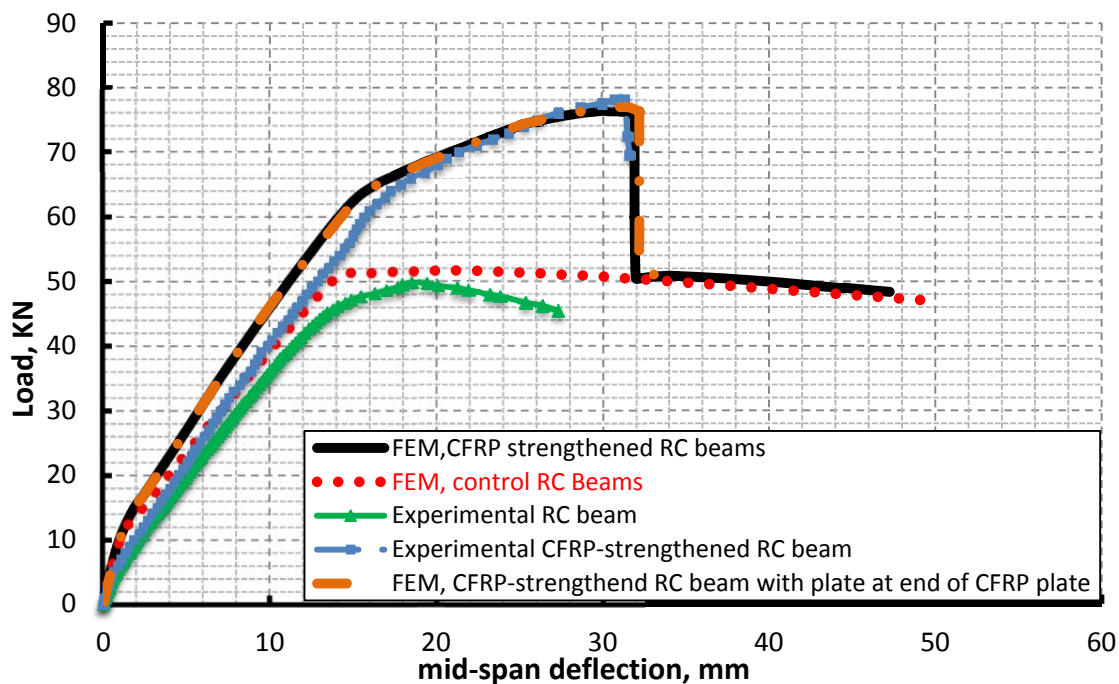
Figure 6-2: load-deflection curve comparison between control beams and CFRP-strengthened RC-beams.

100

6.1.2   **Failure mode**

The failure mode for control RC-beam was due to flexural cracks in the tension zone and yielding of the steel reinforcement in the tension side, also the failure takes place in a ductile manner. The first crack occurred at load 10 KN and the deflection was 1.07 mm, in the tension side near the applied load point.

The failure mode of CFRP-strengthened RC beams was due to debonding of the CFRP plate from the plate end to near the under load position.

The failure takes place at the concrete-epoxy interface. The crack pattern for control beam and CFRP-strengthened RC-beams were shown in Figure 6-3 (a & b) and Figure 6-4.

(a) damage pattern of RC beam at ultimate load

(b) damage pattern of FRP-strengthened RC beam at ultimate load
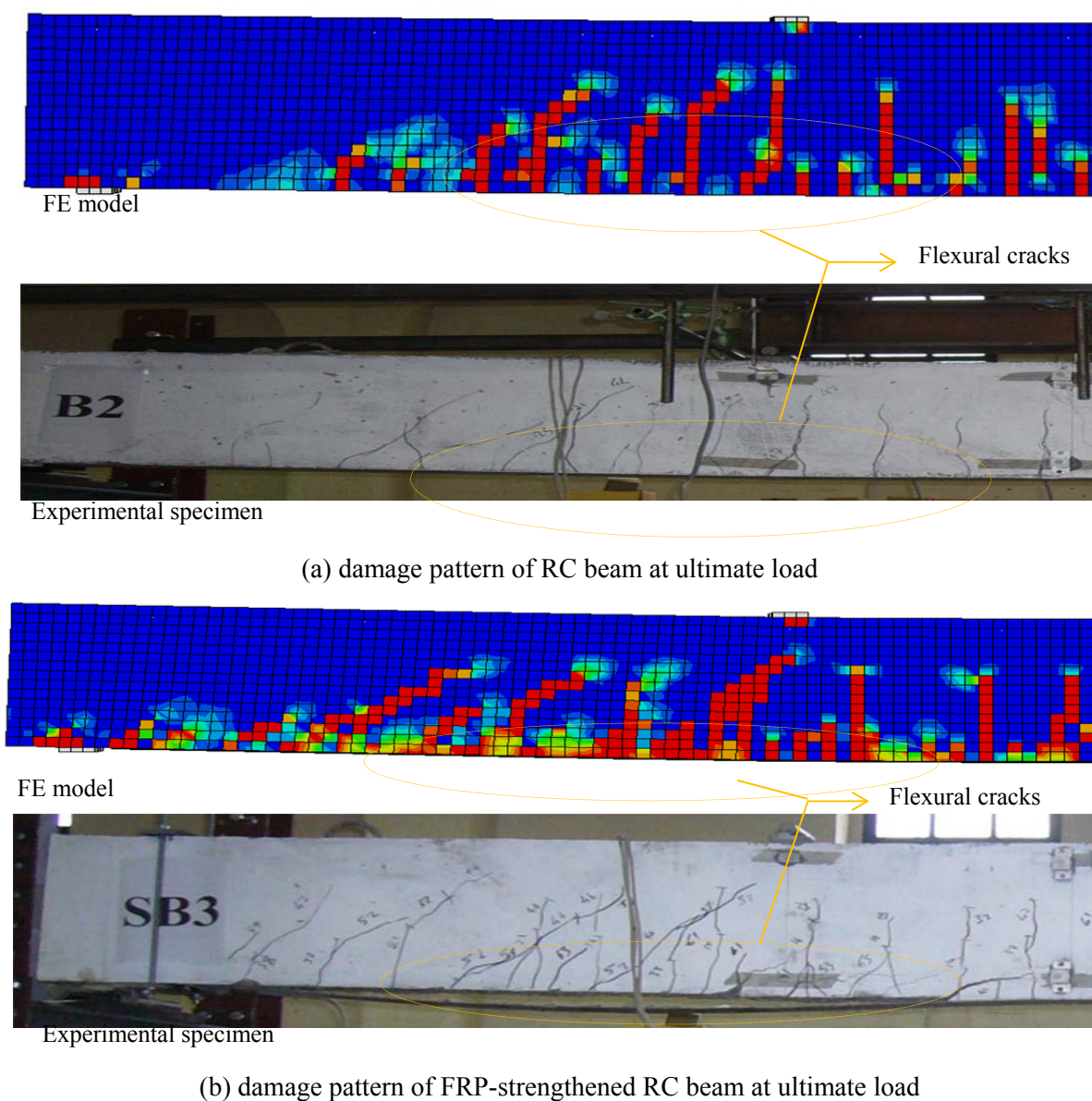
Figure 6-3: FE crack patterns at ultimate load for (a) control RC beam; and (b) CFRP-strengthened RC beam.

FE model

Debonding of FRP plate, interface failure

SB3

Experimental specimen
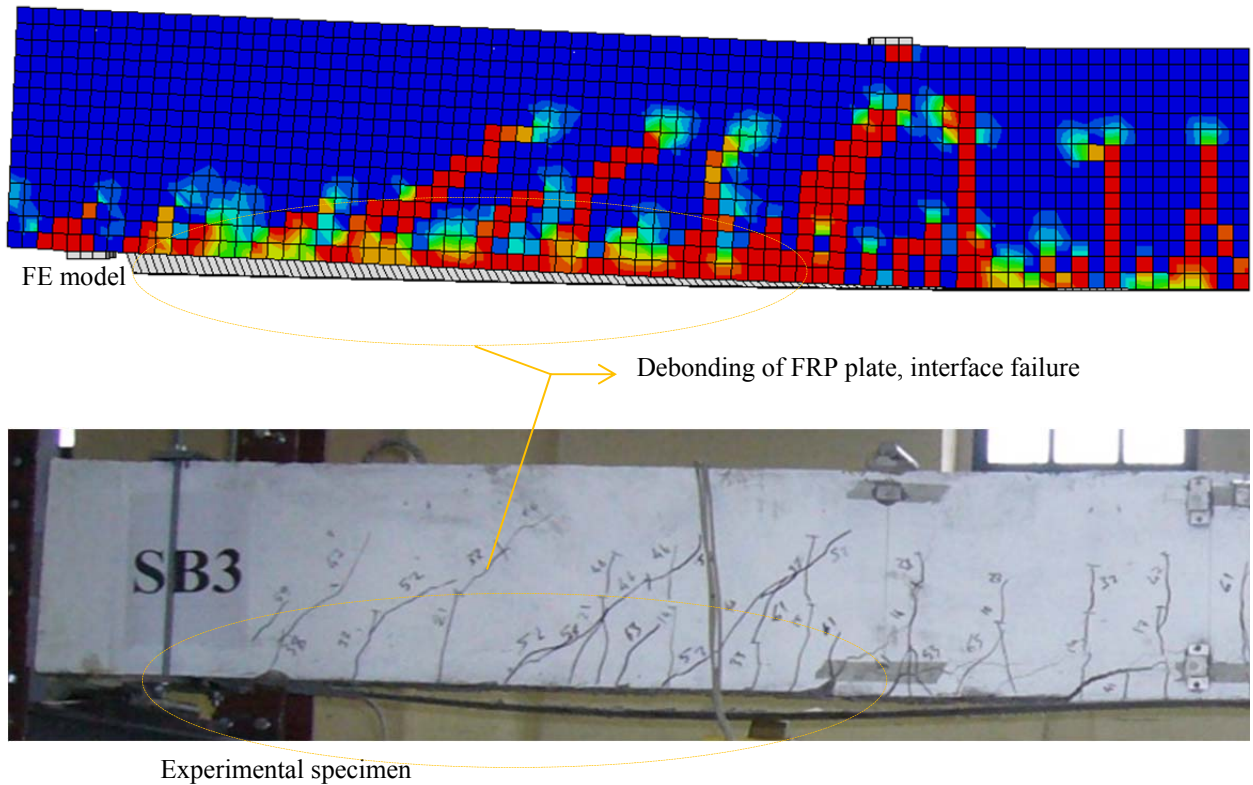
Figure 6-4: FE crack patterns for interface separation of CFRP-strengthened RC beam.

6.1.3   Comparison FE Modeling results with ACI 440

The ultimate capacity obtained from experimental and FE model were compared to that obtained from the ACI 440 equation (See chapter 2; section 2.2.3); the summarized results of ultimate load was shown in Table 6-2

The cross section properties for the strengthened specimen are as follow (Figure 6-5):
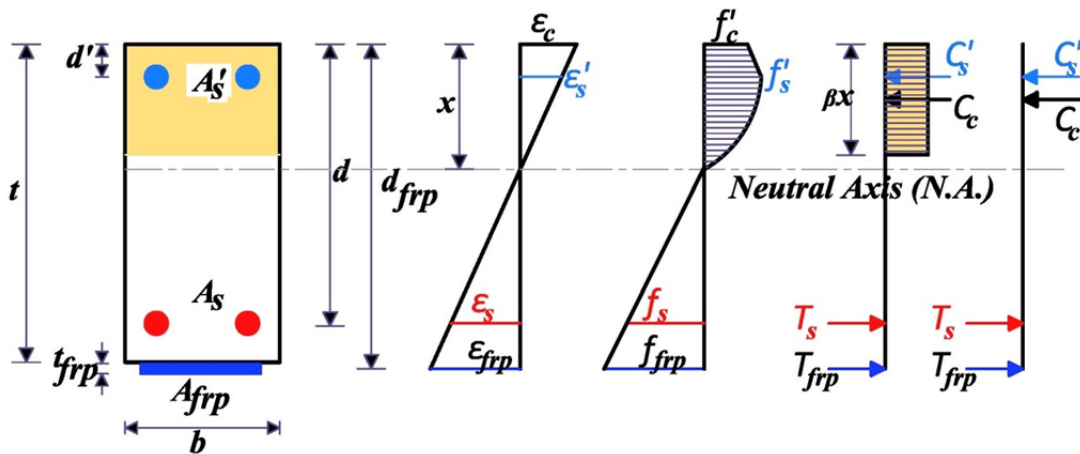
Figure 6-5: Internal strain and stress distribution for a rectangular section under flexure at ultimate stage.

b =120 mm f'_c= 44 MPa

t=300 mm f_t= 2.6 MPa

L= 2900 E_c=23941 MPa

A_s= 402 mm^2 f_y= 490 MPa

A'_s= 157 mm^2 E_s=200000 MPa

d_s= 264 mm E_{FRP}=165000 MPa

d'_s= 33 mm f_{FRP}= 2800 MPa

A_{FRP}= 96 mm^2 ε_{cu} = 0.003

d_{FRP}= 301.6 mm ε_s = 0.007178 > 0.005

                                               ε'_s = 0.001728

                                               ε_{fe} = 0.0111

Using the previous data and the equilibrium of internal forces in the diagram shown in Figure 6-5; the value of x can be determined as dollow:

$$x = \frac{-B + \sqrt{B^2 - 4ac}}{2a}$$ (6-1)

Where a = $0.85f'_c\beta\, b,$

B= $\left(A'_s E_s + A_{frp}E_{frp}\right)\varepsilon_{cu} - A_s f_y$

c= $-(A'_s E_s d' + A_{frp}E_{frp}d_{frp})\varepsilon_{cu}$

x= 77.8154 mm

The ultimate moment can be determined as follow:

$$M_n = f_s A_s \left(d - \frac{\beta x}{2}\right) + \psi_{frp}A_{frp}E_{frp}\varepsilon_{fe}\left(d_{frp} - \frac{\beta x}{2}\right)$$
$$+ A'_s f'_s \left(\frac{\beta x}{2} - d'\right)$$ (6-2)

M_n = 83814 kN.mm

For design, M_u = 0.9 Mn = 75433 kN.mm

P_u = 75.43 kN

For the control RC beams the ultimate moment can be determined from Equation (6-3):

$$M_n = f_y(A_s - A_s')\left[d_s - \frac{f_y(A_s - A_s')}{2(0.85f_c'b)}\right] + f_yA_s'(d_s - d') \qquad (6\text{-}3)$$

M_n = 47860 kN.mm

P_u = 47.86 kN

Table 6-2: ultimate load for control RC beams and FRP-strengthened RC beams comparison

Specimen	P_u (kN)
Experimental CFRP strengthened RC- beam	78.347
FEM CFRP strengthened RC- beam	76.4212
ACI equation CFRP strengthened RC- beam	75.43
Experimental control RC- beam	49.75
FEM control RC- beam	51.56
ACI equation control RC- beam	47.86

It can be observed that the FE model can be used to investigate the ultimate capacity of the CFRP-strengthened RC beams and the result gives good matching with the ultimate capacity obtained using the ACI 440 equation.

The comparison between ultimate load for control RC beams and CFRP-strengthened RC beams for different calculation methods was shown in Figure 6-6.

For the designer it is recommended to use reduction factor for the ultimate capacity between 0.7 to 0.9.

It can be concluded that the FE model was matching both of the experimental and code equation for estimating the ultimate flexural capacity of the CFRP-strengthened RC beams and the verified model can be used to investigate the flexural and long-term behavior of the strengthened beams.
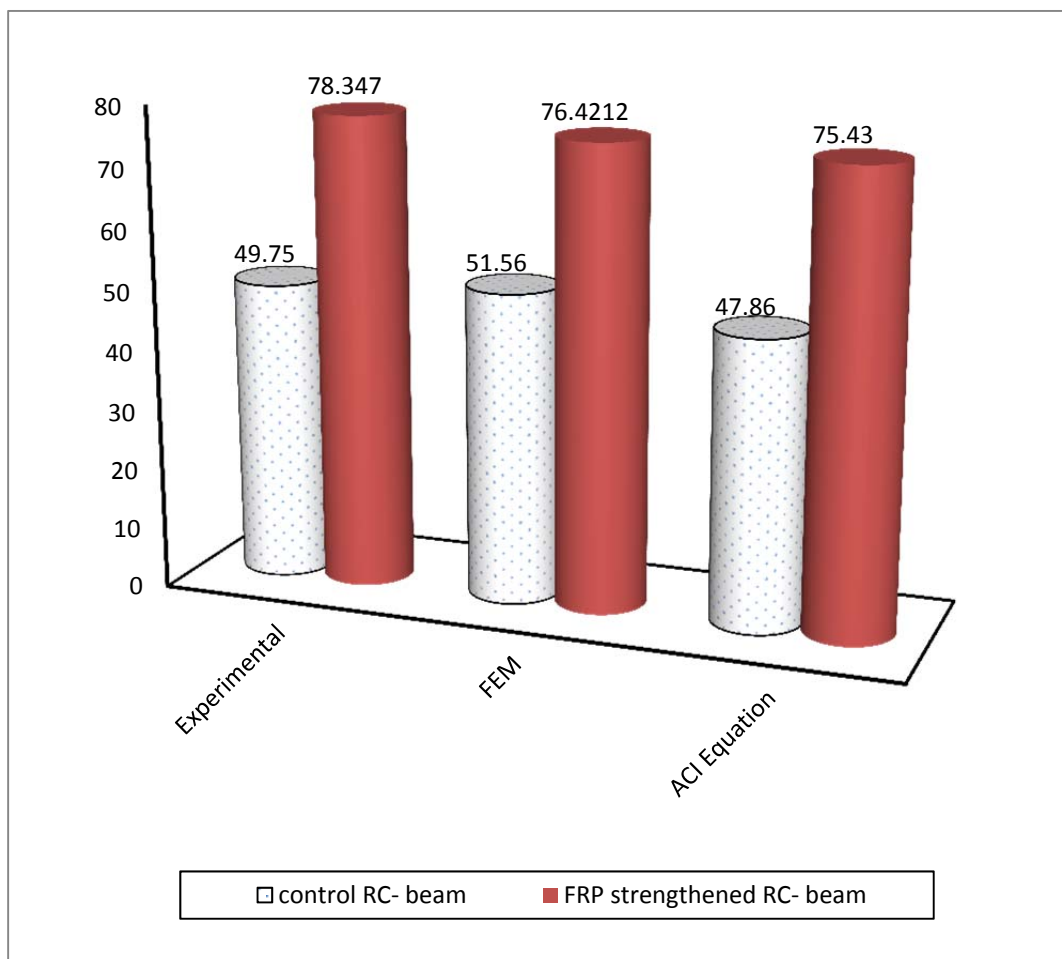
Figure 6-6: ultimate load for control RC beams and FRP-strengthened RC beams comparison.

6.2 Parametric study using FE modeling of CFRP-strengthening RC-beams

The verified FE model for CFRP-strengthened reinforced concrete beams was used to study the effect of changing the CFRP plate to span ratio, CFRP width to beam width ratio, and cohesive properties to evaluate the ultimate flexural load of CFRP-strengthened RC beams which is important to predict the long-term behavior of CFRP-strengthened RC beams under service flexural load.

6.2.1 CFRP plate length to span ratio and FRP width to beam width ratio

The CFRP plate length to span ratio was varied from 40% to 96%; while the variation between CFRP plate breadth to beam width was varied from 41% to 100%.

The load-deflection relationship and failure cracks are shown in Figure 6-7 and Figure 6-8 (1 to 9) respectively.

The ultimate load is compared to the ultimate load for control reinforced concrete beam (P_{rc} = 51.56 kN) as shown in Table 6-3
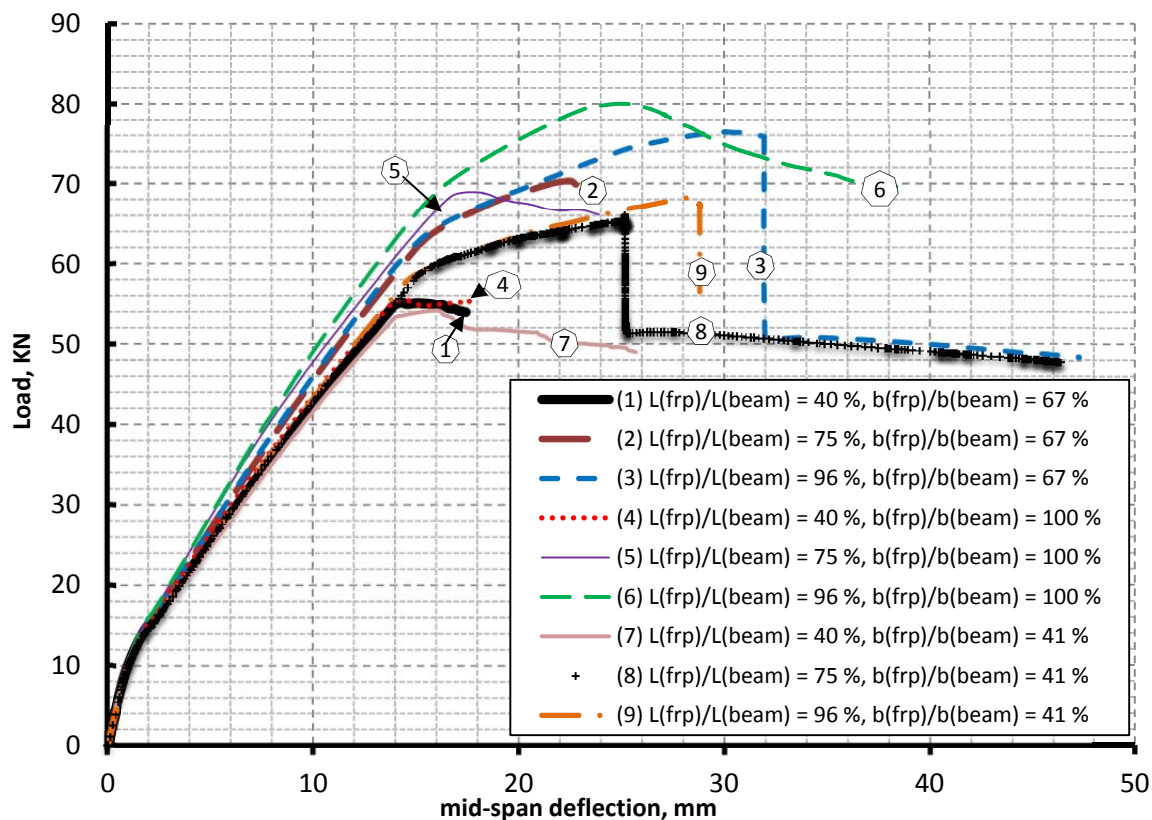
Figure 6-7: load-deflection curves of FRP-strengthened RC-beams with different L_{frp}/L_{beam} and b_{frp}/b_{beam} ratio.

Table 6-3: FE model results for FRP-strengthened RC-beams with different L_{frp}/L_{beam} and b_{frp}/b_{beam} ratio.

L_{frp}/L_{beam} %	b_{frp}/b_{beam} %	P_u (kN)	Δ_u (mm)	$P_{u,frp}/P_{u,rc}$ %	Failure mode
40	41	54.1662	15.9552	105	Yield of tension rebar
	67	55.1332	14.3326	107	CFRP-debonding
	100	55.448	14.2688	107.5	Interface separation
75	41	66.133	25.1571	128	Yield of tension rebar
	67	70.3292	22.4515	136.4	debonding
	100	68.9826	17.7835	134	Yield of tension rebar
96	41	68.32	23.5939	132.5	debonding
	67	76.4212	30.0682	148.22	debonding
	100	80.0254	24.908	155	Concrete cover failure

From the results it can be observed that the ultimate load was increased with increasing both of CFRP plate length and the CFRP plate width. Also the CFRP plate width improved the bond between concrete and CFRP plate. The increasing in flexural capacity was varied from 5% to 55% due to increasing in CFRP plate length to beam span ratio from 40% to 96% respectively. Furthermore, the increasing in CFRP plate breadth can be affected the ultimate capacity when using CFRP plate length more than 75% from the beam span, also improved the ductility of the strengthened beam. For the short plate length the effect of strengthening is less than 10%, it is recommended to use CFRP plate extended with an anchorage length outside the maximum flexural stress to obtain the full effect of the CFRP plate on the strengthening. Also the breadth is very important to increase the ability of the strengthening system to resist the debonding effect at the CFRP plate end due to the concentration of stresses at the plate end.
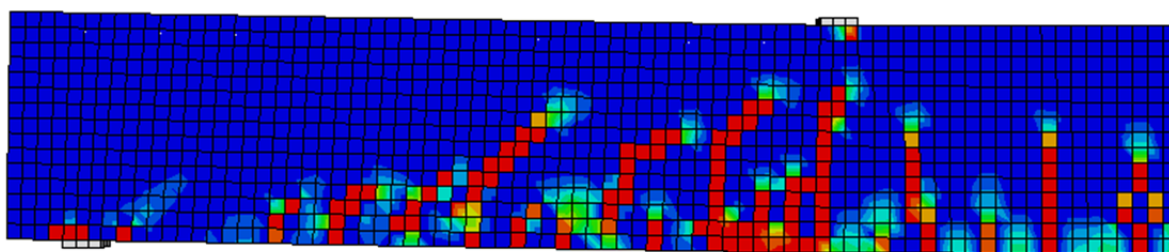
(1) L_{frp}/L_{beam} = 40 %, b_{frp}/b_{beam} = 67 %
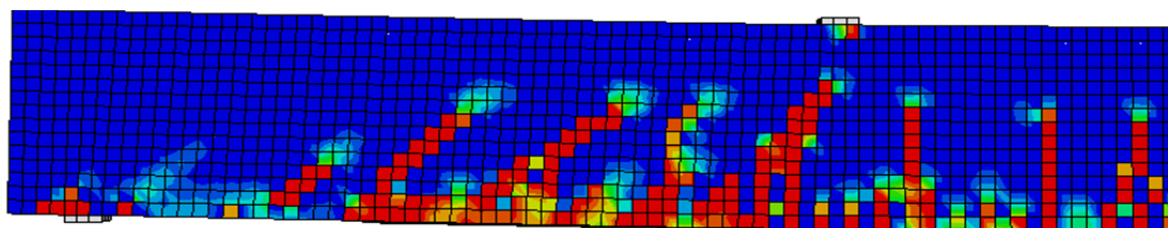
(2) L_{frp}/L_{beam} = 75 %, b_{frp}/b_{beam} = 67 %
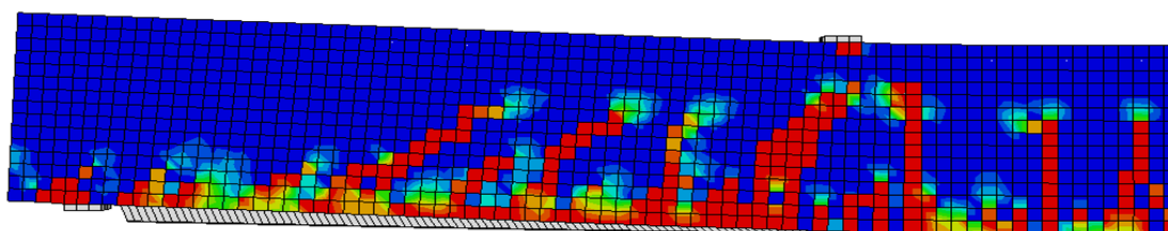
(3) L_{frp}/L_{beam} = 96 %, b_{frp}/b_{beam} = 67 %
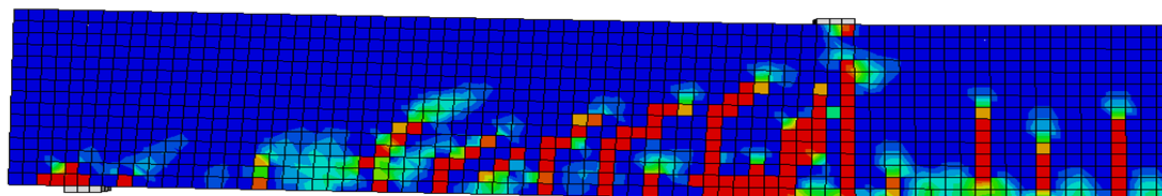
(4) $L_{frp}/Lbeam$ = 40 %, b_{frp}/b_{beam} = 41 %
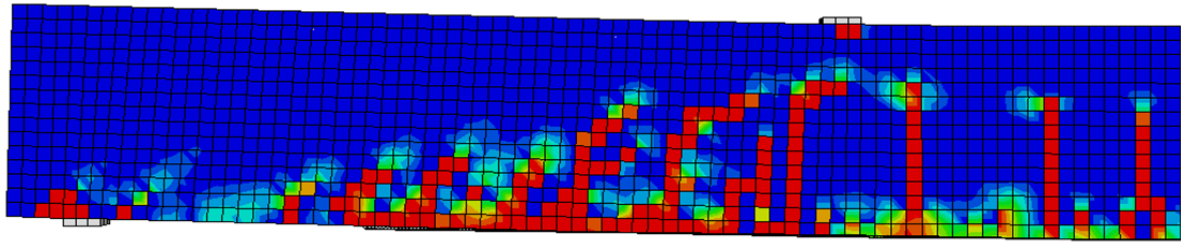
(5) L_{frp}/L_{beam} = 75 %, b_{frp}/b_{beam} = 41 %
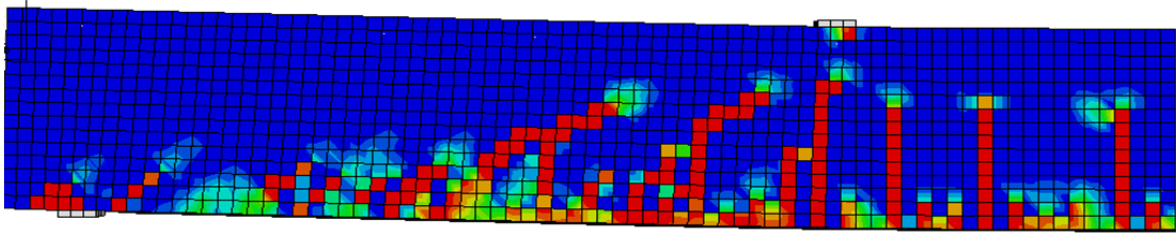
(6) L_{frp}/L_{beam} = 96 %, b_{frp}/b_{beam} = 41 %
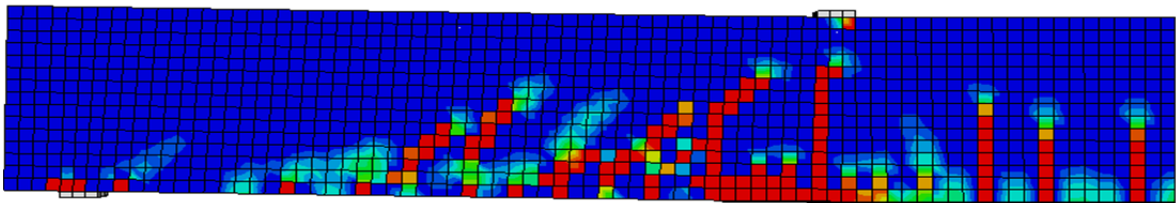
(7) L_{frp}/L_{beam} = 40 %, b_{frp}/b_{beam} = 100 %
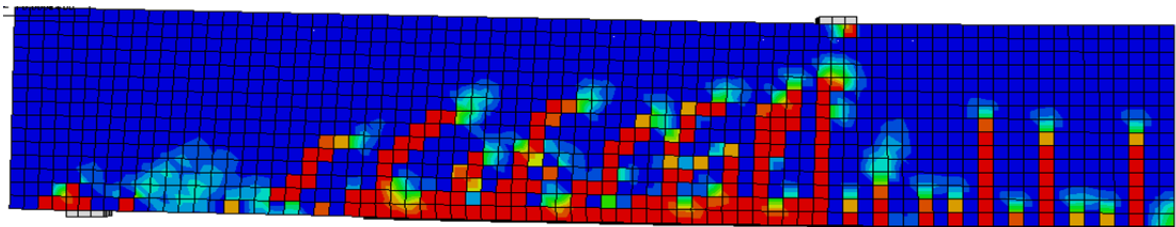
(8) L_{frp}/L_{beam} = 75 %, b_{frp}/b_{beam} = 100 %
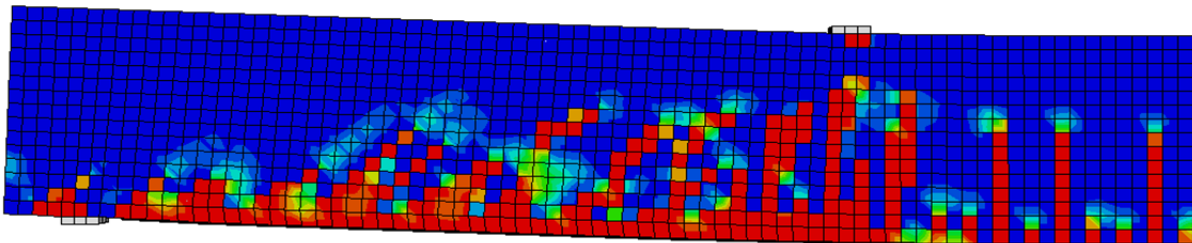
(9) L_{frp}/L_{beam} = 96 %, b_{frp}/b_{beam} = 100 %

Figure 6-8: FE crack patterns at ultimate load for FRP strengthened RC-beams with different L_{frp}/L_{beam} and b_{frp}/b_{beam} ratio.

6.2.2   Effect of epoxy adhesive

Results of ultimate load and deflection obtained from FE model for four types of epoxy adhesive used to bond the CFRP plate to the tension face of the RC beams are shown in Figure 6-9; it can be observed that different epoxy types has no significant effect on the the ultimate load of the CFRP-strengthened RC beams, this is due to the effect of small value of tensile strength of the concrete compared to that for epoxy, which is control the bond stress between concrete and epoxy and has the major effect in failure of the strengthened system. The data of epoxy used in FE model was summarized in Table 6-4
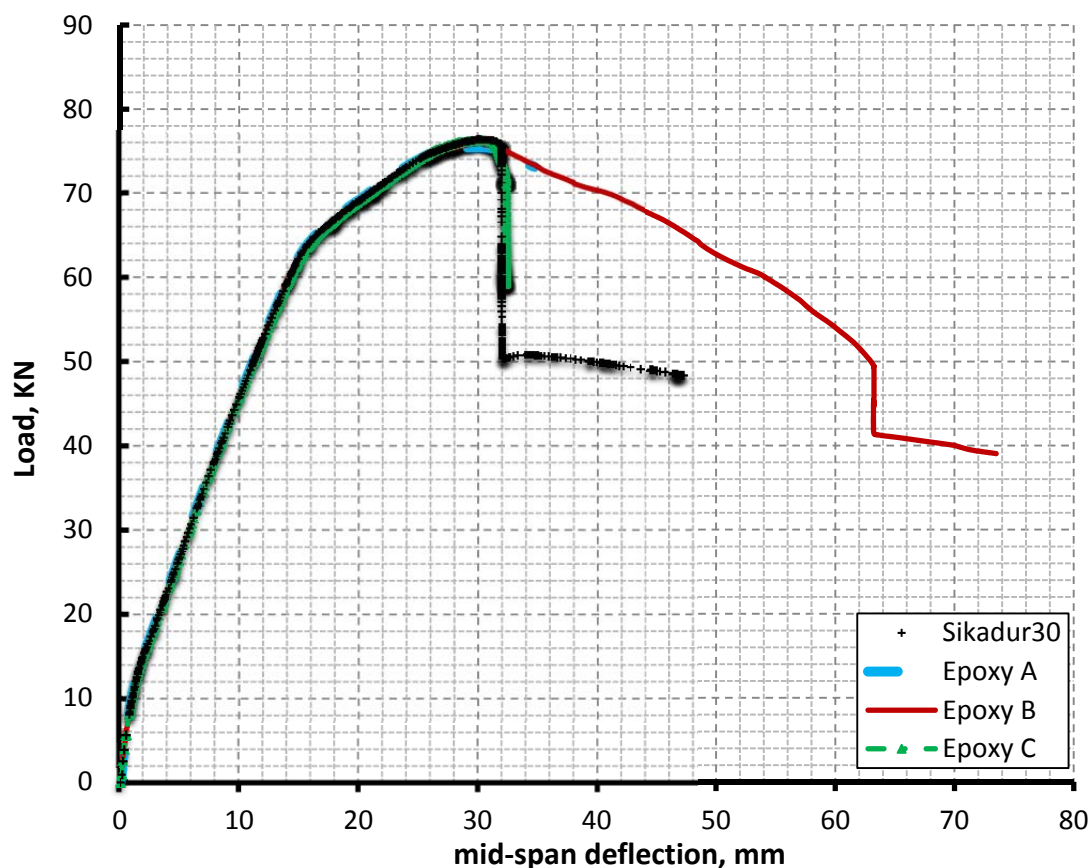
Figure 6-9: load-deflection curve comparison between control beams and CFRP strengthened RC-beams.

Table 6-4: material charactaristics for epoxy interface used in FE analysis

Material	Sikadur 30	Epoxy A	Epoxy B	Epoxy C
Young modulus (GPa)	12	5.29	6	3.2
Poisson's ratio, v	0.38	0.364	0.35	0.32

6.3 Numerical results of long-term behavior of CFRP-strengthened RC beams

The time-creep deflection curves obtained from the FE modeling and the corresponding experimental test results are compared in Figure 6-10. The experimental results and FE model result under applied load 17 kN and 26 kN were ploted and analysied. A good correlation between the FE and experimental results confirms that the creep behavior of CFRP-strengthened reinforced beams can be successfully predicted based on the creep properties of the epoxy, CFRP, and reinforced concrete beam using the developed 3D model.
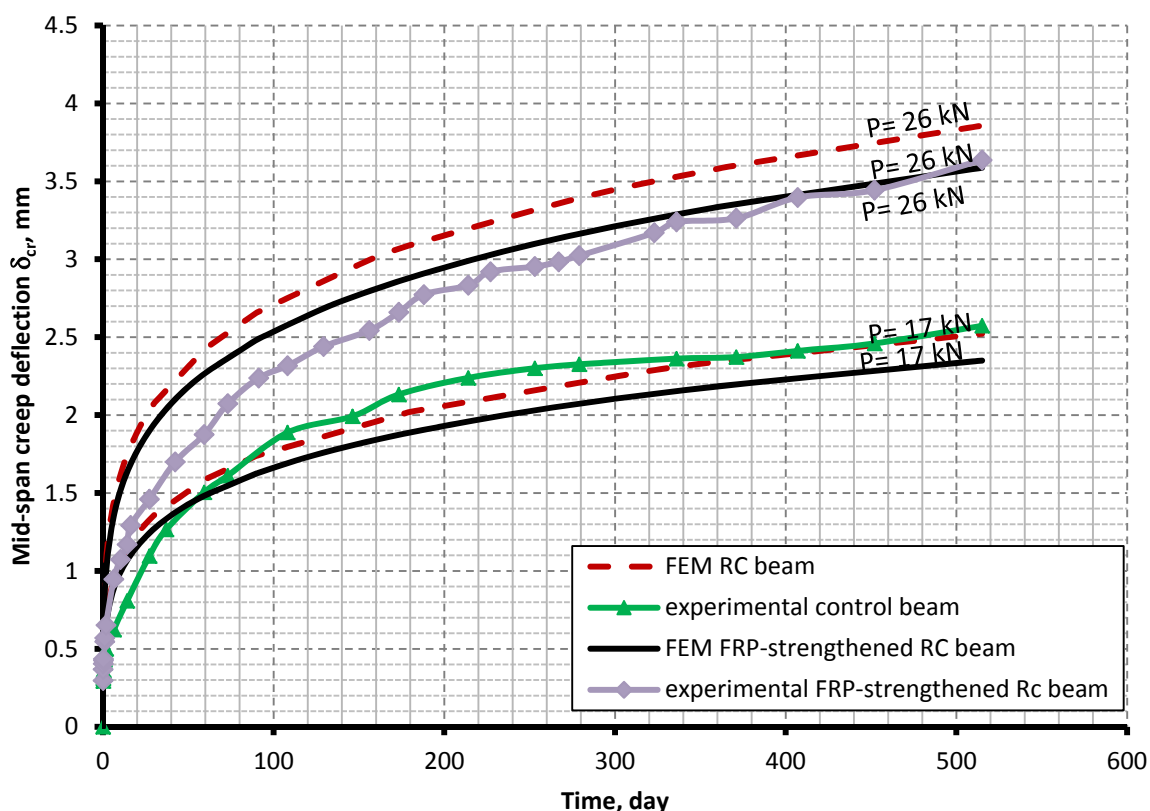
Figure 6-10: creep deflection at mid-span of control beam and FRP-strengthened RC beam

The FE model was then employed for conducting a parametric study to investigate the influence effect of the CFRP, and epoxy on the long-term performance of CFRP-strengthened reinforced concrete beams. Also the results from the finite element modeling will be compared with the recommended code equation for determining the creep deflection of the strengthened system.

To study the creep effect of the CFRP-strengthened RC beams; first the creep deformation of reinforced concrete beam was simulated by Abaqus FE program; after that the effect of epoxy adhesive alone was taken into consideration to evaluate the creep deflection of the CFRP strengthened RC beams.

110

Then the creep of the CFRP was taken in the simulation FE model to evaluate the effect of every material in the creep deformation. The results of the FE model were discussed as follow:

6.3.1 Effect of neglecting CFRP creep in Creep deflection deformation of CFRP-strengthened RC beams

The creep deflection-time relationship at mid-span for control RC beam and CFRP-strengthened RC beam was shown in Figure 6-11, in this model the creep of reinforced concrete beam and the creep of the epoxy interface is included in the model, while the creep of the CFRP plate was neglected.

The applied load was constant (P = 34% from the ultimate load of RC beam) with time and the young's modulus assumed to be constant to eliminate the FE model problems.

It can be observed that the creep deflection of CFRP-strengthened RC beams is less than the creep deflection for control beam by about 7% due to the effect of the strengthening on increasing the stiffness of the CFRP-strengthened RC beams and decreasing the immediate deflection.

Table 6-5 summarized the FE result for creep deflection at mid-span for RC beam and CFRP-strengthened RC beam.
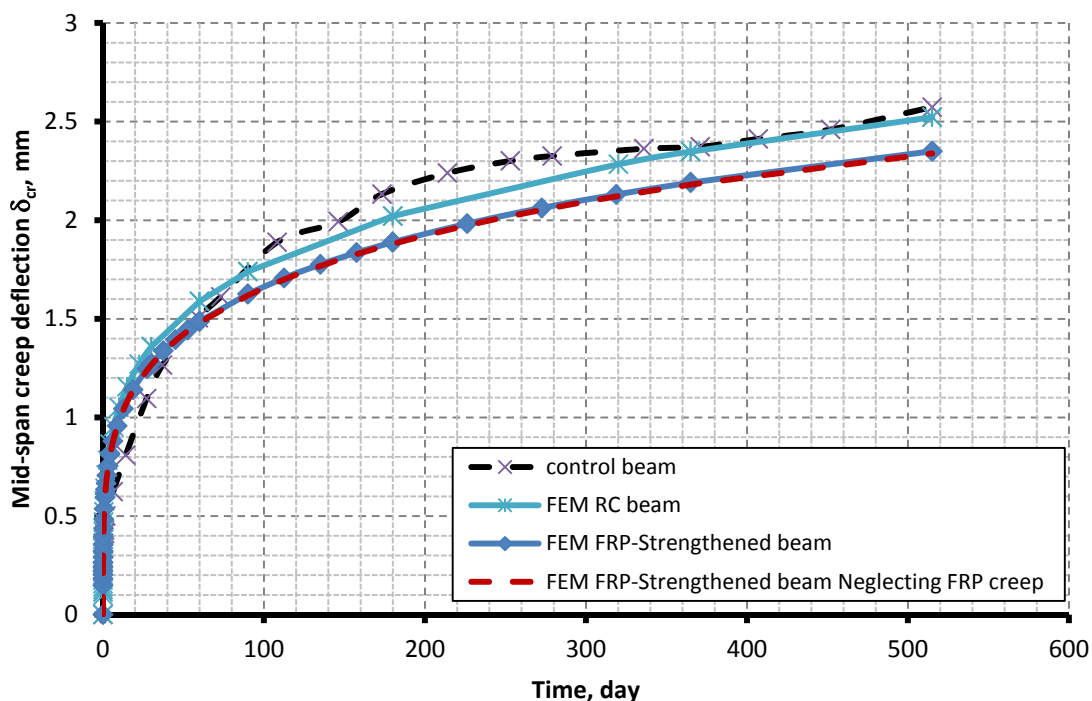
Figure 6-11: creep deflection at mid-span of control beam and CFRP-strengthened RC beam

Table 6-5: long-term creep deflection at mid-span of FE model at load 17kN.

Time, day / Specimen	0	30	60	90	180	365	515	1825
Control beam	0	1.36	1.59	1.74	2.021	2.35	2.52	3.25
CFRP-strengthened RC beam	0	1.27	1.48	1.625	1.89	2.19	2.35	3.01
CFRP-strengthened RC beam neglecting FRP creep	0	1.27	1.48	1.61	1.88	2.18	2.34	2.99

Figure 6-12 shows the effect of the applied load in the creep deflection of control beam and CFRP-strengthened RC beam when neglecting creep effect of CFRP plate; from the results it can be observed that the creep deflection of the strengthened beams is less than the creep deflection of the unstrengthened beams by about 7%, this is due to the effect of the CFRP on the decreasing the immediate deflection of the strengthened beams. Also the creep deflection is increased proportionally to the applied load as expected.
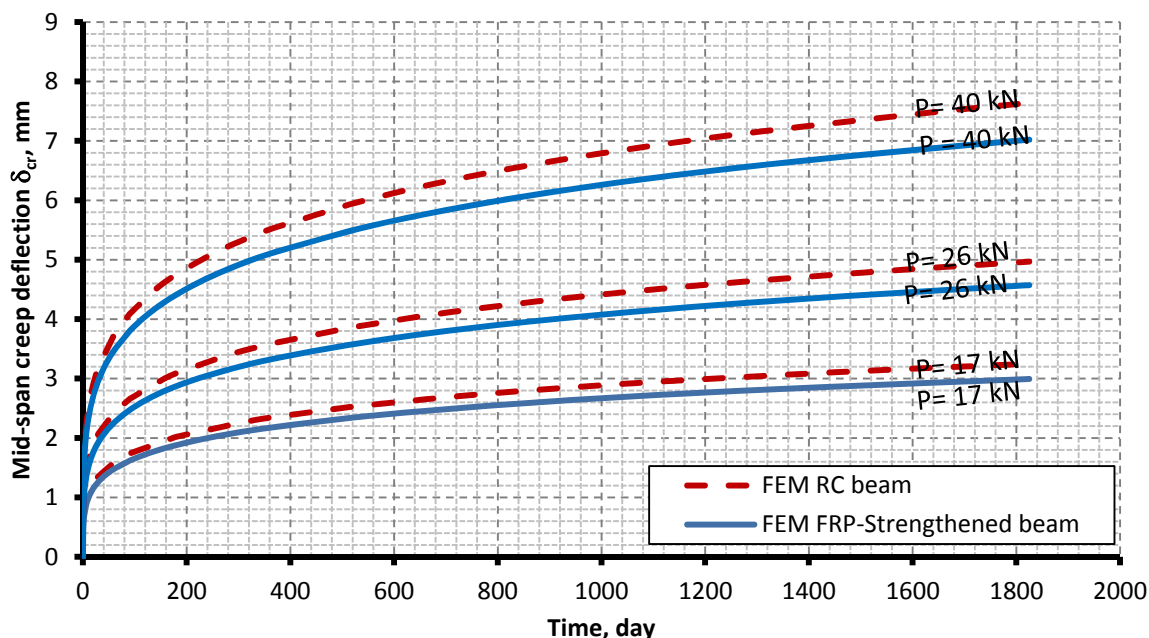
Figure 6-12: creep deflection at mid-span at different applied load without CFRP creep.

6.3.2   Effect of interface and CFRP creep in Creep deflection deformation of FRP strengthened RC beams

Figure 6-13 shows the effect of CFRP, epoxy interface, and reinforced concrete creep in the creep deflection at mid-span of the CFRP-strengthened RC beam and comparing it to the FE model of the control beam at different applied load; from the relationship the CFRP creep increases the creep deflection of CFRP-strengthened RC beam with a very small value about 0.5 % from the creep deflection of the strengthened beams with neglecting effect of CFRP creep in the model.
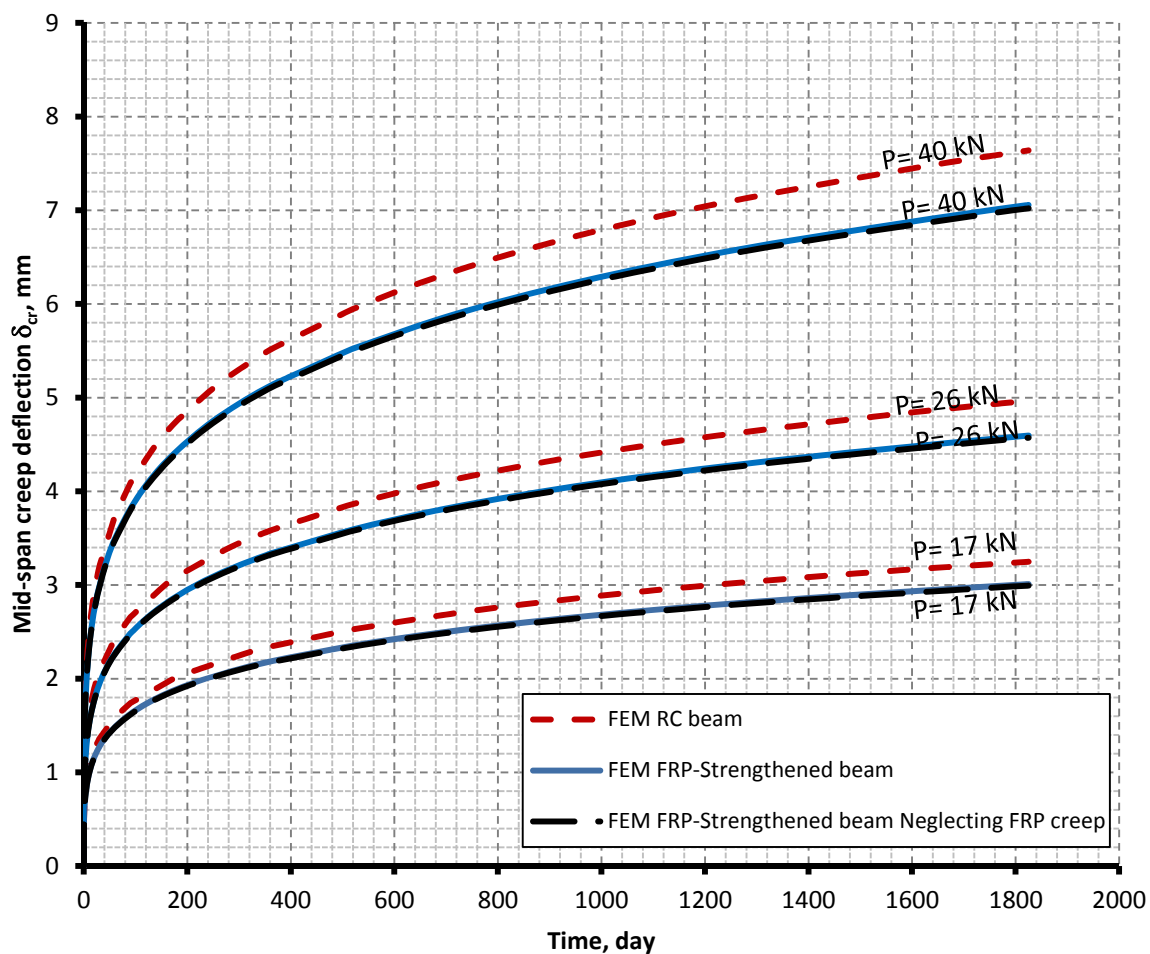
Figure 6-13: creep deflection at mid-span at different applied load.

From the results and comparing with the experimental creep deflection of CFRP-strengthened RC beam it can be concluded that the FE model can evaluate the creep behavior of CFRP-strengthened RC beam at different applied load levels and the results had good matching with experimental results, as shown in Figure 6-14.
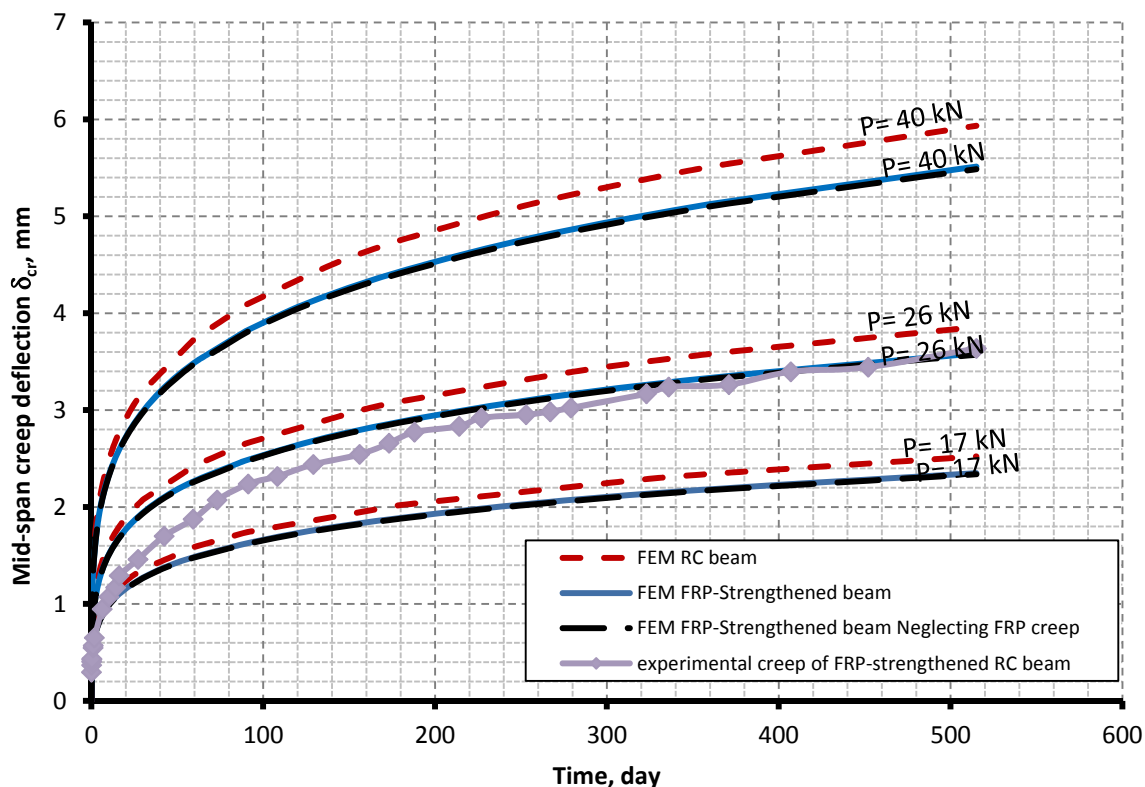
Figure 6-14: creep deflection at mid-span at different applied load comparison.

6.3.3   Reinforcement steel bar creep strain

The FE model results for long-term creep strain of reinforcement steel bar at different applied load level are shown in Figure 6-15, it can be observed that the creep strain of the reinforcement steel bars in the tension side of the CFRP-strengthened RC beams was decreased by about 15% from that of the RC control beam; due to the effect of CFRP plate. But the steel reinforcement strain at the compression side of the beam was decreased by about 3%; this value can be neglected in the design consideration.

Also the creep strain proportional to the applied load; with increasing the applied load by 58 % and 135 % the creep strain of reinforcement steel increases with 55% and 137% respectively; it is nearly the same percent of increasing in the applied load. It should be taken into account the effect of the applied load to be limited with the design service load for the CFRP strengthened RC beams.
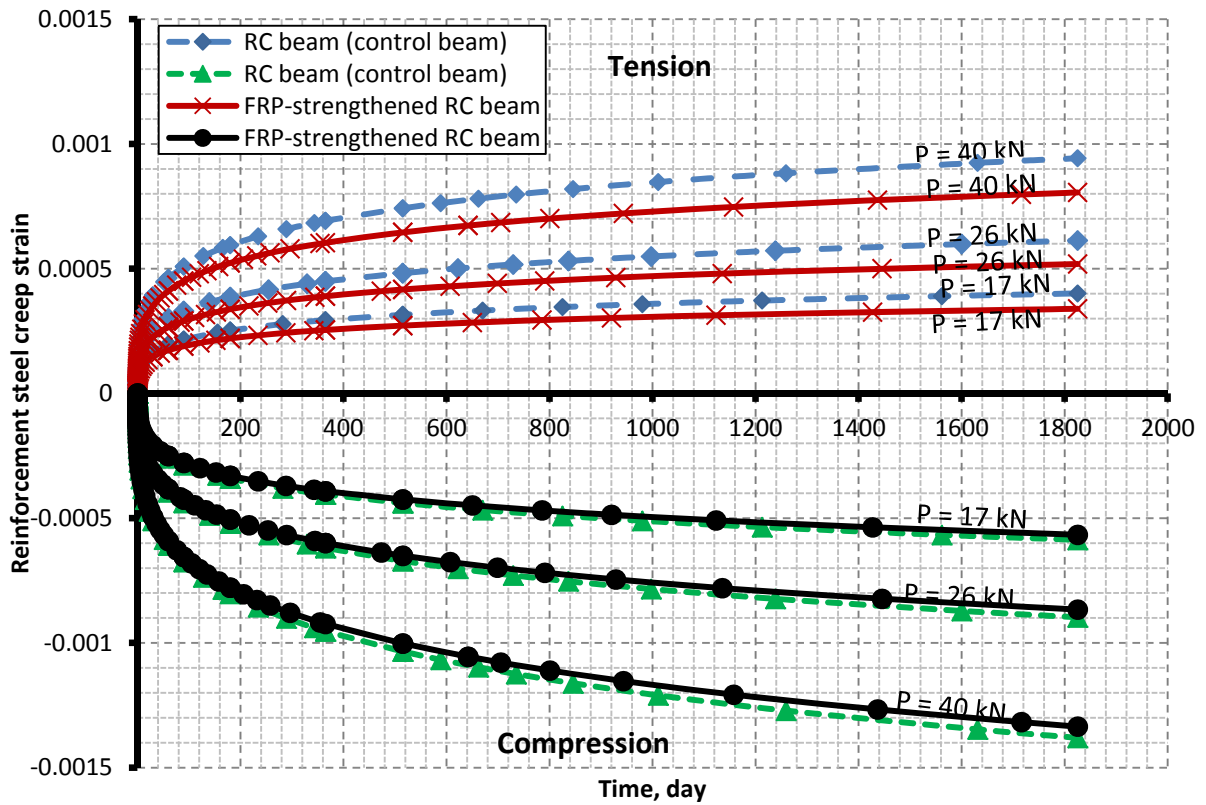
Figure 6-15: reinforcement creep strain at mid-span at different applied load comparison.

6.3.4 CFRP creep strain

The creep of CFRP plate at the mid-span is proportional to applied load and there is neither damage nor failure occur due to creep. The creep strain of CFRP-plate at mid-span at different applied load level is shown in Figure 6-16.
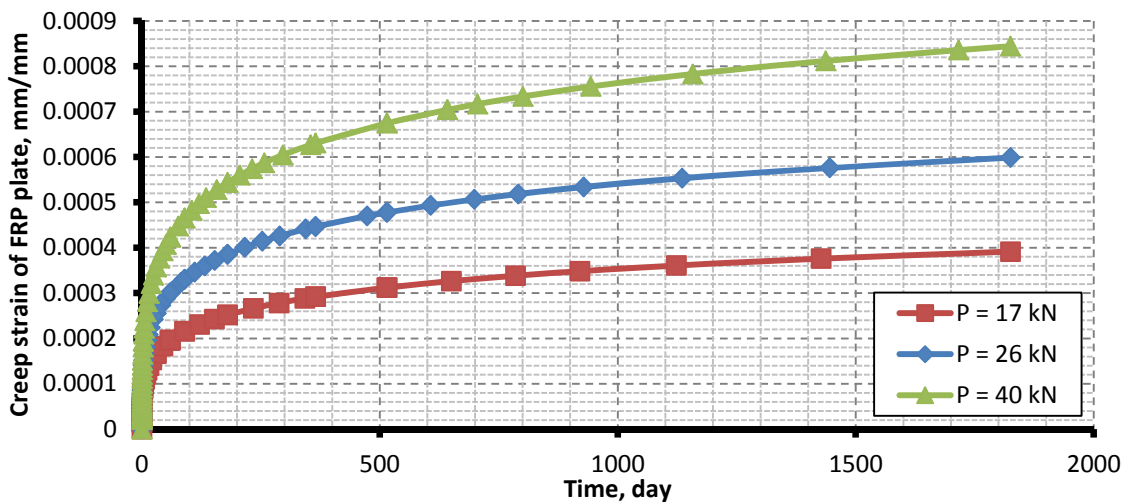
Figure 6-16: CFRP creep strain at mid-span at different applied load comparison.

6.3.5   CFRP-plate end slip

The long-term CFRP slip at the end of the CFRP plate at different applied load levels are shown in Figure 6-17; the slip increased with 50% and 124 % for increasing of the applied load from 53% to 135% respectively compared to slip at load level 17 kN. From the results it can be observed that the applied load level should be within the service load level to avoid the increasing in CFRP plate end slip due to increasing of the stress at the plate end.
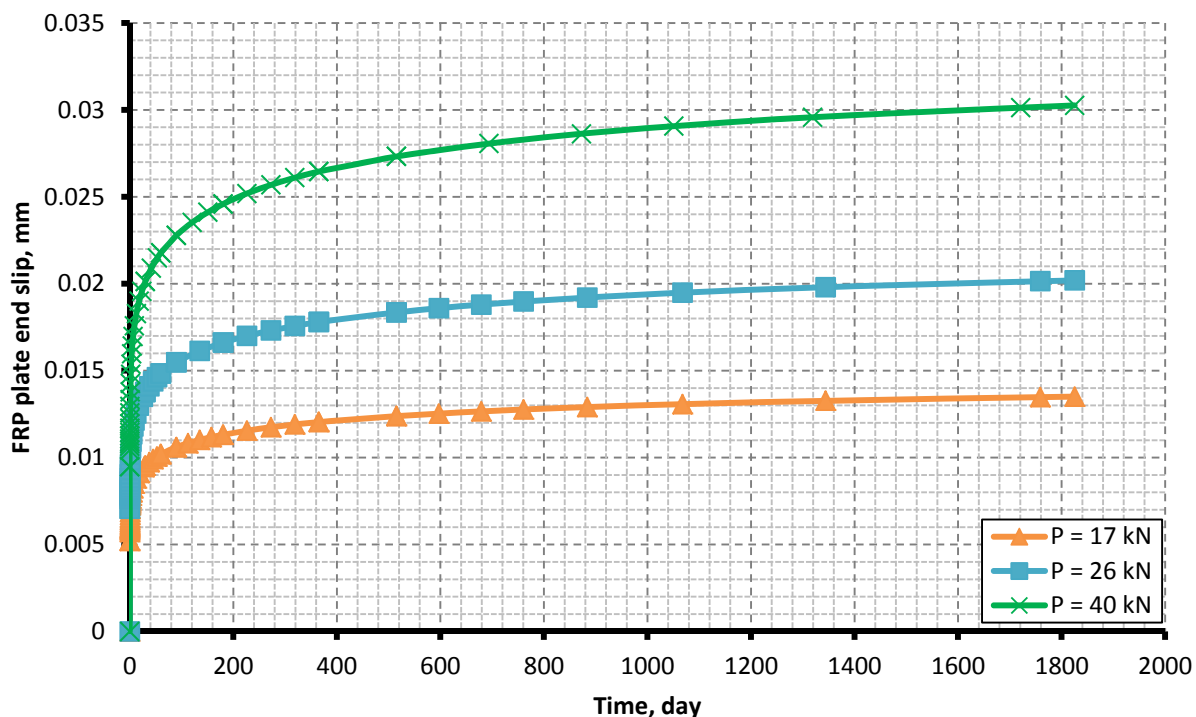
Figure 6-17: CFRP slip at plate end at different applied load comparison.

6.3.6   Shear stress along interface

The shear stress on the epoxy interface is varied along the length of the interface; it was high at the end of the CFRP plate and decreased to its minimum value at the mid-span; due to the concentrated shear stress at the end of the CFRP plat as shown in Figure 6-18.

It can be observed that there is neither failure nor debonding occur along the interface. Also the FE modeling can be used to predict the creep behavior of the CFRP-strengthened RC beams.
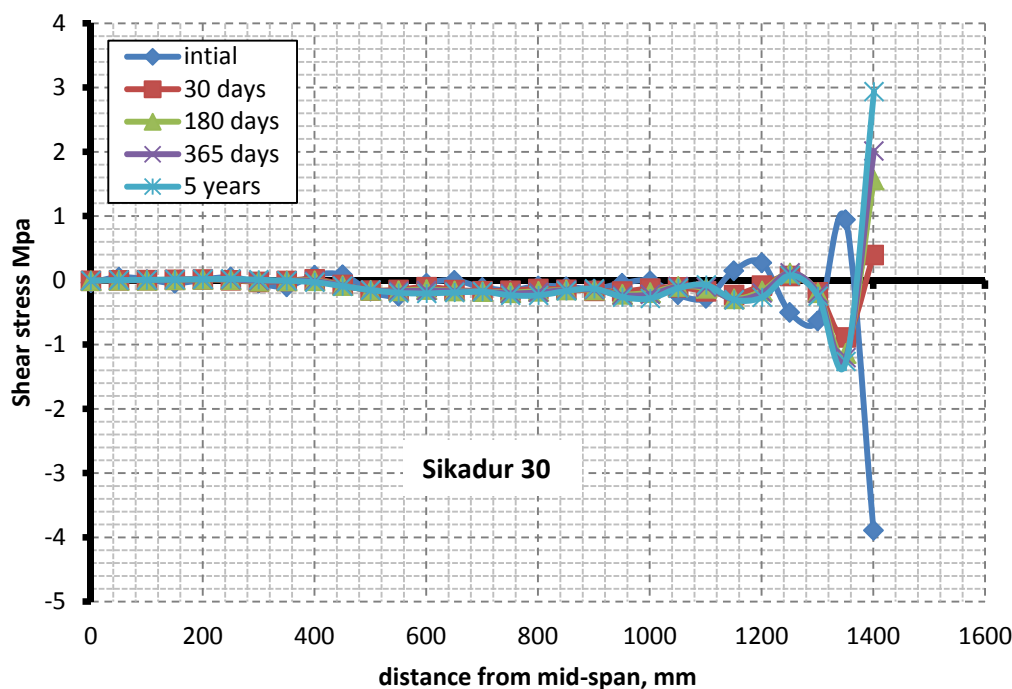
Figure 6-18: shear stress along the interface at different time.

6.4 Parametric study of creep behavior of CFRP-strengthening RC-beams using FE modeling

The verified FE model was used to predict the creep behavior of CFRP-strengthened reinforced concrete beams. The effect of the interface epoxy properties, applied load level and effect of CFRP plate length/breadth to beam span/breadth ratio on the creep behavior of the CFRP-strengthened RC beams are the parameters used in this study.

6.4.1 Effect of epoxy interface properties

The epoxy interface has an important effect on the behavior of strengthened RC beams because the property of epoxy was affected by the temperature and the material properties of the epoxy. And also this material used to transfer the stresses from RC beam to CFRP plate.

6.4.1.1 Type of epoxy interface

To study the effect of the epoxy interface on the creep behavior of CFRP-strengthened RC beam; four types were selected based on the previous study of epoxy adhesive creep (Miguel Miravalles & IIP Dharmawan, 2007), the properties and creep parameters are shown in Table 6-6.

Table 6-6: creep parameters for epoxy interface used in FE analysis

Material	Epoxy A	Epoxy B	Epoxy C	Epoxy D
Young modulus (GPa)	5.29	4.57	6	6.54
Poisson's ratio, ν	0.364	0.312	0.35	0.329
A	7.87 E-05	0.000297	1.23E-04	1.19E-06
n	1.344	0.7658	0.9913	2.709
m	-0.67813	-0.73529	-0.65207	-0.71435

Figure 6-19 shows the effect of type of epoxy adhesive in mid-span creep deflection; it can be observed that the effect on creep deflection can be neglected.
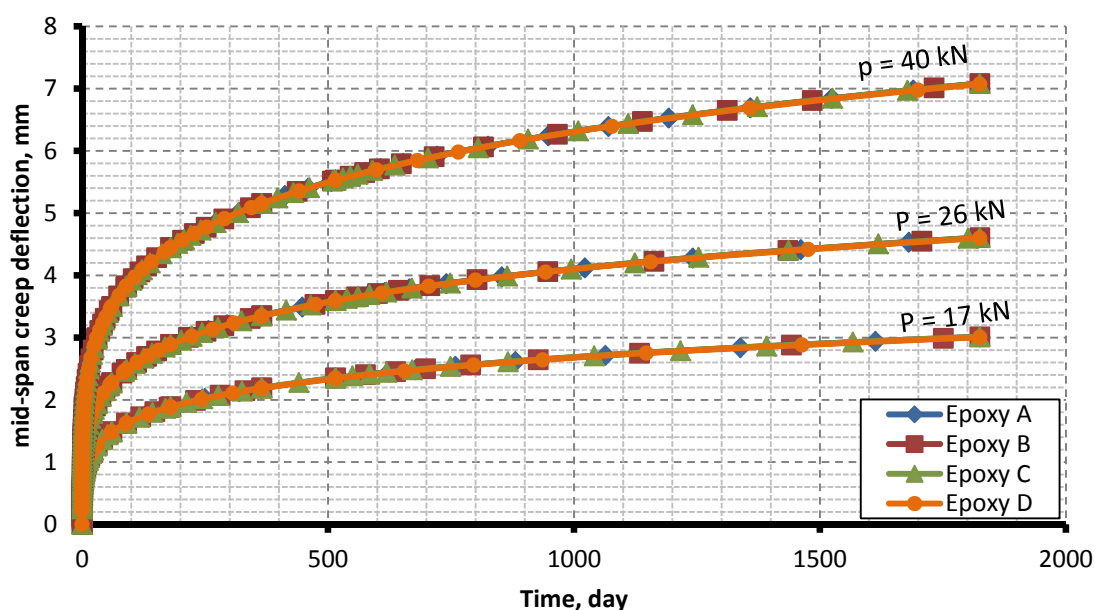
Figure 6-19: creep deflection at mid-span at different applied load for different epoxy adhesive comparison.

The long-term slip of the end of CFRP plate was increased by about 3 to 3.6 times the initial slip at applied load P = 40 kN; as shown in Figure 6-20 this due to the increase in the strain along the interface. The creep strain along the interface after 5 years for different type of epoxy is shown in Figure 6-21, it can be seen that the strengthened creep has limited effect on the interface creep strain for epoxy type A, D, and Sikadur 30 and the effect of the creep of the strengthened beams on the interface creep strain is increased for epoxy B more than other types of epoxy.
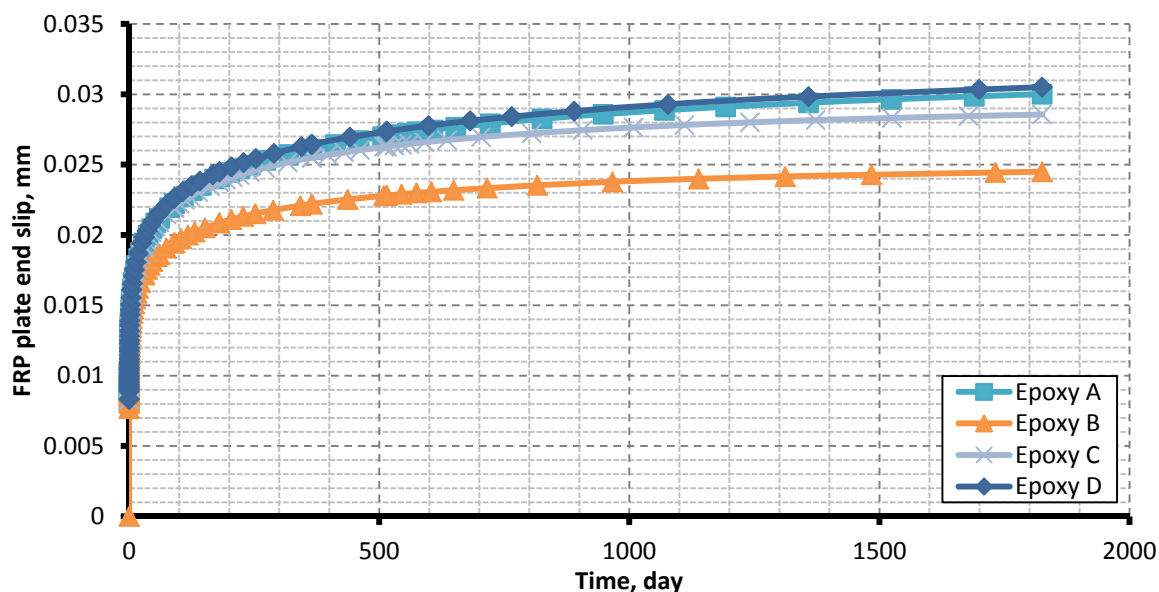
Figure 6-20: CFRP slip at plate end at different applied load comparison.
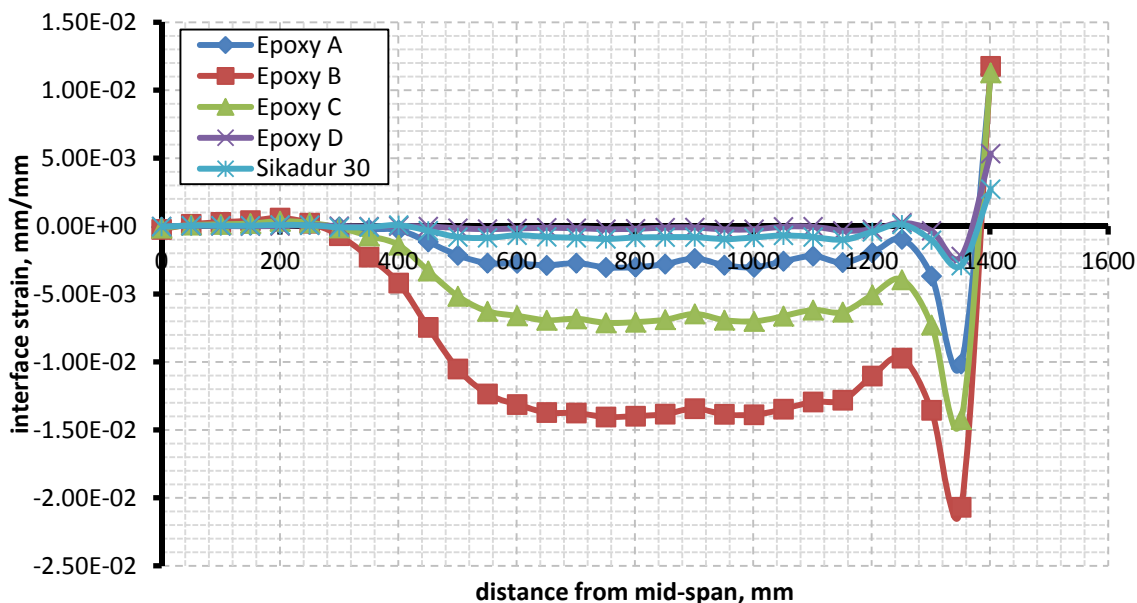
Figure 6-21: interface creep strain for different epoxy adhesive comparison.

The shear stress along the interface at applied load P=40 kN at time 30, 180, 365, 1825 days for different epoxy types are shown in Figure 6-22; the sikadur30 epoxy has very good resistance to creep and also the epoxy type D is good, while for the other types of epoxy the shear stress increase along the interface with time and this is affect the bond between CFRP and concrete.

From the results of different epoxy types it can be observed that the epoxy type has no significant effect on the creep deflection of the CFRP-strengthened RC beams, on the other hand the effect of the epoxy type can limit the change on the interface strain due to creep.
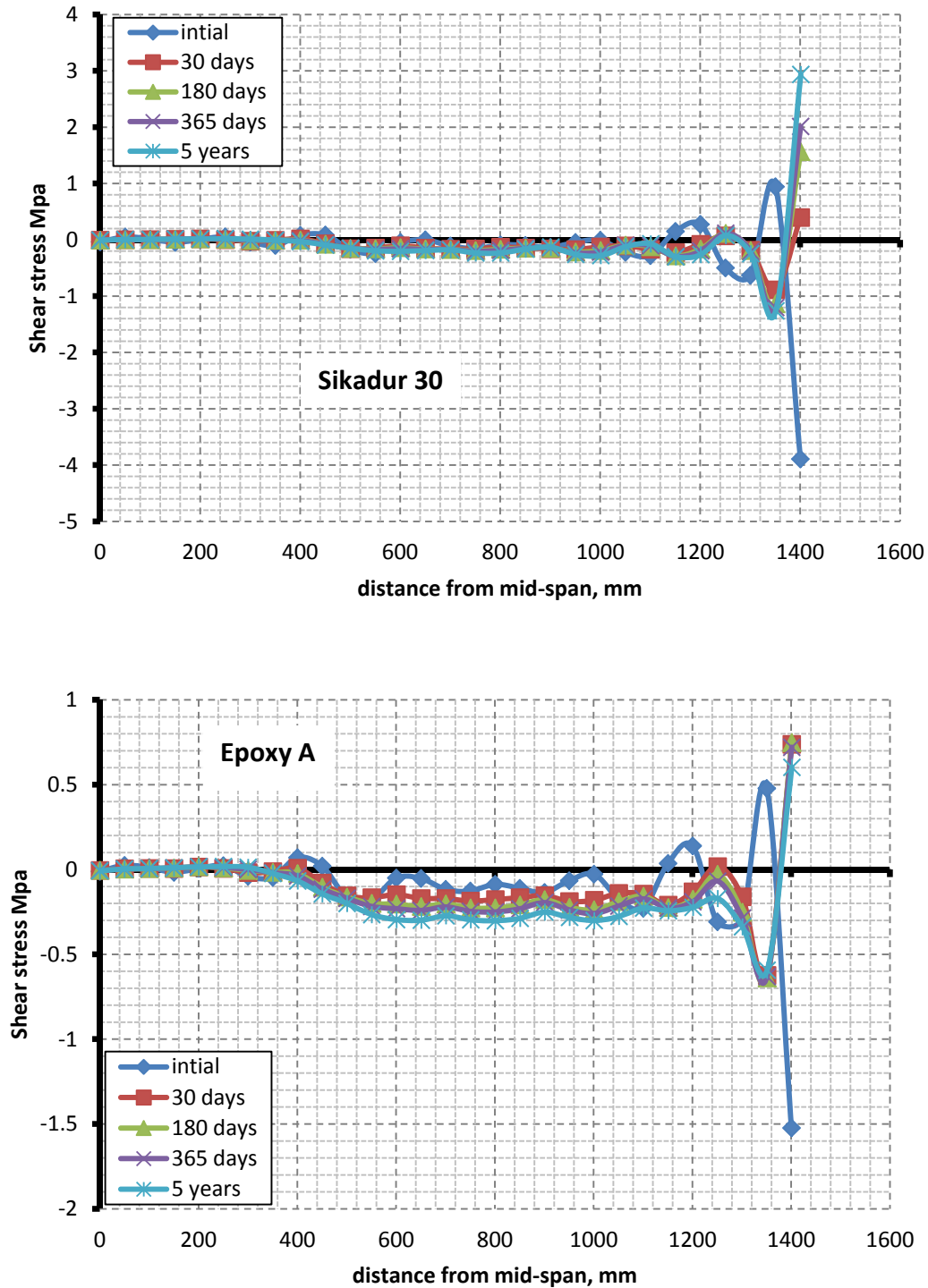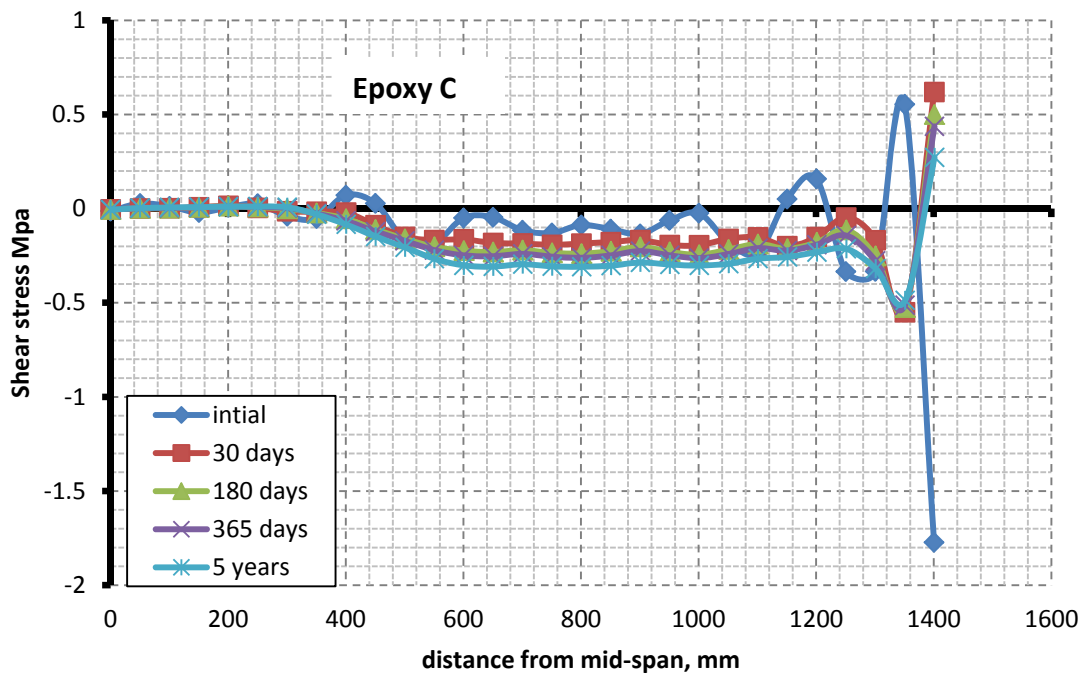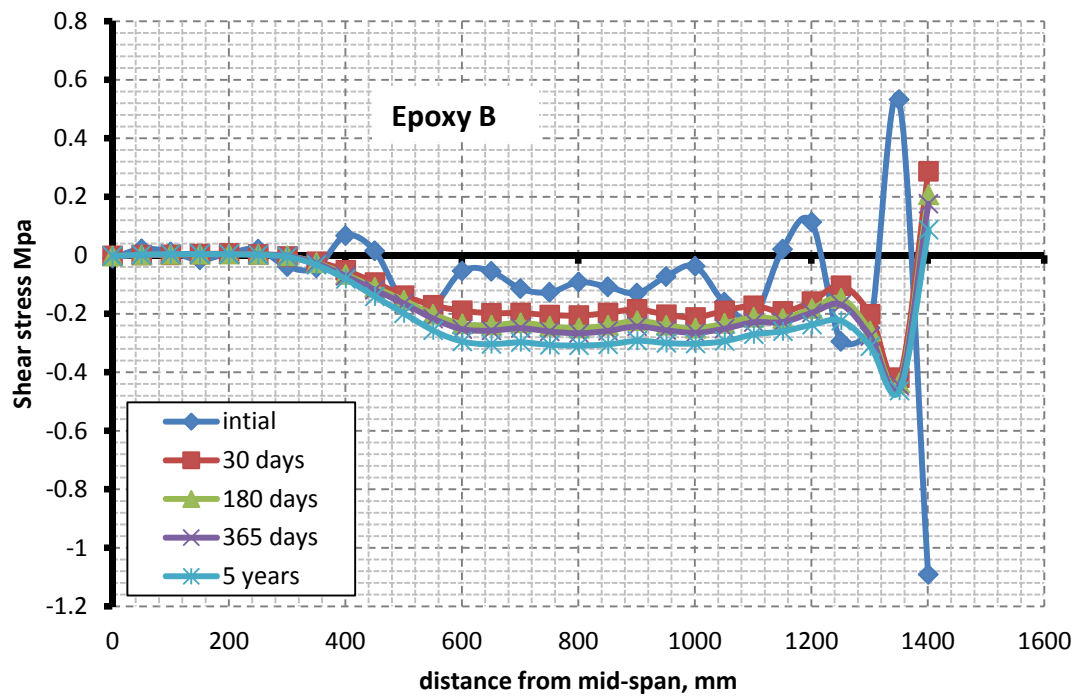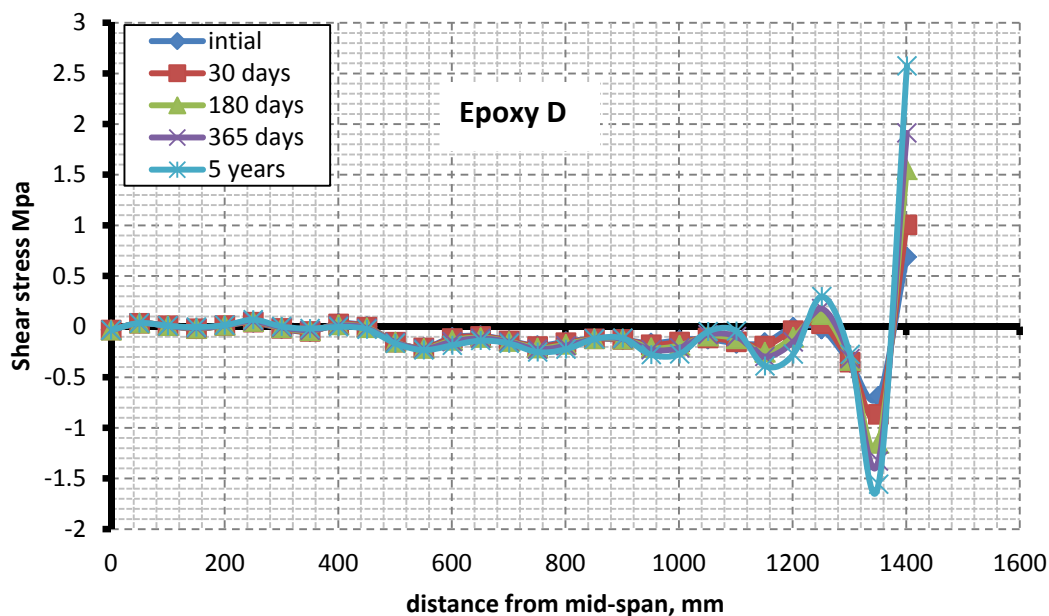
Figure 6-22: shear stress along the interface for different epoxy type.

6.4.1.2   *Effect of temperature on creep of epoxy interface*

In this study the epoxy interface properties and the creep parameters evaluated based on the data from the previous study of (E. Ferrier , et al., 2011) shown in Table 6-7.

Table 6-7: creep parameters for epoxy adhesive used in FE analysis

Material		Epoxy A	Epoxy B	Epoxy C
Young modulus (MPa)		3200	3200	12000
Glass transition temperature T (^{o}C)		55	80	55
T = 20 ^{o}C	A	4.58605E-05	8.76142E-05	3.16036E-05
	n	0.9769	1.0946	0.7573
	m	-0.9095	-0.8467	-0.8241
T = 40 ^{o}C	A	8.40539E-05	0.000137827	5.7885E-05
	n	0.9239	1.0862	0.994
	m	-0.8871	-0.8412	-0.8488
T = 60 ^{o}C	A	0.00019246*	0.000168762	6.95357E-05*
	n	1.1178*	0.9873	1.0164*
	m	-0.8565*	-0.8148	-0.8972*

* The creep parameter evaluated at 50 ^{o}C

122

It should be noticed that the effect of temperature not included in evaluated the creep parameter of reinforced concrete and CFRP.

The mid-span creep deflection for different type of epoxy was shown in Figure 6-23
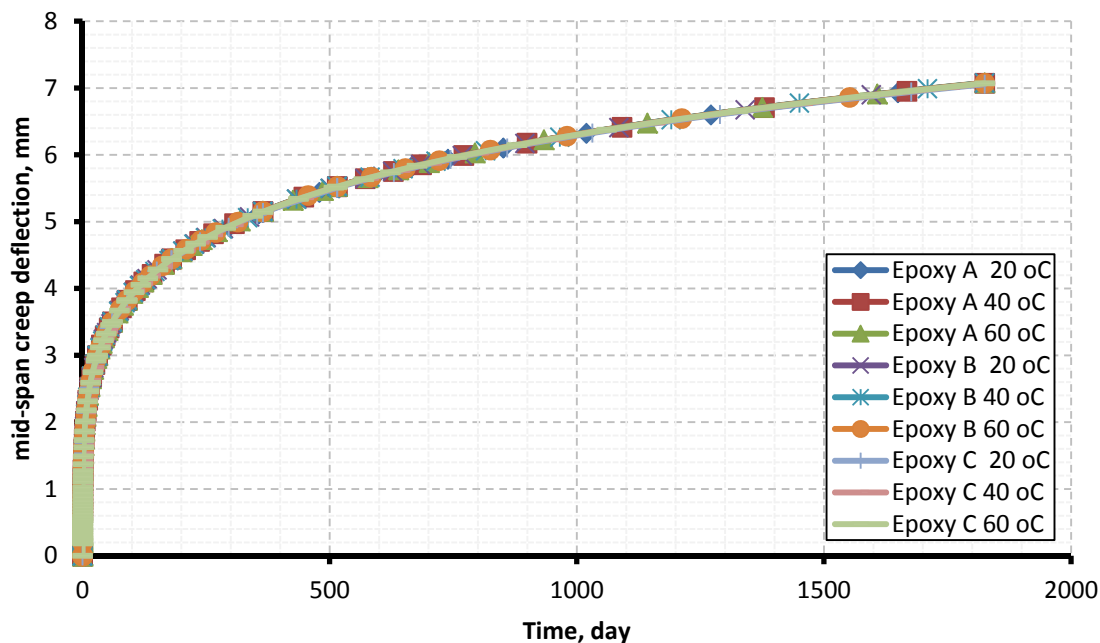
Figure 6-23: creep deflection at mid-span of CFRP-strengthened RC beam for different epoxy type

From the results it can be seen that the epoxy type has no significant effect on the creep deflection of the CFRP-strengthened RC beams at different temperature level. This is due to the very small thickness of the epoxy compared to the concrete section, also the effect of the temperature level was on the strain and stiffness of the epoxy layer.

The interface strain at different temperature level for different epoxy types are shown in Figure 6-24. From the results it can be observed that there is no significant effect on the creep deflection of the CFRP-strengthened RC beams due to the high level of the interface type at different temperature levels. Also the creep strain along the interface was increased from 2 to 3 times more than the immediate interface strain when the temperature was changed from 20 ^{o}C to 50 ^{o}C, but for the epoxy with combined high modulus of elasticity (high shear modulus) and high glass transition temperature the interface strain was decreased by about 40 % less than the other types of epoxy.

From the results for the previous epoxy types in this parametric study, it can be concluded that, using epoxy with combined high modulus of elasticity (more than 6 GPa) and high glass transition temperature (more than 55 ^{o}C) will improve the interface strain but did not affect the creep deflection of the strengthened RC beams. This result can be approved

with the experimental results obtained by (E. Ferrier , et al., 2011) he recommended to use epoxy adhesive with high shear modulus (more than 10 GPa) and in my study the shear modulus can be decreased to be 20% (shear modulus more than 2.3 GPa, and modulus of elasticity more than 6 GPa) from the results obtained by (E. Ferrier , et al., 2011).
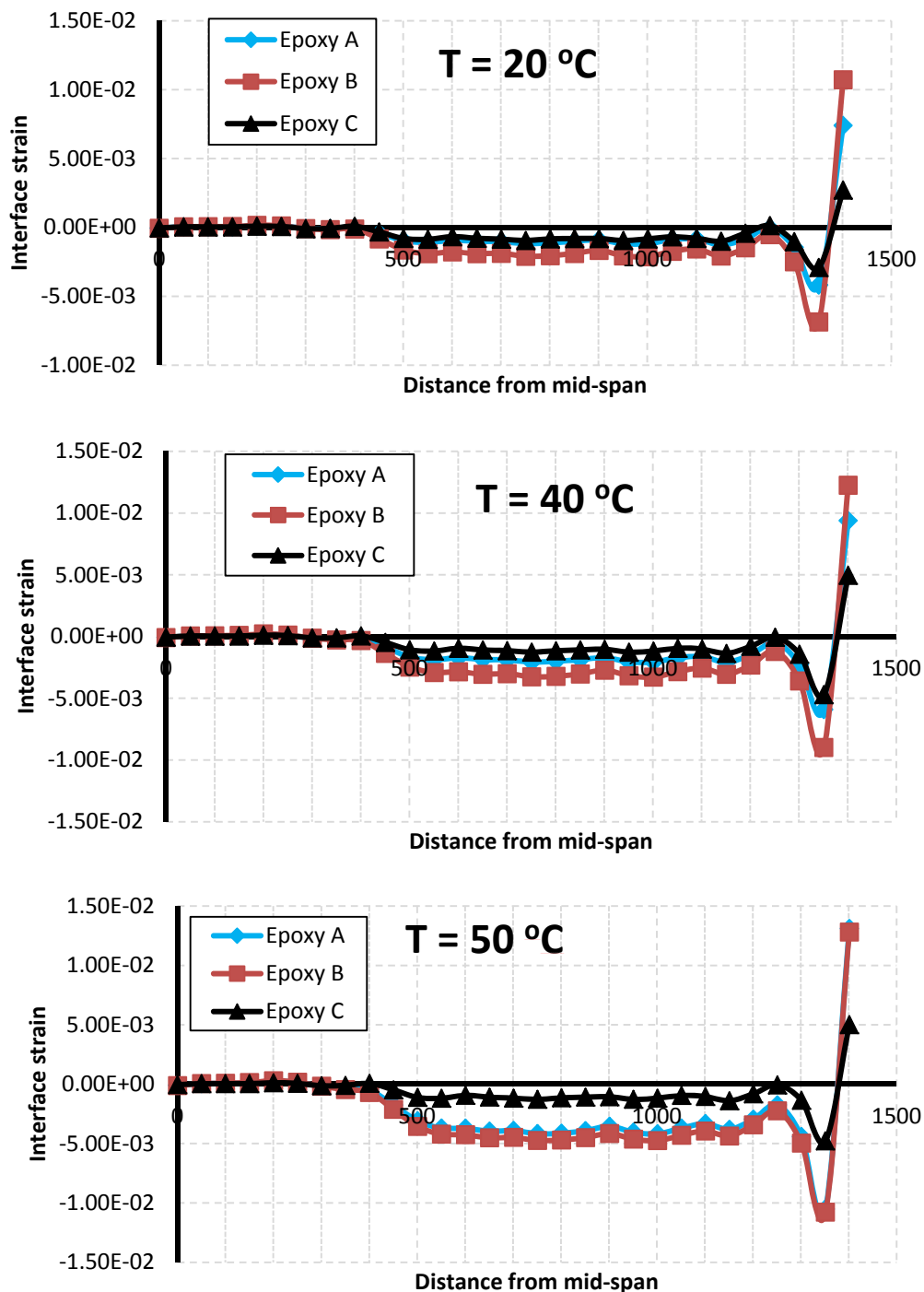
Figure 6-24: shear strain along the interface for epoxy type A, B and C at different temperature after 5 years

124

6.4.2 Effect of applied load level

Figure 6-25 shows the effect of applied load on the creep deflection at mid-span of the CFRP-strengthened RC beam, it can be showed that the deflection due to creep was 3.86 mm, 5.896 mm, 9.052 mm, 13.882 mm at applied load P= 17 kN, P= 26 kN, P= 40 kN and P= 60 kN respectively. Also the increasing in the deflection due to creep was gradually and proportion to the increase in the applied load. The variation of the increase in applied load were 0, 0.53, 1.35, and 2.53 for applied load P= 17 kN, P= 26 kN, P= 40 kN and P= 60 kN respectively; while the increase in the deflection due to creep of the CFRP-strengthened RC beams were 0, 0.53, 1.34, and 2.53.
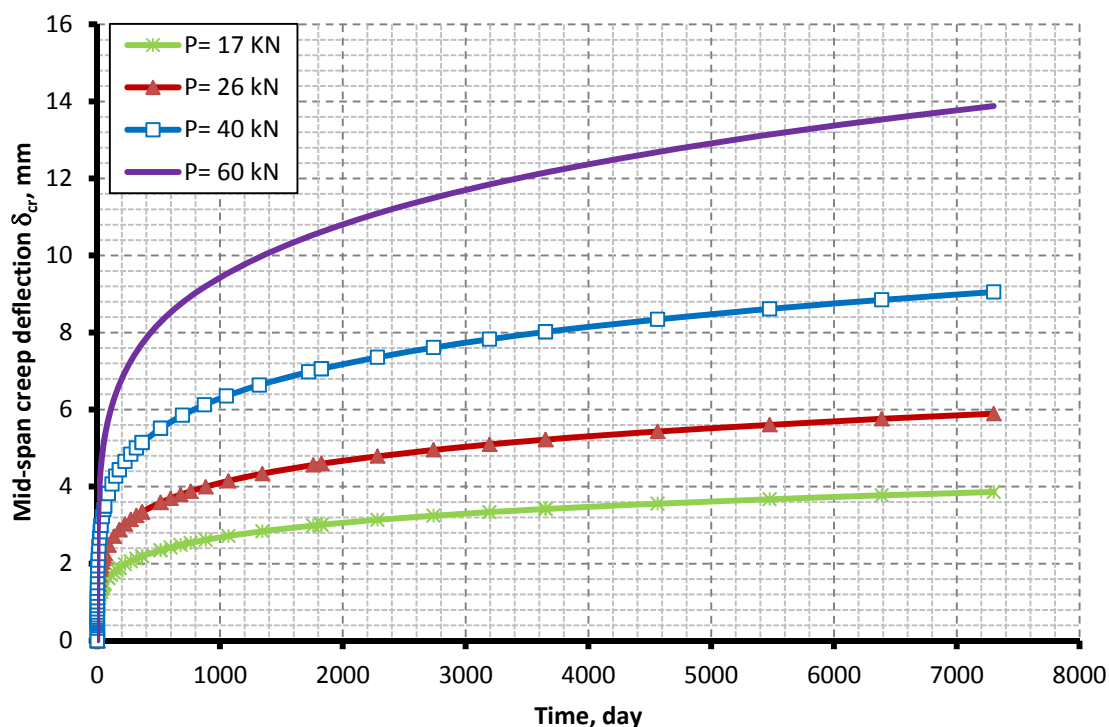
Figure 6-25: creep deflection at mid-span of FRP-strengthened RC beam at different applied load

From the results it can be concluded that the applied load level should be within the service load limit (about 59% from ultimate capacity).

6.4.3   Effect of CFRP plate length/breadth to beam span/breadth ratio

To study the effect of CFRP plate length/breadth as a ratio from the beam span length/breadth; three groups were studied using the calibrated finite element model. Each group consists of three CFRP-strengthened RC beams with same CFRP plate length to beam span length ratio and different CFRP plate breadth. In the FE model the applied load (40kN) was constant for all the beams to predict the effect of changing CFRP plate dimensions on the creep deflection of the strengthened beams. Also the results obtained from the finite element model were compared to the creep deflection of the control RC beam under the same load. The details of the studied groups were summarized in Table 6-8.

Table 6-8: Mid-span creep deflection for different CFRP length/breadth to beam span/breadth ratio obtained from FE model

L_{cfrp}/L_{beam} %	b_{cfrp}/b_{beam} %	Creep deflection Δ_{cr} (mm)					percentage of decreasing in creep deflection due to strengthened %
		30 days	90 days	6 months	1 year	5 years	5 years
40	41	3.095	3.955	4.596	5.335	7.354	3.74
	67	3.037	3.880	4.506	5.229	7.197	5.80
	100	2.970	3.788	4.398	5.100	7.011	8.23
75	41	3.067	3.915	4.549	5.279	7.271	4.83
	67	2.995	3.820	4.435	5.144	7.072	7.43
	100	2.909	3.706	4.299	4.982	6.834	10.55
96	41	3.064	3.916	4.552	5.283	7.268	4.87
	67	2.991	3.818	4.434	5.141	7.059	7.60
	100	2.901	3.700	4.293	4.973	6.814	10.81
Control RC beam		3.197	4.088	4.756	5.527	7.640	0

The effect of CFRP plate length to beam span ratio and CFRP plate breadth to beam breadth ratio were studied in this section using the calibrated finite element model, the CFRP plate length to beam span ratio was varied from 0.4 to 0.96, and CFRP plate breadth to beam breadth ratio was varied from 0.4 to 1, the load to mid-span relationship is shown in Figure 6-26. From the results it can be seen that using CFRP with varied length and breadth from 40% - more than 96% to beam span and breadth ratio decreases the creep deflection by 3.74% - 10.81% after 5 years. The relationship between percentage of decreasing in creep deflection and different CFRP plate length/breadth ration was shown in Figure 6-27.
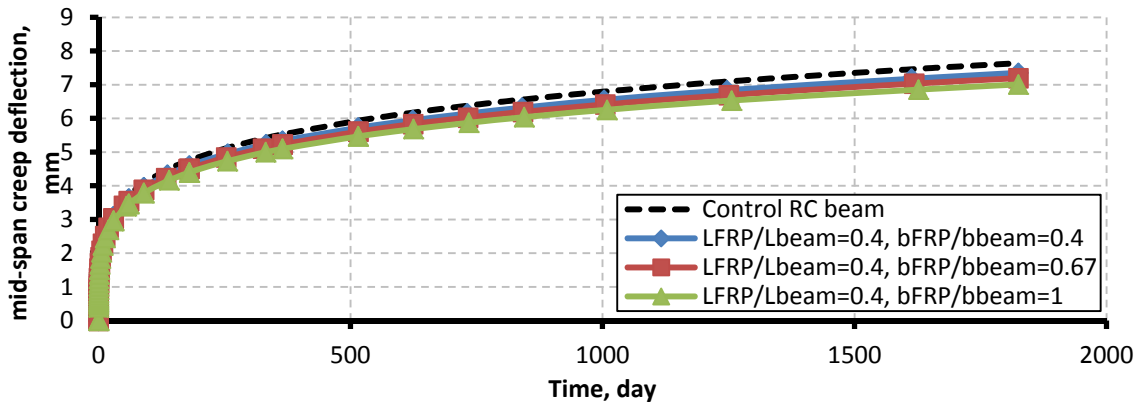
a)   creep deflection at mid-span of CFRP-strengthened RC beam for 40% CFRP plate length ratio and different breadth ratio
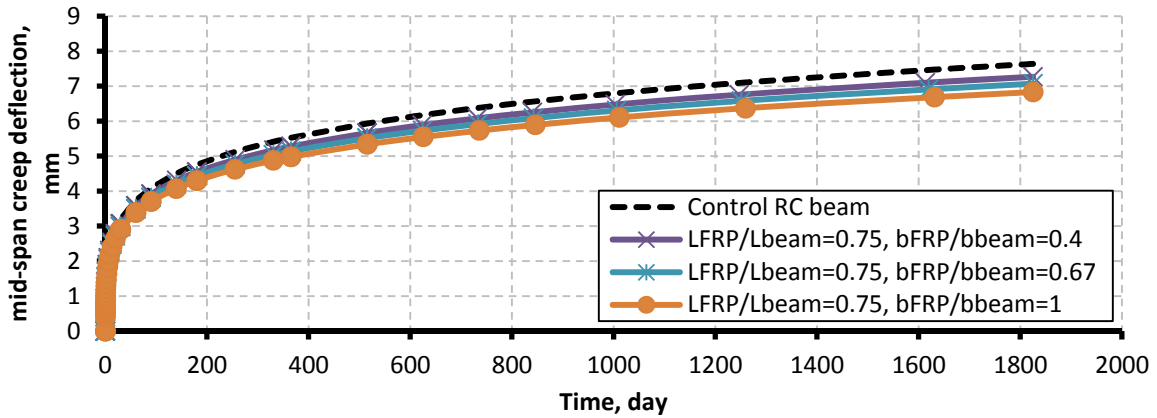
b)   creep deflection at mid-span of CFRP-strengthened RC beam for 75% CFRP plate length ratio and different breadth ratio
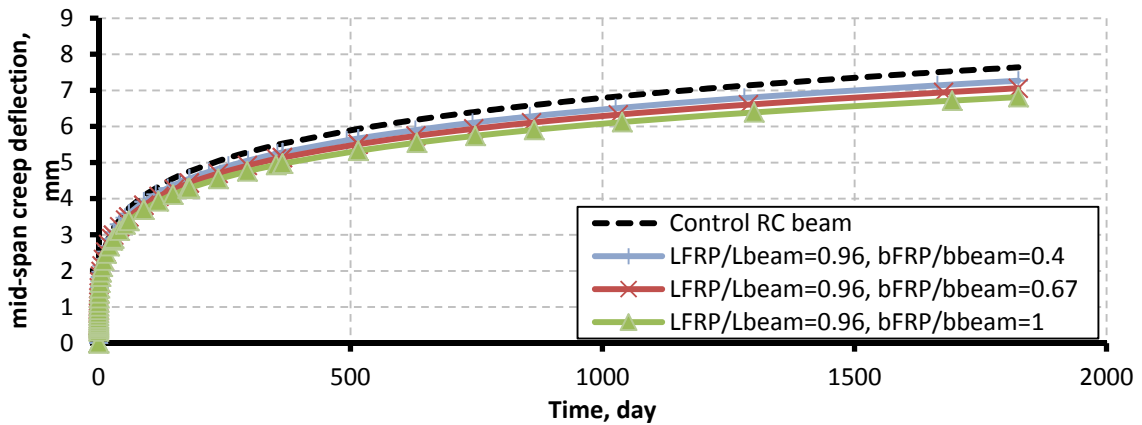
c)   creep deflection at mid-span of CFRP-strengthened RC beam for 96% CFRP plate length ratio and different breadth ratio

Figure 6-26: creep deflection at mid-span of CFRP-strengthened RC beam for different CFRP plate length/ breadth ratio
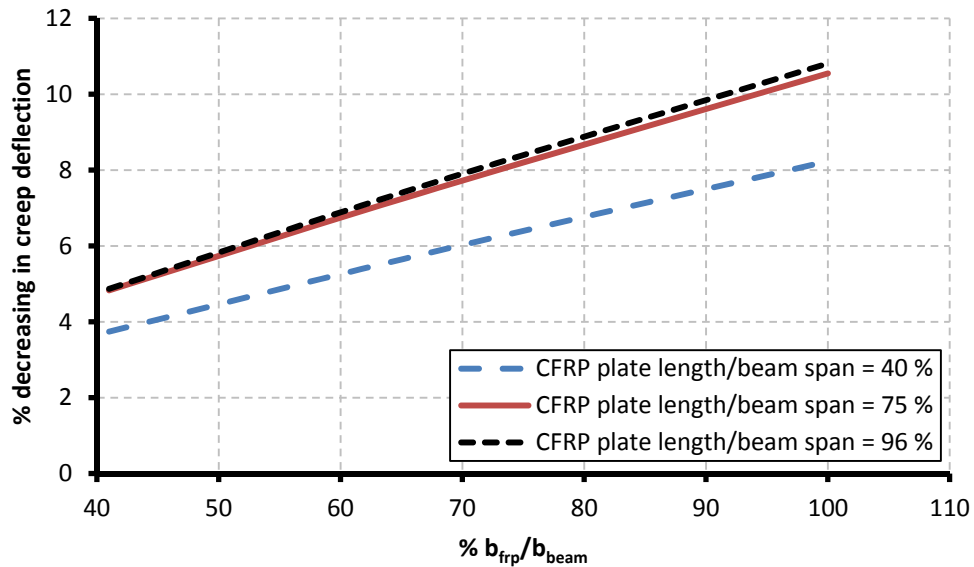
Figure 6-27: percentage of decreasing in creep deflection at mid-span of CFRP-
strengthened RC beam for different   CFRP plate length/ breadth ratio

From Figure 6-27, it can be predict the percentage of decreasing in mid-span creep deflection of the CFRP-strengthened RC beams for different CFRP plate length/breadth ratio under service load from the unstrengthened RC beams.

It can be concluded that the creep deflection of the unstrengthened beams can be used for estimating the creep deflection of the CFRP-strengthened RC beams. The creep deflection of both CFRP-strengthened RC beams and unstrengthened RC beams can be calculated as immediate deflection multiplying by creep coefficient, the creep coefficient for concrete calculated using the code equation will be checked in the next section to validate its ability to estimate the creep deflection of the CFRP-strengthened RC beams.

6.5 Comparison results with ACI 209R-92 and CEB-FIP 1990

In this section; a comparison between creep coefficient obtained from experimental results and numerical results for CFRP-strengthened RC beams and the creep coefficient of concrete results estimated from code equation to verify the ability of creep coefficient of concrete for determining the creep coefficient and creep deflection of the CFRP-strengthened RC beams.

6.5.1 ACI 209R-92

The creep coefficient of concrete is estimated as follows:

$$\varphi(t, t_o) = \varphi_\infty(t_o) \cdot \frac{(t - t_o)^{0.6}}{10 + (t - t_o)^{0.6}} \tag{6-4}$$

Where

$\varphi(t, t_o)$: Creep coefficient at time t

$\varphi_\infty(t_o)$: Ultimate creep coefficient

t_o : Time of loading

The ultimate creep coefficient can be expressed as:

$$\varphi_\infty(t_o) = \gamma_c \cdot \varphi_\infty \tag{6-5}$$

The constant $\varphi_\infty = 2.35$ is recommended. The correction factors γ_c consist of the following terms:

$$\gamma_c = \gamma_{la} \cdot \gamma_{RH} \cdot \gamma_{at} \cdot \gamma_s \cdot \gamma_\rho \cdot \gamma_a \tag{6-6}$$

Where

γ_{la} : Correction factor for loading age.

For loading ages later than 7 days and moist cured concrete, $\gamma_{la} = 1.25$ x $t_o^{-0.118}$

For loading ages later than 1-3 days and steam cured concrete, $\gamma_{la} = 1.13$ x $t_o^{-0.094}$

γ_{RH} : Correction factor ambient relative humidity. For ambient relative humidity greater than 40%, $\gamma_{RH} = 1.27 - 0.0067$ RH; (RH is the ambient relative humidity in %)

γ_{at} : Correction factor for thickness of member. When the average thickness or volume to surface ratio of a structural member differs from 150 mm or 38 mm, respectively.

γ_s : Correction factor for slump of fresh concrete;

$\gamma_s = 0.82 + 0.00264\ S_1$

S_1 : is the slump in mm.

γ_ρ : Correction factor for fine to total aggregate ratio.

$\gamma_\rho = 0.88 + 0.0024\ \rho_a$

ρ_a : is fine to total aggregate ratio

γ_a : Correction factor for air content. $\gamma_a = 0.46 + 0.09 a_a$

a_a is air content.

The data used in this study are as following:

b =120 mm	f'_c= 44 MPa
t=300 mm	f_t= 2.6 MPa

L= 2900 E_c=23941 MPa

A_s= 402 mm^2 f_y= 490 MPa

A'_s= 157 mm^2 E_s=200000 MPa

d_s= 264 mm E_{FRP}=165000 MPa

d'_s= 33 mm f_{FRP}= 2800 MPa

A_{FRP}= 96 mm^2 t_o=260 days

d_{FRP}= 301.6 mm

$\gamma_{la} = 0.65$

$\gamma_{RH} = 0.935$ for RH = 50 %

$\gamma_{at} = 1$

$\gamma_s = 1$

$\gamma_\rho = 1$

$\gamma_\rho = 1$

$\gamma_c = \gamma_{la} \cdot \gamma_{RH} \cdot \gamma_{at} \cdot \gamma_s \cdot \gamma_\rho \cdot \gamma_a = 0.61$

$\varphi_\infty(t_o) = \gamma_c \cdot \varphi_\infty = 1.43$

6.5.2   CEB-FIP 1990

The creep strain can be predicted by the following equation:

$$\varepsilon_{cr}(t, t_o) = \frac{\sigma_c}{E_c} \cdot \varphi(t, t_o)$$
(6-7)

Where;

$\varepsilon_{cr}(t, t_o)$: is the creep strain at time t

σ_c : is the applied stress

$\varphi(t,t_0)$: is the creep coefficient

E_c : is the concrete modulus of elasticity at 28 days.

The creep coefficient, $\varphi(t,t_0)$, is usually used to describe the magnitude of the creep deformations. It is defined as the total deformation (including creep) divided by the instantaneous deformation

The creep coefficient of concrete $\varphi(t,t_0)$ can be calculated from the following expression:

$$\varphi(t, t_o) = \varphi_o \beta_c(t, t_o)$$
(6-8)

Where

φ_o : is the notional creep coefficient

$\beta_c(t, t_o)$: is a coefficient that describes the progress of creep with time after loading.

The notational creep coefficient can be estimated as follows:

$$\varphi_o = \varphi_{RH} \cdot \beta(f_{cm}) \cdot \beta(t_o)$$
(6-9)

Where

φ_{RH} : is a factor that takes the relative humidity into account,

$\beta(f_{cm})$: is a factor for the effect of concrete strength, and

$\beta(t_o)$: is a factor for the effect of concrete age at loading, t_o.

The factor φ_{RH} is calculated with the following equation:

$$\varphi_{RH} = 1 + \frac{1 - RH/100}{0.46(\frac{h}{100})^{1/3}}$$
(6-10)

where

RH : is the relative humidity for the surrounding, expressed in percentage and

131

h : is the notional size of the concrete member in mm, calculated as:

$$h = \frac{2A_c}{u} \tag{6-11}$$

Where

A_c: Cross-sectional area (in mm^2)

u : Perimeter of the member in contact with the atmosphere (in mm)

The factor $\beta(f_{cm})$ is calculated with the following expression:

$$\beta(f_{cm}) = \frac{5.3}{\sqrt{f_{cm}/10}} \tag{6-12}$$

Where

f_{cm} : is the mean compressive strength of concrete, in MPa at the age of 28 days

The factor $\beta(t_o)$ is calculated from the following equation:

$$\beta(t_o) = \frac{1}{0.1 + t_o^{0.2}} \tag{6-13}$$

The coefficient $\beta_c(t, t_o)$ can be calculated using the following expression:

$$\beta_c(t, t_o) = \left[\frac{(t - t_o)/t_1}{\beta_H + (t - t_o)/t_1}\right]^{0.3} \tag{6-14}$$

$$\beta_H = 150\left[1 + \left(1.2\frac{RH}{100}\right)^{18}\right] \cdot \frac{h}{100} + 250 \leq 1500 \tag{6-15}$$

Where

t: is the age of concrete in days at the moment considered,

t_0 : is the age of concrete in days when loaded

$t_1 = 1\ day$

β_H: is a coefficient depending on the relative humidity and the notional size of the concrete member

The data used in this study are as following:

       b = 120 mm f'_c = 44 MPa

t=300 mm f_t= 2.6 MPa

L= 2900 E_c=23941 MPa

A_s= 402 mm^2 f_y= 490 MPa

A'_s= 157 mm^2 E_s=200000 MPa

d_s= 264 mm E_{FRP}=165000 MPa

d'_s= 33 mm f_{FRP}= 2800 MPa

A_{FRP}= 96 mm^2 t_o=260 days

d_{FRP}= 301.6 mm

u = 840 $\beta(f_{cm})$= 2.65

2A_c = 72000 $\beta(t_o)$ = 0.318

h = 85.72 φ_o = 1.809

RH = 50 % β_H = 378.58

φ_{RH} = 2.14 $\beta_c(t, t_o)$ = 0.457, 0.551, 0.61, 0.711, 0.808, 0.848, and 0.945

$$\varphi(t, t_o) = \varphi_o \beta_c(t, t_o)$$

The creep deflection = $\varphi(t, t_o)$ x initial deflection

The comparison between results obtained from experimental, FE model, ACI 209-2R, ACI 318 and CEB-FIP 1990 are summarized in Figure 6-28 and Table 6-9

It can be observed that the value of the creep coefficient of concrete which calculated using ACI 209 equation when using initial creep coefficient φ_∞ = 2.35 is higher than creep the creep coefficient of CFRP-strengthened RC beams obtained from both of experimental and FE model results. Also the creep coefficient estimated using CEB-FIP 1990 is the highest one. Furthermore the concrete creep coefficient of concrete calculated using ACI 209 equation when using initial creep coefficient φ_∞ = 1.60 gives good matching creep coefficient results with both experimental and FE modelling for CFRP-strengthened RC beams.

It is recommended to use initial creep coefficient φ_∞ = 1.6 when estimating the creep coefficient of concrete to predict the creep deflection of CFRP-strengthened RC beams using the code equation.

It can be concluded that the creep coefficient of concrete estimated from code equation can be used to predict the creep deflection of both unstrengthened and CFRP-strengthened RC beams.

133
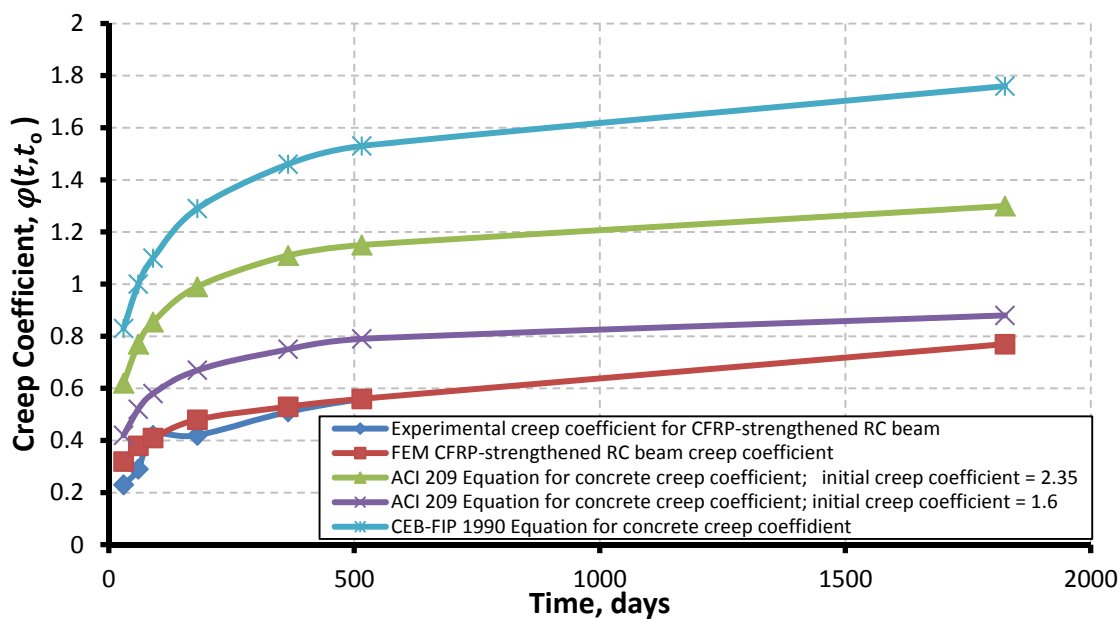
Figure 6-28: creep coefficient for CFRP-strengthened RC beam and concrete comparison

Table 6-9 creep coeffecent comparison

Time, day \ Specimen	0	30	60	90	180	365	515	5 years
Experimental FRP-strengthened RC beam	0	0.23	0.29	0.42	0.42	0.51	0.56	--
FEM CFRP-strengthened RC beam	0	0.32	0.38	0.41	0.48	0.53	0.56	0.77
ACI 209 Equation for concrete; $\varphi_\infty = 2.35$	0	0.62	0.77	0.855	0.99	1.11	1.15	1.30
ACI 209 Equation for concrete; $\varphi_\infty = 1.6$	0	0.42	0.52	0.58	0.67	0.75	0.79	0.88
CEB-FIP 1990 Equation concrete; $\varphi_o = 1.809$	0	0.83	1	1.1	1.29	1.46	1.53	1.76

6.6   Summary of numerical analysis

In this chapter, the finite element program (Abaqus) was used to simulate the long-term behavior of CFRP-strengthened RC beams, the results obtained from the finite element model was compared to the results obtained from the experimental program to validate the ability of the model for investigating the long-term behavior of the CFRP-strengthened RC beams. The results obtained from the FE model had good agreement with the experimental results and the calibrated model was used for parametric study to predict the flexural and long-term behavior of the CFRP-strengthened reinforced concrete beams. The results obtained from the finite element modeling were plotted and analyzed and the following can be drawn:

➢ The FE model can predict the flexural and long-term behavior of the CFRP-strengthened RC with good agreement with experimental and codes equations.

➢ The FE model can predict the slip at the end of CFRP plate and also can be used to predict the CFRP/concrete interface stress (strains) at any load step, which is very difficult to evaluate it in the experimental test.

➢ Using CFRP plate with length near to the span of the beam and with breadth not less than the half of the reinforced concrete beam breadth was improving the behavior of the strengthening system because the length of CFRP plate should be extended with an anchorage length outside the maximum flexural stress to obtain the full effect of the CFRP plate on the strengthening system. Also the breadth is very important to increase the ability of the strengthened beams to resist the debonding effect at the CFRP plate end due to the concentration of stresses at the plate end.

➢ The properties of the epoxy adhesive had no significant effect in the ultimate capacity of the strengthened system because the interface stress depends on the concrete tensile strength, beam breadth and CFRP breadth which controls the interface failure stresses.

➢ The externally bonded CFRP decreased the creep deflection of the CFRP-strengthened RC beams by varied value which depends on the ratio of the CFRP plate length/breadth to the beams span/breadth. This decreasing of creep deflection was due to the effect of the CFRP plate on increasing the stiffness of the beam and decreasing the initial deflection of the strengthened beams.

➢ The deflection due to creep was increased proportionally to the applied load level with nearly the same value of the increasing in the applied load level. It should be considered in design that the applied load should be in the limit of the service load used by the international codes.

➢ The interface strain was decreased at high temperature level (50 °C) by about 40 % for the epoxy type with high modulus of elasticity from epoxy type with low modulus of elasticity, while the interface strain was increased to 2-3 times due to varying in temperature level from 20 °C to 50 °C. Using epoxy with combined high glass transition temperature and high modulus of elasticity will improve the interface strain (stress) and limit the creep effect on the interface. The modulus of elasticity of the epoxy decreases due to increasing of temperature. In this case, the interface bond stress will decrease due to the decreasing in the interface stiffness at high level of temperature.

➢ The creep coefficient of concrete estimated from any code equation can be used to evaluate the creep deflection of the strengthening system because of the insignificant effect of CFRP and epoxy on the creep deflection of the strengthening system and the higher factor of safety used by the code equations for estimating the creep coefficient of the concrete.

➢ The creep deflection of strengthening system obtained from experimental and FEM results in this study had good agreement with the creep deflection estimated from ACI code equations when using initial creep coefficient φ_∞ = 1.6 for estimating the creep coefficient of the concrete.

Chapter 7   Summary and Conclusions

7.1 Summary

Strengthening reinforced concrete beams with externally bonded carbon fiber reinforced polymer was widely used as a retrofitting technique for reinforced structures. Engineers have to be able to predict the behavior of the strengthening system using a simplified method for preliminary design. Evaluation of flexural short- and long-term behavior of the CFRP-strengthened RC beams, especially the effect of the creep phenomenon on the behavior of the strengthening beams during the life time of the structure, was set as the aim of this thesis. To achieve this aim, experimental and numerical models were carried out to evaluate the flexural short- and long-term behavior of CFRP-strengthened reinforced concrete beams.

Experimental program consisting of twelve simply supported beams, (six of them were strengthened with externally bonded CFRP plates), was carried out and divided into two parts. In Part I, three CFRP-strengthened RC beams were tested to evaluate the flexural behavior up to failure and the results were compared to the unstrengthening reinforced concrete beams, while in Part II, three CFRP-strengthened RC beams were tested to evaluate the long-term behavior of the CFRP-strengthened RC beams under constant load in the lab condition and the results were compared to the unstrengthening reinforced concrete beams.

3D numerical model using Abaqus finite element program was developed and validated with the experimental results to investigate the flexural and long-term behavior of CFRP-strengthened RC beams. The material properties for concrete, steel, epoxy interface and CFRP were evaluated based on the available data from experimental and literature. The time hardening power law creep equation available in Abaqus program was used to evaluate the creep behavior of the and the results were compared to the unstrengthening reinforced concrete beams. Furthermore, a parametric study using the calibrated finite element model was also carried out. The effect of CFRP, epoxy type, temperature level at interface, and the applied load level were the parameters used in evaluating the long-term behavior of the CFRP-strengthened RC beams.

7.2 Conclusions and Recommendation

In this study, the short and long-term behavior of CFRP-strengthened RC beams were investigated. Based on the experimental and finite element modeling results the following general conclusions can be drawn:

1. It is recommended to use externally bonded CFRP with length closed to the span of the RC beams, and width equal to the RC beam section width if possible, to get the full increasing effect in the flexural behavior of the CFRP-strengthened

RC beams. The length of the CFRP plate should be extended with enough length to cover the area of the maximum flexural stress to obtain the full effect of the CFRP plate on the ultimate behavior of CFRP-strengthened RC beams. Also the breadth is very important to increase the ability of the CFRP-strengthened RC beams to resist the debonding effect at the CFRP plate end due to the concentration of stresses at the plate end.

2. Most of the creep deformation occurs in the first 90 days and the total deflection of the strengthening system after about one and half year was about 1.55 times the initial deflection of the strengthening system. This value of total deflection increased to about 2.3 times the initial deflection after about 20 years under service load level due to creep. The creep deflection must be taken into consideration in the design of the CFRP-strengthened RC beams.

3. The externally bonded CFRP decreases the creep deflection of the CFRP-strengthened RC beams by decreasing rate depends on the CFRP plate length/breadth to beam span/breadth ratio, because the CFRP plate increases the stiffness of the beams and decreases the immediate deflection, this will improve to the creep deflection which was a function of immediate deflection.

4. The creep coefficient of concrete estimated from any international code equation can be used to evaluate the creep deflection of the CFRP-strengthened RC beams because of the higher factor of safety used in the code equations for estimating the creep coefficient of the concrete.

5. Based on long-term results of the CFRP-strengthened RC beams, there is no slip observed between CFRP and concrete, also the cracks are limited in the tension side of the RC beam due to the effect of the strengthening with CFRP in increasing the stiffness of the beams and the limitation of the applied service load level.

6. The deflection due to creep was increased proportionally to the applied load level for both strengthened and unstrengthened systems. It should be considered the service load of the strengthening system to be limited with the code value.

7. Based on the FE model for creep of the CFRP-strengthened RC beams at different temperature levels for different epoxy types it can be concluded that the epoxy adhesive is very sensitive to the change of the temperature and the interface strain due to creep was increased with about 2 to 3 times its initial strain due to increasing the temperature level from 20 $^{\circ}$C to 50 $^{\circ}$C; although there is no failure occurs in the interface due to creep. It is suggested to use epoxy adhesive with high modulus of elasticity and it is recommended to be

with high glass transition temperature more than 55 ^{o}C to resist the change in the interface behavior due to the creep of the strengthened system at high temperature level. The modulus of elasticity of the epoxy decreases due to increasing of temperature level. In this case, the interface bond strength will decrease due to the decreasing in the interface stiffness at high level of temperature. Using epoxy with combined high glass temperature and high modulus of elasticity will improve the interface strain (stress) and limit the creep effect on the interface at high temperature levels.

8. Based on the results obtained for 5 years creep deflection of the CFRP-strengthened RC beams from the FE model; it is suggested to use an initial creep factor of 1.6 to estimate the creep coefficient of the concrete using ACI 209 equation to evaluate the creep deflection of the CFRP-strengthened RC beams for the designer because the initial creep factor of 2.35 is a little high.

7.3 Future study

❑ Effect of fire in the behavior of FRP-strengthened RC structures.

❑ Experimental effect of high temperature on the creep behavior of FRP-strengthened RC structures for different types of FRP, epoxy and concrete compressive strength.

❑ Extracting design charts to evaluate the ultimate capacity of FRP-strengthened RC beams for different concrete section dimensions, steel reinforcement ratio, FRP types/area ratio, epoxy type, and concrete compressive strength.

References

Paulson K.A., Nilson A.H. & Hover K.C. , 1991. Long-term deflection of high-strength concretebeams. *ACI Mater J,* 88(2), pp. 197-206.

Abaqus , 2010. *Abaqus V6.10.1, User's Manual, ABAQUS, Inc., Providence.* RI, USA: s.n.

ACI Committee 318, 1999. *Building code requirements for structural concrete and commentary (ACI 318-99).* Detroit (MI): American Concrete Institute.

ACI Committee 435R , 1995. Control of Deflection in Concrete Structures. In: Redford Station, Detroit, Michigan: American Concrete Institute, pp. 66-71.

ACI Committee 440, 2002. Guide for the design and construction of externally bonded FRP systems for strengthening concrete structures. In: *Draft report, American Concrete Institute,.* Framington Hills, MI.: s.n.

ACI Committee-209R-92, 1997. *Prediction of Creep, Shrinkage, and Temperature Effects in Concrete Structures.* Detroit, Michigan.: American Concrete Institute (ACI).

Al Chami, G., Therialt, M. & Neal, K., 2009. Creep behaviour of CFRP-strengthened reinforced concrete beams. *Construction and Building Materials ,* pp. 1640-1652.

Almusallam T. H., Al-Salloum Y. A., Alsayed S. H. & Mosallam A. S, 2001. Durability & Long-Term Behavior of Reinforced Concrete Beams Strengthened with FRP Composites. *FRP Composites in Civil Engineering,* Volume 2 ed. J. G. Teng, pp. 1579-1588.

Amélie Grésille, 2009. *Carbon fiber strengthening and jacking of engineering structures,* Sweden: Division of Structural Engineering, Faculty of Engineering, Lund University.

Amélie Grésille, 2009. *Carbon fiber strengthening and jacking of engineering structures,* Lund, Sweden: Division of Structural Engineering, Faculty of Engineering, Lund University.

Amir, M., 2002. Creep and Durability of Environmentally Conditioned FRP-RC Beams Using Fiber Optic Sensors. *Journal of REINFORCED PLASTICS AND COMPOSITES,* pp. 351-373.

An W., Saadatmanesh H. & Ehsani M. R., 1991. RC beams strengthened with FRP plates II: Analysis and parametric study." Journal of Structural Engineering. *Journal of Structural Engineering, ASCE,* 117(11), pp. 3434-3455.

Andrade, E., 1910. *The viscous flow in metals and allied phenomena.* London: Proc. R. Soc..

Aqeel Ahmed & Venkatesh Kodur, 2011. The experimental behavior of FRP-strengthened RC beams subjected to design fire exposure. *Engineering Structures,* Volume 33, pp. 2201-2211.

Aram MR, Czaderski C & Motavalli M , 2008. Debonding failure mode of flexural FRP-strengthened RC beams. *Composite Part B: Engineering,* Volume 39, pp. 826-841.

ASTM. E119, 2002. *Standard test methods for fire tests of building construction and materials..* West Conshohocken, Pennsylvania: American Society for Testing and Materials.

Bazant Z.P., 1988. *Mathematical Modelling of Creep and Shrinkage of Concrete..* Wiley, New York.: s.n.

Bazant ZP & Becq-Giraudon E, 2002. Statistical prediction of fracture parameters of concrete and implications for choice of testing standard. *Cement Concrete Res,* 32(4), pp. 529-556.

Benmokrane B., et al., 2000. Effects of Alkaline Environment, Gap Analysis for Durability of Fiber Reinforced Polymer Composites in Civil Infrastructure. *ASCE Publications,* pp. 24-28.

Benzeggagh M. L. & Kenane M. , 1996. Measurement of Mixed-mode Delamination Fracture Toughness of Unidirectional Glass/epoxy Composites with Mixed-mode Bending Apparatus. *Compos. Sci. Technol,* 56(4), pp. 439-449.

Brea Williams, et al., 2006. Fire insulation schemes for FRP-strengthened concrete slabs. *Composites: Part A,* Volume 37, p. 1151–1160.

C. Mazzotti & M. Savoia, 2005. Long term properties of bond between concrete and FRP. *Proceedings of the International Symposium on Bond Behaviour of FRP in Structures (BBFS 2005), Chen and Teng (eds), 2005 International Institute for FRP in Construction,* pp. 531-537.

CEB-FIP Model Code, 1990. *CEB-FIP Model Code 90, Euro-Internationale du beton: CEB Bulletin 213/214.* Lausanne, Switzerland: s.n.

Ceroni F , 2010. Experimental performances of RC beams strengthened with FRP materials. *Construction and Building Materials,* Volume 24, pp. 1547-1559.

Chajes M. J., Thomson T., Finch W. W. & Januszka T., 1994. Flexural strengthening of concrete beams using externally bonded composite materials. *Construction and Building Materials,* 8(3), pp. 191-201.

Chen W-F., 1982. *Plasticity in reinforced concrete.* xv ed. New York: McGraw-Hill.

Christensen, J. B., Gilstrap, J. M. & Dolan, C. W., 1996. Composite Materials Reinforcement of Masonry Structures. *Journal of Architectural Engineering,* pp. 63-70.

Costa IG & Barros JAO, 2010. Flexural and shear strengthening of RC beams with composite materials - The influence of cutting steel stirrups to install CFRP strips. *Cement and Concrete Composites. ,* Volume 32, pp. 544-553.

Dai J G & Ueda T, 2003. Local bond stress slip relationship for FRP sheets-concrete interfaces. *Proceedings of the 6th International Symposium on FRP Reinforcement for Concrete Structures, K. H. Tan, ed,* Volume 1, pp. 143-152.

Dat Duthinh & Monica Starnes, 2001. Strengthening of Reinforced Concrete Beams with Carbon FRP. *Composites in Constructions,* pp. 493-498.

David E. & Neuner J. D, 2001. *Environmental Durability Studies for FRP Systems. Definition of Normal Conditions of Use of FRP for Structural Strengthening Applications.* Hong Kong, China,, Proceedings of the International Conference of FRP Composites in Civil Engineering, pp. 1551-1558.

E. Ferrier , L. Michel, B. Jurkiewiez & P. Hamelin, 2011. Creep behavior of adhesives used for external FRP strengthening of RC structures. *Construction and Building Materials,* Volume 25, pp. 461-467.

El-Mihilmy MT & Tedesco JW, 2001. Prediction of anchorage failure for reinforced concrete beams strengthened with fiber-reinforced polymer plates. *ACI Struct J,* 98(3), pp. 301-314.

Eurocode 2, 1992. *[ENV 1992-1-1], 'Design of Concrete Structa.tres: Part 1.1 General Rules and Rules for Buildings' Commission of the E.U..* Brussels, 1992: s.n.

Findley W. N. , 1960. Mechanism and mechanics of creep of plastics. *SPE journal, Society of Plastic Engineering, Brookfield, Conn.,,* pp. 57-65.

Fuhr, P. L., Huston, D. R., Ambrose, T. P. & Snyde, D. M., 1993. Stress monitoring of concrete using embedded optical fiber sensors. *Journal of Structural Engineering,* p. 2263–2269.

Fukuta Y., Matsuda T. & Kawai M., 2008. Homogenized creep behavior of CFRP laminates at high tempreature. *International Journal of Modern Physics B,* 22(31), pp. 6161-6166.

Ghali A. & Favre R., 1986. Concrete structures: Stresses and deformations. In: London: Chapman and Hall, pp. 9-10.

Gilbert R. I., 1999. Deflection calculation for reinforced concrete structures—Why we sometimes get it wrong. *ACI Struct. J.,* 96(6), p. 1027–1032.

Gilbert R.I., 1988. *Time Effects in Concrete Structures..* B.V., Amsterdam.: Elsevier Science Publishers.

142

Guo ZG, Cao SY, Sun WM & Lin XY., 2005. Experimental study on bond stress-slip behaviour between FRP sheets and concrete. *International Institute for FRP in Construction, proceedings of the international symposium on bond behaviour of FRP in structures,* pp. 77-84.

H. Blontrock , L. Taerwe & S. Matthys, 1999. *Properties of Fibre Reinforced Plastics at Elevated Temperatures with Regard to Fire Resistance of Reinforced Concrete Members.* s.l., In: Proceedings, 4th International Symposium on Non-Metallic (FRP) Reinforcement for Concrete Structures, American Concrete Institute, Baltimore, MD, p. 43–54.

Hearing B. & Buyukozturk O., 2000. *Delamination in reinforced concrete retrofitted with fibre reinforced plastics,* s.l.: Research Rep., Department of Civil and Environmental Engineering, MIT..

Hillerborg, A., 1985. The theoretical basis of a method to determine the fracture energy Gf of concrete. *concrete. Materials and Structures,* Volume 108, pp. Saenz, L. Discussion equation for the stress.

Hillerborg, A., Modéer, M. & Petersson, P. E., 1976. Analysis of Crack Formation and Crack Growth in Concrete by means of Fracture Mechanics and Finite Elements. *Cement and Concrete Research,* 6(6), pp. 773-781.

Hollaway L. C. & Mays G. C., 1999. *Strengthening of reinforced concrete structures Using externally-bonded FRP composites in structural and civil engineering.* s.l.:Woodhead Publishing Limited, Abington Hall, Abington Cambridge CB1 6AH.

Holmes M. & Just D. J, 1983. GRP in structural engineering,. In: Essex, U.K.,: Applied Science Publishers, pp. 213-229.

Hu, H.-T. & Schnobrich, W., 1989. Constitutive modelling of concrete by using nonassociated plasticity. J Mater Civil Eng. *ASCA,* Issue 4, pp. 199-216.

Hundley, A. & Dolan, C., 1996. Non-accelerated creep-rupture of fiber-reinforced-plastics in a concrete environment. *Proceedings of Materials Engineering Congress, ASCE,* p. 519–526.

Huston, D., Fuhr, P., Kajenski, P. & Snyder, D., 1992. Concrete beam testing with optical fiber sensors. *Structures Congress, San Antonio, TX, ASCE,* p. 60–66.

ISIS Canada, 2001. *Strengthening reinforced concrete structures with externally-bonded fiber reinforced polymers.* Design Manual, No. 4 ed. s.l.:s.n.

J. G. Teng, J. F. Chen, S. T. Smith & L. Lam, 2003. Behaviour and strength of FRP-strengthened RC structures: a state-of-the-art review. *Structures & Buildings,* 156(1), pp. 51-62.

143

JCI, 2003. *Technical report on retrofit technology for concrete structures,* s.l.: Technical Committee on Retrofitting Technology for Concrete Structures.

Jinlong Pan & Christopher K.Y. Leung, 2007. Debonding along the FRP–concrete interface under combined pulling/peeling effects. *Engineering Fracture Mechanics,* Volume 74, p. 132–150.

Jumaat MZ & Alam MA , 2010. Experimental and numerical analysis of end anchored steel plate and CFRP laminate flexurally strengthened r. c. beams. *Int. J. Phys. Sci,* Volume 5, pp. 132-144.

Juska T., Dutta P., Carlson L. & Weitsman J., 2000. Thermal Effects Gap Analysis for Durability of Fiber Reinforced Polymer Composites in Civil Infrastructure. *ASCE Publications,* pp. 40-45.

Kachlakev D & McCurry DD., 2000. Behavior of full-scale reinforced concrete beams retrofitted for shear and flexural with FRP laminates. *Composites,* Volume 31, pp. 445-452.

Kak Tien Chong, Stephen J. Foster & R. Ian Gilbert, 2008. Time-dependent modelling of RC structures using the cracked membrane model and solidification theory. *Computers and Structures,* Volume 86, p. 1305–1317.

Kalamkarov, A. L., Fitzgerald, S. B., MacDonald, D. O. & Georgiades, A., 2000. Mechanical performance of pultruded composite rods with embedded fiber optic sensors. *Composites Science and Technology,* p. 1161–1169.

Karbhari V. M. & Engineer M., 1996. Effect of Environmental Exposure on the External Strengthening of Concrete with Composites - Short-Term Bond Durability. *Journal of Reinforced Plastics and Composites,* pp. 1194-1216.

Kinloch , A., 1987. *Adhesion and adhesives..* New York : Chapman & Hall.

L.A. Bisby, 2003. *Fire Behavior of Fibre-Reinforced Polymer (FRP) Reinforced or Strengthened Concrete,* Kingston, ON, Canada: Doctoral thesis, Queen's University at Kingston.

Lee S.M, 1989. *Reference Book for Composite Technology. ,.* Lancaster, PA.: Technomic Publishing.

Lee J & Fenves LG., 1998. Plastic-damage concrete model for earthquake analysis of dams.. *Earthquake Eng Struct Dyn,* 27(9), pp. 937-956.

Leung C. K. Y, 2001. Delamination failure in concrete beams retrofitted with a bonded plate J. Mater. *J. Mater. Civ. Eng.,* 13(2), pp. 101-113.

Leung H. Y. , Balendran R. V. & Lim C. W. , 2001. Flexural Capacity of Strengthened Concrete Beams Exposed to Different Environmental Conditions. *FRP Composites in Civil Engineering, Volume 2 ed. J. G. Teng,, pp. 1597-1606.

Liew Y. S. & and Tan K. H. , 2003. *Durability of GFRP Composites under Tropical Climate.* s.l., Proceedings of the Sixth International Symposium on FRP Reinforcement for Concrete Structures (FRPRCS-6), pp. 769-778.

Liew, Y., 2003. *Durability of FRP composites under tropical climate.MEng thesis.* National University of Singapore: s.n.

Lubliner J, Oliver J, Oller S & Onate E., 1989. Plastic-damage model for concrete. *Int J Solids Struct,* 25(3), pp. 299-326.

Lu, X. Z., Ten, J. G., Ye, L. P. & Jaing, J. J., 2005. Bond-slip models for FRP sheets/plates bonded to concrete.. *Engineering Structures,* pp. 920-937.

M.R. Esfahani, M.R. Kianoush & A.R. Tajari, 2006. Flexural behaviour of reinforced concrete beams strengthened by CFRP sheets. *Engineering Structures,* pp. 1-17.

Maaskant, R. et al., 1997. Fiber-optic bragg grating sensors for bridge monitoring. *Cement and Concrete Composites,* p. 21–33.

MacGregor, J., 1997. Reinforced concrete: mechanics and design. In: 3rd ed. Upper Saddle River NJ: Prentice Hall, p. 939.

Maksimov R.D. & Plume R., 2001. Long-term creep of hybrid aramid/glassfiber-reinforced plastics. *Mechanics of Composite Materials,* 37(4), p. 271e280.

Meier U, 1992. Carbon fiber reinforced polymers, modern materials in bridge engineering. *Struc Engrg Int ,* 2(1), pp. 7-12.

Meier, U., Deuring, M., Meier, H. & Schwegler, G., 1995. Strengthening of structures with CFRP Laminates: Research and application in Switzerland. *Advanced Composite Materials in Civil Engineering Structures, ASCE,* pp. 243-251.

Meier, U. & Kaiser, H., 1991. Strengthening of structures with CFRP laminates. *Advanced Composite Materials in Civil Engineering Structures, ASCE,* pp. 224-232.

Michael J. Chajes, Theodore A. Thomson Jr. & Cory A. Farschman, 1995. Durability of concretebeamsexternallyreinforced with composite fabrics. *Construction and Building Materials,* 9(3), pp. 141-148.

145

Miguel Miravalles & IIP Dharmawan, 2007. *The creep behaviour of adhesives; A numerical and experimental investigation,* Göteborg, Sweden: Master Thesis. Department of Structural Engineering, Chalmers University of Technology.

N. Pesic & K. Pilakoutas, 2005. Flexural analysis and design of reinforced concrete beams with externally bonded FRP reinforcement. *Materials" and Structures,* Volume 38, pp. 183-192.

Nabil F. Grace, 2004. Concrete Repair with CFRP Evaluating the durability of externally bonded carbon fiber-reinforced polymer plates and fabric exposed to the environment. *Concrete international,* pp. 45-52.

Naumenko, K. & Altenbach, H., 2007. *Modeling of Creep for Structural Analysis (Foundations of Engineering Mechanics).* s.l.:Springer.

Nikolaos Plevris & Thanasis C. Triantafillou, 1994. Time-Dependent behavior of RC members strengthened with FRP laminates. *Journal of Structural Engineering, ASCE,* 120(3), pp. 1016-1042.

Nilson, H., Darwin, D. & Dolan, C. W., 2004. *Design of Concrete structures.* 13th edition ed. s.l.:McGraw Hill Higher Education.

Pania Meshgin, Kyoung-Kyu Choi & Mahmoud M. Reda Taha, 2009. Experimental and analytical investigations of creep of epoxy adhesive at the concrete–FRP interfaces. *International Journal of Adhesion & Adhesives,* Volume 29, pp. 56-66.

Pham H & Al-Mahaidi R , 2004. Assessment of available prediction models for the strength of FRP retrofitted RC beams. *Composite Structures,* Volume 66, pp. 601-610.

Philip A. Ritchie, David A. Thomas, Le-Wu Lu & Guy M. Conelly, 1991. External Reinforcement of Concrete Beams Using Fiber Reinforced Plastics. *American concrete Institute, ACI Structural Journal,* 88(4), pp. 490-500.

Phillips L.N. , 1989. Design with Advanced Composite Material. In: London, England: Springer-verlag, p. 77–80.

Piggott, M., 2002. *Load bearing fibre composites.* 2nd ed. Boston/Dordrecht/London: Kluwer Academic.

Ritchie PA, Thomas DA, Lu LW & Connely GM, 1991. Connely GM. External reinforcement of concrete beams using fiber reinforced plastics. *ACI Structural Journal,* 88(4), pp. 490-500.

Ross C. A., Jerome D. M. , Tedesco J. W. & Hughes M. L., 1999. Strengthening of reinforced concrete beams with externally bonded composite laminates. *ACI Structural Journal,* 96(2), pp. 65-71.

S. Benyoucef , A. Tounsi , K.H. Benrahou & E.A. Adda Bedia, 2007. Time-dependent behavior of RC beams strengthened with externally bonded FRP plates: interfacial stresses analysis. *Mech Time-Depend Mater,* Volume 11, p. 231–248.

Saadatmanesh H, & Malek AM., 1998. Design guidelines for strengthening of RC beam with FRP plates. *J Compos Construct,* 2(4), pp. 158-164.

Saadatmanesh, . H. & Tannous , F. E., 1998. Durability of fiber reinforced plastic (FRP) rebars and tendons in aggressive environments. *Proceedings of the International Seminar on Repair and Rehabilitation of Reinforced Concrete Structures,* p. 120–133.

Saenz, L., 1964. Discussion of ''Equation for the stress-strain curve of concrete'' by Desayi P, Krishman S.. *ACI Journal ,* Volume 61, pp. 1229-1239.

Saha M. K. & Tan K. H., 2004. *Long-term Deflections of FRP-strengthened Beams under Sustained Loads.* s.l., Proceedings of the Second International Conference on FRP Composites in Civil Engineering, pp. 261-266.

Saha, M. & Tan, K., 2005. GFRP-Bonded RC Beams under Sustained Loading and Tropical Weathering. *American Concrete Institute, Advancing concrete knowledge, ACI,* pp. 1379-1396.

Sen, R., Mariscal, D. & Shahawy, M., 1993. Durability of fiberglass pretensioned beams. *Structural Journal, ACI,* p. 525–533.

Sika Detuschland, n.d. *http://deu.sika.com/de/group.html.* [Online].

Smith ST & Teng JG., 2002. FRP-strengthened RC beams. II: assessment of debonding strength models.. *Engineering Structures,* 24(4), pp. 397-417.

Soudki, K. A. & Green, M. F., 1997. Freeze-Thaw Response of CFRP Wrapped Concrete. *Concrete International,* pp. 64-67.

Steckel, G., Hawkins, . G. & Bauer, J., 1999a. Durability Issues for Composites in Infrastructure. *44th International SAMPE Symposium,* pp. 2194-2208.

Stierwalt D.D. & Hamilton III H.R. , 2005. Creep of concrete masonry walls strengthened with FRP composites. *Construction and Building Materials,* Volume 19, pp. 181-187.

Tan K. H., Paramasivam P. & Tan K. C. , 1994. Creep and shrinkage deflections of RC beams with steel fibers. *J. Mater. Civ. Eng.,* 6(4), pp. 474-494.

Tan KH, Saha MK & Liew YS , 2009. FRP-strengthened RC beams under sustained loads and weathering. *Cement and Concrete Composites,* Volume 31, pp. 290-300.

Tan T.H. & Saha M.K., 2006. Long-Term Deflections of Reinforced Concrete Beams Externally Bonded with FRP System. *Journal of Composites for Construction,* 10(6), pp. 474-482.

Tannous, F. & Saadatmanesh, H., 1999. Durability of AR glass fiber reinforced plastic bars. *Journal of Composites for Construction,* p. 12–19.

Teng GJ, Smith TS, Yao J & Chen JF, 2003. Intermediate crack-induced debonding in RC beams and slabs. *Construction and Building Materials,* Volume 17, pp. 447-462.

Teng J. G., et al., 2000. Retrofitting of deficient RC cantilever slabs using GFRP strips. *J. Compos. Constr,* 4(2), pp. 75-84.

Toutanji, H., 1999. Stress-Strain Characteristics of Concrete Columns Externally Confined with Advanced Fiber Composite Sheets. *ACI Materials Journal,* pp. 397-404.

Toutanji, H., Zhao, L. & Zhang, Y., 2006. Flexural behavior of reinforced concrete beams externally strengthened with CFRP sheets bonded with an inorganic matrix. *Engineering Structures ,* pp. 557-566.

W.K. Goertzen & M.R. Kessler, 2006. Creep behavior of carbon fiber/epoxy matrix composites. *Materials Science and Engineering,* Volume A 421, p. 217–225.

Wang YC & Hsu K , n.d. Design recommendations for the strengthening of reinforced concrete beams with externally bonded composite plates. *Composite Structures,* Volume 88, pp. 323-332.

Wang, Z., Joh, O. & Goto, Y., 1999. Bond creep behavior of FRP rods and their bond strength after sustained loading. *Transactions of the Japan Concrete Institute, Japan Concrete Institute,* p. 221–226.

Washa G.W. & Fluck P.G. , 1952. Effect of compressionreinforcement on plastic flow of reinforcedconcretebeams. *ACI Journal,* 24(2), p. 89–108.

Wei An, Hamid Saadatmanesh & Mohammad R. Ehsani, 1991. RC Beams Strengthened with FRP Plates. II: Analysis and Parametric Study. *Journal of Structural Engineering,* 17(11), pp. 3434-3455.

Wu Z., Matsuzaki T. & Tanabe K., 1997. Interface crack propagation in FRP-strengthened concrete structures, In: Non-metallic (FRP) reinforcement for concrete structures. *Japan Concrete Institute,* Volume 1, pp. 319-326.

Yasmeen T.O., et al., 2011. Review: Retrofitting of reinforced concrete beams using composite laminates. *Construction and Building Materials,* Volume 25, pp. 591-597.

Yousef A. Al-Salloum & Tarek H. Almusallam, 2007. Creep effect on the behavior of concrete beams reinforced with GFRP bars subjected to different environments. *Construction and Building Materials,* Volume 21, p. 1510–1519.

Curriculum Vita

Personal Data

Name:	Mohamed Morsy Abd El-Ghaffar Salem
Date of Birth:	01. June. 1972
Place of Birth :	El-Fayoum - Egypt
Family status:	Married with Marwa Hassanein since 2007 and have 2 children; Ahmed and Mariam.
Nationality:	Egyptian
Telephone:	+20 1005883131 +4917653455160
Email:	mm.aladawy@gmail.com mm_aladawy@yahoo.com

Education

Aug. 1991	Secondary School certificate of grade: 87.5 % Rank: 3rd of the Fayoum Governorate
Sep. 1991- July1996	Bachelor of Civil Engineering Cairo University (Fayoum Branch), El-Fayoum, Egypt Grade: Very Good with honor degree; 81.48%
	Graduation project: Structures, (Study & analysis of wide beam) Grade: Excellent
December 2004	Master of Science in Civil Engineering (Structural Engineering) from faculty of Engineering, Cairo University, Cairo, Egypt
	Master Thesis: Flexural behavior of continuous composite concrete beams with embedded steel sections
December 2012	Doctor of Engineering (Dr.-Ing) in Civil Engineering from faculty of Engineering, Hannover University, Hannover, Germany
	Thesis: "Flexural and Long-Term Behavior of CFRP-Strengthened Reinforced Concrete Beams"

Professional Experience

Jan. 1997 – Feb. 1998	Site Engineer for constructing reinforced concrete bridges during the period of Military Service
April 1998 – Jan. 1999	Site Engineer for constructing school buildings and Irrigations and drainages work

Jan 1999 – Sep. 2000	Engineer in Concrete Construction Research Institute of Housing and Building National Research Center (HBRC) http://www.hbrc-journal.gov.eg/ 87 Tahrir Street, Dokki – Giza, Egypt
	Site project: Supervisor Engineer for constructing 18 multi-story buildings
Oct. 2000 – Oct. 2001	Supervisor for Partition work in Al Nafea Trading Est. Partition Division Riyadh, Kingdom of Saudi Arabia
March 2002 – Jan. 2003	Supervisor for for Roads and high way constructions in Tabuk (KSA). **AAW**, Prof .Dr. Ahmed Abd Alwares Consulting Engineering Riyadh, Kingdom of Saudi Arabia (KSA)
March 2003 – Dec. 2004	Assistant researcher in Concrete Construction Research Institute, Housing and Building National Research Center (HBRC) http://www.hbrc-journal.gov.eg/ 87 Tahrir Street, Dokki – Giza, Egypt
	Site project: Supervisor Engineer for strengthening & rehabilitation of existing buildings in Arish, Egypt.
Jan. 2005 – Sep. 2007	Assistant Lecturer in Concrete Construction Research Institute, Housing and Building National Research Center (HBRC) http://www.hbrc-journal.gov.eg/ 87 Tahrir Street, Dokki – Giza, Egypt
	Site project: Supervisor Engineer for strengthening & rehabilitation of existing buildings in Beni-Suef and Arish, Egypt. Supervisor Engineer for constructing buildings in Luxor, Aswan, and Qena

Computer Program

Auto CAD Program.
Microsoft office.
SAP Program.
Abaqus FE program
Matlab
Very Good knowledge for computer software and hardware

Mohamed Salem
Hanover, December 2012